

**TECHNICAL  
TRANSACTIONS**

---

**CIVIL  
ENGINEERING**

**ISSUE  
4-B (28)**

---

**YEAR  
2015 (112)**

**CZASOPISMO  
TECHNICZNE**

---

**BUDOWNICTWO**

**ZESZYT  
4-B (28)**

---

**ROK  
2015 (112)**



**WYDAWNICTWO  
POLITECHNIKI  
KRAKOWSKIEJ**

# TECHNICAL TRANSACTIONS

# CZASOPISMO TECHNICZNE

## CIVIL ENGINEERING

## BUDOWNICTWO

ISSUE 4-B (28)  
YEAR 2015 (112)

ZESZYT 4-B (28)  
ROK 2015 (112)

Chairman of the Cracow  
University of Technology Press  
Editorial Board

**Jan Kazior**

Przewodniczący Kolegium  
Redakcyjnego Wydawnictwa  
Politechniki Krakowskiej

Chairman of the Editorial Board

**Józef Gawlik**

Przewodniczący Kolegium  
Redakcyjnego Wydawnictwa  
Naukowych

Scientific Council

**Jan Błachut**  
**Tadeusz Burczyński**  
**Leszek Demkowicz**  
**Joseph El Hayek**  
**Zbigniew Florjańczyk**  
**Józef Gawlik**  
**Marian Giżejowski**  
**Sławomir Gzell**  
**Allan N. Hayhurst**  
**Maria Kušnierova**  
**Krzysztof Magnucki**  
**Herbert Mang**  
**Arthur E. McGarity**  
**Antonio Monestiroli**  
**Günter Wozny**  
**Roman Zarzycki**

Rada Naukowa

Civil Engineering Series Editor  
Editor of Issue

**Marek Piekarczyk**  
**Jolanta Gintowt**

Redaktor Serii Budownictwo  
Redaktor wydania

Section Editor  
Native Speaker  
Typesetting  
Cover Design  
Cover Photo

**Dorota Sapek**  
**Tim Churcher**  
**Adam Bania**  
**Michał Graffstein**  
**Jan Zych**

Sekretarz Sekcji  
Weryfikacja językowa  
Skład i łamanie  
Projekt okładki  
Zdjęcie na okładce

Basic version of each Technical Transactions magazine is its online version  
Pierwotną wersją każdego zeszytu Czasopisma Technicznego jest jego wersja online  
[www.ejournals.eu/Czasopismo-Techniczne](http://www.ejournals.eu/Czasopismo-Techniczne) [www.technicaltransactions.com](http://www.technicaltransactions.com) [www.czasopismotechniczne.pl](http://www.czasopismotechniczne.pl)

© Cracow University of Technology/Politechnika Krakowska, 2015

**Civil Engineering Series**  
**4-B/2015**

**Editor-in-Chief:**

Marek Piekarczyk, Cracow University of Technology, Poland

**Editorial Board:**

Marek Cała, AGH University of Science and Technology, Poland  
Andrzej Cholewicki, Building Research Institute, Poland  
Wit Derkowski, Cracow University of Technology, Poland  
Jean-François Destrebecq, French Institute for Advanced Mechanics, France  
Grzegorz Dzierżanowski, Warsaw University of Technology, Poland  
Andrzej Flaga, Cracow University of Technology, Poland  
Dariusz Gawin, Lodz University of Technology, Poland  
Jacek Gołaszewski, Silesian University of Technology, Poland  
Kocsán Lajos György, University of Miskolc, Hungary  
Bożena Hoła, Wrocław University of Technology, Poland  
Maria E. Kamińska, Lodz University of Technology, Poland  
Oleg Kapliński, Poznan University of Technology, Poland  
Tadeusz Kasprowicz, Military University of Technology, Poland  
Renata Kotynia, Lodz University of Technology, Poland  
Robert Kowalski, Warsaw University of Technology, Poland  
Mária Kozlovská, Technical University of Košice, Slovakia  
Andrzej Łapko, Białystok University of Technology, Poland  
Marco Menegotto, Sapienza University of Rome, Italy  
Peter Mesároš, Technical University of Košice, Slovakia  
Piotr Noakowski, TU Dortmund University, Germany  
Andrzej Nowak, University of Michigan, United States  
Zygmunt Orłowski, AGH University of Science and Technology, Poland  
Hartmut Pasternak, Brandenburg University of Technology Cottbus–Senftenberg, Germany  
Edyta Plebankiewicz, Cracow University of Technology, Poland  
Maria Polak, University of Waterloo, Canada  
Elżbieta Radziszewska-Zielina, Cracow University of Technology, Poland  
Charles Rodrigues, Universidade Nova de Lisboa, Portugal  
Tomasz Siwowski, Rzeszow University of Technology, Poland  
Marcela Spišáková, Technical University of Košice, Slovakia  
Zuzana Struková, Technical University of Košice, Slovakia  
Maria Szerszeń, University of Nebraska – Lincoln, United States  
Jolanta Tamošaitienė, Vilnius Gediminas Technical University, Lithuania  
Alena Tažiková, Technical University of Košice, Slovakia  
Balázs Tóth, University of Miskolc, Hungary  
Martins Vilnītis, Riga Technical University, Latvia  
Szczepan Woliński, Rzeszow University of Technology, Poland

# BUILDING PHYSICS



ARTUR BOROWCZYŃSKI, DARIUSZ HEIM\*

## SUPPLEMENTARY LIGHTING CONTROL IN OFFICE ROOM WITH MINIMIZED GLAZING AREA

---

### UZUPEŁNIAJĄCE STEROWANIE OŚWIETLENIEM W POMIESZCZENIU BIUROWYM O ZMINIMALIZOWANEJ POWIERZCHNI PRZESZKLENIA

#### Abstract

The paper is dedicated to present and compare two methods of controlling supplementary lighting system in office with limited glazing area. The lighting energy demand was evaluated taking into account positioning of light sensors and room occupancy. Comparison of daylight conditions in the rooms with different orientations was carried out. The results shows the effect of occupancy scenario on lighting control strategy.

*Keywords: control, daylighting, artificial lighting, simulation, office room*

#### Streszczenie

W artykule przedstawiono dwie metody sterowania uzupełniającym systemem oświetlenia w budynku biurowym o ograniczonej powierzchni przeszklenia. Oszacowano zapotrzebowanie na energię do oświetlenia, biorąc pod uwagę rozmieszczenie czujników promieniowania oraz liczbę osób pracujących w pomieszczeniu. Dokonano porównania pomiędzy pomieszczeniami o różnej orientacji. Na podstawie otrzymanych wyników stwierdzono wpływ użytkowania pomieszczenia na strategię sterowania oświetleniem.

*Słowa kluczowe: sterowanie, światło dzienne, oświetlenie sztuczne, symulacja, pomieszczenie biurowe*

**DOI: 10.4467/2353737XCT.15.385.5016**

---

\* MSc. Eng. Artur Borowczyński, PhD. DSc. Eng. Dariusz Heim, Department of Environmental Engineering, Faculty of Process and Environmental Engineering, Lodz University of Technology.

## 1. Introduction

New artificial lighting technologies e.g. light emitting diode (LED) solution, give a new possibilities to control light intensity in offices and other public utility buildings occupied during a day [1]. Some limitations of artificial light intensity as well as shorter operating time, can lead to lower energy requirements. These savings are possible to be achieved through selected control strategies, when daylight is mixed with electrical light [2]. However, in buildings with minimized size of transparent components the daylight utilization is lower than for highly glazed facades. On the other hand limited surface of glazing also provides higher comfort level by avoiding of daylight glare effects and heighten solar heat gains [3].

Another issue related with supplementary lighting control is positioning of light sensors. Their location must be adjusted to the room geometry. Minimized glazing area imposes additional limitations. Furthermore, lighting in larger offices often works in groups, what further complicates sensor positioning [4].

The presented study was devoted to find the appropriate control strategy for supplementary artificial lighting in office rooms dedicated for work with computer. Additionally, changeable occupancy and daylight accessibility were taken into account. Finally, the energy which is necessary to power supplementary lighting system was measured and correlated with a sensor positioning.

## 2. Supplementary lighting control

As supplementary lighting the most commonly used are lights with the low power consumption, because such systems have to operate only periodically. Additionally, to achieve greater accuracy lighting should be able to work on the different levels of intensity [5]. Artificial light should have an ability to brighten or to dim for several levels. It is necessary to provide precise response to the continuously changing daylight conditions. Because of these two characteristics as supplementary lighting LED systems are the most suitable choice, they are a control subjects of this work.

Electric lights can be controlled according to the availability of natural daylight. When lighting control is switched on, illuminance levels are calculated to determine how much the electric lighting can be reduced. The daylight illuminance level in a zone depends on many factors, including sky condition, sun position, light sensor position, as well as glass transmittance, location and size of window, window shades and reflectance of interior surfaces. Reduction of electric lighting depends on daylight illuminance level, illuminance set point, fraction of zone controlled and type of lighting control [6].

Two control strategies were analysed in this work: linear/off and stepped models. With linear/off control, the lights dim continuously and linearly from maximum electric power, maximum light output to minimum electric power, minimum light output as the daylight illuminance increases. The lights switch off completely with further increase in the daylight illuminance. Linear/off control provides an idealised lighting control mechanism. Stepped control allows to switch lighting on/off according to the availability of natural daylight in discrete steps. Whereas the linear/off control provides precisely controlled illuminance by dimming the lights, the stepped control models blocks of lights switching on/off according to

the electric lighting requirement. The electric power input and light output vary in discreet, equally spaced steps. The number of steps can be set individually [7].

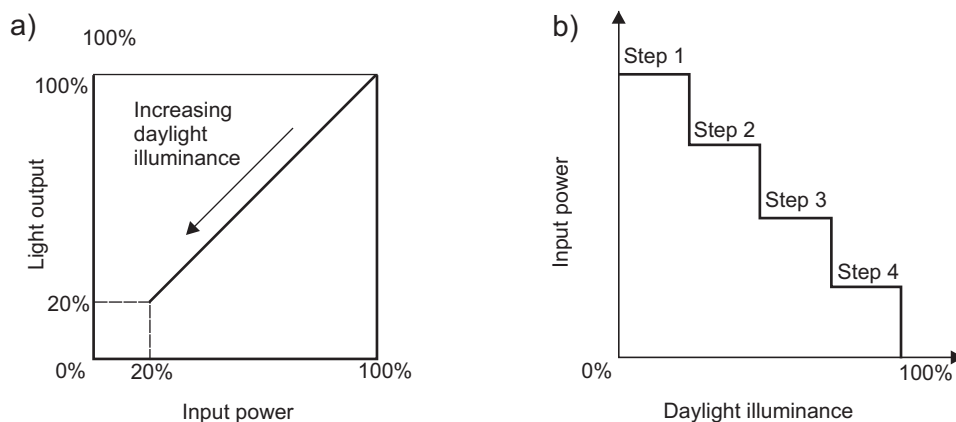


Fig. 1. Control a) linear/off, b) stepped model

### 3. Experimental office room

For the purpose of the comparative analysis two office rooms were taken into consideration: one faced east, other west direction. Its dimensions were assumed as 5.0 m length and 3.0 m width and height. The rooms are painted with light grey colour. They represent typical offices for work with computer for up to two persons. These rooms used in the analysis are a models of real offices located at the Lodz University of Technology.

Rooms have only a single window with a minimized window area (1.2 m width and 1.2 m height) estimated based on the maximum UDI and the proper view of the external environment. During morning hours the west oriented room was lighted by a diffuse daylight while during afternoon for specific weather conditions also some direct light were available inside. Opposite situation appears for east oriented room. Because of small window's surface during cloudy days it will not provide a necessary access to the daylight. To deal with that problem the room was equipped with three LED luminaires. They are operating in two groups: one closest to the window acts as single lamp, two next are coupled. This solution gives an opportunity to implement a complex control systems described in the previous section.

Rooms are equipped with two light sensors each. Their height is on 0.8 m (working plane), first is located in the distance of 1.0 m from window, second 1.5 m deeper. It represents groups of lamps as well as spaces of office workers.

Furthermore, the analysis includes 3 occupancy variants. Scenarios are based on the three characteristics: occupancy, minimum illuminance required for work and control by the use of one or two light sensors. It was assumed, that for a single person only one sensor is required, while for two persons second sensor will be also introduced. Variants with the minimum required illuminance are listed in (Table 1). Additionally, assumption was made for scenario III, that work space closer to window does not require 500 lux to meet requirements for work with computer due to vicinity of window and additional light emitted by computer screen.



The software used for simulation of lighting conditions in rooms was DesignBuilder, which is developed on Energy Plus, therefore radiosity method was used to calculate effects of light.

Table 1

**Office occupancy variants**

Name	Occupancy	Minimum illuminance [lux]	
	[Persons]	Sensor 1	Sensor 2
Variant I	1	500	–
Variant II	2	500	500
Variant III	2	250	500

#### 4. Results and discussion

In order to examine presented lighting control method, two types of control algorithm were taken into consideration. Conducted analysis showed that total lighting energy demand has different values for linear/off and stepped control. In general, power demand obtained for stepped control method is higher in each case, regardless of chosen occupancy variant. The major reason is that linear/off is idealized method, that enable to control lighting with perfect accuracy with amount of daylight illuminance actuated by sensor. On the other hand, stepped control is closer to typical office LED controls, which do not offer such precision and require more power to operate.

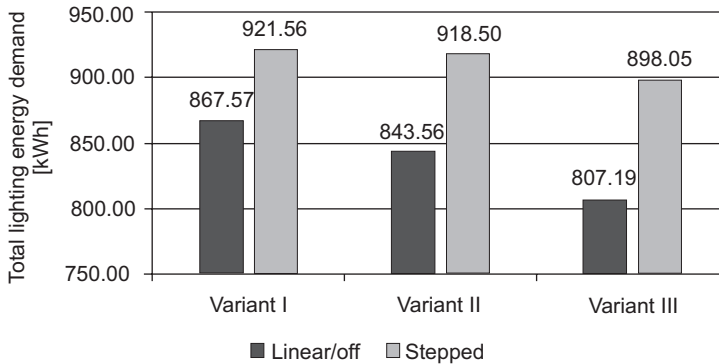


Fig. 2. Total lighting energy demand

Furthermore, it can be noted that lighting energy demand values obtained in calculation differ depending on the occupancy variant. Introduction of second light sensor and its implementation into control method allow for significant reduction in lighting energy. What is more, by lowering minimum required illuminance in the working plane closer to the window another energy savings can be noted. It is positive for both control methods, however for stepped control differences are much lower.

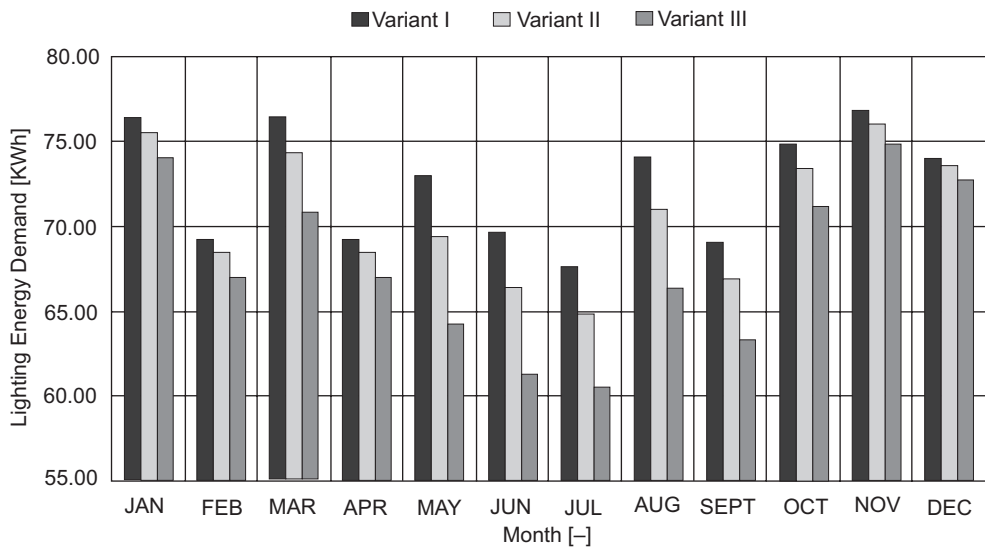


Fig. 3. Lighting energy demand for linear/off control

Final analysis was related to office rooms oriented on the east and west. Results (Fig. 4) show the daylight illuminances actuated by light sensors. It can be noted that east room receives slightly more daylight, especially in the summer period. Furthermore, sensor 1 located closer to the window acquire more daylight than one placed deeper, therefore controlling supplementary lighting only on the basis of one sensor may be unreliable and can lead to insufficiency of light in the further parts of the room.

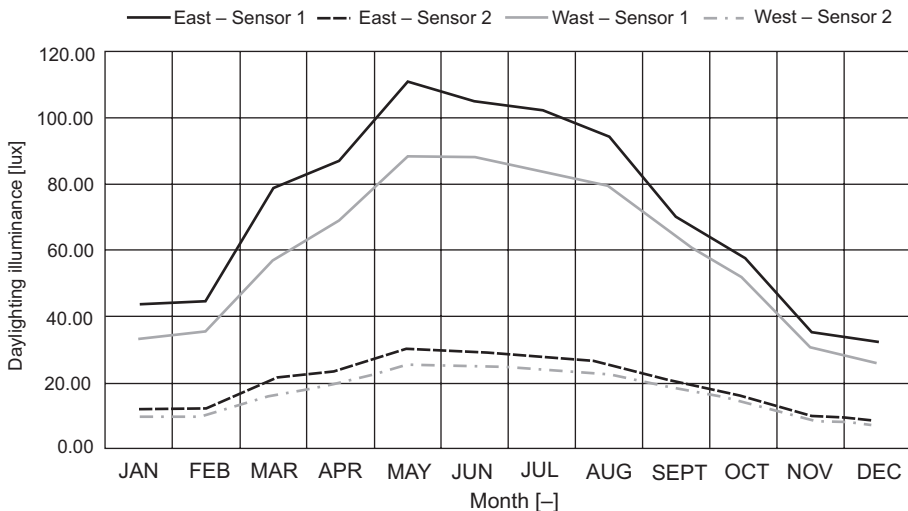


Fig. 4. Values of daylight illuminance for office rooms

## 5. Summary

Performed analysis showed that selection of an appropriate control strategy for supplementary lighting has a great impact on the quality of light in office room. Control method should include indoor daylight conditions, electric lighting should operate only when it is required to reach necessary illuminance level. Moreover, room occupancy scenario strongly influence control method as well as the positioning of sensors. For rooms with limited glazing area location of sensors should be carefully thought, their insufficient number or too large distance between them may lead to incorrect operation of electric lighting. Furthermore, the proper window orientation (even with minimized glazing area) may have positive effect on supplementary lighting system, decreasing its light intensity, therefore reducing energy costs.

Based on the obtained results it was possible to justify the effectiveness of lowly glazed office buildings considering energy efficiency of indoor lighting. Additionally, the most proper control strategy could be applied and analyzed taking into account irregular presence in the office.

## Acknowledgements

This work was funded by The National Centre for Research and Development as part of the project entitled: “Promoting Sustainable Approaches towards Energy Efficiency in Buildings as Tools Towards Climate Protection in German and Polish Cities: developing facade technology for zero-emission buildings” (acronym: GPEE).

## References

- [1] Bin-Juine Huang, Po-Chien Hsu, Min-Sheng Wu, Chun-Wen Tang, *Study of system dynamics model and control of a high-power LED lighting luminaire*, Energy, 32, 2007, 2187–2198.
- [2] Ihm P., Nemri A., Krarti M., *Estimation of lighting energy savings from daylighting*, Building and Environment, 44, 2009, 509–514.
- [3] Heim D., Szczepańska E., *Daylight distribution in a building space: A comparison of real conditions and theoretical sky models*, Proceedings of Building Simulation, Sydney 2011, 2718–2723.
- [4] Khalid Y. A., *Controllability of Building Systems*, PhD Thesis, University of Strathclyde, Glasgow 2011.
- [5] Shen E., Hu J., Patel M., *Energy and visual comfort analysis of lighting and daylight control strategies*, Building and Environment, 78 (2014), 155–170.
- [6] Tzempelikos A., Shen H., *Comparative control strategies for roller shades with respect to daylighting and energy performance*, Building and Environment, 67, 2013, 179–192.
- [7] *DesignBuilder 2.1 User's Manual*, October 2009.

HENRYK NOWAK, PAWEŁ NOSZCZYK \*

## APPLICATION OF THE ACTIVE IR THERMOGRAPHY FOR THE DETECTION OF NON-UNIFORMITY OF MATERIALS IN BUILDING PARTITIONS

### ZASTOSOWANIE TERMOGRAFII AKTYWNEJ DO DETEKCJI NIEJEDNORODNOŚCI MATERIAŁOWYCH W PRZEGRODACH BUDOWLANYCH

#### Abstract

The paper describes the problem of building envelope investigation with active thermography. Mainly emphasized is its application to detect different material of wall inclusions. Examples of active thermography application and description of experimental investigation has been shown on a model envelope, with inclusion of significantly different thermal conductivity and heat capacity materials; XPS polystyrene, steel and granite. Thermograms received for every kind of inclusion have been compared and analyzed. Finally, the summary and conclusion have been shown along with the prospects of development and practical application of this kind of investigation in construction.

*Keywords: building partition, material inclusions, active IR thermography*

#### Streszczenie

Artykuł porusza problem wykonywania badań przegród budowlanych za pomocą termografii aktywnej. Podkreślono w nim możliwość detekcji różnych wtrąceń materiałowych w przegrodzie. Praca przedstawia wykonane badanie doświadczalne na modelu przegrody, w którym zamodelowano wtrącenia z materiałów o znacznie różniącym się współczynniku przewodzenia ciepła tj. styropian XPS oraz stal. Otrzymane termogramy porównano ze sobą i poddano analizie. W podsumowaniu przedstawiono wnioski wraz z perspektywami rozwoju badań i praktycznego zastosowania termografii aktywnej w budownictwie.

*Słowa kluczowe: przegroda budowlana, wtrącenia materiałowe, termografia aktywna*

**DOI: 10.4467/2353737XCT.15.396.5027**

\* Prof. DSc. PhD. Eng. Henryk Nowak; MSc. Eng. Paweł Noszczyk, Division of Building Physics and Computational Design Methods, Faculty of Civil Engineering, Wrocław University of Technology.

## 1. Introduction

Thermography is a form of nondestructive testing, which means that such testing does not affect the properties of the object being tested and does not interfere with its structure. The thermovision testing is performed noninvasively, with a contactless method. It uses the electromagnetic radiation within the wave length of  $3.0 < \lambda < 100 \mu\text{m}$  [4], called infrared radiation or, commonly, thermal radiation. The measurements are made using a thermovision camera, that records thermal radiation emitted by each object being tested. The signal reaching the camera is processed into a thermogram, that shows the temperature field distribution over the surface of the element being tested. The thermovision testing is used in various fields of life and science, e.g., industry, medicine or in building industry [1, 2, 3]. Both passive and active method can be used when testing the temperature distribution field on the surface of a building partition. The former consists of performing the testing without interfering with the thermal processes occurring within the partition, which is a typical thermovision testing process for buildings. This method is practical in the heating season only, since the testing requires a difference in the air temperature at a level of circa  $15^\circ\text{C}$  [2]. On the other hand, the active IR thermography method introduces an additional source of heat/cold, as well as intensive heating/cooling of the building partition, followed by the recording of thermograms during the cooling/heating of the partition being tested, performed at certain time intervals. Depending on the type of the temperature source, the active IR thermography can be split into four types: pulse, modulation, pulse-phase and vibration [4]. This paper takes a closer look at the application of the pulse active thermography in building industry. The paper focuses on the presentation of the model of a building partition, that was subjected to experimental testing, along with the description of the built test and its method, followed by the quotation of exemplary test results. A particular problem with the use of active IR thermography is to achieve uniform heating of a large surface area along with limited penetration of thermal waves in the thick building partitions.

## 2. Active IR thermography in the thermal analysis of buildings

The active IR thermography is a relatively young field of science, that became globally acknowledged in the 80s. In Poland this method has been investigated since ca. 2000. Presently, various research centres throughout the world conduct work on the development of the active IR thermography in building industry. An interesting trend of the active IR thermography's development seeks to find its application for the contactless investigation of the properties of building materials to determine their heat conductivity. Another application focuses on the detection of defects in the tested partitions. This investigation can be particularly helpful in such building facilities, where more invasive tests are impossible to carry out. The detection of inclusions and their general location by itself does not pose a problem to the operator of a thermovision camera. On the other hand, an interesting issue to resolve is to determine the precise dimensions of such inclusions/defects or their depth, especially on a macro scale of a building partition. The investigation can be conducted both in the reflection mode (the camera and the source of temperature are located on the same side of the wall) and the transmission mode (the camera and the source of temperature are located on two different sides of the partition).

### 3. Adopted partition model and test stand

The building partition model was adopted as a construct comprising two major elements. The first one constitutes a homogenous material, that reflects the major wall building material. The other element constitutes material inclusions located inside the partition. A OSB-3 board type was adopted as a homogenous material, having a heat conductivity amounting to  $0.13 \text{ W/m}\cdot\text{K}$ . The model partition is made up of 4 board layers of varying thicknesses: 22 mm; 10 mm; 10 mm and 22 mm, successively. Such structure is fitted with 20 mm thick inclusions inside the model partition. Three different material inclusions, with a considerably differentiated heat transfer conductivities (steel, XPS polystyrene and granite) were used. Each inclusion is characterized by a different heat conductivity amounting to:  $50.0 \text{ W/m}\cdot\text{K}$  for steel,  $0.033 \text{ W/m}\cdot\text{K}$  for polystyrene and  $2.80 \text{ W/m}\cdot\text{K}$  for granite. Each of the inclusions has the size of  $100 \times 200 \times 20 \text{ mm}$ . They are located both vertically (steel) and horizontally (polystyrene, granite) over the whole surface of the homogenous material – an OSB board of  $1250 \times 1250 \text{ mm}$ . The partition model applied will allow good observation of the temperature field variation during the test conducted with the active IR thermography. Should the building partition of an order of 20 – 40 cm had been applied from the very beginning, it might have been impossible to notice the impact of the inclusions in the material in the reflection mode in the initial investigation conducted with active IR thermography. Conclusions were drawn on the basis of the previously conducted investigation, where a similar partition of 13 mm was applied on the OSB board [3]. The proposed partition model increases the thickness of the front plate up to 22 mm and at the same time introduces three different inclusions in the same partition.

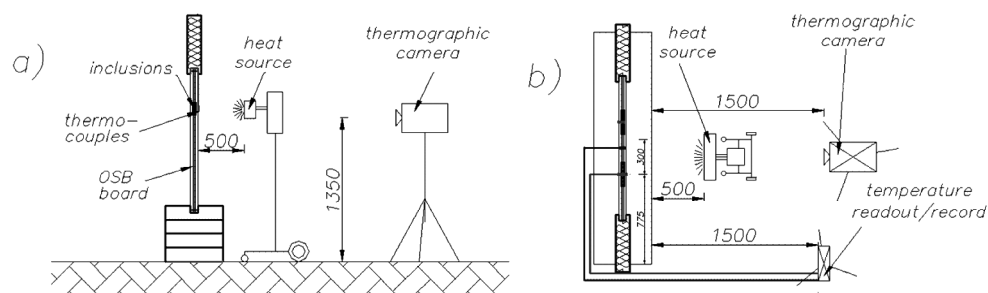


Fig. 1. Schematic of the built test stand. Section of the test stand (a) and its horizontal projection (b)

The schematic of the test stand is shown in Fig. 1. Its core element is the partition model made of an OSB board with inclusions, around which a 50 cm broad frame of 12 cm thick polystyrene boards was placed. The whole segment was supported by a layer of polystyrene boards. The above operation was conducted taking into account the convective heat transfer to the back of the partition. Without a polystyrene band an uncontrolled heat flow and warming-up of the other side of the OSB board would take place. A thermovision camera made by the Flir company, model P65, K type thermocouples, an infrared radiator type FOBO EP 102 of 1.0 kW power (to warm up the partition) and the Ahlborn unit for carrying out the recording of temperatures and relative humidity of air were used. The camera was placed at the distance of 1.5 m from the partition being warmed up, while the infrared radiator was set

at the distance of 50 cm from the OSB board. Beside the recording of the thermograms of the cooling-down partition, the temperature in the vital places of the tested section was also recorded by thermocouples.

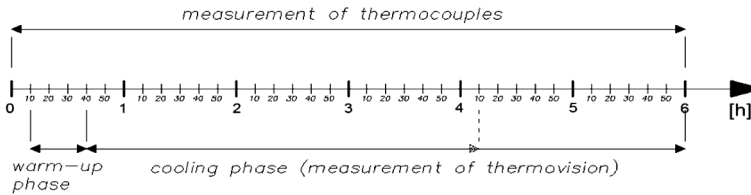


Fig. 2. Schematic of the graphic schedule of the conducted test

The thermocouples were placed in alignment over the inclusions and 20 cm from the edge of the inclusion, 4 thermocouples in each section: on the OSB board surface, on both sides of the inclusion surface and at the rear of the partition model. As the result, the temperature distribution in time throughout the section can be observed. The thermocouple wires were placed in the outer cut-out grooves of the partition boards. Measurements started with the activation of the temperatures recording from all thermocouples placed on the partition, as well as the temperatures and relative air humidity. After 10 minutes, the switch-on of the heat radiator occurred, warming up the board for exactly 30 minutes. Afterwards, the heat radiator was removed from before the board and the recording of thermograms started, lasting for a minimum of 4 hours, until a uniform temperature over the partition surface was reached. The recording of thermograms followed periodically every 1 minute, while the recording of temperature and humidity values followed every 10 seconds (Fig. 2).

#### 4. Selected experimental results

Figs. 3–4 below present the selected experimental measurements made with a thermovision camera. The white colour areas show the warmest places, whereas the violet areas show the coolest places. Fig. 3 (top) shows how – after a time period of 30 minutes after the start time of the element’s cooling – the zone of warmest temperatures moves over the defect from polystyrene, that “does not allow” the heat flow to the other side of the partition. A reciprocal situation (Fig.3 at the bottom) takes place with a steel inclusion. After a time period of around 30 minutes, a zone of lower temperatures in relation to a homogenous section without an inclusion is visible. It comes from the fact, that steel (having a high heat conductivity) “allows” easy heat displacement onto the other side of the partition. An interesting temperature distribution is also visible in Fig. 3 on its extreme right side.

A slightly cooler zone is visible over the polystyrene inclusion, while the partition surface over an inclusion from steel is slightly warmer than the other area visible on the thermogram. This happens due to a different volumetric heat capacity of materials. Polystyrene of a low volumetric heat capacity yields heat more quickly, on the other hand, steel having a high volumetric heat capacity radiates out heat for a significantly longer time, which is shown in the thermogram in form of a temperate increase on the graph.

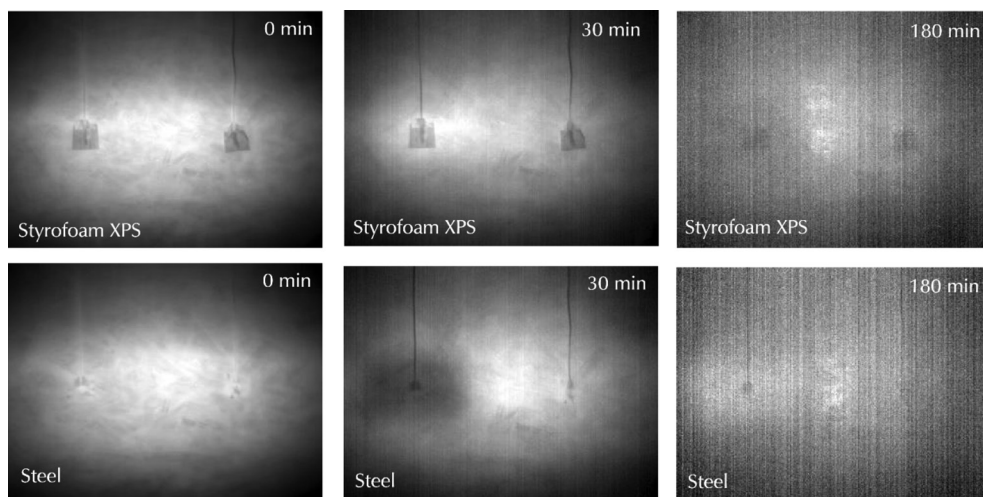


Fig. 3. Thermovision pictures in crucial moments of the element's cooling; styrofoam XPS inclusion (top line), and steel inclusion (bottom line)

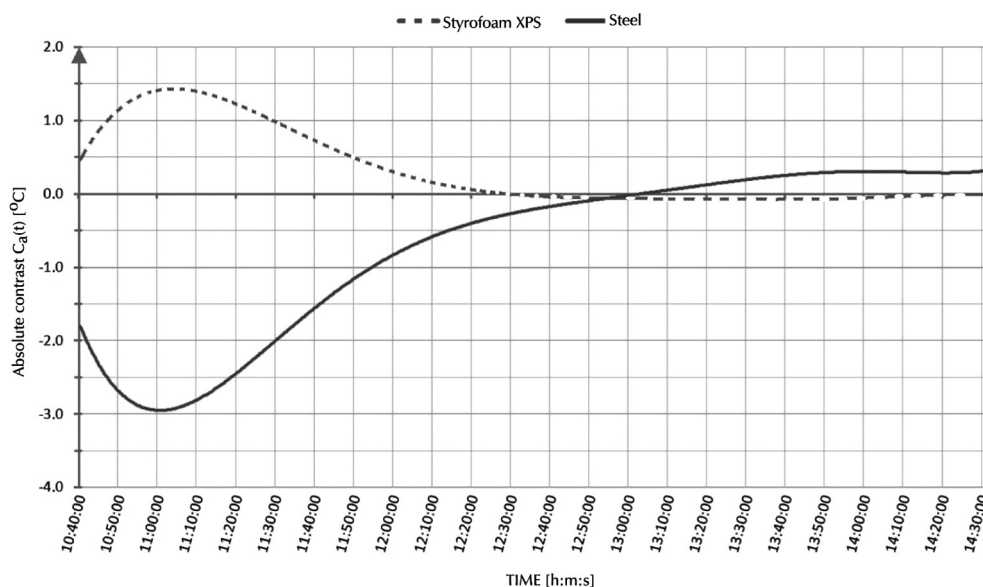


Fig. 4. The temperature difference between the surface of the section with a defect and a homogenous section for styrofoam XPS inclusion and steel inclusion (absolute contrast)

A conclusion may be drawn, that with the pre-set geometry (a hidden defect under a homogenous material of a thickness above 20 mm), using the active IR thermography exclusively, it is possible to simply identify the inclusions' material. In order to show various dynamic changes in both sections of the surface of the object being tested, the absolute



contrast for a steel inclusion and a styrofoam XPS inclusion were compared (Fig. 4). The absolute contrast defines the difference between the temperature at a freely selected point on the surface (over an inclusion) and the temperature of the surface over a homogenous area. The maximum absolute contrast is perceptible circa 25–30 minutes after the initiation of the element's cooling. Also at that time, for the assumed partition model, a material inclusion is best visible in the thermogram.

## 5. Summary

The investigation conducted emphasizes a special suitability of active thermography in the reflection mode to detect material inclusions in building partitions. A significant advantage of such investigation is its non-destructive nature, thanks to which it can be used in investigations of the existing building facilities. In the next step of the experimental investigation a test of a granite inclusion will take place. The test will also feature the comparison of temperature contrasts, depending on the degree of the element's warm-up and an attempt to find a reciprocal solution of the heat transfer issue [5–7]. To compare the test results, an additional analysis consisting of warming-up of the whole partition with all inclusions installed simultaneously will be carried out. Under the research work conducted, the investigation on real objects is also scheduled.

## References

- [1] Maierhofer Ch., Brink A., Rollig M., Wiggenhauser H., *Quantative impulse-thermography as non-destructive testing method in civil engineering – Experimental results and numerical simulations*, Construction and Building Material, 19, 2005, 731–737.
- [2] Nowak H., *Zastosowanie badań termowizyjnych w budownictwie*, Oficyna Wydawnicza Politechniki Wrocławskiej, Wrocław 2012.
- [3] Nowak H., Kucypera M., *Zastosowanie termografii aktywnej w nieniszczących badaniach przegród budowlanych*, Energia i Budynek, nr 7 2011, 13–18.
- [4] Maldague X., Marinetti S., *Pulse phase infrared thermography*. Journal Applied Physics, 79, 1996, 2694–2698.
- [5] Minkina W., *Wybrane problemy współczesnej termografii i termometrii w podczerwieni*, Wydawnictwo Politechniki Częstochowskiej, Częstochowa 2011.
- [6] Oliferuk W., *Termografia podczerwieni w nieniszczących badaniach materiałów i urządzeń*, Biuro Gamma, Warszawa 2008.
- [7] Taler J., Duda P. *Rozwiązywanie prostych i odwrotnych zagadnień przewodzenia ciepła*. Wydawnictwa Naukowo-Techniczne, Warszawa 2003.

KATARZYNA NOWAK-DZIESZKO, MAŁGORZATA ROJEWSKA-WARCHAŁ\*

## SYMULATION OF NIGHT COOLING IN A SINGLE DWELLING OF A LARGE PANEL BUILDING

---

### SYMULACJA NOCNEGO CHŁODZENIA W POJEDYNCZYCH MIESZKANIACH W BUDYNKU Z WIELKIEJ PŁYTY

#### Abstract

When analyzing large panel buildings, it is very rare to take into consideration the requirements connected with the overheating effect. The paper presents the results of the annual computational simulations of thermal comfort conducted for one flat of W70 multi-family large panel building. Basing on the simulations the authors analyzed the influence of night cooling on thermal comfort inside the flat. Different simulation steps were taken into consideration: windows with and without shading systems, opened during entire night or just during given periods of time to keep specific thermal conditions.

*Keywords: large panel building, thermal comfort, PMV (Predicted Mean Vote), balcony framings, loggia*

#### Streszczenie

Podczas analizy budynków wielkopłytowych bardzo rzadko uwzględniane są wymagania związane z ich przegrzewaniem. W artykule przedstawiono roczne symulacje komfortu cieplnego przeprowadzone dla pojedynczego mieszkania w wielorodzinnym budynku wielkopłytowym w systemie W70. Na podstawie symulacji autorzy przeprowadzili analizę wpływu nocnego chłodzenia na komfort wewnątrz mieszkania. Analizie poddano różne warianty: okna z systemem zacienień zewnętrznych i wewnętrznych, otwierane w okresach nocnych w celu obniżenia temperatury.

*Słowa kluczowe: budynki wielkopłytowe, komfort cieplny, PMV, loggia, balkon*

**DOI: 10.4467/2353737XCT.15.397.5028**

---

\* MSc. Katarzyna Nowak-Dzieszko, MSc. Małgorzata Rojewska-Warchał, Institute of Building Materials and Structures, Faculty of Civil Engineering, Cracow University of Technology.

## 1. Description of problem

Overheating problems in buildings are very common and seem to be very important from occupants' point of view. Taking into consideration the fact that almost a quarter of Poles lives in large system panel buildings the issues related to this subject are very important and common. Occupants can control their thermal environment by means of clothing, operable windows, fans, heaters, internal and external sun shades.

Unfortunately at the simulation stage it is very difficult to predict the way the individual flat will be used. Looking globally at the multi-family building probably each flat should be analyzed separately after considering the requirements and expectations of inhabitants regarding temperature and humidity conditions. Many analyses were conducted by the authors and results were described in [1–4]. All of them under the assumption that all windows are closed during the entire day. For those unfavorable conditions there are problems with overheating of internal spaces even after using of internal and external shading systems. This assumption is however only theoretical as in practice the inhabitants open the windows when temperature inside exceeds uncomfortable values. Internal cooling through the windows makes sense especially during the night when external temperature is lower than internal. From the safety reasons sometimes opening of the windows during the night is impossible, especially at the lowest levels.

## 2. Description of analyzed building

The simulations were conducted for the W70 panel dwelling building, built in 1974. Plan area  $21.5 \text{ m} \times 13.2 \text{ m}$ ; usage building area –  $2279 \text{ m}^2$ , 25 m high with 11 levels. Basement below the entire building, flat roof.

The building has natural ventilation and a central heating system with convection heaters. A communication area is located in the central part of the building. There are four flats at every single level. Exterior walls made of prefabricated panels in the W70 system, insulated with 15 cm of styrofoam with plasters at both sides:  $U = 0.20 \text{ [W/m}^2\text{K]}$ . Triple glazing windows:  $U = 1.1 \text{ W/m}^2\text{K}$  to keep current national requirements (Warunki Techniczne), SHGC (solar heat gain coefficient) equal to 0.63. SHGC is a description of windows used in United States, refers to the solar energy transmittance of the glass. In Europe the g value describes the same parameters of the glazing.

The simulations conducted for the Polish climatic conditions (building located in Cracow). The calculations were carried out in Design Builder v.3. The program has been specifically developed around Energy Plus, allowing the simulation of the building envelope and building interiors.

Analysis based on standard PN-EN ISO 7730, 'Ergonomics of the thermal environment. Analytical determination and interpretation of thermal comfort using calculation of the PMV and PPD indices and local thermal comfort criteria'.

### 3. Simulation settings

Simulations were conducted for one flat, located at 7<sup>th</sup> floor with balcony at south elevation and windows at west side. The flat was analyzed as one thermal zone, an assumption that all internal doors are open was made. The main aim of simulations was to determine the temperature and PMV (Predicted Mean Vote) index during the summer months. The period of time between 15th May and 15th September was taken into consideration because at this time in Poland, there is a risk of overheating.

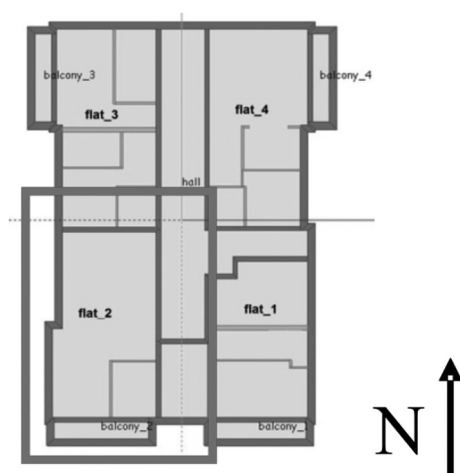


Fig. 1. Typical zones' visualization at every building level. Analyzed flat #2

The assumptions to the simulations:

- Heating system on from September to March (22°C), 7 days a week, 24 hours a day.
- Occupancy density: flats – about 1 person per 15 m<sup>2</sup>.
- Operating schedule: flats – 100% occupancy density between 4 pm and 7 am, 5 days a week; at the weekends between 6 pm and 9 am; 50% reduced occupancy between 9 am and 6 pm.
- Metabolic activity: factor 1.2 met, winter clothing – clo = 1.0, summer clothing clo = 0,5.
- Ventilation requirements per Polish national standards PN-83/B-03430, in every flat 70 m<sup>3</sup>/hour for kitchen and 50 m<sup>3</sup>/hour for bathroom.
- Internal solar shadings (blinds with high reflexivity slats), and external shading panel (7 panels – louvre blades).

### 4. Test results

Six different simulation steps were analyzed and compared with one another.

1. All windows closed.
2. All windows closed, internal and external shading systems used.
3. Night cooling of the flat between 8p.m. and 6 a.m. without shading systems.

4. Night cooling of the flat during the night until the internal temperature drops to 20°C, without shading systems.
5. Night cooling of the flat between 8p.m. and 6 a.m. with shading systems.
6. Night cooling of the flat during the night until the internal temperature drops to 20°C, without shading systems.

#### 4.1. Influence of shadings

In the first simulation step there is an assumption that all building windows are closed for the entire day. It affects the internal temperatures significantly. All simulation results have shown that during some days in the analyzed period of time the average interior air temperature exceeds 30°C and the PMV factor is even higher than 2. Those microclimate building conditions exceed the optimal internal summer temperature of 25°C and recommended value  $-0.5 < PMV < +0.5$ . In the second step, the internal and external shading systems were used at all windows. Those solutions affected the results significantly however did not eliminate the overheating temperatures entirely. Figures 3 and 4 present the number of overheating hours in the analyzed months. The number of discomfort hours, with the temperature above 25°C in the first simulation step is 2549, usage of shading systems reduces this number by about 35% to 1659.

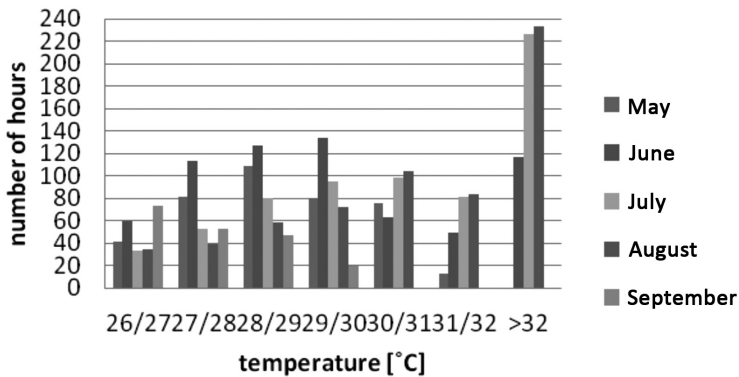


Fig. 2. Number of overheating hours in different months

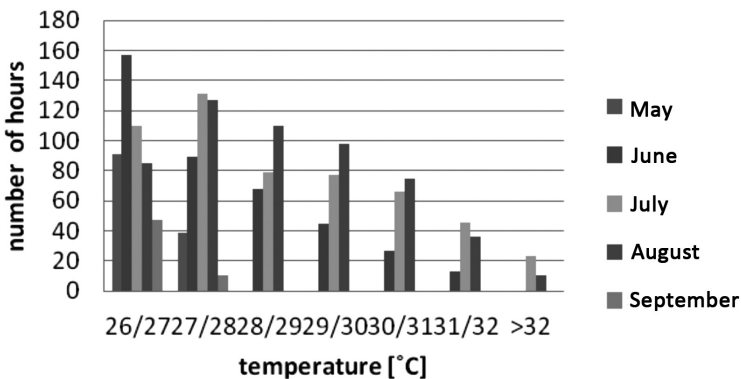


Fig. 3. Number of overheating hours, with internal and external shading systems, in different months

#### 4.2. Influence of night cooling on thermal conditions

Simulation steps #3 through #6 assume night cooling of the flat which, in program, was modelled as additional ventilation rate. It represents the cooling of the flats by opened windows and was modelled as 5 air ventilation exchanges of the flat volume for a flat with and without shading systems. Night cooling itself was also analyzed in two different options. First case when the windows are opened between 8 p.m. and 6 a.m. (steps 3 and 5), second option – windows are opened until the internal temperature drops to 20°C, then windows are closed (steps 4 and 6).

Table 1 presents comparison of the number of discomfort hours in all analyzed cases.

Table 1

**Number of overheating hours (above 25°C) in different simulation steps.**

Simulation step	Number of overheating hours	Temperatures above 30°C
Step 1	2549	1144
Step 2	1659	296
Step 3	591	71
Step 4	727	79
Step 5	229	0
Step 6	278	0

Night cooling exerts significant influence on the internal thermal conditions. In all cases (3 thru 6), night cooling affected the number of discomfort hours significantly, decrease up to 80% can be observed comparing to the assumption when all windows are closed (steps 1 and 2). Temperatures above 30°C were almost entirely eliminated.

Using both shading systems and night cooling eliminated temperatures above 30°C entirely. From the overheating point of view the most favorable solution is using of night cooling together with internal and external shading systems (steps 5 and 6). However in those cases low temperatures even below 20°C can be observed. Figures 5 through 7 present the number of hours below 25°C and PMV factor in 6<sup>th</sup> simulation step. Values are even lower than -2.0 and temperatures drops down to 15°C. Number of hours below 20°C is 433 and those are very unfavorable conditions for inhabitants.

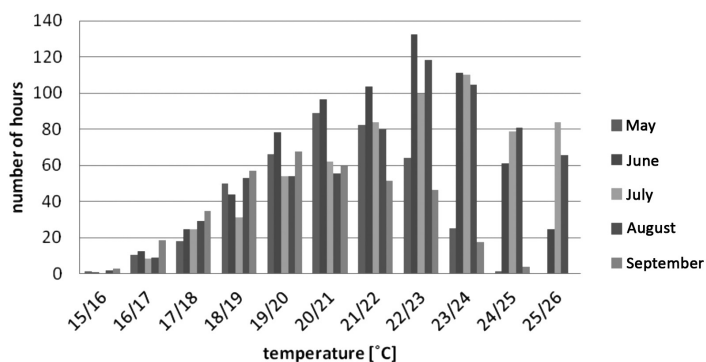


Fig. 4. Number of hours below 25°C in different months

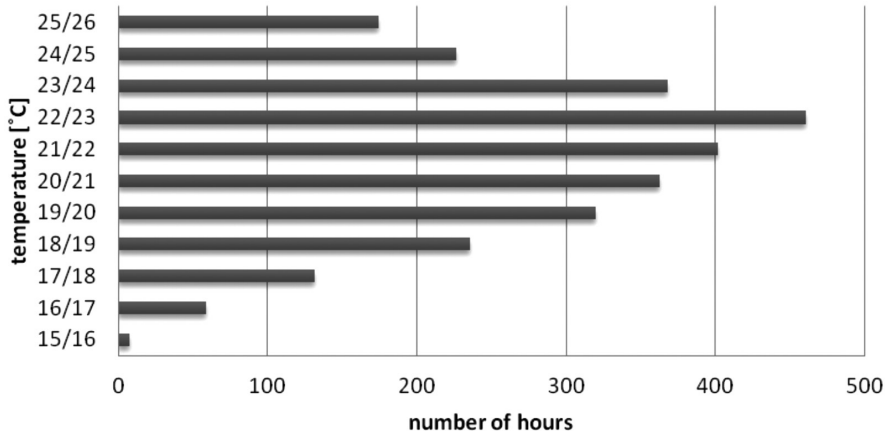


Fig. 5. Total number of hours below 25°C

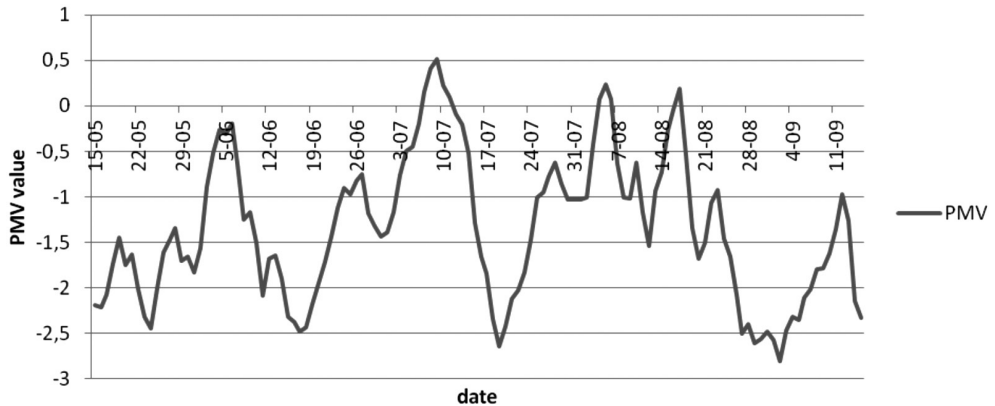


Fig. 6. PMV factor in 6<sup>th</sup> simulation step (night cooling plus internal and external shading systems)

## 5. Conclusions

The results of the conducted analysis show that the overheating problem occurs in large panel buildings. Windows in the prefabricated panel buildings in most cases are poorly shaded from solar radiation. Glazing is the source of the excessive heat gains and results in the overheating of the dwellings. Using of internal and external shading systems reduces the number of discomfort hours however the most significant results are observed when internal spaces are cooled by opening the windows during the night. In practice this solution is commonly used by inhabitants. Modelling of this process is however complicated and difficult as it depends on the way separate flats are used. Cooling of the flats during every night would result in too low temperatures which affects the thermal conditions unfavorably. Simulations of night cooling by ventilation air exchanges is a simplification

used for analyses purposes. Modelling of different air exchanges is the subject of authors' future works.

## References

- [1] Nowak-Dzieszko K., Rojewska-Warchał M., *Analiza symulacyjna komfortu cieplnego w wielkopłytkowym budynku wielorodzinnym*, Materiały Budowlane 8/2014, 47 – 49.
- [2] Nowak-Dzieszko K., Rojewska-Warchał M., *Simulation analysis of microclimate conditions in a multi – family large panel building*, Technical Transactions, vol. 3-B/2014, Cracov University of Technology Press.
- [3] Nowak-Dzieszko K., Rojewska-Warchał M., *Influence of shadings systems on the microclimate conditions in the large panel building*, Technical Transactions, vol. 3-B/2014, Cracov University of Technology Press.
- [4] Nowak-Dzieszko K., Rojewska-Warchał M., *Thermal Comfort of the individual flats of multi – family panel building*, Technical Transactions, vol. 5-B/2014, Cracov University of Technology Press.
- [5] Rozporządzenie Ministra Infrastruktury z dnia 12 kwietnia 2002 w sprawie warunków technicznych, jakim powinny odpowiadać budynki i ich usytuowanie (Dz.U. nr 75, poz. 690 z późn. zm. ogłoszonymi w Dz.U. z 2003 r. Nr 33, poz. 270, z 2004 r. Nr 109, poz. 1156, z 2008 r. Nr 201, poz. 1238, z 2009 r. Nr 56, poz. 461, z 2010 r. Nr 239, poz. 1597, z 2012 r. poz. 1289 oraz z 2013 r., poz. 926).
- [6] Rozporządzenie Ministra Transportu, Budownictwa i Gospodarki Morskiej z dnia 5 lipca 2013 r. zmieniające rozporządzenie w sprawie warunków technicznych, jakim powinny odpowiadać budynki i ich usytuowanie (Dz.U. z 13 sierpnia 2013 r., poz. 926).
- [7] PN-EN ISO 7730 Ergonomics of the thermal environment. Analytical determination and interpretation of thermal comfort using calculation of the PMV and PPD indices and local thermal comfort criteria.
- [8] PN-83/B-03430 Wentylacja w budynkach mieszkalnych zamieszkania zbiorowego i użyteczności publicznej – Wymagania.
- [9] Nowak, K., *Modernizacja budynków a komfort cieplny pomieszczeń*, Energia i Budynek, 29–33.





ANDRZEJ SMOLEŃ\*

## PERFORMANCE ANALYSIS OF THE HYBRID POWER SYSTEM USED FOR SUPPLYING THE AUTONOMIC ROAD LIGHT INSTALLATIONS

### ANALIZA WYDAJNOŚCI HYBRYDOWEGO UKŁADU ZASILANIA AUTONOMICZNEGO SYSTEMU OŚWIETLENIA DROGOWEGO

#### Abstract

The performance of hybrid power system used for supplying power to the autonomous road light system is analyzed in this paper. The calculations were based on data describing the typical climatic conditions in the selected location on Polish territory. The power flow simulation results were presented. The results show that the efficiency of micro-wind turbine is low. This leads to the conclusion that there is no economic justification to use it in such systems.

*Keywords: autonomic, road light, hybrid, simulation, photovoltaic*

#### Streszczenie

W artykule przedstawione zostały wyniki analizy wydajności hybrydowego układu zasilania autonomicznego systemu oświetlenia drogowego. Obliczenia przeprowadzone zostały metodą symulacji komputerowej na podstawie danych opisujących typowe lata meteorologiczne w miejscowości Szczecinek. Ponadto przedstawiony został przewidywany poziom naładowania zasobnika energii systemu. Otrzymane wyniki świadczą o niskiej przewidywanej wydajności mikro-turbiny wiatrowej. Prowadzi to do wniosku, iż jej zastosowanie w analizowanym układzie nie ma uzasadnienia ekonomicznego.

*Słowa kluczowe: autonomiczny, oświetlenie, hybrydowy, symulacja, fotowoltaika*

**DOI: 10.4467/2353737XCT.15.403.5034**

\* Eng. Student Andrzej Smoleń, Department of Electrical and Computer Engineering Fundamentals, Faculty of Electrical and Computer Engineering, Rzeszow University of Technology.

## Denotations

$G_{STC}$	– solar radiation under STC conditions 1000 [W/m <sup>2</sup> ]
$G_c$	– hourly average of solar radiation [W/m <sup>2</sup> ]
$I_{scmr}$	– short-circuit current of module under under STC conditions [A]
$V_{ocmr}$	– open-circuit voltage under STC conditions [V]
$dV/dT$	– module voltage temperature coefficient [-]
$dI/dT$	– module current temperature coefficient [-]
$I_{mppSTC}$	– maximum power point current of module under STC conditions [A]
$T_{pv}$	– PV module temperature [K]
$N_s$	– number of cells connected in series
$R_{sm}$	– module series resistance
$n$	– P-N junction quality coefficient [-]
$l_m$	– number of modules in PV panel
$V_d$	– velocity of wind, which start the turbine
$V_o$	– a minimum value of wind speed, at which the turbine reaches the rated power
$V_g$	– wind speed limit, at which the turbine turns off
$N_n$	– wind turbine nominal power
$\gamma$	– Rayleigh distribution shape coefficient 2 [-]
$A$	– rotor surface [m <sup>2</sup> ]
$\rho$	– typical air density 1.225 [kg/m <sup>3</sup> ]

## 1. Introduction

In recent years, autonomic road light systems became much more popular. The power supply unit uses renewable energy from wind and the Sun. Installation of such systems is not preceded by a long-term analysis of the location when it comes to renewable energy potential. For this reason a lot of this applications do not fulfill its function properly, especially when the configuration was selected incorrectly. Considered supply system comprises: photovoltaic panel, micro wind turbine and a lead-acid battery. Quasi-static mathematical models of each component were used to simulate the system. Such an approach requires the input data in a form of time series average values describing the temperature, wind speed, solar radiation and system load. For the purposes of this study the data describing typical climatic conditions (TCC) in Szczecinek (Poland) were used.

## 2. Method

### 2.1. Photovoltaic panel

In order to calculate the expected energy yield of the photovoltaic panel it is necessary to calculate the temperature of its modules for each step in the simulation. For this purpose the single layer PV thermal models described in [1] were used. In this approach the temperature

of the module is treated as a linear function of the solar radiation with straight angle of incidence. The influence of forced convection was neglected in this model, for increased

accuracy the simulation step in which the wind speed exceeds  $1 \frac{\text{m}}{\text{s}}$  were calculated using the other model described in [2]. Values of natural convection coefficient  $h = 25.3 \frac{\text{W}}{\text{m}^2\text{K}}$

and the forced  $h_f = 6 \frac{\text{W}}{\text{m}^2\text{K}}$  have been adopted in accordance with [3]. The influence of module temperature for open circuit voltage was taken into account.

$$V_T = \frac{dV}{dT} T_{PV} \quad (1)$$

The temperature-caused change of module current was calculated as:

$$I_T = \frac{dI}{dT} (T_{PV} - T_{STC}) \quad (2)$$

To calculate the time series energy produced by a photovoltaic panel, on the basis of [4], [5] and [6] the quasi-static PV model was created. The method of calculation of the hourly average generated power is presented below.

The current of module under the given conditions of solar radiation is given by:

$$I_{scm} = \frac{G_c}{G_{STC} (I_{scmr} + I_T)} \quad (3)$$

The average value of the open circuit voltage is given by:

$$V_{ocm} = V_{ocmr} + \frac{dV}{dT} (T - T_{STC}) n N_s V_T \log \left( \frac{I_{scm}}{I_{scmr}} \right) \quad (4)$$

The average value of module MPP current, under given conditions is calculated as:

$$I_{mpp} = \frac{I_{mppSTC} G_c}{G_{STC} + I_T} \quad (5)$$

The average value of module voltage corresponding to the same conditions is given by:

$$V_{mpp} = n N_s V_T \log \left( \frac{1 + I_{scm} - I_{mpp}}{I_{scm} e^{\frac{V_{ocm}}{n N_s V_T}} - 1} \right) - I_{mpp} R_{sm} \quad (6)$$

The average value of generated power is calculated as:

$$P_g = V_{mpp} I_{mpp} I_m \quad (7)$$

Additionally the conversion losses (contacts and wires resistance) are about 5 percent of produced energy [4]. Module parameter values have been adopted in accordance with the note sheet of BP-Solar-380. The relations have been analyzed in Mat-lab. Exemplary calculations results carried out for the PV panel which rated power is 240 W are presented below.

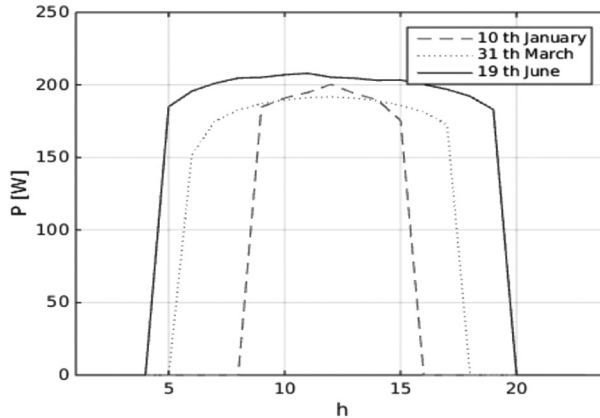


Fig. 1. The hourly average value of power generated by PV module with angle of elevation 30° and south orientation

The results show that the total daily value of generated power depends mostly on ratio of the length of day and night. Occurring in the course of the year, changes of this ratio are most important for the autonomic road light systems, where load increases relatively to the length of nights.

## 2.2. Estimate of the energy yield of micro wind turbine

In a considered system the micro-wind turbine is mounted directly on the lamppost. For this reason the axis of the rotor is usually located at an altitude between 7 to 11 m above the ground. It is very important for the amount of energy supplied to the turbine by the air stream. According to [7] the measurements were performed at similar heights above the ground. According to [8] wind velocity distribution as a function of time, a density function can be approximated by Weibull or Rayleigh. The practical possibilities of using wind energy are limited by the construction of turbine and this can be estimated with a method given in [8] as follows:

The amount of energy produced by the turbine into the wind speed range from  $V_d$  to  $V_o$  was calculated as:

$$E_1 = \frac{3}{2} N_n T \int_{V_d}^{V_0} \left[ \left( \frac{V}{2} \right)^{(s-1)} e^{-\left( \frac{V}{2} \right)^s} \right] \sin \left( \frac{\pi}{2} \frac{V - V_d}{V_0 - V_d} \right) dV \quad (8)$$

For the wind speed range from  $V_o$  to  $V_g$ :

$$E_2 = \frac{\gamma}{\beta} N_n T \int_{V_0}^{V_g} \left( \frac{V}{\beta} \right)^{(s-1)} e^{-\left( \frac{V}{\beta} \right)^s} dV \quad (9)$$

The total energy produced by micro-turbine in a given period of time:

$$E_c = E_1 + E_2 \quad (10)$$

To the future calculations the Rayleigh distribution was used, where  $\beta = 1.1258$  coefficient is taken as an example according to [7]. On this basis, values of annual energy yield were estimated for a turbine with rated power 400 W. The calculations were conducted for different values of turbine starting speed ( $V_d$ ).

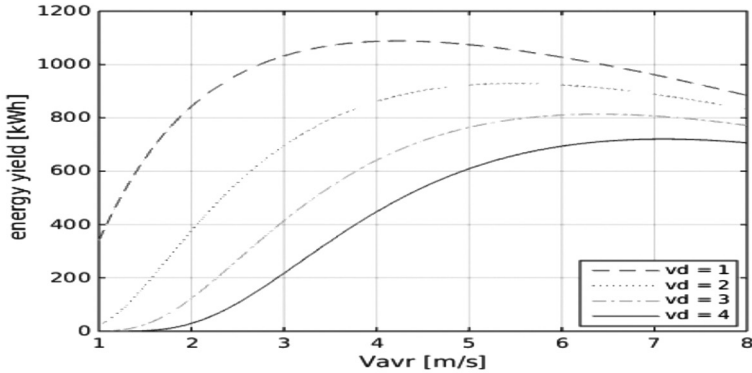


Fig. 2. Annual yield of turbine as a function of average wind speed, for different values of  $V_d$

The results show that the values of  $V_d$  affect the annual yield of turbine, especially for low wind speeds. The most frequently value of this parameter, reported by the manufacturers, is about  $2 \frac{\text{m}}{\text{s}}$ . For the purpose of this study the experimental verification of parameter  $V_d$  has not been made. For this reason, for further calculations  $V_d = 3 \text{ m/s}$  were adopted. The parameters of considered turbine are as follows:

- turbine has a three-bladed rotor
- rotor blade design provides a maximum value of power coefficient  $C_p = 0.4$
- rotor diameter is 1.5 m

For those parameters the minimum value of  $V_o$  is approximately given by:

$$V_0 = \sqrt[3]{\frac{N_n}{\rho A C_p}} \quad (11)$$

For a rated power  $N_n = 400$  W the value of  $V_0 = 7.73 \frac{\text{m}}{\text{s}}$  is assumed to the further calculations. For the purpose of energy flows, simulations of the hourly energy yield of turbine were calculated using the method presented above for each average value of wind speed. The hourly average value of generated power was calculated by dividing it by corresponding time unit.

### 2.3. Energy storage

For the purpose of power flow simulation in systems with energy storage the kinetic model of battery was developed in National Renewable Energy Laboratory (USA). The model has been described in details in [4]. This model considers the limitations of available power stored in the battery, in the case of rapid unloading and access to free capacity of the battery during charging. The dependences was implemented in Mat-lab in accordance with [4]. Additionally the charging and discharging losses were treated as constant and equal. The value of these processes: efficiency coefficient was assumed as 0.8. The parameters of the model were adopted for a lead-acid battery in accordance with Homer software database.

### 2.4. System load

The LED lamps with rated voltage of 12 V, are most frequently used as a load of autonomic road light systems. Load power between 20 to 120 W is usually used in such installations, 80 W was adopted to the further calculations. In order to simulate the system energy flows, the hourly time series of energy consumption was created with following assumptions:

- the light source operates from dusk to dawn
- the load power is constant during simulation step (the influence of temperature is neglected)

Distribution of daily averages load power has been calculated.

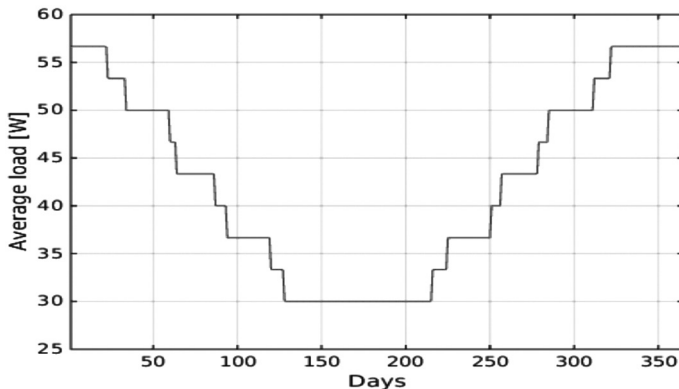


Fig. 3. Daily averages of load power [W]

### 3. Results

The simulation was performed with a quasi-static approach which means that all of variables are constant during the simulation step. The simulation process is based on energy conservation law, the system energy balance is calculated for each step and on this basis the battery state of charge is determined. According to [4] such calculations can provide acceptable accuracy at time step 1 h. For this reason the hourly averages of generated and consumed power were used. The considered system configuration is:

- photo-voltaic panel is composed of three modules with a total capacity 240 W
- micro wind turbine rated power is 400 W
- nominal load power is 80 W
- battery capacity is 2400 Wh

In order to compare the performance of each energy sources during the year, the daily averages of their power generation were calculated.

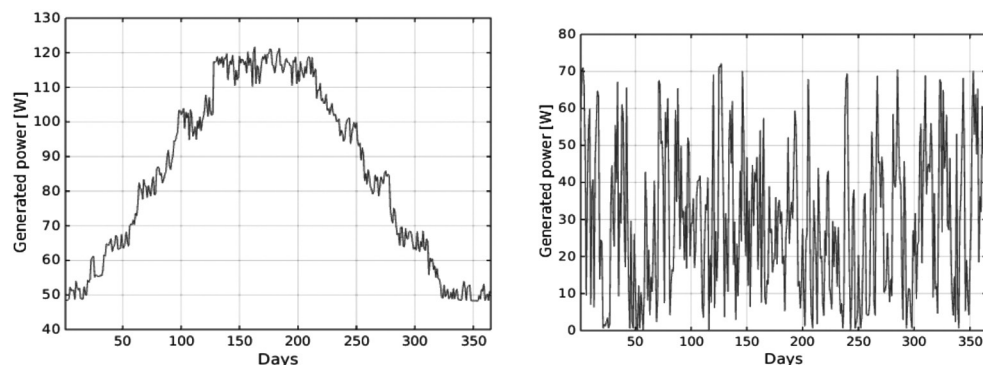


Fig. 4. Daily averages of photovoltaic collector output (left) and micro wind turbine output (right)

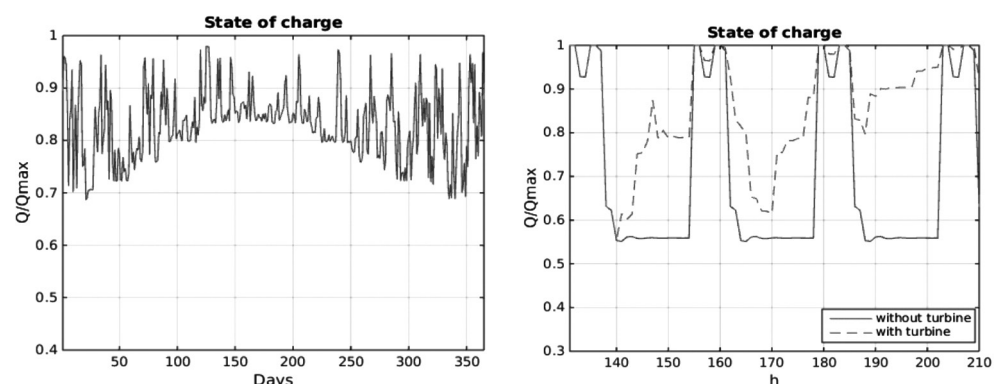


Fig. 5. Battery state of charge – daily averages (left), and without wind turbine support (right)

The results show that the differences between the collector performance in winter and summer period are significant. It is particularly important in view of annual load profile of



considered system. The daily averages of power generated by micro-wind turbine practically do not exceed 70 W, with rated power 400 W. The calculated annual average of turbine output power is only 29.43 [W]. For reference, the average output power of photovoltaic panel is more than three times higher, and equals 89.62 W. In order to assess whether the system is able to work autonomously, the battery state of charge was calculated.

#### 4. Conclusions

The considered configuration of standalone road light system could be able to work autonomously, but the influence of ambient temperature for a total battery capacity was neglected in this study. The battery state of charge does not fall below 0.4. It is important in the view of battery service life [9]. In accordance with the expectations the wind turbine has a greater share in energetic balance of system in a winter period and during the nights. The contribution of wind turbine yield, in total energy balance of the system is slight and unpredictable. For this reason it is doubtful to consider it in optimization calculations of battery capacity. This leads to the conclusion that there is no economic justification to support such systems by a micro wind turbine.

#### References

- [1] Bardhi M., Grandi G., Tina G. M., *Comparison of PV Cell Temperature Estimation by Different Thermal Power Exchange Calculation Methods*, 2012.
- [2] Mattei M., Notton G., *Calculation of the polycrystalline PV module temperature using a simple method of energy balance*, *Renewable Energy* vol. 31, 553–567.
- [3] Faiman D., *Assessing the outdoor operating temperature of photovoltaic modules*, *Progress in Photovoltaic: Research and Applications* vol. 16, 307-315.
- [4] Manwell J., *HYBRID2 – A Hybrid System Simulation Model – Theory Manual*, National Renewable Energy Laboratory, 1997.
- [5] Caster L., Silvester S., *Modeling Photovoltaic Systems using PSpice*, John Wiley & Sons, 2002.
- [6] Marciniak W., *Przyrządy półprzewodnikowe i układy scalone*, WNT, Warszawa 1987.
- [7] Narowski P. G., *Dane klimatyczne do obliczeń energetycznych w budownictwie, Ciepłownictwo, Ogrzewnictwo, Wentylacja*, vol. 11, 2006.
- [8] Gumuła S., Knap T., Strzelczyk P., *Energetyka wiatrowa*, Kraków 2006.
- [9] Czerwiński A., *Akumulatory, baterie, ogniwa*, WKiŁ, 2005.

# BUILDING STRUCTURE



KATARZYNA FRAN CZYK\*, ALICJA KOWALSKA-KOCZWARA\*\*

## ANALYSIS OF THE INFLUENCE OF SHAPING STEEL HALL PILLARS OF ITS DYNAMIC CHARACTERISTICS

### ANALIZA WPŁYWU KSZTAŁTOWANIA SŁUPÓW HALI STALOWEJ NA JEJ CHARAKTERYSTYKI DYNAMICZNE

#### Abstract

In this paper, the analysis of the influence of the changes in shaping steel hall pillars of its dynamic characteristics, in particular of the value of the natural frequency, has been subjected. The moment of inertia about the axis of the transverse profile of a typical arrangement of the pile and its mass influence on the dynamic characteristics of the steel pillars hall. These factors are different for different types of steel poles profile. The article presents the results of the analysis of the influence of the shape of the three selected types of profiles on the dynamic characteristics of the steel hall. Steel hall selected for the analysis is a workshop, a single nave hall with a frame structure covered with a gable roof. Profile sections of load bearing pillars used for the analysis are: IPE 450, 280 HEB, HEM 220. These profiles were selected due to similarities between stress levels. The evaluation shall assess the influence of such dimensional manipulation on change of the construction costs of the steel hall selected for analysis. Static design and modal analysis was made in Robot Structural Analysis which is FEM engineering program.

*Keywords: modal analysis, natural frequencies of the structure, dynamic, numerical model*

#### Streszczenie

W artykule analizie poddano wpływ zmiany kształtowania słupów hali stalowej na jej charakterystyki dynamiczne, a w szczególności na wartości częstotliwości drgań własnych. Na charakterystyki dynamiczne słupów hali stalowej mają wpływ moment bezwładności względem osi poprzecznej profilu przy typowym układzie słupa oraz jego masa. Czynniki te są różne dla różnych typów profili słupów stalowych. W artykule przedstawiono wyniki analizy wpływu kształtu trzech wybranych typów profili na charakterystyki dynamiczne hali stalowej. Wybrana do analizy hala stalowa to hala warsztatowa, jednonawowa o ramowej konstrukcji przykryta dwuspadowym dachem. Profile kształtowników słupów nośnych użyte do analizy to: IPE 450, HEB 280, HEM 220. Profile te zostały wybrane ze względu na podobny stopień wyęźnienia. Ocenie podlegał także wpływ takiej manipulacji wymiarowej na zmianę kosztów budowy wybranej do analizy hali stalowej. Wymiarowanie statyczne oraz analizę modalną konstrukcji hali stalowej wykonano w inżynierskim programie Robot Structural Analysis.

*Słowa kluczowe: analiza modalna, częstotliwości drgań własnych konstrukcji, dynamika, model numeryczny*

**DOI: 10.4467/2353737XCT.15.394.5025**

\* Eng. Katarzyna Franczyk, Faculty of Hydraulic and Civil Engineering of Wrocław University Technology.

\*\* PhD. Eng. Alicja Kowalska-Koczwarą, Institute of Structural Mechanics, Faculty of Civil Engineering, Cracow University of Technology.

### 1. Introduction

Dynamic forces and dynamic characteristics of a building determine the dynamic response of structures [1]. It is widely known a relationship between the natural frequency and stiffness of the building – the higher is value of the frequency,  $f$ , the greater is stiffness of the structure. The influence of parameters such as the height or width of the hall on the value of natural frequency is the subject of many studies include [2]. Also under consideration is sometimes influence of static scheme on the dynamic characteristics of halls for example [2].

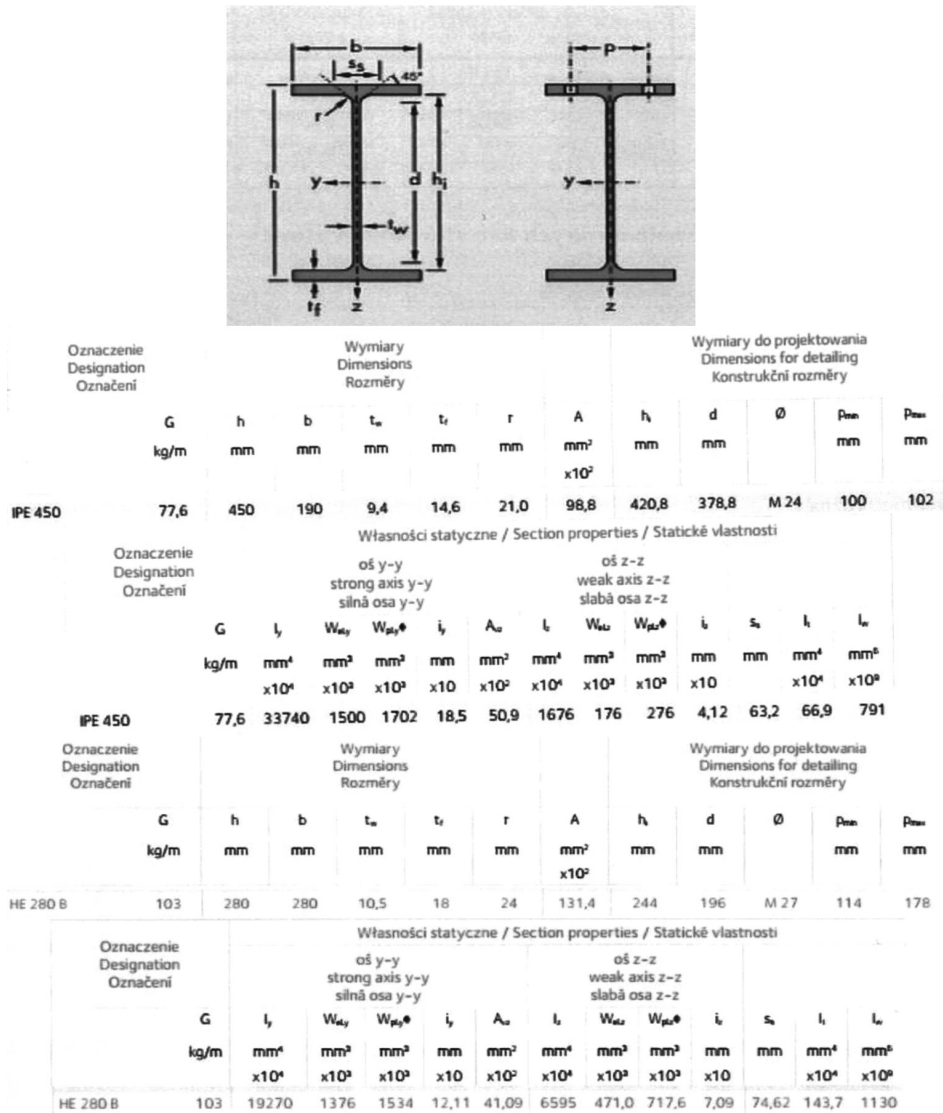


Fig. 1. adopted steel profiles

The aim of the study is to analyze the influence of the selection of steel profiles of hall pillars on its dynamic characteristics. The scope of work includes: developing a model of the hall using the Robot Structural Analysis, checking the structure under static loads, calculation of the dynamic characteristics of the chosen steel hall for three variants of pillars profiles: IPE 450, 280 HEB, HEM 220 - chosen due to the similar similarities between stress levels as well as analysis of the cost of each profiles. The characteristics of the profiles shown in Fig. 1 by [3]. The scope of work includes analysis of the cost of individual profiles.

The concept of dynamic characteristics are defined as: natural frequencies, mode shapes and damping coefficients. In this study, because of numerical calculation, it was possible to achieve natural frequencies and mode shapes of chosen steel hall. Values of damping ratio of such a structure are possible to obtain only during *in-situ* measurements [4].

## 2. Description of chosen steel hall

Chosen steel hall is a workshop, a single nave hall with a frame structure covered with a gable roof. Height of the hall is equal 6,06 m in the roof ridge and the cross-section is  $18.3 \times 54$  m in the axes of pillars.

Elements of the steel hall are as follows:

- bidding rafters – I-section profile IPE 180,
- roof transom – I-section profile IPE 400,
- frame pillars – I-section profile IPE 450 (in the beginning),
- steel bracing – circular bar  $\phi$  10 mm,
- roof encasing – laminar panels 140/100 mm.

Steel used for the structure is S 355.

Connection between the structure of steel hall with the foundation is fixed. Foundation are reinforced concrete feet with the dimensions as follows: B/L/h: 1,5m/2m/0,56m Length of the span of frame structures is equal 54m, and the frame spacing is 6m. Bidding rafters are placed on roof transoms in spacing equal 3,05m.

## 3. Numerical model

Chosen steel hall was examined as 2d frame. Numerical model was carried out in FEM program named Robot Structural Analysis [5]. The model assumes the following material coefficients:

- for concrete C20/25 acc. [6]:
  - $f_{ck} = 20$  MPa – characteristic strength of cylindrical concrete compressive strength after 28 days
  - $f_{cm} = 28$  MPa – the average value of the strength of cylindrical concrete compressive,
  - $f_{ctm} = 2.2$  MPa – the average value of the concrete tensile axial,
  - $E = 30$  GPa –Young modulus,
  - $\nu = 0.2$  –Poissons ratio.

- For steel S355, acc [7]:
  - $f_y = 355$  MPa – yield strength
  - $f_u = 510$  MPa – tensile strength,
  - $E_s = 200$  GPa –Young modulus,
  - $G = 80$  GPa – Kirchoff modulus,
  - $\nu = 0,27$  – Poissons ratio

Soil – structure interaction was taken into account with using elastic foundation (Fig. 2). Elastic foundation takes into account possibility of settlement occuring and makes model of foundation more realible. After including soil conditions (types of soil in different stratum) the Robot soil-calculator gives as a result value of substitute modulus of elasticity of soil in z-direction called Kz. Values of substitute modulus of elasticity of soil in x and y-direction were calculated according to rules enclosed in [8].



Fig. 2. The definition of the elastic support in Robot

Modal analysis was chosen to obtain natural frequencies and mode shapes of the selected structure [9]. Calculations of these dynamic characteristics of the chosen steel hall were made for three variants of pillars profiles: IPE 450, 280 HEB, HEM 220 as mentioned previously. Mode shapes for all three variants of the structure look almost the same, they differ insignificantly in amplitudes. The two first mode shapes of variant I (profile IPE 450) are presented on Fig. 3 and 4.

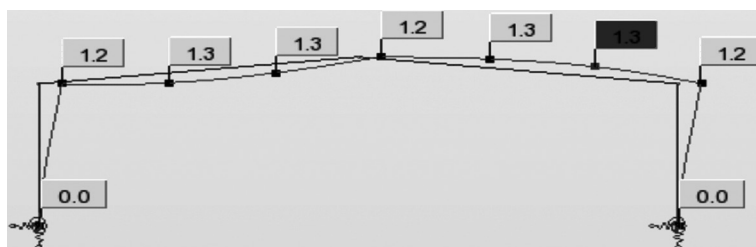


Fig. 3. First mode shape of variant I

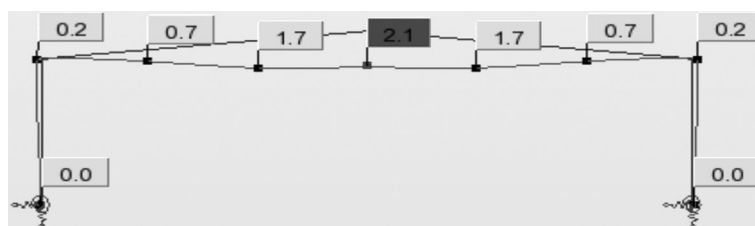


Fig. 4. Second mode shape of variant I

#### 4. Results of modal analysis

Pillar profiles were selected due to similarities between stress levels from I-section type profiles such as IPE, HEB and HEM. The results of analysis shows that changing in pillar profiles influence on dynamic characteristic of whole structure. Values of natural frequencies of selected variants of numerical model are listed in Table 1.

Table 1

Values of natural frequencies for 3 variants

No variant	Section	Degree of effort	Natural frequencies				
			1	2	3	4	5
type of mode shape		–	antisym.	sym.	antisym.	sym.	antisym.
V 1	IPE 450	0,62	4,16	4,19	11,27	17,76	28,14
V 2	HEB 280	0,66	3,46	3,86	10,55	17,15	27,52
V 3	HEM 220	0,69	3,15	3,67	10,17	16,85	27,19

The highest values of frequencies were obtained for basic variant: IPE 450, and the lowest values were obtained for third variant: HEM 220. This results from the fact that



factors which determine the values of frequencies are the moment of inertia  $I_y$  (according to the axis of local systems as shown in Figure 3) and mass section according to the following formula (ex. [10]):

$$\sqrt{\frac{EI}{m}}$$

where:

$E$  – Young's modulus,

$I$  – moment of inertia with respect to the corresponding axis,

$m$  – mass.

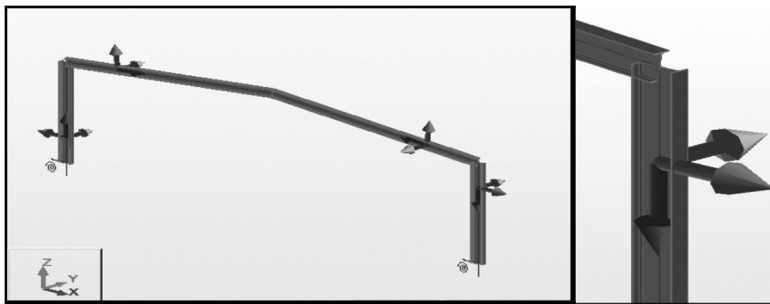


Fig. 5. The local systems of bearing frame elements

Table 2 shows the percent differences in values of natural frequency for three different variants.

Table 2

**Differences in values of natural frequencies for the first mode shape**

	Variant I	Variant II	Variant III
Frequency for the first mode shape	4,16	3,46	3,15
Difference to the variant I		16,8 %	24,3 %

The difference in natural frequencies of over 24% between I and III variant demonstrates the significant influence of shaping steel pillars on dynamic characteristics of steel hall.

Changing the sections of pillars also effects on costs of the whole building. Prices per kg for each section (acc. [11]) are close to each other for all three variants but when we consider the mass of each section, differences in cost between I and III is almost equal 120 zlotys per section (see Tab. 3).

### Costs per section

section	Price per kg [zł]	Mass [kg/m]	Price per meter of section [zł]
IPE 450	2,7	77,6	209,52
HEB 280	2,6	103	267,80
HEM 220	2,8	117	327,60

## 5. Conclusion

This paper was intended to analyze the influence of shaping steel hall pillars on its dynamic characteristics. Selected steel hall has been designed and verified in Robot FEM program in terms of statics. Soil Structure interaction was taken into account through the use of elastic support using for this purpose soil calculator included in Robot and the rules specified by standards.

In order to test the influence of shaping steel hall pillars in its dynamic characteristics, the three variants of the cross section steel pillars were taken for analysis: IPE 450, 280 HEB, HEM 220.

Based on the analysis of the three model variants it can be concluded that the various shaping steel hall pillars has a significant influence on the natural frequency. The differences in results reach approx. 24%. Variant I- section profile IPE 450 showed the highest frequency in the longitudinal direction of the profile (direction of z, cf. Fig. 3). Variants II and III - H sections, which due to a much larger mass and a much lower moment of inertia "I<sub>y</sub>" show a lower stiffness in the longitudinal direction z.

The article also performed a cost analysis of individual profiles and found that the profile IPE 450 is the cheapest, or the most optimal for the pillars for this steel hall.

## References

- [1] Brooks N.B., Newmark N.M. *The response of simple structures to dynamic loads*, Technical Report to Office of Naval Research, University of Illinois, April 1953.
- [2] Kwiatkowski T. *Trójwymiarowa analiza dynamiczna ramy nośnej hali stalowej*, Budownictwo 17,119–128.
- [3] Bogucki W., Żybertowicz M., *Tablice do projektowania konstrukcji metalowych*, wyd. 7, Arkady, Warszawa 2007.
- [4] Flaga A., Szulej J., Wielgos P., *Comparison of determination methods of vibration's damping coefficients for complex structures*, Budownictwo i Architektura 3, 2008, 53–61
- [5] Autodesk Robot Structural Analysis Professional. Verification Manual for American Codes, March 2014.
- [6] Eurokod 2, PN-EN 1992-1-1:2008 Projektowanie konstrukcji z betonu.

- [7] Eurokod 3, PN-EN 1993-1-1:2006 Projektowanie konstrukcji stalowych.
- [8] PN-80/B-03040 Foundations and supporting structures for the machine. Calculation and Design (Polish Standard).
- [9] H e J., F u Z. F., *Modal Analysis*, Elsevier 2001.
- [10] Osiński Z., *Teoria drgań*. PWN Warszawa 1978.
- [11] <http://www.a20.pl/10010> (14.01.15 r.).

PAWEŁ GAŁEK\*

## AN ATTEMPT TO EVALUATE THE APPLICATION OF 3D SCANNERS IN CONSTRUCTION DIAGNOSTICS AND TESTS

---

## PRÓBA OCENY MOŻLIWOŚCI ZASTOSOWANIA SKANERÓW 3D W DIAGNOSTYCE BUDOWLANEJ I BADANIACH

### Abstract

For over a decade there has been a rapid development of technology in the construction of 3D scanners, resulting in increased precision, speed and reliability. The scope of their application has also been continuously extending. This paper describes possible applications for 3D scanners in construction measurement and evaluation. The uses described include measuring concrete surface roughness and surveying architectural details.

*Keywords: scanner 3D, optical triangulation, time-of-light, surface topography*

### Streszczenie

Od ponad dekady notuje się burzliwy rozwój techniki w zakresie budowy skanerów 3D, które charakteryzują się coraz większą precyzją skanowania, szybkością i niezawodnością. Stale zwiększa się też zakres ich stosowania. W artykule omówiono przykłady możliwych zastosowań skanerów 3D w pomiarach i diagnostyce budowlanej. Przedstawiono pomiar chropowatości powierzchni betonu oraz inwentaryzację detali architektonicznych.

*Słowa kluczowe: skaner 3D, triangulacja optyczna, czas przelotu, topografia powierzchni*

**DOI: 10.4467/2353737XCT.15.389.5020**

---

\* PhD. Eng. Paweł Gałek, Institute of Building Materials and Structures, Faculty of Civil Engineering, Cracow University of Technology.

## 1. Optical methods of coordinate measuring

3D scanners allow non-contact measurement of the geometry of spatial elements. For over a decade there has been a rapid development of technology in the construction of these devices. This is possibly thanks to the fast development of electronics, especially optoelectronics and the progress in microprocessor technology (increase in computing power). 3D scanners use light as information carrier for measured sizes. They are based on measuring the reflection or scattering of light from the surface of the examined object. Optical measurement methods used in 3D scanners can be divided into passive and active ones [1]. Passive methods (e.g. photogrammetry) do not require any additional, artificial source of light. However, these are the methods of giving small measurement resolution. Active methods are based on the use of an additional, artificial light source (projectors, lasers) by means of which different kind of structure points, lines, patterns (Fig. 1) or coded patterns [2] are displayed on the surface of the tested element. The most commonly used active methods are: the method of time-of-flight (TOF), structured light projection, laser triangulation method, a laser tracker system or moiré projection.

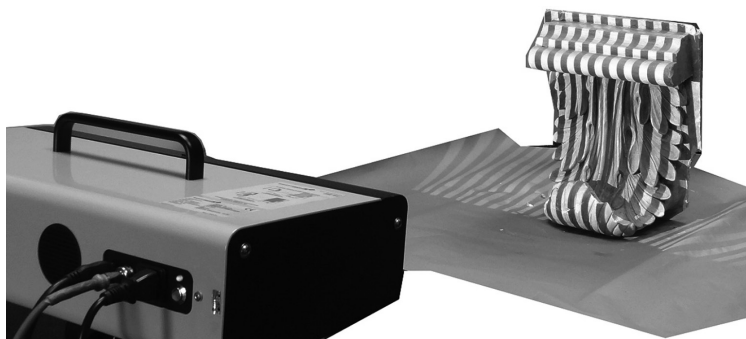


Fig. 1. Projection of stripes on the scanned object. Scanner: Smarttech Surface Scan3D

TOF and laser triangulation methods use the light emitted by the laser so they can be used to measure large and distant objects – ranging up to 2 km. The TOF method uses precise measurement of time between the emission of light impulse and its return, which allows to record the distance between the measured point and the measuring device. The laser triangulation method uses a picture (points, stripes) which is displayed by the laser on the surface of the measuring element. The methods based on structured light allow the measurement of smaller objects due to low energy efficiency of light sources used.

### 1.1. The principle of measurement methods based on the structural light

Scanners using structured light are characterized by a simple structure and high accuracy. The device consists of two basic components: a projector and a camera. The projector displays the characteristic raster pattern (stripes, waves, circles) [3], which distorts the uneven surface of the measured object (Fig. 2).

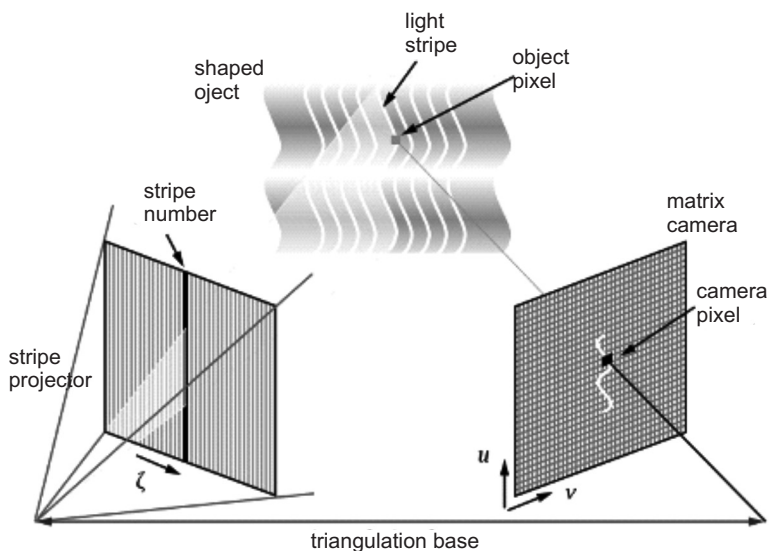


Fig. 2. The measuring principle based on the structured light [4]

In the image registered by the light-sensitive matrix of the camera, a thrown pattern is discovered. On this basis angles in a triangle formed by the camera, projector and scanned point of the object shall be calculated. Knowing the distance between the camera and the projector the location of a given point in space can be determined.

## 1.2. Description of 3D scanner selected for testing

In measurements of small objects, scanners, whose operation is based on structural light can be used. Currently, manufacturers use in their devices the LED light of different colors (white, blue, green). Regardless of the type of the light used, scanned objects cannot be exposed to other strong light sources. It is one of the drawbacks of this type of equipment. In further studies a scanner **Smarttech Surface Scan3D** of white light technology has been used. The resolution of used matrix is 10 megapixels which enables the measurement, in one cycle, of about 10 million points. The scanner has an uncertainty of measurement at the level of 0.015 mm. Scan resolution is 0.05 mm. The constant measurement volume ( $x, y, z$ ) is 200 mm  $\times$  150 mm  $\times$  120 mm. The use of constant measurement volume and closing projector and the camera in a compact, rigid casing allows a single calibration. There is no need to calibrate the scanner before each measurement. The certificate issued by an accredited laboratory confirms the scanner parameters.

## 2. The use of 3D scanners in the studies

The primary use of 3D scanners is in reverse engineering and quality control of products. However, they were widely applied in many other areas. In the construction industry they are most commonly used in the inventory and digitization of objects and architectural details (Fig. 3). This allows to control the movements of the objects and the evaluation of destructive changes in materials exposed to aggressive environment. In the future, it will be possible to restore damaged objects with high accuracy.

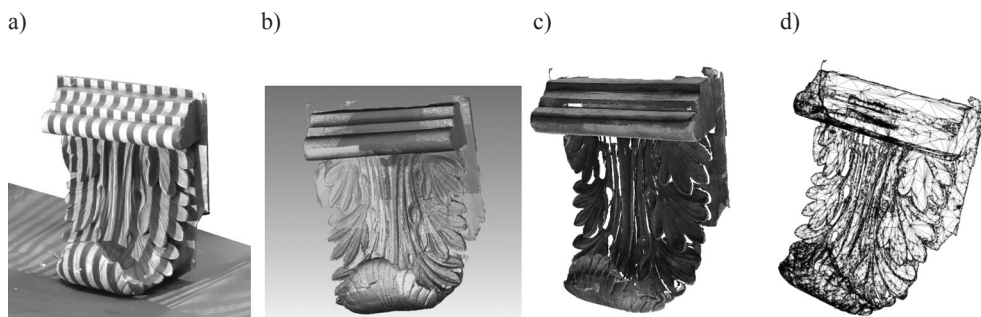


Fig. 3. Stages of the inventory of architectural details: a) the effect of the stripes on the object, b) point cloud, c) render, d) triangle mesh

In laboratory studies, in the field of construction, 3D scanners have been used among other things in the measurement of material defects due to destruction during destructive testing (fire resistance, frost resistance, durability), in assessing the scratch of concrete elements, in the measurement of deformation of the structure and its elements subjected to load and in 3D thermography. The author proposes the use of 3D scanners for measurement of the surface topography of concrete surfaces that require fixation with a new concrete.

### 2.1. Measurement of the surface topography of concrete

The strength and durability of anastomosis of two concretes at different age groups depends on many factors. One of them is the preparation of the old concrete surface which can be achieved by various methods (sand blasting, shot blasting, chiseling etc.). This results in the different surface topography, which influences the strength of anastomosis [5]. The parameters describing the surface topography are discussed in standard ISO 25178:2 [6]. The list of these parameters is presented in Table 1.

For initial assessment of the potential use of a 3D scanner on white structural light for measurement the surface, a topography test was carried out on a small concrete element of which one surface was prepared by chiseling (Fig. 4). The point cloud obtained as a result of measurement was converted in Geomagic software so as to obtain the orientation of the coordinate system required by the standard [6]. At the same time a part of the cloud of points representing an area of 50 mm × 50 mm was isolated. The isolated part of the point cloud was

imported to the CPP software, a custom program enabling the analysis of surface topography according to the ISO 2517:2 standard. The calculations obtained with the CPP software were compared with MountainsMap [7], a commercial software with similar application. The calculation results are shown in Table 1. Fig. 4b shows the graphical representation of the measured surface obtained in the MountainsMap.

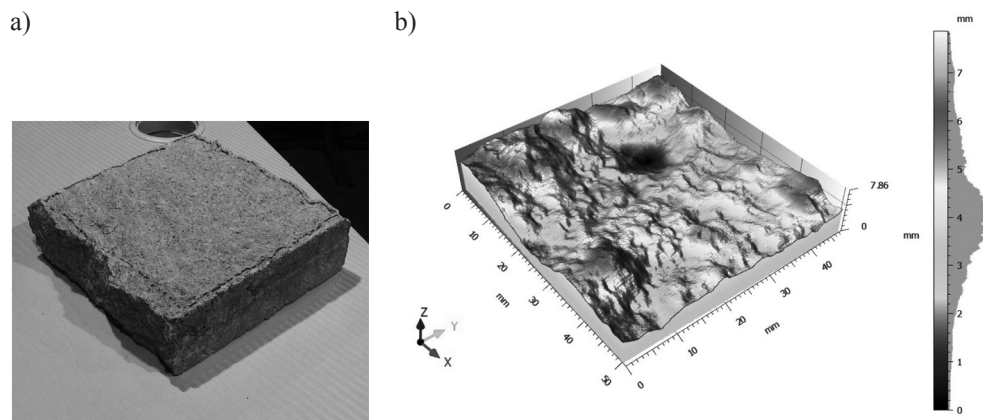


Fig. 4. a) a photography of a concrete sample testing, b) a graphical presentation of the surface obtained in the program MountainsMap

Table 1

**Parameters of the surface topography according to ISO 25178: 2 derived from the measurement by 3D scanner**

Symbol	Parameter	Value MM	Value CPP	Unit	Diff. [%]
Sq	Root Mean Square Roughness	1.25	1.23	[mm]	1.34
Ssk	Skewness	0.157	0.154	–	1.76
Sku	Kurtosis	3.29	3.22	–	2.21
Sp	Maximum Peak Height	3.77	3.77	[mm]	0.00
Sv	Maximum Valley Depth	4.09	4.09	[mm]	0.00
Sz	Maximum Height of Surface	7.86	7.86	[mm]	0.00
Sal	Autocorrelation Length	6.73	6.63	[mm]	1.45
Str	Texture Aspect Ratio	0.282	0.279	–	1.22
Sdq	Root Mean Square Surface Slope	0.492	–	–	–
Sdr	Developed Interfacial Area Ratio	10.8	–	[%]	–



### 3. Conclusion

A dynamic development of technology in terms of optoelectronics and microprocessors enables wide application of 3D scanners, also in research in the construction sector. The measurement results in the form of a cloud of points, obtained with a scanner using white, structural light, are correctly processed by custom and dedicated software for determining surface topography parameters according to ISO 25178:2. The results obtained in both programs are comparable, and the difference in results does not exceed 3%. Therefore, it is possible to use 3D scanners to test the surface of concrete prepared for reinforcement with new concrete, and the application of custom software makes it possible to obtain reliable results.

### References

- [1] El-Hakim S. F., Beraldin J.-A., Blais F., *A Comparative Evaluation of the Performance of Passive and Active 3-D Vision Systems*, Proceedings of the St. Petersburg Conference on Digital Photogrammetry, St. Petersburg 1995.
- [2] Schwenke H., Neuschaefer-Rube U., Pfeifer T., Kunzmann H., *Optical Methods for Dimensional Metrology in Production Engineering*, CIRP Annals – Manufacturing Technology, 51, 2002, 685–699.
- [3] Salvi J., Pagès J., Batlle J., *Pattern codification strategies in structured light systems*, Pattern Recognition, 37, 2004, 827-849.
- [4] <http://nick.onetwenty.org/index.php/2009/08/07/digital-camera-to-3d-scanner/>, online: 25.10.2015.
- [5] Garbacz A., Piotrowski T., Courard L., *Inżynieria powierzchni betonu. Część 1. Struktura geometryczna powierzchni*, Materiały Budowlane, 409, 2006, 3–7.
- [6] ISO 25178:2 Reaction Geometrical product specifications (GPS) – Surface texture: Areal – Part 2: Terms, definitions and surface texture parameters.
- [7] <http://www.digitalsurf.com/en/index.html>, online: 25.10.2015.

ALICJA KOWALSKA-KOCZWARA\*, PAWEŁ KISZKA\*

## ANALYSIS OF THE INFLUENCE OF REINFORCED CONCRETE BEAM-AND-SLAB FLOOR FORMING ON DYNAMIC CHARACTERISTICS OF A BUILDING

### ANALIZA WPŁYWU KSZTAŁTOWANIA MODELU STROPU PŁYTOWO-ŻEBROWEGO NA CHARAKTERYSTYKI DYNAMICZNE BUDYNKU

#### Abstract

A dynamic response of structures determine its dynamic characteristics, i.e. the natural frequency, the corresponding figures of vibration and damping coefficient. Designing of a building in terms of dynamics lets us interfere in its stiffness and mass which allows the derivation of the structure of the resonance zone early in the design stage. It is known that the larger the value of the natural frequency the greater the stiffness of the whole structure. The article examined how the natural frequencies of the object change under the influence of adjustments in the development of the floor model. The main purpose of the analysis carried out in the article was to determine the relationship between stiffness and mass matrices and the results of the modal analysis of the chosen structure. The article hypothesized that the natural frequency is inversely proportional to the mass of the floor raised to a suitable exponent. A formula derived from this relationship has been verified on a number of variants of the building model made in the program for numerical calculation Dlubal.

*Keywords: modal analysis, natural frequencies of the structure, dynamic, numerical model.*

#### Streszczenie

Odpowiedź dynamiczną budowli determinują jej charakterystyki dynamiczne tj.: częstotliwości drgań własnych, odpowiadające im postacie drgań i współczynnik określający tłumienie drgań. Projektując budowlę pod względem dynamicznym można ingerować w jej sztywność i masę co pozwala na wyprowadzenie konstrukcji ze strefy rezonansowej już na etapie projektu. Wiadomym jest, że im większe wartości częstotliwości drgań własnych tym większa sztywność całej konstrukcji. W artykule sprawdzono w jaki sposób zmieniają się właśnie częstotliwości drgań własnych obiektu pod wpływem zmian w kształtowaniu modelu stropu konstrukcji. Głównym celem przeprowadzonych w artykule analiz było ustalenie zależności pomiędzy macierzami sztywności i mas a wynikami analizy modalnej wybranej konstrukcji. W artykule wysunięto hipotezę, wg której częstotliwości drgań własnych są odwrotnie proporcjonalne do masy stropu podniesionej do odpowiedniej potęgi. Wyprowadzony z tej zależności wzór został zweryfikowany na wielu wariantach modelu budynku wykonanym w programie do obliczeń numerycznych Dlubal.

*Słowa kluczowe: analiza modalna, częstotliwości drgań własnych konstrukcji, dynamika, model numeryczny*

**DOI: 10.4467/2353737XCT.15.395.5026**

\* PhD. Eng.. Alicja Kowalska-Koczwarą, Eng. Paweł Kiszka, Institute of Structural Mechanics, Faculty of Civil Engineering, Craciv University of Technology.

## 1. Introduction

Nowadays a civilization progress causes a series of new problems in modern civil engineering. Among them, without any doubts, very relevant is a matter of building dynamics, connected with designing higher buildings (where the most important factor in design is the dynamic influence of the wind) or with occurring new sources of vibration, like underground, railways, mining activities and earthquakes.

One of the dynamic characteristic of the structure is natural frequency, which is also known as resonance frequency. In case of designing buildings subjected to dynamic influence we try to control natural frequencies of the building in a way where we can avoid resonances of a structure. Appropriate control of natural frequencies of the building is possible through the selection of proper values of stiffness and mass matrixes, because those two parameters have large influence on natural frequency of the structure (acc. [1]).

In these article the influence of beam-and-slab floor forming on the dynamic characteristic of a building is taken into consideration, which means finding dependence between forming stiffness or mass matrix on building resonance frequencies. Because of that frequencies which occur, in the real structure the resonance area can be avoided only by changing the forming of the floor.

## 2. Description of the structure and model variants

The structure analyzed is a reinforced concrete frame structure which has six floors without basement, designed as open-space office building. All reinforced concrete elements were made of concrete C30/37, reinforced with steel A-IIIIN, RB-500W. The dimensions of the building in axes are 37.50 × 30.00 m. Beam-and-slab floor is composed of 5 five-span binders with span length 7.50 m, sixteen four-span ribs with span length 7.50 m and unidirectionally reinforced plates with dimensions in rib axes equal to 2.50 m. Floors are supported by internal columns with dimensions of cross section 350 × 350 mm and external columns with dimensions of cross section 350 × 450 mm. The whole structure is completed by internal and external walls, allowing the use of the internal open-space plan. These walls also stiffen the building in both horizontal directions.

The building chosen was modeled in Dlubal RFEM, in thirty-six variants of beam-and-slab floors formation. The cross section of chosen three elements (binder, rib and slab) was modified between each variant. Firstly the limits for the height of binder  $h_b$  and rib  $h_r$  depending on the elements length were determined (acc. [2]).

$$h_r = l_r \cdot \left( \frac{1}{18} \div \frac{1}{12} \right) = 7.50 \text{ m} \cdot \left( \frac{1}{18} \div \frac{1}{12} \right) = (420 \text{ mm} \div 625 \text{ mm}) \quad (1)$$

$$h_{db} = l_{db} \cdot \left( \frac{1}{18} \div \frac{1}{12} \right) = 7.50 \text{ m} \cdot \left( \frac{1}{15} \div \frac{1}{10} \right) = (500 \text{ mm} \div 750 \text{ mm}) \quad (2)$$

In the next step several heights of the elements were determined, all of them had to be included inside determined intervals earlier. The width of each rib and binder were determined according to the formula (acc. [2]):

$$b_{db,r} = h_{db,r} \cdot \left( \frac{1}{2,5} \div \frac{1}{2} \right) \quad (3)$$

Using the above described method, six cross sections of binders were determined numbered from 1 to 6 and four cross sections of ribs were also named from A to D. Determined cross sections were combined into pairs: binder – rib, assuming, that each next two variants have only different cross section of a binder or of a rib. All 9 variants were tested with four versions of slab thickness: 120, 160, 200, 240 mm as presented in Table 1.

Table 1

**Different variants of the floor**

Rib	Binder						
Symbol:	Number:	1	2	3	4	5	6
	Cross sections [mm]	250 × 500	250 × 550	300 × 600	300 × 650	350 × 700	350 × 750
<b>A</b>	200 × 450	1A	2A				
<b>B</b>	250 × 550		2B	3B	4B		
<b>C</b>	250 × 550				4C	5C	
<b>D</b>	300 × 600					5D	6D

### 3. Description of foundation, dynamic soil coefficient and computer modeling

Three soil layers were taken:

- humus soil, layer thickness 0.30 m,
- loamy sand with  $I_L < 0$ , layer thickness 2.20 m,
- half-compact loam with  $I_L = 0$ , as the deepest layer.

Building foundations were divided into groups, due to their dimensions. For each group the dynamic soil coefficient was calculated, according to [3] and [4]. It was proven, that the dynamic soil coefficient calculated from relations created by Sawinow for multilayer ground are directly proportional to the square root of the tension on the border of soil – the foundation. This assumption allowed to calculate precisely dynamic soil coefficient for each variant.

The mash consists of 3D square elements with side dimension equal to 0.5 m. Binders were modeled as reinforced concrete beams, cooperated with reinforced concrete slab on width equal to  $L/6$ .

#### 4. Analysis of the results

Analyses of calculation results show that with increasing mass of floors, values of natural frequencies are decreasing (com. Fig. 1.)

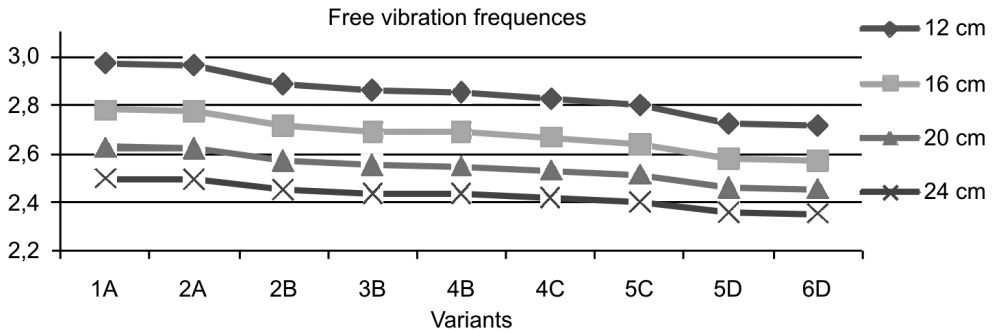


Fig. 1. Changes of the values of first natural frequency depending on the model variant

Inversely proportional character of the dependence between natural frequencies and the mass of the floor was a base to make a hypothesis, according to which natural frequency is inversely proportional to floor mass, raised to the  $\mu$  power (com.eq. 4).

$$f \cdot M_s^\mu = k \quad (4)$$

where:

- $f$  – natural frequency of the structure,
- $M_s$  – floor mass,
- $\mu$  – power of floor mass,
- $k$  – proportionality constant.

With known values of coefficient  $\mu$  and  $k$ , we are able to control floors masses in a way which allows us to obtain desirable natural frequencies of the building. To prove the hypothesis, a series of calculations were made, which proved that for each vibration mode a constant coefficient  $\mu$  exists, for whose proportional coefficient  $k$ , for each variant, is also constant.

Masses of each floor are shown in Table 2 and first natural frequencies for each variant were shown in Table 3. Values of coefficient  $k$  were calculated using formula (4) with control of value of coefficient  $\mu$  in such a way to get the smallest differences between all variants. Finally after transforming formula (4), new values of first natural frequencies for different variants of the model were determined, based on  $M_s$ ,  $\mu$  and average value of  $k$  coefficient. Results of this analysis are shown in Table 5.

Table 2

**Floor mass for each variant of the model (in tons)**

Slab thickness	Variant								
	1A	2A	2B	3B	4B	4C	5C	5D	6D
12 cm	485.39	491.57	527.72	545.77	553.19	568.77	590.53	636.03	644.68
16 cm	589.18	595.36	629.01	646.08	653.50	669.08	689.85	732.86	741.51
20 cm	692.97	699.15	730.31	746.39	753.81	769.39	789.17	829.68	838.34
24 cm	796.76	802.94	831.61	846.70	854.12	869.70	888.49	926.51	935.17

Table 3

**First natural frequency of each model variants**

Slab thickness	Variant								
	1A	2A	2B	3B	4B	4C	5C	5D	6D
12 cm	2.969	2.962	2.886	2.860	2.852	2.827	2.799	2.723	2.716
16 cm	2.780	2.775	2.714	2.691	2.687	2.668	2.641	2.577	2.570
20 cm	2.626	2.622	2.571	2.552	2.549	2.532	2.514	2.460	2.455
24 cm	2.497	2.495	2.451	2.435	2.433	2.418	2.401	2.356	2.352

Table 4

**Value of coefficient  $k$  for each model variant**

Slab thickness	Variant								
	1A	2A	2B	3B	4B	4C	5C	5D	6D
12 cm	27.86	27.92	27.91	28.00	28.06	28.09	28.20	28.18	28.24
16 cm	27.98	28.04	27.97	28.01	28.08	28.12	28.14	28.07	28.11
20 cm	28.03	28.08	27.97	27.98	28.05	28.07	28.13	28.03	28.08
24 cm	28.03	28.09	27.95	27.95	28.01	28.02	28.04	27.94	27.98

Table 5

**New values of first natural frequency**

Slab thickness	Variant								
	1A	2A	2B	3B	4B	4C	5C	5D	6D
12 cm	2.988	2.975	2.899	2.864	2.850	2.822	2.783	2.710	2.696
16 cm	2.786	2.775	2.721	2.694	2.683	2.660	2.631	2.574	2.563
20 cm	2.627	2.618	2.577	2.557	2.548	2.529	2.506	2.461	2.452
24 cm	2.497	2.490	2.459	2.443	2.435	2.419	2.401	2.365	2.357

Calculation is made for first three natural frequencies of the structure, results are shown in Table 6.

Table 6

### Results of natural frequency calculation

Free vibration shape	$\mu$	average $k$ value	Average standard deviation of $k$ value	Average value of error of $f$ value
First mode (longitudinal)	0.362	28.04	0.08	0.23%
Second mode (transverse)	0.345	26.08	0.07	0.20%
Third mode (torsion)	0.330	34.19	0.10	0.21%

## 5. Summary

The purpose of this paper was to analyze the influence of beam-and-slab floor model on natural frequencies of the building which are the part of dynamic characteristic (ex. [5]). It has been shown that the change in slab forming causes changes in mentioned frequencies and it was shown that these dependences can be presented as exponential equation. This opens new possibilities in designing of the structure subjected to dynamic influence. This gives the possibility of controlling resonance zone only by proper design of the structure instead of installing expensive and difficult to design devices (such as dampers ex.[6–8]) that reduce the influence of vibration on the structure.

In the next step of calculation there are predicted calculation of  $k$  and  $\mu$  for any case. The influence of floor stiffness on natural frequencies of the building will also be considered in future.

## References

- [1] Langer J., *Dynamika budowli*, Wydawnictwo Politechniki Wrocławskiej, 1980.
- [2] Starosolski W., *Konstrukcje żelbetowe według Eurokodu 2 i norm związanych*, Wydawnictwo Naukowe PWN, 2012.
- [3] Lipiński J., *Fundamenty pod maszyny*, Wydawnictwo Arkady, 1985.
- [4] Kisiel I., *Dynamika fundamentów pod maszyny*, Państwowe Wydawnictwo Naukowe, 1957.
- [5] Ward H. S., *Dynamic characteristic of a multi-storey concrete building*, Proceedings, Institution of Civil Engineers vol.43, Canada 1969, 553–572.
- [6] Webster A.C., Vaicaitis R., *Application of tuned mass dampers to control vibration of composite floor systems*, Engineering Journal, American Institute of Steel Construction 2003.
- [7] Guideline\_Floors\_EN02.doc – 27.10.2008.
- [8] Arnold C., *Designing for earthquake. Chapter 4. Earthquake effects on buildings*, FEMA 454, US December 2006.

DAWID ŁĄTKA\*, MICHAŁ REPELEWICZ\*

## THE INFLUENCE OF SUPERSTRUCTURE STIFFNESS ON INTERNAL FORCES DISTRIBUTION IN RAFT FOUNDATIONS

### WPLYW SZTYWNOŚCI NADBUDOWY NA WIELKOŚĆ SIŁ WEWNĘTRZNYCH W PŁYTACH FUNDAMENTOWYCH

#### Abstract

The article presents the changes in designing rules of raft foundations according to Eurocodes in relation to structural stiffness of: superstructure–foundations–soil. The results from two numerical models (wall-type and slab-column superstructure) were analyzed. The subject of the analysis was to assess the influence of the raft foundation effective stiffness and Winkler's spring constant on internal forces distribution in the foundation.

*Keywords: superstructure stiffness, Winkler's spring constant, raft foundation, Eurocodes*

#### Streszczenie

W artykule przedstawiono zmiany w przepisach normowych przy projektowaniu posadowień bezpośrednich na płycie fundamentowej w odniesieniu do sztywności układu: nadbudowa – fundament – podłoże gruntowe. Przeanalizowano wyniki z dwóch modeli numerycznych (dla nadbudowy ścianowej i płytowo-słupowej) pod kątem wpływu sztywności efektywnej płyty fundamentowej i parametrów podłoża Winklera na dystrybucję sił wewnętrznych w fundamencie.

*Słowa kluczowe: sztywność nadbudowy, współczynnik sprężystości podłoża Winklera, płyta fundamentowa, Eurokody*

DOI: 10.4467/2353737XCT.15.402.5033

\* MSc. Eng. Dawid Łątka, MSc. Eng. Michał Repelewicz, Institute of Building Materials and Structures, Faculty of Civil Engineering, Cracow University of Technology.



## Symbols

- $(EJ)_s$  – approximate value of flexural rigidity per structure width unit of the building structure concerned, [MN·m]
- $(EI)_f$  – approximate value of flexural rigidity per structure width unit of the foundation raft and the structure directly bound with it, [MN·m]
- $E$  – deformation modulus of the ground, [MPa]
- $b, l$  – dimensions of the foundation,  $b < l$ , [m]
- $K_R$  – relative stiffness of the structure acc. EN 1992-1-1:2004, [-]
- $K_f$  – stiffness index acc. DIN 4018:1974-09, [-]
- $h_z$  – replacement thickness of the raft foundation (taking into account rheology), [m]
- $E_{cm}$  – secant elasticity modulus for foundation concrete and superstructure, [MPa]
- $I_f$  – moment of inertia of the foundation cross section and the structure directly bound with it (e.g. foundation walls), [m<sup>4</sup>]
- $M_0$  – compression modulus of the ground (value reduced for layered ground), [MPa]
- $E_f$  – elasticity modulus of concrete in the foundation and superstructure, [MPa]
- $M_{xx}$  – bending moments in the raft foundation, [kNm/m]

### 1. Changes in standard requirements

The requirement to take into account the effect of the superstructure stiffness when determining the value and distribution of internal forces in raft foundation, has until recently, not been included in any Polish standard concerning structural design. The withdrawn standard, PN-81 / B03020 [1] concerning the design of direct foundation of buildings assumed the ground as a homogeneous elastic half-space, and the structure as perfectly elastic, without considering the overall stiffness of the superstructure–foundation–ground system. Both of these sub-systems (superstructure as the first and foundation–ground as the second) were treated separately, and the active element was the deformable soil. The building, or actually only its foundation is, in this approach, merely a passive receiver of forces transmitted from the ground [2]. As a result, the significant influence of the building’s actual stiffness on the behaviour of its elements is omitted, especially in the form of settlement and internal forces generated in direct foundations. Unfortunately, the standard applicable at the same time, PN-B-03264 [3], does not contain any provisions regarding the discussed issue.

The situation radically changed with the introduction of common European Standards in design practice. The provisions of Eurocode 7 [4] repeatedly point at the legitimacy of the use of models enabling the consideration of a full interaction between the structure and the substrate (Chapters 2 and 6) – in the serviceability limit state, clearly preferring FEM numerical models. At the stage of determining interaction values, and the calculation of differences in settlement, the referenced standard directly “requires that the structure stiffness during construction and after its completion should be taken into account.” In contrast to no longer valid reinforced concrete standard [3] much more attention is attached to the topic in Eurocode 2 [5], especially in Annex G. The so far applied separation of computational methods used in analyses of the superstructure–foundation–ground system has been validated, among others, in the dependence of the so-called relative stiffness ( $K_R$ ) of this system.

4 analysis levels were introduced (0 to 3) into structural designs. The most demanding is level 3, which basically means building a model (e.g. FEM) of the entire superstructure-foundation-subsoil system, in order to assess interactions. Unfortunately, as it can be found in numerical analyses and on-site observations carried out by numerous authors [6–9], this level seems to be the most suitable for analyses of buildings erected on raft foundations. The core of the problem is to determine the relationship between: load distribution from the superstructure onto the foundation – stiffness of the whole building structure – distribution of the soil vertical bearing resistance; while maintaining conformity of the displacement of the foundation footing with the soil. Thus only designating the soil vertical bearing resistance distribution allows the determination of internal forces at any raft foundation cross-section. A theoretical development deserving attention is presented in [10].

The relative stiffness quoted above for EC2 is defined by the formula:

$$K_R = \frac{(EJ)_S}{El^3} \quad (1)$$

The structural system under consideration can be regarded as rigid when parameter  $K_R > 0.5$ . Literally, this means that the soil stiffness should be less than twice with regard to doubled stiffness of the building and the foundation. As Starosolski noted [11], this is a very conservative limitation, and contains a substantial safety margin. The fulfilment of this criterion is also considered sufficient for the adoption of a linear distribution of pressure under the raft foundation, for which the following condition is fulfilled:

$$\frac{l}{h_z} < 0,55\sqrt[3]{\frac{E_{cm}}{E}} \quad (2)$$

For example, for a raft foundation with dimensions of 30 m × 40 m, situated on ground with a deformation modulus of  $E_0 = 30\text{MPa}$ , and made of concrete C25/30 ( $E_{cm} = 31000\text{MPa}$ ) the thickness  $h > 6,2$  m which, according to [12] roughly corresponds to the actual thickness of a non-cracked plate  $h > 8.2$  m, or  $h > 9.3$  m for a cracked plate.

The relative rigidity formula (1) is not a novelty in estimating the susceptibility of the brand superstructure-foundation-subsoil system, and is only a small modification of index ( $K_f$ ) cited by Motak in [6], after an old German DIN 4018:1974-09 standard:

$$K_f = \frac{bl^3}{I_f} \frac{M_0}{E_f} = \frac{M_0 l^3}{\frac{E_f I_f}{b}} = \frac{M_0 l^3}{(EI)_f} \quad (3)$$

Based on the calculated value of  $K_f$ , it could be initially determined whether the whole system is rigid ( $K_f \leq 1$ ), elastic ( $1 < K_f \leq 100$ ), or flexible ( $K_f > 100$ ). It can be clearly seen, on the basis of algebraic transformations applied to equation (3) that formula  $K_f$  by DIN and  $K_R$  by EC2 are similar. The main difference is the replacement of module  $M_0$  determined in a laboratory (by an oedometer); module  $E$ , determined in-field (e.g. by a pressuremeter), which stems from the thinking in the new standards – normally  $E < M_0$ . In addition, the impact of superstructure stiffness on the stiffness of the entire system was increased, replacing, as introduced by the authors of the article,  $(EI)_f$  by  $(EJ)_S$  value, – where  $(EI)_f < (EJ)_S$  – which

further underlined the difference between  $K_f$  and  $K_R$ . In structures erected on coarse-grain, compacted soils, such as gravels ( $M_0 \approx E$ ), with a flexible superstructure ( $(EI)_f = (EJ)_s$ ), rate  $K_f \approx 1/K_R$  can be assumed.

## 2. Impact of the superstructure stiffness on the distribution of bending moments in a raft foundation for a simple engineering model – qualitative approach

### 2.1. Adapted numerical models

For a rough estimation of changes in the raft foundation bending moments under the influence of changes in the overall stiffness of the superstructure, two opposing models were analysed. The first model (slab-column type) reflects a flexible structure, while the second (wall type) reflects structure with a rigid superstructure. In both cases, the Winkler model was used, with soil constant elasticity in the vertical direction equal to 5 MPa/m, and in both directions horizontally 0,5 MPa/m. The change in stiffness of the superstructure was simulated by reducing the number of floors, retaining a constant total of vertical loads (load from the reduced section was applied at the highest node of columns/walls, in order to exert the least impact possible on the distribution of bending moments).

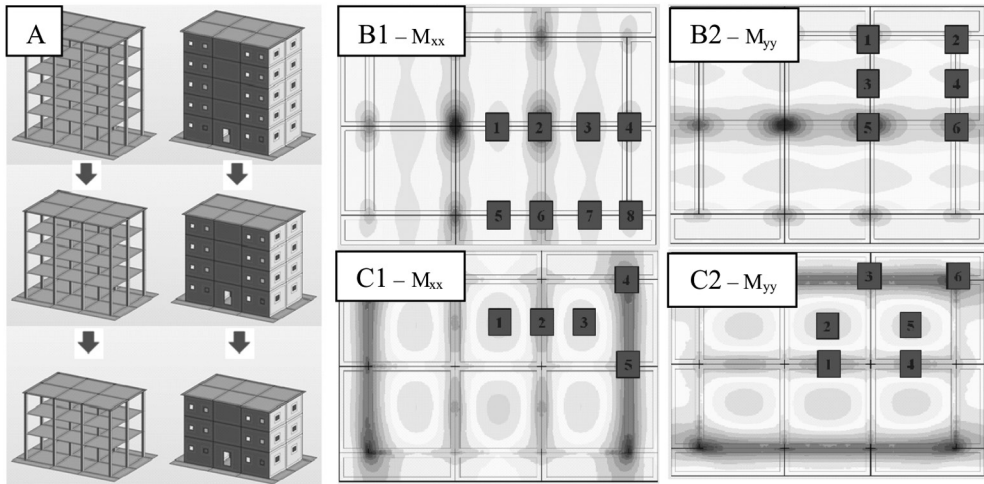


Fig. 1. A) Reduction of superstructure stiffness; B1-2) Location of points on the foundation for flexible superstructure; C 1-2) Location of points on the foundation for a rigid superstructure

The raft foundation with dimensions of  $16 \times 22$  m was analyzed in thickness variants of 50 cm and 100 cm. The height of the buildings was 21m, and floor slabs were 22 cm thick. For numerical calculations, Autodesk Robot Structural Analysis Professional 2014 was used [13] – a popular engineering software for linear analysis of structures.

The analysis was based on tracking changes in moments  $M_{xx}$  and  $M_{yy}$  at specific points on the raft foundation in both models – the location of points is shown in Fig.1.B1-2) and C1-2).

The concept to modify the superstructure stiffness in the form of a gradual reduction in the number of storeys from 5 to 2 is presented in Fig. 1.A).

## 2.2. Results obtained

Analysing the results obtained for the slab-column structure (Fig.2.A), one can observe high sensitivity of the model to decrease in the number of storeys. For 50cm thick raft foundations, a more stable trend can be observed, tending to decrease the value of moments in the span. In a variation solution, where the plate thickness was 1m, the change in moment values was much more evident. The largest  $M_{xx}$  increase occurred in the span middle lane, while the largest decrease was recorded in the last (edge) span strip. Relative changes in the columns were insignificant, which is associated with a very high value of reference moments at this point. For  $M_{yy}$  moments, the largest increase occurred in central columns, while decrease occurred in the last span. However, when analyzing the absolute moment values, regardless of the selected direction, the greatest changes occurred in the column area.

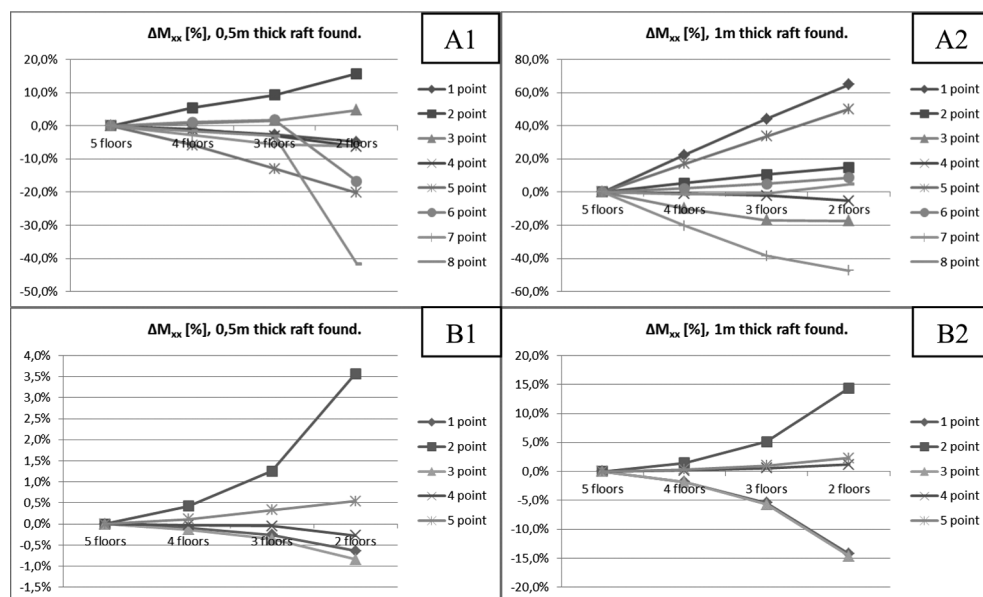


Fig. 2 A) Relative  $M_{xx}$  change for flexible superstructure with 0,5m (A1) and 1m (A2) foundation;  
 B) Relative  $M_{xx}$  change for rigid superstructure with 0,5m (B1) and 1m (B2) foundation

For the wall construction (Fig. 2.B), changes in the bending moment value with a foundation at the thickness of 50 cm were fully negligible – with a maximum reduction of stiffness, they did not even achieve 6%. Just as before, along with doubling of the foundation thickness, the impact of the superstructure reduction was multiplied. However, due to low absolute values of reference moments, these changes are insignificant.

### 3. Conclusion

With the increase in the stiffness of a raft foundation, the range of moments stretching lower fibres grows significantly. Based on the above analysis, it can be stated that the building with a wall construction is characterized by high effective stiffness in the foundation, which takes into account the stiffening impact of the superstructure. This justifies the use of solid, reinforced concrete walls in the raft foundation floor, even for structures with framework superstructures. This floor acts as a rigid box that positively influences on the behaviour of the entire structure.

### References

- [1] PN-81/B03020. Grunty budowlane. Posadowienie bezpośrednio budowli. Obliczenia statyczne i projektowanie.
- [2] Majewski S., *Sprężysto-plastyczny model współpracującego układu budynek – podłoże poddanego wpływom górniczych deformacji terenu*, Zeszyty Naukowe Politechniki Śląskiej Nr 1271, Gliwice 1995.
- [3] PN-B-03264:2002. Konstrukcje betonowe, żelbetowe i sprężone. Obliczenia statyczne i projektowanie.
- [4] EN 1997-1:2004. Eurocode 7: Geotechnical design – Part 1: General rules.
- [5] EN 1992-1-1:2004. Eurocode 2: Design of concrete structures – Part 1-1: General rules and rules for buildings.
- [6] Motak E., *Inżynierskie modele obliczeniowe układu fundament – podłoże gruntowe*, Inżynieria i Budownictwo, nr 2/1995.
- [7] Świniański J., *Ocena podatności podłoża przy wymiarowaniu płyt fundamentowych*, Inżynieria Morska i Geotechnika, nr 5/2003.
- [8] Sun H.H., Zhao X., Li X.P., Ding J.M., Zhou Y., *Performance Analysis of Basement Fin Wall of the Shanghai Tower Based on the Interaction Between Pile-Raft Foundation and Superstructure*, The Twelfth East Asia-Pacific Conference on Structural Engineering and Construction, Procedia Engineering 14 (2011).
- [9] Russo G., Abagnara V., Poulos H.G., Small J.C., *Re-assessment of foundation settlements for the Burj Khalifa, Dubai*, Acta Geotechnica, Volume 8, Issue 1, 2013.
- [10] Król W., *Statyka fundamentów żelbetowych z uwzględnieniem sztywności nadbudowy*, Arkady, Warszawa 1964.
- [11] Starosolski W. *Techniczne metody obliczania fundamentów płaskich*, Geoinżynieria – Drogi Mosty Tunele 03/2009 (22).
- [12] Starosolski W., *Metody obliczania płyt fundamentowych*, Geoinżynieria – Drogi Mosty Tunele 03/2008 (18).
- [13] Robot Structural Analysis 2011 – user’s manual, 2010.

IZABELA MURZYN\*, JOANNA DULIŃSKA\*, MAREK WAZOWSKI\*\*

## AN EXPERIMENTAL AND NUMERICAL ASSESSMENT OF THE DYNAMIC CHARACTERISTICS OF THE FOOTBRIDGE LOCATED OVER THE NATIONAL EXPRESSWAY DK-1

---

### DOŚWIADCZALNE I NUMERYCZNE WYZNACZANIE CHARAKTERYSTYK DYNAMICZNYCH KŁADKI DLA PIESZYCH USYTUOWANEJ NAD DK-1

#### Abstract

In this paper the experimental and numerical results of dynamic characteristics (i.e. natural frequencies and modes of vibrations) of the cable-stayed footbridge, located in Czestochowa, are presented. The numerical analysis was carried out with the ABAQUS package. The *in situ* tests methodology and the results are also presented on the basis of the spectral analysis of vibrations caused by a group people jumping. The theoretical and experimental results are in good agreement as far as both the natural frequencies and eigenmodes are concerned.

*Keywords: footbridges, dynamic characteristics of footbridges, in situ experiments*

#### Streszczenie

W artykule przedstawiono charakterystyki dynamiczne (postaci i częstotliwości drgań własnych) podwieszanej kładki dla pieszych zlokalizowanej w Częstochowie uzyskane na drodze teoretycznej jak i eksperymentalnej. Analizę numeryczną konstrukcji przeprowadzono z wykorzystaniem programu ABAQUS. W trakcie badań *in situ* zarejestrowano przebiegi czasowe drgań wymuszonych przez podskoki grupy ludzi. Analiza spektralna przebiegów pozwoliła na wyznaczenie charakterystyk dynamicznych kładki. Uzyskano dobrą zgodność częstotliwości i postaci drgań wyznaczonych teoretycznie i eksperymentalnie.

*Słowa kluczowe: kładki dla pieszych, charakterystyki dynamiczne kładek, badania in situ*

**DOI: 10.4467/2353737XCT.15.387.5018**

---

\* MSc. Eng. Izabela Murzyn, Prof. DSc. PhD. Eng. Joanna Dulińska, Institute of Structural Mechanics, Faculty of Civil Engineering, Cracow University of Technology.

\*\* PhD. Eng. Marek Wazowski, ASPECT, Testing Laboratory, Limited Liability Company.

## 1. Introduction

Pedestrian bridges are objects of public infrastructure which are designed to allow their users to pass over an obstacle [1, 3]. It is important to note that the application of advanced technology, calculation and materials gives engineers the opportunity to create footbridges that are more slender, lighter and longer than bridges designed for cars or trains [3]. Because of this, in a vast majority of cases, footbridges have the lowest natural frequency, which coincides with the frequency of pedestrian steps (whether walking or running). Such situations are very dangerous because resonance phenomena can occur [3, 4].

In the contemporary history of bridge construction, one of the most publicized examples is Millennium Bridge located in London. From the day of its opening on 10 June 2000, the bridge exhibited very dangerous tendencies that attracted the attention of scientists, including more than 1000 articles and 150 broadcasts in the media around the world [3].

The first step in the analysis is to determine the dynamic characteristics of the structure. There are two ways to do it: numerical and experimental [2].

In this paper, the comparison of both the experimental and the numerical results of dynamic characteristics (i.e. frequencies and modes of natural vibrations) of the existing footbridge are presented.

## 2. Basic geometry and material data of the analysed footbridge

The dynamic characteristics were determined for an existing two-span footbridge located in Czestochowa, Poland. The primary purpose of the structure is to allow pedestrians to cross over the national expressway DK-1. It was designed according to the technical requirements demanded of footbridges (PN-85/S-10030). The cross-section of the footbridge span is shown in Fig. 1, whereas the side view of the structure and its main dimensions are presented in Fig. 2. In both figures the locations of accelerometers, used for the *in situ* experiment, are also presented.

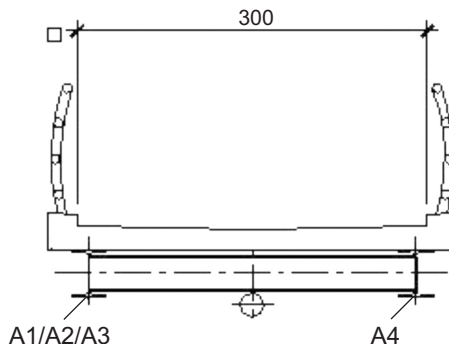


Fig. 1. The cross-section of the footbridge span along with the locations of sensors (A- accelerometer)

The total length is 46.9 m, with the lengths of the spans 21.1 and 25.8 m. The width of the footbridge is 3.5 m. The primary structural system of the footbridge consists of steel girders (I-section HEB 400) located at a distance of 2.8 m and connected by crossbars (I-section HEA

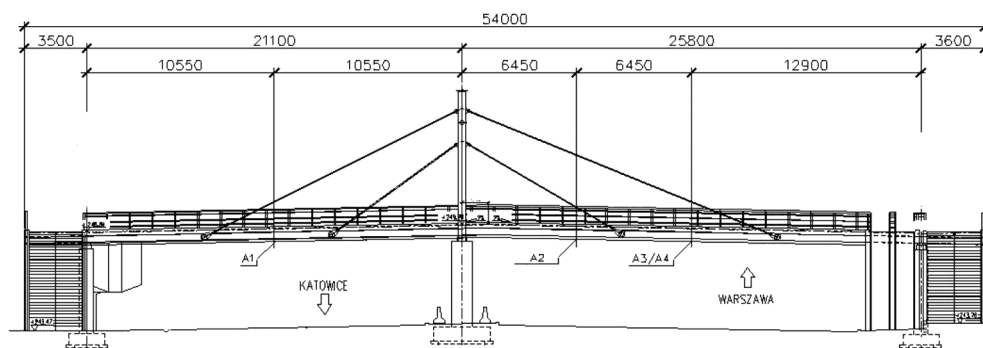


Fig. 2. The side view of the footbridge along with the locations of sensors (A – accelerometer)

300). The main girders are integrated with a concrete deck by steel bolts. The thickness of the deck varies from 0.17 to 0.20 m. The superstructure has been suspended (4 trusses on both sides of the deck) from a pylon 13.20 m high situated above the middle support. The pylon is constructed of steel pipes with a diameter 457 mm and concrete inside. The trusses (type ASDO M42) are hinged to the pylon and to the deck. Three supports are constructed as reinforced concrete pillars with a cross section of 1.0 x 1.2 m and 0.8 x 0.8 m for the middle and the extreme pillars, respectively.

The modulus of elasticity of steel was taken as 210 GPa. The Poisson's ratio was assumed to be 0.29. The material data of concrete were assumed: the modulus of elasticity at 39 GPa, the Poisson's ratio at 0.17 and the mass density at 2500 kg/m<sup>3</sup>.

### 3. Experimental determination of dynamic characteristics of the footbridge

For an experimental determination of the dynamic characteristics of the footbridge, an impulse load – a jump by a group of nine people – was applied as a vibration source. The footbridge was equipped with sensors (accelerometers) arrayed vertically (see Figs 1 and 2). The natural frequencies of the structure were assessed on the basis of the spectral analysis of the registered time history of the vibrations caused by the jump.

The time history of accelerations registered by sensor A1 is shown in Fig. 3a. The amplitude-frequency spectra calculated from the time histories of accelerations recorded by sensors A1, A2, A3, A4 are presented in Fig. 3b. It can be observed from the spectral analysis of all signals in Fig. 3b that the first, second and third natural frequencies equaled 2.7, 4.9 and 6.2 Hz, respectively.

The mode shapes associated with the obtained natural frequencies have also been detected from the registered signals. The analysis of the first mode shape is presented in Fig. 4. To abstract the accelerations associated with the first natural frequency a bandpass filter with the lowest frequency of 2.4 Hz and the highest frequency of 2.9 Hz was used. The filtered time histories of accelerations registered by sensor A1 located on the first span and by sensor A3 located on the second span are compared in Fig. 4a. Then, the comparison of the accelerations registered by sensor A3 and situated on the opposite sides of the second span is illustrated in Fig. 4b. It should be noted that the accelerations of the first and the second span are out of phase (sensors A1 and A3), whereas the accelerations of both sides of the deck (sensors A3 and A4) are almost identical.



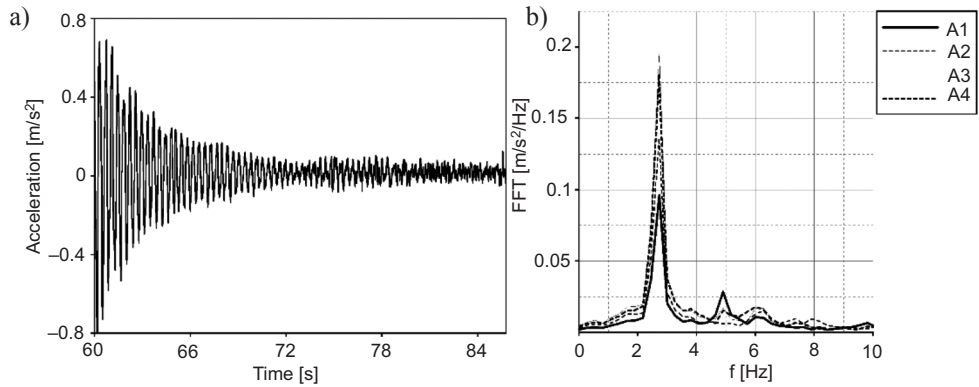


Fig. 3. (a) Time history of accelerations registered by sensor A1; (b) amplitude-frequency spectra calculated from the time histories of accelerations recorded by sensors A1, A2, A3, A4

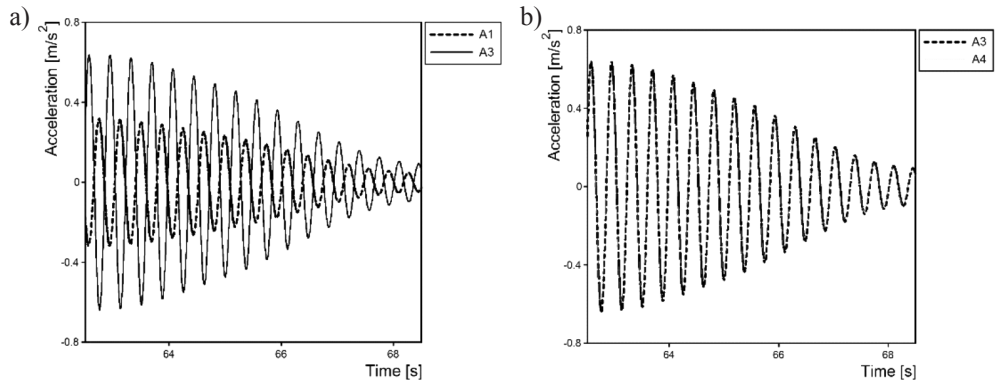


Fig. 4. Comparison of accelerations (filtered to 2.4-2.9 Hz) recorded by sensors: (a) A1 located on the first span and A4 located on the second span; (b) A3 and A4 located on the opposite sides of the deck on the second span

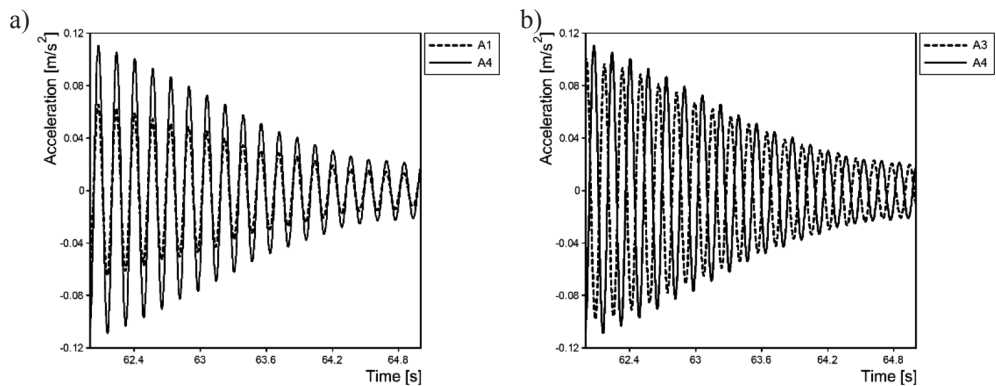


Fig. 5. Comparison of accelerations (filtered to 5.9-6.3 Hz) recorded by sensors: (a) A1 located on the first span and A4 located on the second span; (b) A3 and A4 located on the opposite sides of the deck on the second span

A similar analysis was carried out for the second and third mode shapes. The acceleration histories recorded by sensors A1, A3 and A4, filtered around the second natural frequency 4.9 Hz, are all in phase. Finally, the analysis demonstrated that the acceleration histories recorded by sensors A3 and A4, filtered around the third natural frequency 6.2 Hz, are out of phase (see Fig. 5).

#### 4. Comparison of the experimental and numerical results

As a result of the numerical analysis, the natural frequencies of the footbridge were also calculated. The model was created in ABAQUS software. In Table 1 the experimental and numerical results of natural frequencies are compared. The differences between the experimental and the numerical results did not exceed 10%.

The modes of natural vibration are presented in Fig. 6. It should be noted that, in the case of the first mode, the shape obtained from the numerical analysis of the vertical displacements of the first and the second span were out of phase. In the case of the second mode, the shape the vertical displacements of both spans were in phase. In the case of the third torsional mode, the shape of both sides of the footbridge deck moved out of phase. These results are in good agreement with the experimental results registered by accelerometers located at points A1-A4.

Table 1

Comparison of experimental and numerical values of natural frequencies of the footbridge

No. of frequency	Frequency [Hz]			Description of mode shape
	Experimental	Numerical	Difference [%]	
1	2.7	2.6	3.7	Bending
2	4.9	5.0	2.0	Bending
3	6.3	6.9	9.5	Torsion

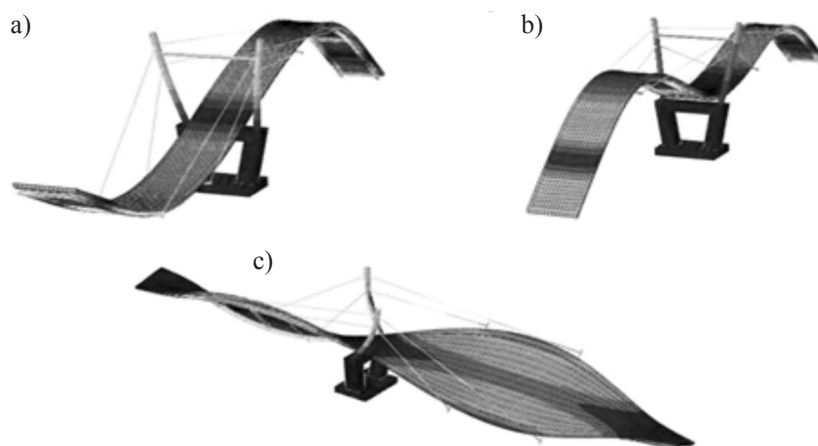


Fig. 6. Modes of natural vibrations of the footbridge: (a) first; (b) second; (c) third

## 5. Conclusions

In this paper the dynamic characteristics of the cable-stayed pedestrian footbridge obtained in numerical and experimental ways are presented. On the basis of the obtained results, the following conclusions can be drawn, as well as some general remarks for engineering practice:

1. The comparison of the analytical and experimental results are in very good agreement as far as both the natural frequencies and modes of vibrations are concerned. Hence, the numerical model of the cable-stayed footbridge was positively verified.
2. The obtained natural frequencies are within the range of 2.7-3.3 [3], which is typical for fast pedestrian running. Hence, the resonance phenomenon resulting in the amplification of the dynamic response may occur.

## References

- [1] Bilszczuk J., W. Barcik. et al., *Design of steel footbridges*, Lower Silesia Educational Publisher House (DWE), Wrocław 2004.
- [2] Dulińska J., *Evaluation of Dynamic Characteristics of Masonry Arch Bridges: Linking Full-Scale Experiment and FEM Modeling*, *Advanced Materials Research*, 133–134: 605–610.
- [3] Flaga A., *Mosty dla pieszych*, WKŁ, Warsaw 2011.
- [4] Murzyn I.J., *Dynamic characteristics of cable-stayed pedestrian and cyclists footbridge 120 m long*, *International Journal of Earth Sciences And Engineering*, 7(1): 313–319.

DAWID PAWŁOWSKI, MACIEJ SZUMIGAŁA\*

## AN EXPERIMENTAL AND THEORETICAL STUDY OF DEFLECTIONS OF BFRP RC BEAMS

---

### UGIĘCIA BELEK ZBROJONYCH PRĘTAMI BAZALTOWYMI BFRP – BADANIA LABORATORYJNE I ROZWAŻANIA TEORETYCZNE

#### Abstract

Basalt fiber-reinforced polymer (BFRP) bars are a new material used in reinforced concrete (RC) structures. They present such properties as high tensile strength, low modulus of elasticity and shear strength. Due to these mechanical properties, flexural behavior of BFRP RC elements is significantly different to that of traditional steel RC. This paper presents the results of an experimental and theoretical study of the short-term flexural behaviour of a series of simply supported BFRP RC beams. The beams were tested under four-point bending. The main objective of this paper was to investigate deflections of the beams depending on reinforcement ratio. The results of experiments were compared with code formulations and prediction models.

*Keywords: composite materials, BFRP bars, BFRP RC beams, deflections*

#### Streszczenie

Bazaltowe pręty zbrojeniowe (BFRP) są stosunkowo nowym materiałem stosowanym w budownictwie. Charakteryzują się one wysoką wytrzymałością na rozciąganie, niskim modułem sprężystości oraz niską wytrzymałością na ścinanie. W artykule przedstawiono wyniki badań laboratoryjnych zachowania się belek zbrojonych prętami BFRP poddanych działaniu obciążenia statycznego. Głównym celem badań było określenie wpływu stopnia zbrojenia na ugięcia zginanych elementów. Rezultaty badań porównano z wynikami obliczeń teoretycznych.

*Słowa kluczowe: materiały kompozytowe, zbrojenie bazaltowe, belki zbrojone BFRP, ugięcia*

**DOI: 10.4467/2353737XCT.15.399.5030**

---

\* MSc. Eng. Dawid Pawłowski, DSc. PhD.Eng., Prof. PUT, Maciej Szumigała, Institute of Structural Engineering, Faculty of Civil and Environmental Engineering, Poznan University of Technology.

## 1. Introduction

Fiber-reinforced polymer (FRP) bars present such properties as corrosion resistance, electromagnetic neutrality, light weight and high cutability [1, 2]. As a result they can be a good alternative to traditional steel for reinforced concrete (RC) elements, especially used in aggressive environments (e.g. offshore constructions, bridges), when electromagnetic neutrality is needed, or in temporary structures.

Basalt fiber-reinforced polymer (BFRP) bars are a relatively new type of FRP reinforcement. They have low modulus of elasticity and high tensile strength [3]. Moreover, they do not present any yielding before failure and behave almost linearly up to tensile rupture. Due to their mechanical properties, deflections and cracking in BFRP RC beams are larger than these found in traditional RC members [4]. Consequently, the design of BFRP RC flexural members is often governed by the serviceability limit states [5, 6].

The main aim of this study was to evaluate the stiffness of simply supported BFRP RC beams depending on the reinforcement ratio. This paper presents chosen results of a larger research programme in which 12 beams have been tested under static four-point bending. The results of experiments were compared with the results of theoretical analysis.

## 2. Experimental programme

Tests of 6 (3 pairs) simply supported BFRP RC beams subjected to four-point bending were carried out in the laboratory of the Institute of Structural Engineering at Poznan University of Technology. Three different amounts of BFRP reinforcement were used: 0.19% for beam BFRP 3#7, 0.32% for beam BFRP 3#9 and 0.52% for beam BFRP 5#9.

### 2.1. Test specimens

Fig. 1 illustrates the geometry and the reinforcement of test specimens. All the beams had a cross-section of  $0.20 \times 0.30 \text{ m}^2$ , a total length of 3.05 m and a span of 2.70 m. The shear reinforcement consisted of 8 mm round steel stirrups placed at intervals of 100 mm.

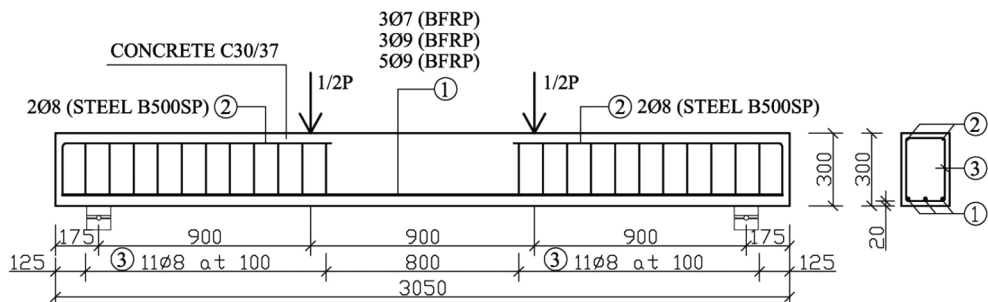


Fig. 1. Geometry and reinforcement of BFRP RC beams (dimensions in mm)

In the pure bending zone no stirrups were provided. Two 8 mm steel bars were used as top reinforcement to hold the stirrups. Reinforcing steel grade B500SP was used.

## 2.2. Materials properties

### 2.2.1. Concrete

All the beams were made of C30/37 concrete. The properties of this material were evaluated from core samples taken from the beams after the tests had been carried out. Table 1 presents the mechanical properties of concrete.

Table 1

**Mechanical properties of concrete**

Compressive strength $f_{ck}$ [MPa]	Modulus of elasticity $E_{cm}$ [GPa]	Tensile strength $f_{ctm}$ [MPa]	Age [days]
54.0	38.450	2.7	280

### 2.2.2. BFRP bars

BFRP ribbed bars were used as the flexural reinforcement. The experimentally determined mechanical properties of reinforcement [3] are shown in Table 2. According to the results of experiments [7, 8] the bond strength of these rebars is similar to that of steel bars.

Table 2

**Mechanical properties of BFRP bars**

Equivalent diameter [mm]	Tensile strength $f_u$ [MPa]	Modulus of elasticity $E_f$ [GPa]	Ultimate strain $\epsilon_{fu}$ [%]
6.7	1185	52.800	22.5
8.7	1485	56.300	26.2

More details of the experiments (instrumentation and test procedure) are presented in the paper [9].

## 3. Tests results

Fig. 2 shows evolution of the concrete strain along the depth of the section of beam BFRP 5#9 for different load levels. As can be observed in this figure, the neutral axis before cracking is located at the mid-height of the section. After cracking the neutral axis depth increases and then its value is constant.

Fig. 3 shows load – midspan deflection curves for all considered elements. All the beams behaved almost linearly until failure. This is the result of the mechanical properties of BFRP bars, which present a linear elastic behaviour under tensile loading. Because of the low modulus of elasticity of BFRP reinforcement, ultimate deflections of the beams were more than six times greater than these permissible (SLS graph in Fig. 2 – deflection limit =  $L/250$ ).

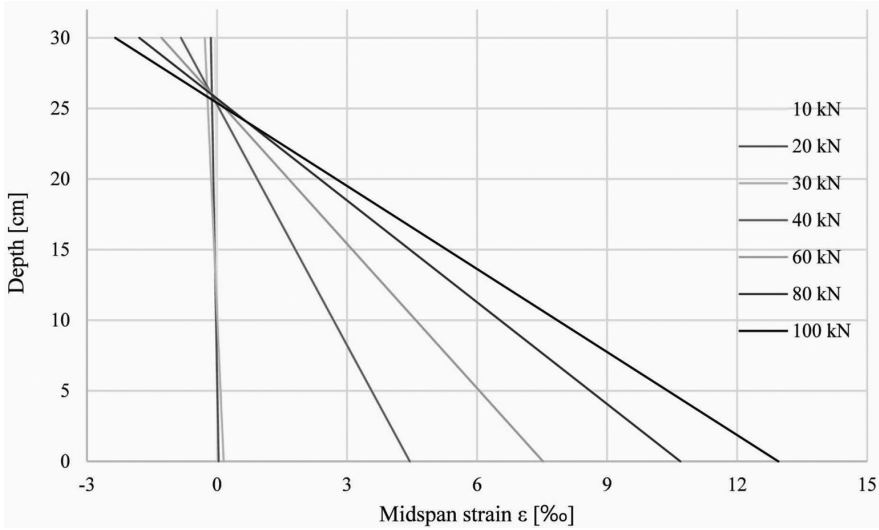


Fig. 2. Strain along midspan depth of beam BFRP 5#9

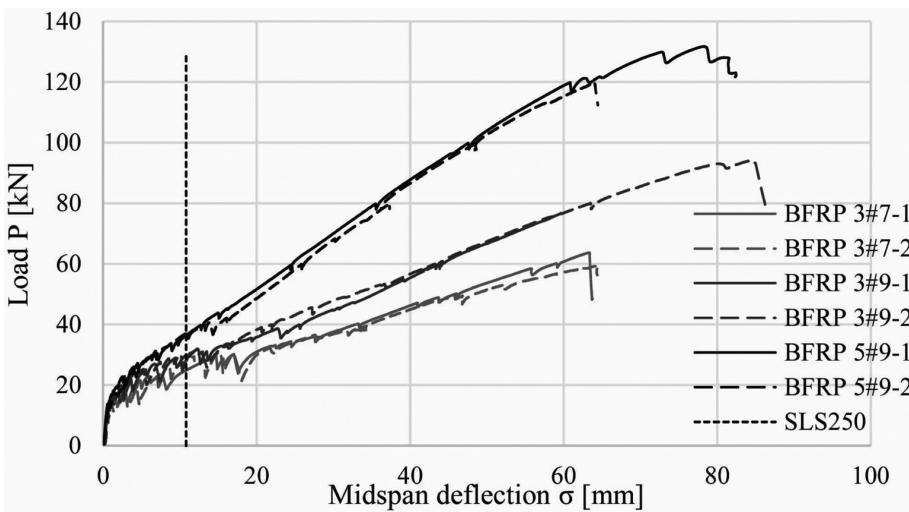


Fig. 3. Experimental load – midspan deflections

It is clear from Fig. 3 that the reinforcement ratio had a considerable effect on the stiffness of the beams. Loads for permissible deflections (equal to about  $L/250$ ) of the beams were about 28%, 36% and 39% of the limit loads for BFRP 5#9, BFRP 3#9 and BFRP 3#7, respectively. These values correspond well with the values obtained for RC elements with other types of FRP reinforcement [5, 10, 11].

#### 4. Theoretical analysis of deflections

Table 3 presents seven models for calculation deflections of BFRP RC beams.

Table 3

##### Expressions for the effective moment of inertia/deflections of FRP RC beams

Expression	Procedure
$\delta_{\max} = \left[ 1 - \left( \frac{M_{cr}}{M_a} \right)^2 \right] \delta_2 + \left[ 1 - \left( 1 - \left( \frac{M_{cr}}{M_a} \right)^2 \right) \right] \delta_1 \quad (1)$	EN 1992-1-1:2004 [12]
$I_e = \left( \frac{M_{cr}}{M_a} \right)^3 \beta_d I_g + \left[ 1 - \left( \frac{M_{cr}}{M_a} \right)^3 \right] I_{cr} \leq I_g \quad (2)$ $\beta_d = \frac{1}{5} \frac{\rho_f}{\rho_{fb}} \leq 1 \quad (3)$	ACI 440.1R-06 [13, 14]
$I_e = \frac{I_T I_{cr}}{I_{cr} + \left[ 1 - 0.5 \left( \frac{M_{cr}}{M_a} \right)^2 \right] (I_T - I_{cr})} \quad (4)$	ISIS Canada [15]
$\delta_{\max} = \frac{P \cdot L_a}{48 E_c \cdot I_{cr}} \left[ 3L^2 - 4L_a^2 - 8 \left( 1 - \frac{I_{cr}}{I_g} \right) \left( \frac{M_{cr}}{M_a} \right)^3 \cdot L_a^2 \right] \quad (5)$	CSA S806-02 [16, 17]
$I_e = \frac{I_{cr}}{1 - \left( 1 - \left( \frac{I_{cr}}{I_g} \right) \right) \left( \frac{M_{cr}}{M_a} \right)^2} \quad (6)$	Bischoff [18]



$I_e = \frac{I_{cr}}{1 - \left(1 - \left(\frac{I_{cr}}{I_g}\right)\right)\left(\frac{M_{cr}}{M_a}\right)^2} \quad (7)$ $\gamma = \frac{3\left(\frac{L_a}{L}\right) - 4\left[4\left(\frac{M_{cr}}{M_a}\right) - 3\right]\left(\frac{L_a}{L}\right)^3}{3\left(\frac{L_a}{L}\right) - 4\left(\frac{L_a}{L}\right)^3} \quad (8)$	<p>Bischoff and Gross [19]</p>
$I_m = \frac{23I_e I_{cr}}{8I_{cr} + 15I_e} \quad (9)$	<p>Faza and GangaRao [20]</p>

where  $M_{cr}$  is the cracking moment,  $M_a$  is maximum service moment,  $d_1$  is uncracked-state deflection,  $d_2$  is fully cracked-state deflection,  $I_e$  is the effective moment of inertia,  $I_g$  is the moment of inertia of gross section,  $I_{cr}$  is the moment of inertia of the cracked transformed section,  $\rho_f$  is the reinforcement ratio,  $\rho_{fb}$  is the balanced reinforcement ratio,  $I_y$  is the moment of inertia for uncracked section,  $P$  is the total force acting on the tested beam,  $L$  is the span of the beam,  $L_a$  is the distance from the force to the support of the beam,  $E_c$  is the modulus of elasticity of concrete.

Figs. 4 and 5 show experimental and theoretical load-deflection curves for beam BFRP 5#9. Comparing theoretical predictions obtained based on Eq. (1), Eq. (6) and Eq. (7), with the results of experimental tests, it can be observed that up to the service load (deflection  $\sigma < L/250$ ) there is good agreement between theoretical and actual values of deflections. Deflections calculated according to ACI (Eq. 2) are underestimated, whereas deflections calculated according to ISIS (Eq. 4), CSA (Eq. 5) and Faza and GangaRao (Eq. 9) are overestimated up to the service load. For higher loads all the theoretical approaches underestimate deflections.

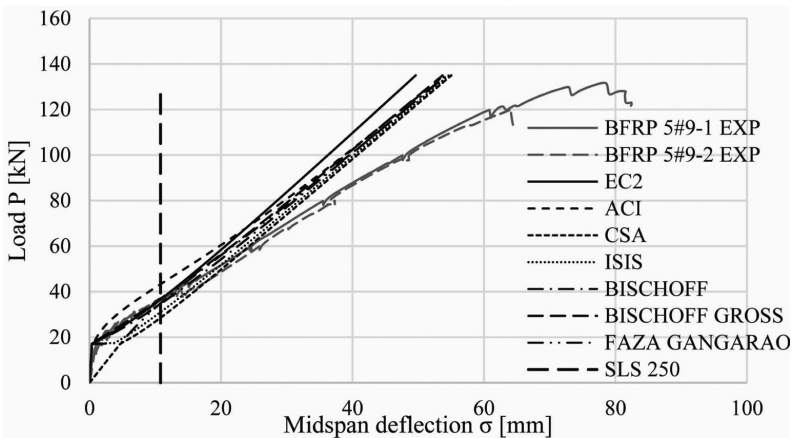


Fig. 4. Experimental vs. theoretical load – midspan deflections of BFRP 5#9

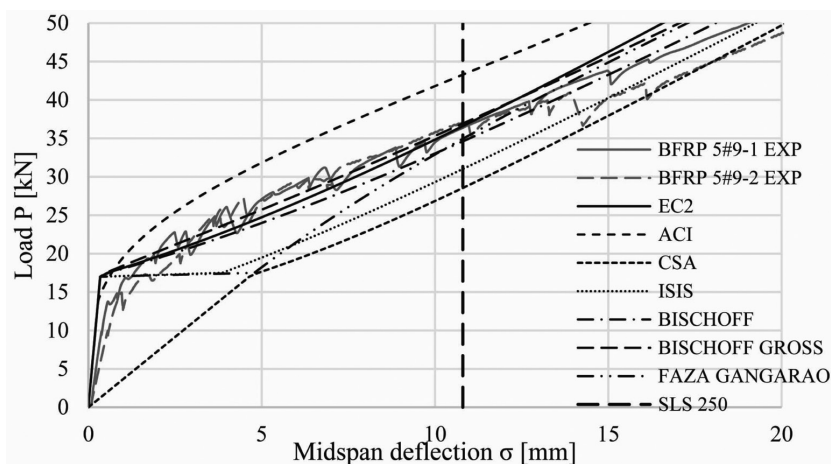


Fig. 5. Experimental vs. theoretical load – midspan deflections of BFRP 5#9 for loads less than service load

## 5. Conclusions

This paper presents the results of an experimental and theoretical study of the flexural behaviour of BFRP RC beams. Based on these results, the following conclusions may be drawn:

- Due to the mechanical properties of BFRP bars, the beams behave almost linearly until failure, which takes place at relatively large deflections.
- Design of the beams is governed by the serviceability limit states.
- At the service load level, deflections calculated according to Eurocode 2 and Bischoff approaches are in close agreement with the results of the experiments. For higher loads these approaches underestimate deflections.
- Deflections calculated according to ACI are underestimated, whereas deflections calculated according to ISIS, CSA and Faza and GangaRao are overestimated up to the service load. For higher loads these theoretical approaches underestimate deflections.

## Acknowledgements

The laboratory tests were partially supported by the Ministry of Science and Higher Education under doctoral grant 01/11/DSMK/0291. The tests specimens were donated by Depenbrock Polska Sp. z o.o. Sp. k.

## References

- [1] fib Bulletin 40/2007, *FRP reinforcement in RC structures, technical report*, International Federation for Structural Concrete (fib), 40/2007, 3–30.

- [2] Pawłowski D., Szumigala M., *Use of FRP reinforcement in building constructions*, Przegląd Budowlany, 3/2014, 47–50 (in Polish).
- [3] Kamińska M., *The results of tests of composite bars made of BFRP and GFRP*, Lodz University of Technology, 2012 (in Polish).
- [4] Garbacz A., Łapko A., Urbański M., *Investigation on concrete beams reinforced with basalt rebars as an effective alternative of conventional R/C structures*, Procedia Engineering 57/2013, 1183–1191.
- [5] Barris C., Torres L., Tauron A., Baena M., Catalan A., *An experimental study of the flexural behaviour of GFRP RC beams and comparison with prediction models*, Composites Structures, 91/2009, 586–295.
- [6] Nanni A., *North American design guidelines for concrete reinforcement and strengthening using FRP: principals, applications and unresolved issues*, Construction and Building Materials, 17/2003, 439–446.
- [7] Kamińska M., *The results of tests of bond between composite bars made of BFRP and GFRP and concrete*, Lodz University of Technology, 2012 (in Polish).
- [8] Fib Mocal Code, International Federation for Structural Concrete (fib), 2010, 257–259.
- [9] Pawłowski D., Szumigala M., *Flexural behaviour of full-scale basalt FRP RC beams – experimental and numerical studies*, Procedia Engineering, 108/2015, 518–525.
- [10] Barris C., Torres L., Miàs C., Vilanova I., *Design of FRP reinforced concrete beams for serviceability requirements*, Journal of Civil Engineering and Management, 18/2012, 843–857.
- [11] Alsayed S.H., Al-Salloum Y., Almusallam T.H., *Performance of glass fiber reinforced plastic bars as a reinforcing material for concrete structures*, Composites: Part B, 31/2012, 555–567.
- [12] CEN, EN 1992-1-1:2004 Design of concrete structures. Part 1-1. General rules and rules for buildings, Comité Européen de Normalisation Brussels, 2004.
- [13] ACI, ACI 440.1R-06 Guide for the design and construction of structural concrete reinforced with FRP bars, American Concrete Institute, 2006.
- [14] Branson D., *Deformation of concrete structures*, McGraw-Hill, New York 1997.
- [15] ISIS Canada, *Reinforcing concrete structures with fiber reinforced polymers*, Canada ISIS Canada Corporation, Manitoba 2007.
- [16] CSA, S806-02: Design and construction of building components with fiber-reinforced polymers, Canadian Standard Association, Canada 2002.
- [17] Yost J., Gross S, Dinehart D., *Effective moment of inertia for glass fiber reinforced polymer concrete beams*, ACI Structural Journal, 6/2003, 732–739.
- [18] Bischoff P., *Deflection calculation of FRP reinforced concrete beams based on modifications of the existing Branson equation*, Journal of Composites for Construction, 1/2007, 4–14.
- [19] Bischoff P., Gross S., *Design approach for calculating deflection of FRP reinforced concrete*, Journal of Composites for Construction, 4/2011, 490–499.
- [20] Faza S., GangaRao H., *Pre- and post-cracking deflection behaviour of concrete beams reinforced with Fibre-Reinforced Plastic rebars*, Proceedings of the First International Conference Advanced Composite Materials in Bridges and Structures, Canadian Society of Civil Engineers, Sherbrook, Canada, 1992, 151–160.

DAWID PAWŁOWSKI, MACIEJ SZUMIGAŁA\*

## SHORT-TERM CRACKING IN BFRP RC BEAMS – EXPERIMENTAL AND THEORETICAL ANALYSIS

### KRÓTKOTRWAŁE ZARYSOWANIE BELEK ZBROJONYCH PRĘTAMI BAZALTOWYMI BFRP – ANALIZA TEORETYCZNA I DOŚWIADCZALNA

#### Abstract

Basalt fiber-reinforced polymer (BFRP) bars can be a good alternative to traditional reinforcing steel. This type of reinforcement has low modulus of elasticity, hence deflections and cracking in BFRP RC flexural elements are larger than these found in typical RC members. As a result, the design of FRP RC beams is often governed by the serviceability limit states (SLS). This paper presents chosen results of a research programme in which 6 beams have been tested under four-point bending. The beams were varied in terms of the reinforcement ratio and diameter of rebars. The main goal of this paper was to investigate crack spacing and crack width of the beams. The results of experiments were compared with code formulations.

*Keywords: BFRP bars, BFRP RC beams, cracking*

#### Streszczenie

Bazaltowe pręty zbrojeniowe (BFRP) mogą być dobrą alternatywą dla klasycznej stali. Charakteryzują się one niskim modulem sprężystości, dlatego to SGU najczęściej decyduje o ostatecznej geometrii zginanego przekroju. W artykule przedstawiono wyniki badań laboratoryjnych zachowania się 6 belek zbrojonych prętami BFRP poddanych działaniu obciążenia statycznego. Głównym celem badań było określenie wpływu stopnia zbrojenia na rozstaw i szerokość rys. Rezultaty badań porównano z wynikami obliczeń teoretycznych.

*Słowa kluczowe: zbrojenie bazaltowe BFRP, belki zbrojone BFRP, zarysowanie*

**DOI: 10.4467/2353737XCT.15.400.5031**

\* MSc. Eng. Dawid Pawłowski, DSc. PhD. Eng., Prof. PUT, Maciej Szumigała, Institute of Structural Engineering, Faculty of Civil and Environmental Engineering, Poznan University of Technology.

## 1. Introduction

Basalt fiber-reinforced polymer (BFRP) bars are a relatively new building material. On the one hand, this type of reinforcement has low modulus of elasticity and high tensile strength [1]. As a result deflections and cracking in BFRP reinforced concrete (RC) beams are larger than these found in traditional RC members [2]. Consequently, the design of BFRP RC flexural members is often governed by the serviceability limit states [3, 4]. On the other hand, BFRP bars have high corrosion resistance [5, 6]. Hence, building standards [7–9] for FRP RC structures allow relatively large crack widths of 0.5–0.7 mm.

The main aim of this study was to evaluate the crack widths in simply supported BFRP RC beams depending on the reinforcement ratio. This paper presents chosen results of a larger research programme in which 12 beams have been tested under static four-point bending. The results of experiments were compared with the results of theoretical analysis.

## 2. Experimental programme

Tests of 6 (3 pairs) simply supported BFRP RC beams subjected to four-point bending were carried out in the laboratory of the Institute of Structural Engineering at Poznan University of Technology. Three different amounts of BFRP reinforcement were used: 0.19% for beam BFRP 3#7, 0.32% for beam BFRP 3#9 and 0.52% for beam BFRP 5#9.

### 2.1. Test specimens

Fig. 1 illustrates the geometry and the reinforcement of test specimens. All the beams had a cross-section of  $0.20 \times 0.30 \text{ m}^2$ , a total length of 3.05 m and a span of 2.70 m. The shear reinforcement consisted of 8 mm round steel stirrups placed at intervals of 100 mm.

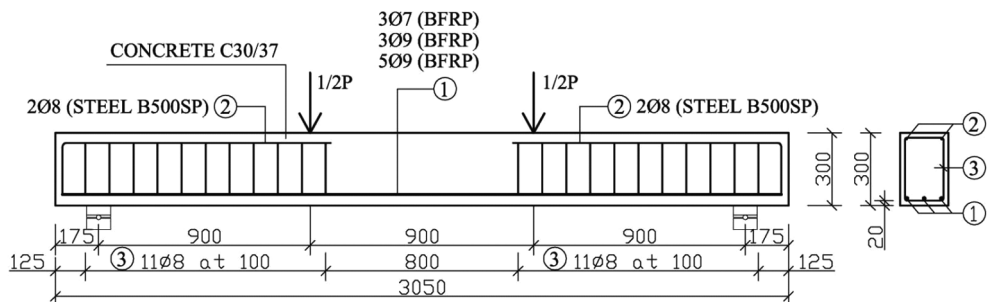


Fig. 1. Geometry and reinforcement of BFRP RC beams (dimensions in mm)

In the pure bending zone no stirrups were provided. Two 8 mm steel bars were used as top reinforcement to hold the stirrups. Reinforcing steel grade B500SP was used.

## 2.2. Materials properties

All the beams were made of C30/37 concrete. The properties of this material were evaluated from core samples taken from the beams after the tests had been carried out. BFRP ribbed bars were used as the flexural reinforcement. The experimentally determined mechanical properties of reinforcement [1] and concrete are shown in Table 1.

Table 1

### Mechanical properties of concrete

Mechanical property	Material		
	concrete C30/37	reinforcement $\Phi = 7$ mm	reinforcement $\Phi = 9$ mm
Compressive strength $f_{ck}$ [MPa]	54.0	–	–
Modulus of elasticity $E_{cm}$ [GPa]	38.450	–	–
Tensile strength $f_{ctm}$ [MPa]	2.5	–	–
Age[days]	280	–	–
Equivalent diameter [mm]	–	6.7	8.7
Tensile strength $f_{ft}$ [MPa]	–	1185	1485
Modulus of elasticity $E_f$ [GPa]	–	52.800	56.300
Ultimate strain $\epsilon_{fu}$ [%]	–	22.5	26.2

## 3. Tests results

Detailed results of the tests are presented in the paper [10]. Table 2 shows the experimental maximum, average and minimum crack spacing measured in the pure bending zone at the height of the reinforcement. The crack spacing ranged between 35 and 223 mm. The average ratio minimum to average and maximum to average crack spacing is found to be 0.48 and 1.82, respectively. The load levels at which cracking stabilized were relatively high – they ranged between 45% and 80% of the ultimate load  $P_{max}$ . These values differ from those found in the literature [3, 11, 12].

Table 2

### Experimental crack spacing and level at which cracking stabilizes

Beam designation	Maximum crack spacing $S_{r,max}$ [mm]	Average crack spacing $S_{r,m}$ [mm]	Minimum crack spacing $S_{r,min}$ [mm]	Force at which cracking stab. $P_{sta}$ [% of $P_{max}$ ]
BFRP 3#7-1	180	107	55	56
BFRP 3#7-2	223	117	52	64
BFRP 3#9-1	151	88	43	45
BFRP 3#9-2	143	80	35	80
BFRP 5#9-1	178	93	45	73
BFRP 5#9-2	186	85	44	61

Table 3 presents the maximum crack widths at every load steps for all the beams. It is clear from the table that the reinforcement ratio has a considerable effect on the crack widths. For loads of 25-35 kN (loads for permissible deflections – equal to about  $L/250$ ) the maximum crack widths were ca. 0.55 mm, 0.43 mm, 0.28 mm for BFRP 3#7, BFRP 3#9 and BFRP 5#9, respectively.

Table 3

#### Maximum crack width

Load [kN]	Maximum crack width $w_{max}$ [mm]				
	BFRP 3#7-2	BFRP 3#9-1	BFRP 3#9-2	BFRP 5#9-1	BFRP 5#9-2
18	–	–	–	0.05	0.05
23	0.55	0.10	0.30	0.10	0.10
28	0.75	0.40	0.45	0.20	0.25
33	1.10	0.60	0.55	0.25	0.30
43	2.75	1.40	1.40	0.65	0.45
53	3.00	–	–	–	–
63	–	1.40	1.75	1.00	0.85
83	–	2.00	2.75	1.40	1.30

#### 4. Theoretical analysis of crack widths

Table 4 presents four models for calculation the maximum crack widths of RC beams.

Table 4

#### Expressions for crack width

Expression	Procedure
$w_k = s_{rm} (\varepsilon_{sm} - \varepsilon_{cm}) \quad (1)$ $s_{rm} = 3.4c + 0.425k_1k_2 \frac{\phi}{\rho_{p,eff}} \quad (2)$ $\varepsilon_{sm} - \varepsilon_{cm} = \frac{\sigma_s}{E_s} - \frac{k_t f_{ctm} (1 + \alpha_e \rho_{p,eff})}{E_s \rho_{p,eff}} \geq 0.6 \frac{\sigma_s}{E_s} \quad (3)$	EN 1992-1-1:2004 [13]
$w = 2 \frac{f_f}{E_f} \beta k_b \sqrt{d_c^2 + \left(\frac{s}{2}\right)^2} \quad (4)$	ACI 440.1R-06 [7]

$w = 2.2k_b \frac{f_{frp}}{E_{frp}} \beta^3 \sqrt{d_c A} \quad (5)$	ISIS Canada [14]
$w = k \left[ 4c + 0.7(c_f - \phi) \right] \frac{\sigma_f}{E_f} \quad (6)$	JSCE [9]

where  $w$  ( $w_k$ ) is the maximum crack width,  $c$  is the concrete cover,  $k_1$  is the bond coefficient (0.8 for high bond – assumed in the study, 1.6 for plain rebars),  $k_2$  is the load coefficient (0.5 for bending, 1.0 for tension),  $\Phi$  is a bar diameter,  $\rho_{p,eff}$  is the effective reinforcement ratio,  $\sigma_s$  ( $\sigma_f$ ) is the tensile stress in the reinforcement,  $E_s$  ( $E_p$ ,  $E_{frp}$ ) is the modulus of elasticity of the reinforcement,  $k_3$  is the load coefficient (1.0 for short-term loading, 0.5 for long-term loading),  $f_{cm}$  is the mean value of the tensile strength of concrete,  $\alpha_c = E_s/E_c$ ,  $f_f$  ( $f_{frp}$ ) is the stress in the tension FRP reinforcement,  $k_b$  is the bond coefficient (1.0 for FRP bars with bond properties similar to steel, > 1.0 for bars with inferior bond behavior, < 1.0 for bars with superior bond behavior, 1.4(ACI), 1.2(ISIS) in the absence of significant test data – assumed in the study),  $d_c$  is the concrete cover measured from the centroid of tension reinforcement to the extreme tension surface,  $s$  ( $c$ ) is a bar spacing,  $\beta = h_2/h_1$  where  $h_2$  is the distance from the extreme tension surface to the neutral axis,  $h_1$  is the distance from the centroid of tension reinforcement to the neutral axis,  $A$  is the effective tension area of concrete,  $k$  is the bond coefficient (1.0~1.30, 1.0 – assumed in the study).

Figs. 2-4 show experimental and theoretical load – maximum crack widths curves for beam BFRP 5#9, BFRP 3#9 and BFRP 3#7, respectively. Comparing theoretical predictions with the results of experimental tests (table 5), it can be observed that all the analytical approaches tend to significant overestimate the crack widths up to the load about  $P = 2.5P_{cr}$  ( $P_{cr} \sim 18$  kN). For higher loads they move closer to the experimental data. Crack widths calculated according to EC2 [13] and ACI [7] present better estimate to the results of experiments than JSCE [9] and ISIS [14]. All the prediction models give better results for the bond coefficient  $k$  similar to that of steel reinforcement.

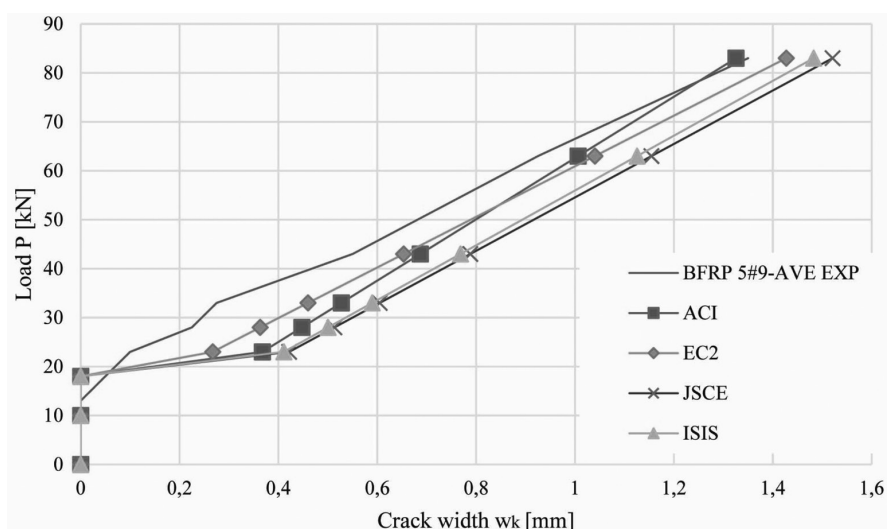


Fig. 2. Experimental vs. theoretical load – crack widths of BFRP 5#9



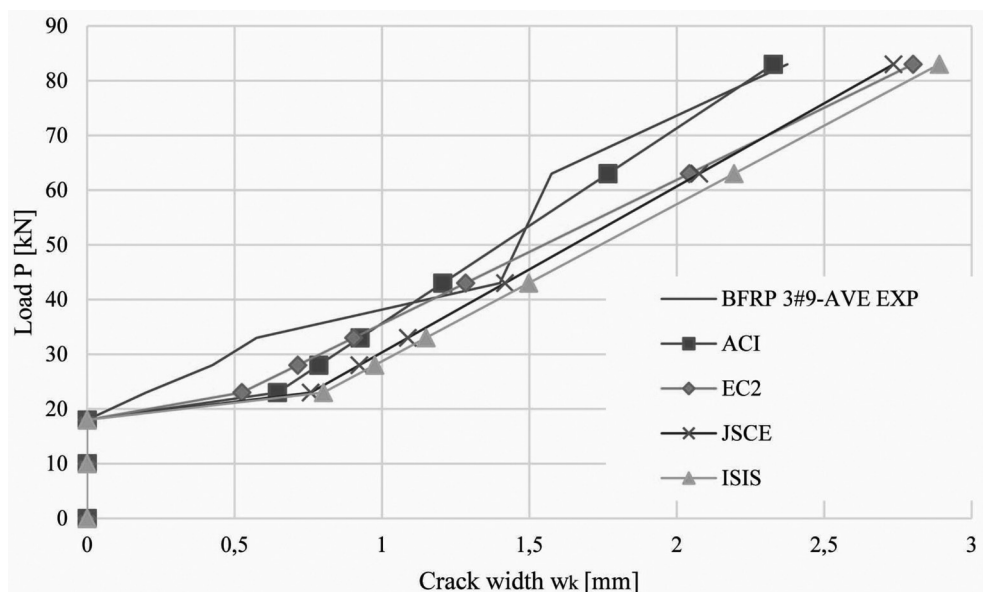


Fig. 3. Experimental vs. theoretical load – crack widths of BFRP 3#9

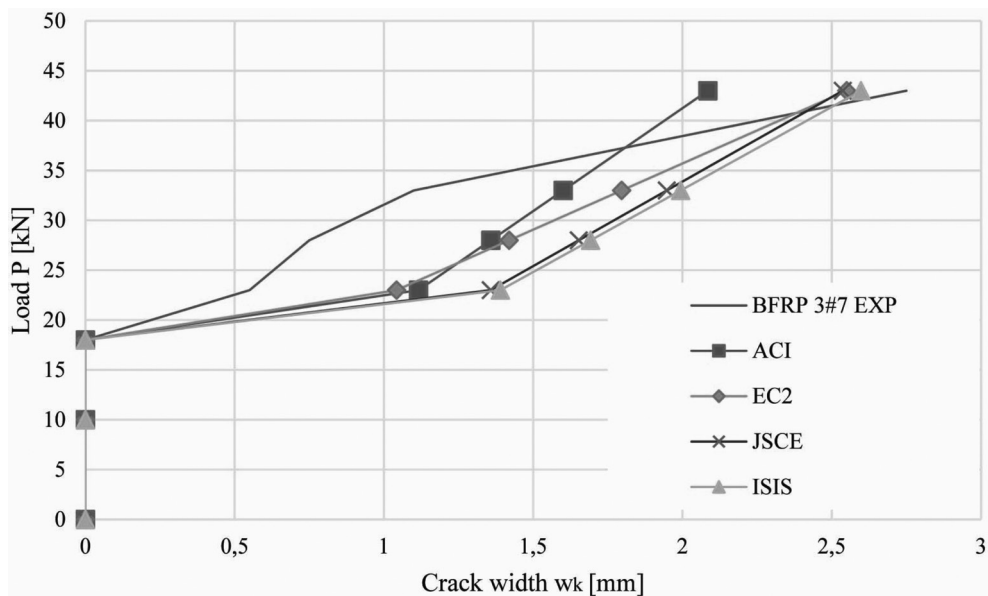


Fig. 4. Experimental vs. theoretical load – crack widths of BFRP 3#7

**Ratios  $w_{th}/w_{exp}$  for BFRP 3#7, BFRP 3#9 and BFRP 5#9**

Load [kN]	Ratio $w_{th}/w_{exp}$											
	BFRP 3#7-2				BFRP 3#9-1 AVE				BFRP 5#9-1 AVE			
	EC2	ACI	ISIS	JSCE	EC2	ACI	ISIS	JSCE	EC2	ACI	ISIS	JSCE
23	1.90	2.03	2.53	2.47	2.62	3.23	4.01	3.79	2.67	3.68	4.11	4.22
28	1.89	1.81	2.26	2.20	1.68	1.85	2.30	2.17	1.61	1.99	2.22	2.28
33	1.63	1.45	1.81	1.77	1.57	1.61	2.00	1.89	1.67	1.92	2.14	2.20
43	0.93	0.76	0.94	0.92	0.92	0.86	1.07	1.01	1.19	1.25	1.40	1.43
63	–	–	–	–	1.30	1.12	1.39	1.32	1.12	1.09	1.22	1.25
83	–	–	–	–	1.18	0.98	1.22	1.15	1.06	0.98	1.10	1.13

## 5. Conclusions

This paper presents the results of an experimental and theoretical study of the flexural behaviour of BFRP RC beams. Based on these results, the following conclusions may be drawn:

- The reinforcement ratio has a significant effect on the crack widths of BFRP RC beams. An increase in the reinforcement ratio results in a decrease in the crack widths.
- The load levels at which cracking stabilize range between 45% and 80% of the ultimate load. These values are higher than those obtained for traditional RC members.
- The average ratio maximum to mean crack spacing equals 1.86 and the average ratio minimum to mean values is 0.48. The first value is higher and the second one is lower than those found in the literature.
- Crack widths for loads for permissible deflections (equal to about  $L/250$ ) of the beams are lower than the maximum allowed ones (0.7 mm).
- Crack widths calculated according to EC2, ACI, JSCE and ISIS are significantly overestimated up to the load  $P=2.5P_{cr}$ . For higher loads they move closer to the experimental data.

## Acknowledgements

The laboratory tests were partially supported by the Ministry of Science and Higher Education under doctoral grant 01/11/DSMK/0291. The tests specimens were donated by Depenbrock Polska Sp. z o.o. Sp. k.

## References

- [1] Kamińska M., *The results of tests of composite bars made of BFRP and GFRP*, Lodz University of Technology, 2012 (in Polish).
- [2] Garbacz A., Łapko A., Urbański M., *Investigation on concrete beams reinforced with basalt rebars as an effective alternative of conventional R/C structures*, Procedia Engineering 57/2013, 1183–1191.
- [3] Barris C., Torres L., Tauron A., Baena M., Catalan A., *An experimental study of the flexural behaviour of GFRP RC beams and comparison with prediction models*, Composites Structures, 91/2009, 586–295.
- [4] Nanni A., *North American design guidelines for concrete reinforcement and strengthening using FRP: principals, applications and unresolved issues*, Construction and Building Materials, 17/2003, 439–446.
- [5] Pawłowski D., Szumigala M., *Use of FRP reinforcement in building constructions*, Przegląd Budowlany, 3/2014, 47–50 (in Polish).
- [6] Wang Z., Wu G., Wu Z., Dong Z., Xie Q., *Evaluation of prestressed basalt fiber and hybrid fiber reinforced polymer tendons under marine environment*, Materials and Design, 64/2014, 721–728.
- [7] ACI, ACI 440.1R-06 Guide for the design and construction of structural concrete reinforced with FRP bars, American Concrete Institute, 2006.
- [8] CSA, S806-02: Design and construction of building components with fiber-reinforced polymers, Canadian Standard Association, Canada 2002.
- [9] JSCE, Recommendation for design and construction of concrete structures using continuous fiber reinforcing materials, Japan Society of Civil Engineering, Japan 1997.
- [10] Pawłowski D., Szumigala M., *Flexural behaviour of full-scale basalt FRP RC beams – experimental and numerical studies*, Procedia Engineering.
- [11] Borosnyoi A., *Serviceability of CFRP prestressed concrete beams*, PhD thesis, Faculty of Civil Engineering. Budapest University of Technology and Economics, 2002.
- [12] Łapko A., Urbański M., *On assessment of cracking of concrete beams reinforced with BFRP bars*, Budownictwo i Architektura, 3/2014, 201–208.
- [13] CEN, EN 1992-1-1:2004 Design of concrete structures. Part 1-1. General rules and rules for buildings, Comité Européen de Normalisation Brussels, 2004.
- [14] ISIS Canada, *Reinforcing concrete structures with fiber reinforced polymers*, Canada ISIS Canada Corporation, Manitoba 2007.

# SUSTAINABLE DEVELOPMENT



DONATAS AVIŽA\*, ZENONAS TURSKIS\*, ADAM ŚWIĘCICKI\*\*

## AN EMPIRICAL ANALYSIS OF THE LITHUANIAN AND POLISH NORMATIVE REQUIREMENTS AND THEIR INFLUENCE ON THE PAYBACK OF A THERMO- INSULATION LAYER OF AN EXTERNAL WALL DETAIL

### ANALIZA LITEWSKICH I POLSKICH WYMAGAŃ OCHRONY CIEPLNEJ ORAZ ICH WPŁYWU NA CZAS ZWROTU TERMOIZOLACJI ŚCIANY ZEWNĘTRZNEJ

#### Abstract

The article provides the empirical analysis of thermo-insulation layer thickness (expanded polystyrene – EPS70) of the typical wall detail and its investment payback period in the traditional new construction single-apartment residential and net-zero energy building. On the basis of the results a simple payback period was calculated. Geographic region of Lithuania and Poland was chosen as the research object. The research results are important for building investors, designers, also for the auditors and experts of buildings energy consumption.

*Keywords: wall, thermo-insulation thicknesses, payback period*

#### Streszczenie

Artykuł stanowi empiryczną analizę grubości warstwy termoizolacji (styropian – EPS70) i okresu zwrotu inwestycji typowego dla nowo wznoszonych jednorodzinnych budynków mieszkalnych i budynków zero-energetycznych rozwiązania przekroju ściany zewnętrznej. Głównym celem było uzyskanie ochrony cieplnej lepszej niż wartości wymagane w przepisach litewskich i polskich oraz zgodnej ze standardami europejskimi. Uzyskane i zaprezentowane wyniki mogą być istotne dla inwestorów, projektantów, a także audytorów i ekspertów zajmujących się zużyciem energii w budynkach.

*Słowa kluczowe: ściana, grubość termoizolacji, czas zwrotu*

**DOI: 10.4467/2353737XCT.15.393.5024**

\* Donatas Aviža, PhD. Student, Prof. DSc. PhD. Zenonas Turskis, Faculty of Civil Engineering, Vilnius Gediminas Technical University.

\*\* PhD. Eng. Adam Święcicki, Department of Building Basis and Building Physics, Faculty of Civil and Environmental Engineering, Białystok Technical University.

## 1. Introduction

All European Union Member States have to ensure that all newly constructed buildings will have to be nearly zero-energy consumption buildings since 31 December 2020, according to requirements of the European Directive 2010/31/EU. A 5-year period is set to achieve this aim [5].

Single-apartment residential buildings with almost unconsumed energy (nearly of zero-energy) are those of very high-energy efficiency where energy consumption equals to almost zero or is very low. These buildings mostly consume the energy produced from renewable sources on site or nearby [1, 2].

According to the requirements for legal acts passed in the Republic of Lithuania and considering European standards – the buildings of classes B, A, A+ and higher can be called low-energy buildings (BUILD UP skills – Lithuania) [3]. Effectively designed and built buildings with almost unconsumed energy (A++ class) is a big challenge not only for Lithuania but also for Poland.

Foreign scientists experience and analysis on this problem is limited. Therefore, scientific achievements in this direction are necessary and timely, this emphasize in articles.

The buildings sector has a large potential for energy savings, because about 40% of the total amount of energy is consumed in this field in the United States or Europe, and nearly 30% in China [4].

Energy saving is an important part of the Energy Policies of the European Union and the Republic of Lithuania and Poland.

The study is aimed at developing correlation functions and determining links between the thickness of the thermal isolation layer of the wall (expanded polystyrene – EPS70) and its payback time according to the energy performance class of the building and the geographical area of building construction.

## 2. Object description

As for Lithuania, according to the currently valid normative requirements and provisions of STR 2.01.09:2012 Energy Performance of Buildings. Certification of Energy Performance [7], buildings are classified and divided into 9 energy efficiency classes, including A++, A+, A, B, C, D, E, F and G (Fig. 1a). The efficiency of energy consumption in the lately erected buildings (building parts) in Lithuania must not be lower than energy performance class “B” by 2016.

To make buildings more energy efficient, minimum energy performance requirements have been raised since 2007 in order to achieve A++ class requirements for buildings with almost unconsumed energy (nearly of zero-energy) performance.

A methodology for calculating the energy performance of a building in Poland is specified in normative documents (Dz. U. poz. 1200, Dz. U. poz. 376 and Dz. U. 75, Poz. 690). According to these documents, the buildings are not grouped in energy performance classes. Their estimated annual energy inputs per one square meter of the useful area of a building is calculated (Fig. 1b).

The research object of the study is the relations between the thickness of the thermo-insulation layer of the typical details of the wall (see Fig. 2) and its simple payback time. The wall was evenly insulated with expanded polystyrene (EPS70) foam having the declared value of the thermal conductivity coefficient (in this study –  $\lambda_{dec} = 0.039 \text{ W}/(\text{m}\cdot\text{K})$ ).

In order to find out the influence of climate and a geographic location on the thickness of the thermo-insulation layer, calculations in 3 Lithuanian and 5 Polish cities were performed. The average outside air temperature discussed in this study has been adopted according to data on (Table 2).

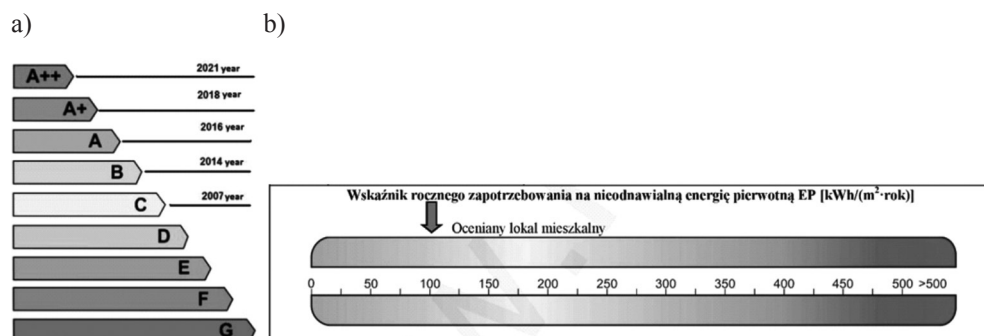


Fig. 1. Classification of energy efficiency of buildings: 1a – Lithuania – classes of energy efficiency (STR 2.01.09:2012); 1b – Poland – graphic method. Source: (Dz. U. Poz. 376)

Normative requirements for the wall partitions of residential buildings of the one and two-room apartment have been investigated in the study (Table 1).

Table 1

#### Normative value of the thermal transmittance coefficient of walls in residential buildings

$$U_{N,w}, \text{ W}/(\text{m}^2\cdot\text{K})$$

Year (PL)/Energy performance class (LT)	In Poland	In Lithuania
2014 (PL)/B (LT)	$0,25 \cdot \kappa$	$0,20 \cdot \kappa$
2017 (PL)/ A (LT)	$0,23 \cdot \kappa$	$0,12 \cdot \kappa$
2021 (PL)/A++ (LT)	$0,20 \cdot \kappa$	$0,10 \cdot \kappa$
Multiplier $\kappa = 20/(\theta_i - \theta_e)$ , where $\theta_i$ – indoor temperature during the heating season is equal to $\theta_i = 20^\circ\text{C}$ ; $\theta_e$ – the average outside air temperature during the heating season (Table 3).		

The problem is that the geographic region of Lithuania in technical documents is evaluated as one climatic region, with an average outside air temperature of  $+0.6^\circ$  during the heating season [2]. Different outside air temperature can be observed in different climatic zones in Lithuania and Poland (Table 2), and therefore, for using correlation dependence functions, a calculation solution to the thickness of the thermo-insulation layer (EPS70) of the typical details of the wall will be presented in this work.



The calculation methodology for the heat transfer coefficient of partitions and correlation dependence are further analysed. Then, on the basis of the obtained results simple payback periods are estimated.

Table 2

**The average outside air temperature during the heating season (Source: The Norm on Construction of the Republic of Lithuania RSN 156-94)**

Location	The average temperature, $\theta_e$ , °C	Duration in days	Location	The average temperature, $\theta_e$ , °C	Duration in days
Gdańsk	-0.05	242	Suwałki	-2.54	252
Poznań	-0.67	227	Klaipeda	1.9	214
Warszawa	-0.63	222	Kaunas	0.7	219
Białystok	-1.9	232	Vilnius	0.2	225

### 3. Calculation methodology

As for this study, general data and formulas for external wall partitions were taken from document STR 2.01.09:2012 *Energy Performance of Buildings. Certification of Energy Performance*. This procedure is also enshrined in Polish normative acts [6, 8, 9, 10].

The total heat transfer coefficient  $U_w$  (W/(m<sup>2</sup>·K)) of the external wall (Picture 2) can be calculated as follows (Eq. 1):

$$U_w = \frac{1}{R_t} = \frac{1}{R_{si} + R_{s1} + R_{se}} \quad (1)$$

where:

- $R_{si}$  – the thermal resistance of the internal surface of the wall (m<sup>2</sup>·K/W);
- $R_{se}$  – the thermal resistance of the external surface of the wall (m<sup>2</sup>·K/W);
- $R_{s1}$  – the sum of the thermal resistance of wall layers (m<sup>2</sup>·K/W);
- $R_t$  – the total thermal resistance of external wall construction (m<sup>2</sup>·K/W).

The main verification condition is the heat transfer coefficient of the external wall partition that must satisfy normative requirements (Eq. 2):

$$U_w \leq U_{N,w} \quad (2)$$

where:

- $U_w$  – the design value of heat transfer coefficient of the wall partition W/(m<sup>2</sup>·K) that directly depends on the investigated object, i.e. thermo-insulation (EPS70) thickness (see Fig. 2);
- $U_{N,w}$  – the normative heat transfer coefficient of the wall W/(m<sup>2</sup>·K) depending on energy efficiency class (see Table 1) and the average outside air temperature during the heating season (Table 2).

When the required thickness of the thermo-insulation layer is obtained, the period of simple materials and salary (investment) payback is calculated (Eq. 3):

$$PS = \frac{I_0}{\Delta S} \quad (3)$$

where:

- $I_0$  – the amount of investment to additional insulation, €/m<sup>2</sup>;  
 $\Delta S$  – annual savings, first year cost, €/(m<sup>2</sup>·years).

The annual savings are calculated according to the following expression (Eq. 4):

$$\Delta S = \left( \frac{\Delta U \cdot \Delta \theta \cdot t \cdot 24}{1000} \right) \cdot E; \quad (4)$$

where:

- $\Delta U = U_1 - U_2$  is the difference value of heat transfer coefficients of the wall (before  $U_1$  and after  $U_2$  additional insulation) W/(m<sup>2</sup>·K);  
 $\Delta \theta$  – the difference of inside and outside air temperature during the heating season, °C;  
 $t$  – the duration of the heating season, days (Table 3);  
 $E$  – heat energy costs, €/kWh.

#### 4. Research model

A research model has been created for determining correlation functions. The solutions to the designed model cover [2]:

1. For the purpose of calculations, the typical details of the wall of the residential building of one and two room-apartment were accepted (Table 4).
2. The thermal resistance of the external surface of the wall is  $R_{se} = 0.04$  m<sup>2</sup>·K/W; the thermal resistance of the internal surface of the wall is  $R_{si} = 0.13$  m<sup>2</sup>·K/W.
3. The adhesive mortar layer was adopted as a thin layer  $R_q = 0.04$  (m<sup>2</sup>·K)/W respectively, according to technical regulations on construction STR 2.01.09:2012.
4. The expanded polystyrene (EPS70) foam was used as insulation according to document ST 124555837.01:2013 *Expanded Polystyrene Foam Thermal Insulation for Building Partitions* (Fig. 2). The declared value of heat conductivity coefficient is  $\lambda_D = 0.039$  W/(m·K). The design value of the accepted heat conductivity coefficient is 0.041 W/(m·K) (according to document STR 2.01.03:2009).
5. Normative values of the heat transfer coefficient of the wall were accepted according to requirements for technical regulations on construction STR 2.01.09:2012 assessing temperature adjustment  $\kappa = 1$ . Effect of the location assessed through temperature adjustment  $\kappa = 20/(20 - \theta_e)$ , when  $\theta_e$  accepted in Table 2.
6. Masonry wall – autoclaved aerated concrete blocks, specific weight – 500 kg/m<sup>3</sup>, thickness – 250 mm;  $\lambda_{ds} = 0.153$  W/(m·K).

7. Thin-reinforced rendering thickness – 5 mm; surface finishing – 15 mm;  $\lambda_{ds} = 0.8 \text{ W}/(\text{m}\cdot\text{K})$ .
8. The price of insulation materials (EPS70) and a salary of 47.47 €/m<sup>3</sup> were accepted.
9. Thermal energy cost was accepted (the average Lithuanian price of central heating systems in 2014)  $E = 0.0724 \text{ €/kWh}$ .

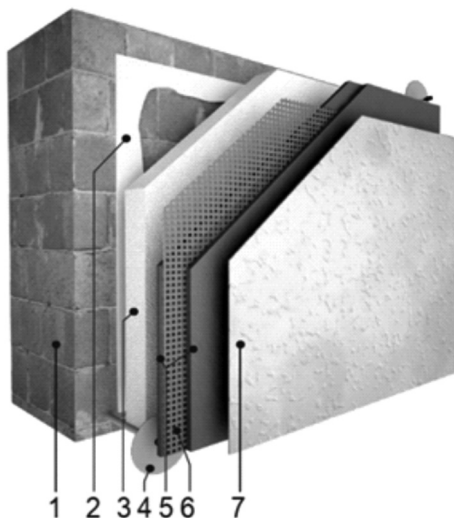


Fig. 2. Details of the wall. Source: (ST 124555837.01:2013). Research object – (3) the thickness of the thermo-insulation layer EPS70 of the wall, mm (for layers see Table 4)

Research calculations were performed using the same model/element and building design solutions, changing only climatic data.

Table 3

**The layers of the details of the external wall**

No.	Wall layer	Thickness, mm
*	Surface finishing	15
1	Autoclaved aerated concrete blocks, (500 kg/m <sup>3</sup> )	250
2	Adhesive mortar layer	5
<b>3</b>	<b>Expanded polystyrene (EPS70) foam</b>	<b>90–330</b>
4	Anchor with plastic nail	–
5	Adhesive mortar coated with masonry sealer	5
6	Reinforcing mesh	
7	Decorative coat	

## 5. Research results

The required thickness of the thermo-insulation layer (EPS70) of the sample of a typical wall was calculated according to the methodology for normative requirements for energy efficiency. As provided in Table 5, the final thickness of the wall was calculated using the approximation method of checking the condition of Eq. (2) and changing climatic data.

Table 4

**The thickness of the calculated thermo-insulation layer (EPS70) (in accordance with regulatory requirements for external walls)**

Year (PL) /Energy performance class (LT)	Thickness of the thermo-insulation (EPS70) layer, mm								Difference, t
	Gdańsk	Warszawa	Poznań	Białystok	Suwałki	Klaipėda	Kaunas	Vilnius	
1	2	3	4	5	6	7	8	9	10
2014 (PL)/ B (LT)	90	95	95	105	110	110	130	130	1.44
2017 (PL)/ A (LT)	105	110	110	120	125	240	260	270	2.57
2021 (PL)/ A++ (LT)	130	135	140	150	155	300	320	330	2.54
Difference, t	1.44	1.42	1.47	1.43	1.41	2.73	2.46	2.54	

The thickness of the thermal insulation layer increases proportionally with a rise in energy efficiency class using traditional insulation materials (in this study – EPS70) for the thermal insulation of external wall partitions. The normative thickness of the thermal insulation layer increases 2.73 times for buildings with almost unconsumed energy (A++ class), compared with the currently valid minimum requirements pertaining to energy efficiency classes “B”, as shown in Table 4.

The simple payback period of the thermo-insulation layer (EPS70) of the wall was estimated using formula presented in Eq. 3. The Lithuanian requirements is the reference level to which payback is applied. The research results are presented in Table 5.

Table 5

**The calculated simple payback period of the thermo-insulation layer of the wall (EPS70)**

Year (PL)/ Energy performance class (LT)	Simple payback period, years								Difference, t
	Gdańsk	Warszawa	Poznań	Białystok	Suwałki	Klaipėda	Kaunas	Vilnius	
1	2	3	4	5	6	7	8	9	10
2014 (PL)/B (LT)	2.3	2.5	2.6	2.5	2.3	3.3	3.5	3.2	1.44
2017 (PL)/ A (LT)	2.6	2.8	2.8	2.7	2.4	5.7	5.6	5.4	2.57
2021 (PL)/A++ (LT)	2.9	3.3	3.2	3.1	2.8	6.8	6.5	6.3	2.54
Difference, t	1.25	1.30	1.24	1.25	1.25	2.06	1.86	1.96	

## 6. Conclusions and implications

- The carried out analysis shows that the variation of the thickness of the thermo-insulation layer of the typical details of the wall depends on energy efficiency class and the type of the geographical location.
- Comparison of the Lithuanian and Polish standard requirements for the energy efficiency of buildings shows that the required thickness of the thermal insulation layer (EPS70) of the typical details of the wall varies and may increase by 2.57 times.
- The evaluation of the buildings of the same energy efficiency class in different climatic zones of Lithuania and Poland has disclosed that the thinnest thermal insulation layer of wall partitions is required in Gdańsk region, while the thickest one – in Vilnius. The greatest influence of fluctuations in climate has been noticed on the buildings of energy efficiency class A++. In this category, the required thickness of the thermal insulation layer (EPS70) pertaining to the wall varies by 20 cm between the warmest and coldest regions of Lithuania and Poland.
- According to the conducted research, the longest payback period of contributed funds (price of thermal insulation materials) is achieved within the period of up to 6.8 years in the city of Klaipėda.

## References

- [1] Aviza D., Turskis Z., *An empirical analysis of correlation between the thickness of a thermal insulation layer of the floor and the payback period*, Journal of Civil Engineering and Management, 20:5, 2014, 760–766.
- [2] Aviza D., Turskis Z., Kaklauskas A., *A Multiple criteria decision support system for analysing the correlation between the thickness of a thermo-insulation layer and its payback period of the external wall*, Journal of Civil Engineering and Management, 21:6, 2015, 827–835.
- [3] *BUILD UP Skills – Lithuania* [online]. (2013). Available on the Internet: <<http://www.buildupskills.eu/en/national-project/lithuania>> [cited 22 January 2015].
- [4] Deng S., Wang R.Z.; Dai I.Y., *How to evaluate performance of net zero energy building – A literature research*, Energy, 71: 2014, 1–16.
- [5] Marszał A. J.P., Heiselberg R., Jensen L., Nørgaard J., *On-site or off-site renewable energy supply options? Life cycle cost analysis of Net Zero Energy Building in Denmark*, Renewable Energy, 2012, 44: 1–2.
- [6] Pogorzelski J.A., *Przewodnik po PN-EN ochrony cieplnej budynków (Instrukcje, Wytyczne, Poradniki, 392/2009)*, Instytut Techniki Budowlanej, Warszawa 2009.
- [7] STR 2.01.09:2012 *Energy performance of buildings. Certification of Energy performance*, Technical Construction Regulation, Vilnius, 2012.
- [8] *Ustawa z dnia 29 sierpnia 2014 r. o charakterystyce energetycznej budynków* (Dz. U. 0 014 r. poz. 1200, z późn. zm.).
- [9] *Rozporządzenie Ministra Infrastruktury i Rozwoju w sprawie metodologii wyznaczania charakterystyki energetycznej budynku lub części budynku oraz świadectw charakterystyki energetycznej* (Dz. U. z 2015 r. poz. 376).
- [10] *Tekst ujednoczony rozporządzenia w sprawie warunków technicznych, jakim powinny odpowiadać budynki i ich usytuowanie* (Dz. U. z 2002 poz. 690, z późn. zm.).

BARBARA DULIŃSKA\*

## SUSTAINABLE DEVELOPMENT IN CITIES DESIGNED IN ACCORDANCE WITH THE SMART CITY CONCEPT

---

### ZRÓWNOWAŻONY ROZWÓJ W MIASTACH PROJEKTOWANYCH ZGODNIE Z IDEAŁ SMART CITY

#### Abstract

The situation of cities, related to a rapid increase in the number of their inhabitants, stimulates the search for solutions counteracting the adverse consequences of this phenomenon. In order to improve the quality of life – both now and in the future – the idea of sustainable development was created, which is reflected in various visions of the twenty-first century cities. The concept of Smart City implemented in the revitalization project of Arabianranta district in Helsinki is a successful example of an action consistent with these concepts.

*Keywords: Smart City, sustainable development, Arabianranta*

#### Streszczenie

Sytuacja miast związana z gwałtownym wzrostem liczby ich mieszkańców, skłania do poszukiwania rozwiązań przeciwdziałającym negatywnym konsekwencjom tego zjawiska. W trosce o poprawę jakości życia – obecnie jak i w przyszłości – powstała idea zrównoważonego rozwoju, która zapisywana jest w wielu różnych wizjach miast XXI wieku. Koncepcja Smart City, zaimplementowana w projekcie rewitalizacji dzielnicy Arabianranta w Helsinkach, jest przykładem działania zgodnego z tymi koncepcjami, zakończonego sukcesem.

*Słowa kluczowe: Smart City, rozwój zrównoważony, Arabianranta*

**DOI: 10.4467/2353737XCT.15.386.5017**

---

\* MSc. Arch. Barbara Dulińska, PhD Student, Faculty of Architecture, Cracow University of Technology.

## 1. Introduction

The subject of the study is presentation of the principles of sustainable development for planning issues in design assumptions, functioning in accordance with the concept of Smart City. The subject was taken up based on the analysis of the revitalized Arabianranta residential district located in Helsinki, where the designers used the concept of Smart City in order to create a comfortable living space that would respect its identity. The author will demonstrate the validity of the thesis that through the use of advanced technologies, which are widely available and used in the infrastructure of modern cities like Smart City, it is possible to effectively implement the principles of sustainable development.

## 2. The current situation of European cities

It can be observed that currently around 70% of Europe's population live in urban areas, and it is expected that this number will continue to grow over the next few years. A rapid development of metropolis, which took place in the past few decades, contributed to the expansion of the areas which they occupy. This process frequently proceeded in an unplanned and uncontrolled manner. Such urban sprawl has adversely affected urban composition of the cities – a rapid creation of monofunctional districts, badly communicated with the rest of the city, have had a direct impact on the deterioration of the quality of life in cities and on the poor air quality there. Currently, cities consume 75% of world energy for their functioning, and emit 70% of global carbon dioxide emissions [1]. The increasing urbanization processes led urban designers and scientists to search for solutions to the problems related to them. This resulted in the emergence of new urban doctrines over the past decades, seeking a way to ensure a comfortable life. A common feature of the concepts such as Compact City, Urban Village, Eco City, New Urbanism, Green Urbanism, Smart City, Sustainable City [2] is their subordination to the **idea of sustainable development**.

## 3. What is sustainable development?

The assumptions of the idea of sustainable development were presented in the 1987 report Our Common Future, prepared by the World Commission on Environment and Development (the so-called Brundtland Commission): “At the current level of civilization, sustainable development is possible, which is such a development that meets the needs of the present without compromising the ability of future generations to meet their own needs” [2]. The implementation of the concept in urban areas is to create good living conditions for their citizens – the space which is both functional and healthy. It refers both to the design (of the whole city, its individual districts and specific buildings), as well as the subsequent management. The idea encourages the rational, efficient and economical management of resources, which include not only **raw materials**, but also **space, energy, human capital and time**. The assumptions of the idea of sustainable development are currently included into numerous development strategies and political declarations, becoming regulations and

guidelines imposed by municipalities. The great role of the users (both entrepreneurs and residents) throughout the process has been emphasized. According to the president of the Responsible Business Forum, Mrs. Mirella Panek-Owiańska, “the city is a special area of business influences. It is a place where the majority of customers are, where employees live. Therefore, the business here should interact with residents and local authorities for sustainable development. Sustainable development is in the interests of both business and citizens” [3].

The idea of sustainable development should be implemented during the work related to the search for tools to solve the problems related to the major challenges which modern cities face. They can be divided into the following 4 groups:

- **Environmental** (carbon dioxide emissions into the atmosphere, biodiversity, waste, clean water)
- **Social** (social polarization, unemployment, migration, homelessness, poverty, meeting the needs of residents, social participation).
- **Economic** (competitiveness of the city, its profitability, lack of jobs for the people coming to live in the cities)
- **Planning** (urban sprawl, development of public spaces, public and individual transport).

#### 4. What is Smart City?

One of the responses to the deteriorating quality of life in cities, based on the principles of sustainable development, is the concept of **Smart City**, which uses the development of advanced technologies. The presence of ICT (Information and Communication Technologies) and the widespread digitization of all areas of life, in the concept of Smart City constitute a tool to create a safe, friendly, convenient, diversified and efficient environment. This idea uses a network and advanced software to prompt, collect and analyze data, and to support urban infrastructure (networks providing media, transportation system) as well as administrative processes. Additionally, free access to broadband Internet is used by the users of the concept (residents, entrepreneurs and public authorities) to communicate with each other. Their dialogue is essential for the effective functioning of public participation, which is essential to the smooth functioning of this type of a concept.

In order to improve the quality of life in cities, the Smart City concept involves:

- development based on network connections between such elements as access to knowledge, technology, human resources, infrastructure and the environment,
- multidimensional development based on ICT and network systems with integrated measurement devices,
- smart city development in the field of economy (smart economy), management (smart governance), humans (smart people), quality of life (smart living), transport and communication (smart mobility) and the environment (smart environment).



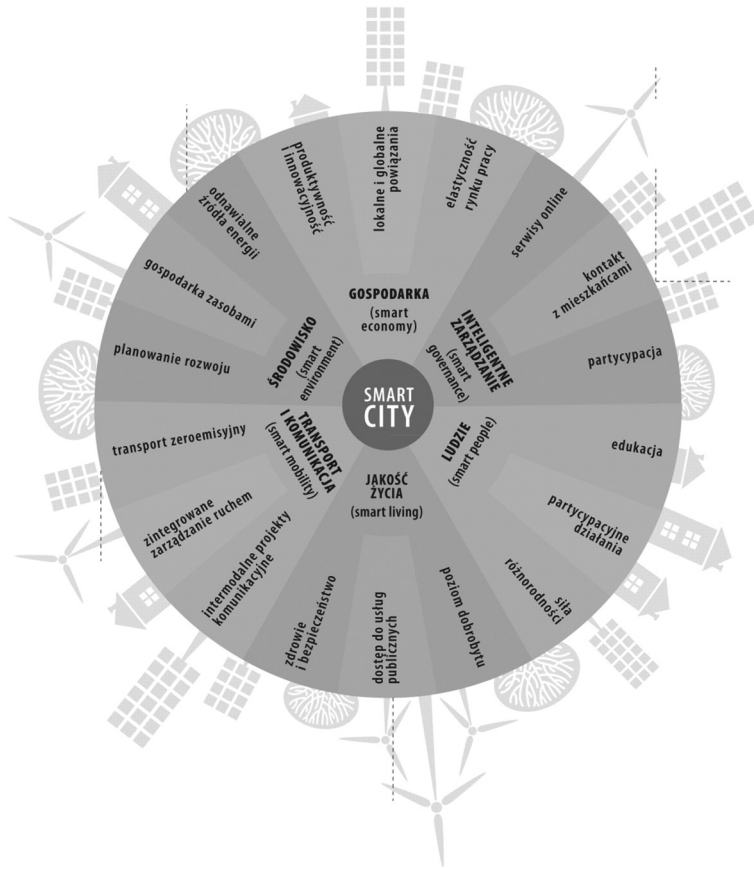


Fig. 1. Fields of development in Smart City

## 5. The tools used in Helsinki's district of Arabianranta, designed according to the concept of Smart City, used to achieve the objectives of sustainable development

The area, currently occupied by Arabianranta residential district, was associated with the industry since the sixteenth century, when a settlement was founded here. In 1992, the city authorities decided to relocate production plants and alter the profile of the district with its vast potential for a multifunctional complex of residential and service buildings, a campus of the Faculty of Art and Design of Helsinki University, as well as recreation areas. The creators of the Masterplan for this site, characterized by complex issues, decided not to treat the heritage of this place as a problem or a barrier to its development. The Arabia ceramics factory, existing since 1874, which is associated with the place and has built its climate, has been treated as an opportunity and inspiration to create an attractive and diversified district. The designers of this assumption have decided that “the starting point of the neighborhood revitalization project is to honor the identity of the place in

which the city was established, and of the culture that was born in this area. The birthplace of the city and the manifestation of technical and industrial culture, including art and music, offer a unique synergy” [4].

The implementation of the settlements of the Masterplan for the district designed according to the concept of Smart City, is to ensure its functioning in accordance with the principles of sustainable development. The area of 85 hectares was developed into 3 zones:

- **green**, located just at the waters of the bay, consisting of both arranged gardens and parks, as well as pristine areas of nature reserves, thus ensuring biodiversity. From the west, the area borders with residential areas and integrates developed sites with open recreational areas and green ecological precincts.
- **residential**, compact development of high intensity and varied forms (collective accommodation, multi-family and single-family housing), thus ensuring a diversified local community. The development of various **form standard and ownership** ensures varied users, who contribute to maintaining a healthy, open local community.
- **universities, office and service buildings**, providing access to services, jobs and education to the residents, allowing them to reduce transportation needs. These facilities also allow to carry out activities related to education and research, making the district an attractive and competitive research center, positively influencing the economic level of the entire unit.

The residential district is well connected with the center of Helsinki, located at a distance of 10 km, thanks to both the low-carbon efficient network of public transportation and the system of cycle lanes. In addition to the compact and varied development, filled with diverse functions, it is a method to minimize the need to use own cars by the residents, by not generating the necessity to travel. Another principle of sustainable development is implemented through the project settlement, which requires that 2% of the financing of each of the implemented investments is assigned for the activities related to art and design. The result was a good system of public spaces, diversified with the works of art that provide cohesion of the district and a friendly neighborhood for both pedestrians and cyclists. The organization of public space and its decoration with the elements associated with the historic porcelain factory Arabia, is conducive for the local community to building attachment to their place of residence and create its identity. The Masterplan required the use of ecological materials, durable and of high quality, which is one of the principles of sustainable development. Another of its objectives is gaining, processing and propagating knowledge, which is accomplished by using modern technology. Telecommunication network enables effective communication, not only within academic institutions and companies having their headquarters here, but also between these organizations.

In order to ensure diversity of the district, the designers marked in the project that it was necessary to design both developed areas and open spaces, attracting private and public investors, as well as effective combination of different functions, including residential, service, educational, and recreational ones. Avoiding monotonous and unidirectional space is conducive to raising the attractiveness of the area and its proper development.

## 6. Conclusions

In 2012, the city of Helsinki announced the completion of the Masterplan for the revitalized district of Arabianranta. The implementation of this complex design made it possible to create a friendly place of residence for approximately 10 thousand people, 15 thousand students and 4 thousand workers employed in 300 enterprises located in this area. The district uses benefits of the twenty-first century, such as modern technologies, to effectively fulfill the principles of sustainable development. With an extensive telecommunication infrastructure, the Helsinki Smart City is a healthy, economical and sustainable environment.

## References

- [1] [www.odpowiedzialnybiznes.pl/wp-content/uploads/2014/07/Analiza-tematyczna-\\_Biznes-na-rzecz-zr%C3%B3wnowa%C5%BConych-miast.pdf](http://www.odpowiedzialnybiznes.pl/wp-content/uploads/2014/07/Analiza-tematyczna-_Biznes-na-rzecz-zr%C3%B3wnowa%C5%BConych-miast.pdf).
- [2] Stangel M., *Kształtowanie współczesnych obszarów miejskich w kontekście zrównoważonego rozwoju*, monografia, Wydawnictwo Politechniki Śląskiej, Gliwice 2013.
- [3] [www.odpowiedzialnybiznes.pl/aktualno%C5%9Bci/7-wyzwan-dla-zrownowazonego-rozwoju-miast-w-polsce/](http://www.odpowiedzialnybiznes.pl/aktualno%C5%9Bci/7-wyzwan-dla-zrownowazonego-rozwoju-miast-w-polsce/) [2015].
- [4] [www.helsinkivirtualvillage.fi](http://www.helsinkivirtualvillage.fi) [2015].
- [5] Stawiasz D., Sikora-Fernandez D., Turała M., *Koncepcja Smart City jako wyznacznik podejmowania decyzji związanych z funkcjonowaniem i rozwojem miasta*, Zeszyty Naukowe Uniwersytetu Szczecińskiego, nr 721, 2012.
- [6] Wdowiarz-Bilska M., *Od miasta naukowego do Smart City*, Czasopismo Techniczne z. 1-A/2/2013, Wydawnictwo Politechniki Krakowskiej.
- [7] Włodarczyk A., *Raport z wizyty studialnej w ramach projektu SMART\_KOM. Kraków w sieci inteligentnych miast*. Helsinki 2014.
- [8] Ghel J., *Miasta dla ludzi*, Wydawnictwo RAM, Kraków 2010.
- [9] [www.arabianranta.fi](http://www.arabianranta.fi) [2015].
- [10] [www.helsinkilivinglab.fi](http://www.helsinkilivinglab.fi) [2015].

WOJCIECH DULIŃSKI\*

## SUSTAINABLE AIRPORT PASSENGER TERMINAL DESIGN – THE REVIEW OF SELECTED EXAMPLES

---

### ZRÓWNOWAŻONY ROZWÓJ W PROJEKTOWANIU PASAŻERSKICH TERMINALI LOTNICZYCH – PRZEGLĄD WYBRANYCH PRZYKŁADÓW

#### Abstract

This paper points out recent tendencies in airport passenger terminal architecture. Taking sustainability of the building as a major concern, examples of the current architectural approaches are presented. Norman Foster's Stansted Airport design is identified as a model solution and three cases of its implementation are pictured and analyzed. Moreover, the rising interest in multi-criteria certification in the aviation infrastructure is depicted on the example of *LEED* certification.

*Keywords: airport design, sustainable airport, multi-criteria certification*

#### Streszczenie

W artykule przedstawiono aktualne tendencje w projektowaniu pasażerskich terminali lotniczych. W ujęciu uwzględniającym ideę zrównoważonego rozwoju, zaprezentowane zostały przykładowe cechy architektury lotnisk. Port lotniczy Stansted, zaprojektowany przez Normana Fostera, został zidentyfikowany jako modelowe rozwiązanie, którego powielenie pokazano na trzech kolejnych projektach. Dodatkowo wskazano, na przykładzie amerykańskiego systemu *LEED*, rosnące zainteresowanie certyfikacją wielokryterialną budynków w sektorze infrastruktury cywilnych lotnisk pasażerskich.

*Słowa kluczowe: zrównoważone projektowanie lotnisk, certyfikacja wielokryterialna*

**DOI: 10.4467/2353737XCT.15.408.5039**

---

\* MSc. Arch. Wojciech Duliński, Institute of Architectural Design, Faculty of Architecture, Cracow University of Technology.

## 1. Introduction

A passenger airport terminal is one of the most complex building typology. Different in sizes and architectural expressions, all airports serve travelers providing a certain standard of mandatory procedures (immigration, customs, security check, etc.) based on high-tech electronic equipment, and additional facilities like duty free stores or restaurants. They operate for the most time of day and night, allowing unobstructed flow of passengers throughout halls, corridors, gates, etc.

The abovementioned factors result in relatively high energy consumption in comparison to other types of buildings [1]. Hence, responsible architectural and engineering designs are inevitable in today's highly developed, sustainability-oriented societies. In this paper recent tendencies in passenger terminals design are presented.

## 2. Transformation towards sustainability

A certain model of optimal 'traditional' airport passenger terminal was developed throughout 20<sup>th</sup> century. Due to large number of people and big volumes with no daylight, followed by continuous increase of rigorous regulations, huge amounts of ductwork, piping, electric installations, etc. were suspended to structural elements under floor slabs to allow maintaining adequate micro-climatic conditions inside the building. This led to overgrown foundations, columns, beams, slabs and, as a consequence, less efficient economic performance of the building in a long-term run. Airports started to generate a huge ecological footprint along with increased operational costs.

A revolutionary idea was invented and first incorporated into the design by a British architect and technocrat – Norman Foster [2, 3]. His design for Stansted Airport (opened for passengers in 1991) represented a new approach to terminal architecture. This concept is now constantly being multiplied and developed by various architects worldwide (including Foster himself).

The model incorporates low-tech solutions and spatial decisions in order to provide better functional operation of the airport not only in terms of investment costs, but also in terms of operational savings. At the same time, it proposes means of reduction of energy consumption and ecological footprint. In terms of design sustainability, the approach is to create a lightweight, 'Big shed'<sup>1</sup> [4] modular canopy structure that offers sunlight and ventilation openings for less energy-consuming interior conditions upkeep (see Fig. 1).

So far, Foster's model is considered to contain the vast majority of desirable solutions, both in terms of operational functionality and life cycle economical and ecological analysis [3]. Even though the diversity amongst airport terminal buildings is very significant, due to external conditions like: desired capacity, climate conditions, economical issues, etc., principles for the design implemented into Stansted's terminal can be described as an emerging trend in passenger terminal architecture.

As sustainability of a building requires a holistic approach to designing process from the very beginning (conceptual design) to the end of construction, it is much easier to incorporate

---

<sup>1</sup> 'Big shed' is a term used to describe trends in the contemporary architecture of public use buildings

sustainable solutions into newly built terminals, rather than building extensions, where the design opportunities are often limited by existing conditions. It does not mean that building extensions should not meet current building standards, but for the purpose of this paper, examples of new designs will be presented as model solutions.



Fig. 1. London-Stansted Airport terminal, designed by Norman Foster. Terminal is roofed by a lightweight canopy structure, allowing natural insulation, daylight penetration and natural ventilation of the building. Source: <http://www.si.wsj.net/>

### **3. Stansted's model implementation**

The continuous growth of aviation industry (dictated by enlarging number of passengers), constant struggles of governments in terms of defining geopolitical nodes on the globe, as well as new emerging cities cause numerous opportunities for architects and engineers to design new airports [5]. As mentioned above, regardless size and range, the majority of recent developments follows Foster's idea [2, 3].

#### **3.1. Queen Alia International Airport, Amman, Jordan**

One of the clearest examples of the idea is Queen Alia International Airport, (completion in 2012). Located in Amman, the airport serves around 8 million passengers per year, which places it in the group of mid-size regional transit airport.

Due to climatic conditions at the airport's location, implementation of the idea was targeted mainly at the efficient use of Sun energy and maximum reduction of heat gains (overheating) from sun rays at the same time. This is why the architect decided to design a canopy roof as a system of modular concrete shells, covered with PV cells and equipped

with small skylights that allow light penetration into the building. Sunrays accessing interior of the terminal reach bright floors that reflect rays towards ceiling in order to spread the natural light throughout the interior (see Fig. 2).

The use of natural light limits the necessity of additional artificial light support to minimum. A concrete sun barrier (canopy roof) limits heat gains, stabilizes humidity on the right level and allows air-conditioning units to work as an additional installation, occasionally and locally lowering interior temperature. The building is also equipped with integrated system of collection and usage of rainwater. Those noticeably decrease ecological footprint of the terminal, causing substantial operational savings at the same time.

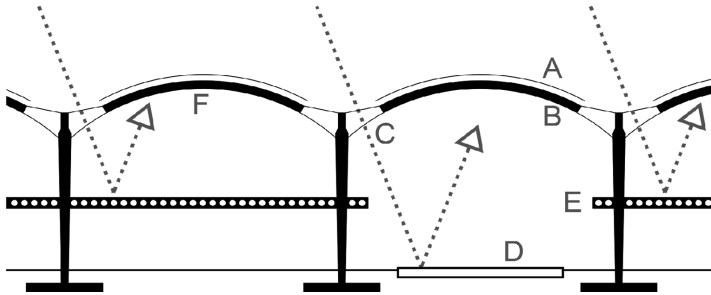


Fig. 2. Cross section of Queen Alia International Airport (Amman, Jordan): (A) photovoltaic panels collecting solar energy, (B) lightweight concrete shell roof structure capturing sunrays and preventing from building overheating, (C) skylights allowing sunlight penetration into the building, (D) interior bright floors reflecting sunlight for better micro-climate, (E) patios for better natural light distribution on all building levels, (F) bright ceilings for better natural light dispersion

### 3.2. Wrocław Airport, Strachowice near Wrocław, Poland

Wrocław's Airport, (completion in 2012), also follows the 'Big shed' [4] pattern for airport construction. Although smaller in size (about 2 million passengers per annum) than Queen Alia airport, it incorporates some of the ideas into design. Lightweight, wavy structure

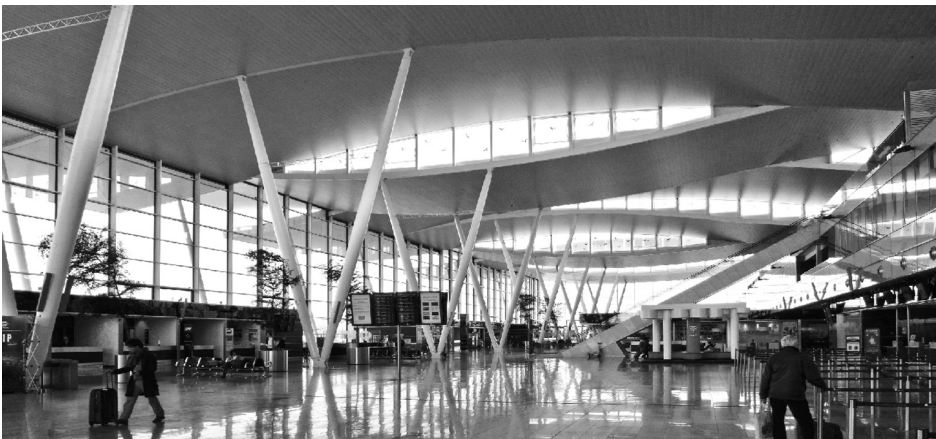


Fig. 3. Wrocław Airport, as an example of Stansted's typology multiplication

of the roof, with vertically situated windows, cleverly brings in sufficient amount of daylight, protecting main hall from direct sun insulation at the same time (see Fig. 3). Adequate volume of the interior prevents from overheating.

#### 4. Multi-criteria certification in airport terminal designs

As today's architecture and building systems become extremely sophisticated, an increasing percentage of investors decide to validate their building's performance by obtaining a certain type of multi-criteria certification<sup>2</sup>. Airports, as a prominent investments in scale of the city, region or even country, are also very often subjected to certification.

Airports' certification is currently mostly developed in United States and, consequently, conducted in LEED Certification system. Many existing airport terminals in U.S. are undergoing renovations and improvement works. Hence, certification of them is based on the *Building Operation + Maintenance*<sup>3</sup> system. The most common enhancements for airports are: renewable energy generation (solar panels), water management (low-flow fixtures, water reuse, draught-tolerant landscaping), natural ventilation and sun access, as well as usage of low volatile and natural finishing materials. Undertaking other actions and renovations is subject to external conditions and preceded by necessary SWOT analysis.

Among the examples of new airport designs, certain number of certified buildings can be distinguished. Recently revealed conceptual design of Mexico City Airport shows the complex and far-reaching development of Stansted's idea, aiming to meet *LEED Platinum* certification standards. Although the project is in very early phase, first descriptive visualizations (see Fig. 4) of the idea, together with other published materials (videos, articles) clearly show that sustainability and high energetic efficiency are the main goals that are to be achieved in the design (materials, building performance, building energy consumption, etc.) and later – during construction (high standard of construction site development, protection of the environment and surroundings during construction).

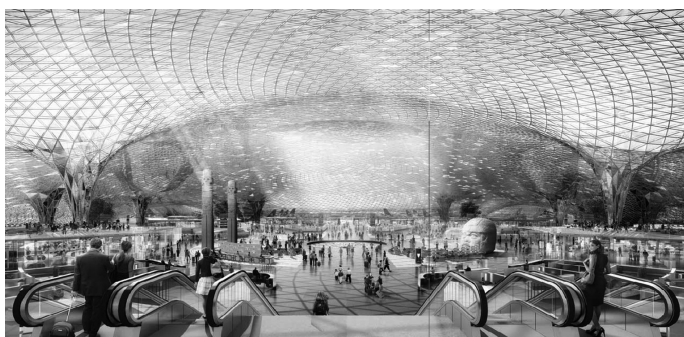


Fig. 4. Mexico City Airport (conceptual design) terminal aims to meet *LEED Platinum* certification standards. Source: <http://www.fosterandpartners.com/>

<sup>2</sup> The widest known certification systems for the building is *LEED*, *BREEAM* and *DGNB*. By evaluating elements of the investment process, they systematize advantages and disadvantages, illustrating building's general performance in terms of sustainability and Life Cycle analysis.

<sup>3</sup> A subgroup of *LEED* certification.



## 5. Conclusions

The progress in technology and building techniques is clearly visible, and so is the society demand for sustainable development. The following conclusions regarding airport design tendencies can be formulated on the basis of presented research:

- Stansted sustainable airport terminal design can clearly be called a model solution for the past 30 years and recent developments;
- Multi-criteria certification becomes popular among airport terminal buildings due to rising ecological society awareness;
- Stansted model further development, combined with conscious sustainable design process subjected to certification seems to set path for the future strategic planning decisions.

## References

- [1] Longhurst J., Gibbs D. C., Raper D. W., Conlan D.E, *Towards sustainable airport development*, Environmentalist, vol. 16, Issue 3, September 1996, 197–202.
- [2] Foster N., *Reinventing the Airport*, 1996, <http://www.fosterandpartners.com/>
- [3] Celadyn W., Duliński W., *The new airport typology. Architectural interventions towards travel time optimization*, 3<sup>rd</sup> Annual International Conference on Architecture and Construction Engineering, Conference Proceedings, Singapore 2015.
- [4] Pryce W., *Big shed*, Thames & Hudson Ltd, London 2007.
- [5] Caves R.E, Gosling G. D., *Strategic Airport Planning*, Pergamon, New York 1999.

IRENA ICKIEWICZ\*, EWELINA KOWALCZUK\*\*

## PASSIVE BUILDING – VERIFICATION OF ACHIEVED EFFECTS

### BUDYNEK PASYWNY – WERYFIKACJA UZYSKANYCH EFEKTÓW

#### Abstract

The article presents a passive building to be used for office purposes that is under construction in Podlaskie region. The building has been designed to meet the characteristics of a passive building – i.e. compact shape, mechanical ventilation with heat recovery, ground heat exchanger, tight external partitions with an indicator  $U < 0.15 \text{ W}/(\text{m}^2\cdot\text{K})$ , heat pump, solar collectors. Calculation indicator of useable energy demand for heating purposes is  $< 15 \text{ kWh}/\text{m}^2\cdot\text{a}$ . In order to verify the achieved effects the building was subjected to tightness test and infrared camera tests are also planned. The building is constructed by the Podlaskie Passive Building Center as part of a project funded by the European Regional Development Fund.

*Keywords: passive building, project guidelines, verification, envelope tightness*

#### Streszczenie

W artykule przedstawiono realizowany w województwie podlaskim budynek pasywny z przeznaczeniem na cele biurowe. Budynek został tak zaprojektowany, aby spełniał cechy budynku pasywnego – zwarta bryła, wentylacja mechaniczna z odzyskiem ciepła, gruntowy wymiennik ciepła, przegrody zewnętrzne szczelne o współczynniku  $U < 0,15 \text{ W}/(\text{m}^2\cdot\text{K})$ , pompa ciepła, kolektory słoneczne. Obliczeniowy wskaźnik zapotrzebowania na energię użytkową na cele grzewcze wynosi  $< 15 \text{ kWh}/\text{m}^2\cdot\text{a}$ . W celu weryfikacji uzyskanych efektów budynek poddany został próbie szczelności, planowane są również badania kamerą termowizyjną. Budynek jest realizowany przez Podlaskie Centrum Budownictwa Pasywnego w ramach projektu finansowanego z Europejskiego Funduszu Rozwoju Regionalnego.

*Słowa kluczowe: budynek pasywny, założenia projektowe, weryfikacja, szczelność obudowy*

**DOI: 10.4467/2353737XCT.15.390.5021**

\* DSc. PhD. Eng. Irena Ickiewicz, Department of Building Basis and Building Physics, Faculty of Civil and Environmental Engineering, Białystok Technical University.

\*\* MSc. Eng. Ewelina Kowalczuk, PhD Student, Faculty of Civil and Environmental Engineering, Białystok Technical University, Podlaskie Passive Building Center.

## 1. Introduction

Passive house as defined by Wolfgang Feist cit. „is a building with very low energy consumption for heating the interior 15 kWh/(m<sup>2</sup>·year), where the thermal comfort is provided by passive heat sources (residents, electrical appliances, solar heat, heat recovered from the ventilation), the building does not need a separate active heating system. Heating demand is met through heat recovery and reheating the air ventilating the building”. The concept of a passive building was developed 20 years ago by W. Feist and his colleagues at the Institute of Housing and the Environment in Darmstadt, Germany. The first passive building with energy consumption of 10 kWh/(m<sup>2</sup>·year) was built in Darmstadt-Kranichstein in Germany in 1991. Over the subsequent years more residential areas with passive buildings were developed. In 1998, the idea of passive houses was supported by the European Union through the project CEPHEUS (part of the THERMIE program). In Germany, Austria, Sweden and France 250 flats were built in 14 passive buildings. In 2003 in Germany, Austria and Switzerland there were more than 3,000 residential housing units in passive house standard, while in 2014 there were over tens of thousands and the number is increasing very fast [1, 2].

### 1.1. The criteria for passive building

The basic criteria to be met by a passive building are presented in Table 1.

Table 1

**The basic criteria for a passive building**

	Specification	Requirements
1	The energy necessary to heat the area of 1 sqm	< 15 kWh/(m <sup>2</sup> ·year)
2	U-value the heat transfer factor for external partitions	< 0.15 W/(m <sup>2</sup> ·K)
3	Tightness of a building – air exchange rate not (n50)	< 0,6 h-1
4	The maximum reduction of thermal bridges	$\Psi \cong 0$
5	Windows of the heat transfer factor U-value	< 0.8 W/(m <sup>2</sup> ·K)
	Total solar energy transmittance for glazing	$g = 50\%$
6	Efficiency of recuperator for recovery of heat from ventilation	>70%
7	Reduction of heat loss in the process of hot water preparation and supply	
9	Efficient use of electric energy	

## 2. Project guidelines for the passive building completed by the Podlaskie Passive Building Centre (PCBP)

### 2.1. Technical description of the completed passive building

The building is located in the 4th climatic zone, it has two stories and no basement. The block consists of 2 parts: office (passive), made in the standard of passive building and the adjacent on the north side industrial hall made in the low-energy building standard. The total usable area of the building (office + hall) is 2400.86 sqm. Basic data for the office part:

- area (heated)  $A_f = 605.33 \text{ m}^2$ ,
- cubature  $1765.65 \text{ m}^3$ ,
- building area of  $368 \text{ m}^2$ ,
- building height  $7.2 \text{ m}$ ,
- length  $30.17 \text{ m}$ ,
- width  $11.64 \text{ m}$ .



Fig. 1. Office building under construction as part of the EU project (PCBP)



Fig. 2. Heating installations 4 heat pumps brine-water used for heating, ventilation and air-water heat pump for domestic hot water needs

**Thermal characteristics of partitions**

	Specification	U [W/(m <sup>2</sup> ·K)]
1	The floor on the ground – the foundation slab ...+ Styrodur 24 cm	0.108
2	The external walls of lime-sand hollow blocks 25 cm thick 30 cm styrofoam (expanded polystyrene)	0.105
3	Flat roof – channell pllates + extruded styrofoam from 30 to 62 cm (average value)	0.062
4	Triple-glazed windows, low-E glass g(G) = 0.8 (U <sub>w</sub> = 0.8, U <sub>g</sub> = 0.5)	0.76*
5	Aluminium door joinery	0.7
4	Maximum reduction of thermal bridges	

\* including “assembly” thermal bridges

### 2.1.1. Sources of heat

The source of heat for the needs of central heating, ventilation and hot water are 4 brine-water heat pumps and air-water heat pump for domestic hot water.

The source of cooling (passive) are two following sources of heat pumps:

- vertical well (ground probes),
- horizontal collector.

The additional source of cooling are heat pumps (active cooling).

### 2.2. Reduction of demand for heat as a result of increased thermal parameters of external partitions

The reduction of demand for heat in the analyzed building in comparison to such a building in which all the external partitions (including windows) are made in accordance with the WT 2013 was calculated on the basis of formulas stipulated in the Regulation of the Minister of Economy [3] and is given in Table 3.

Table 3

**Compilation of designed and constructed thermal insulation partitions, the achieved effects in comparison to the requirements of the standard**

External partitions				Resulting effect	
Specification	area [m <sup>2</sup> ]	heat transfer coefficient U [W/(m <sup>2</sup> · K)]		reduction ΔQ	
		acc. to WT 2015	constructed	[GJ/year]	toe
External walls	319.6	0.25	0.105	11.26	0.27
Windows	65.2	1.3	0.76	101.74	2.42
Flat roof	351.18	0.2	0.062	14.56	0.35
Floor on the ground	351.18	0.3	0.108	7.58	0.18
ΣΔQ =				135.14	3.22

The resulting energy efficiency in form of heat demand reduction is 135.14 GJ/year, which is 3.22 toe (tons of equivalent oil). The greatest thermal effect was achieved when using windows with improved thermal performance.

### 3. Verification – Tightness test

The measurements were carried out by a professional company which: made a tightness test of the building – Blower Door Test, set the air exchange rate  $n_{50}$ , located the spots of uncontrolled leaks.

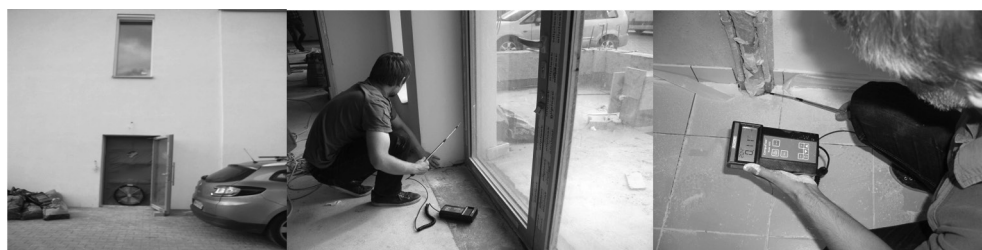


Fig. 3. Tightness test in the office part of the building

As a result of the measurements carried out, an uncontrolled air leakage was found in a few places only. These were mainly the contact points of door frame with the door leaf around the door handle (lock) and contact point of door frame with the fire exit door leaf. After the removal of minor faults the building should meet the required value  $n_{50} \leq 0.6^{-1}$ .

### 4. Analysis of the achieved effects – the compliance with passive building characteristics

The building is under construction, completion date of construction work, commissioning of heating installations and then putting the building into operation is expected in 2015 (the date of the project realization is from 2013 to 2015). Only after a year of operation, a thorough analysis of the achieved energy effects will be possible and after three years the energy marking for the building will be obtainable with measurement method. Table 4 contains the designed and carried out works in regard to the criteria to be met by a passive building.

**Compilation of designed works in regard to the criteria to be met by a passive building**

Specification	Values	Effect	Criteria met
Energy demand for heating 1 sqm	$\leq 15$ kWh/m <sup>2</sup> ·year	Minimum air pollution	Yes *
Thermal insulation of partitions, windows + doors	0.062÷0.105	$\Sigma \Delta Q = 3.22$ toe	Yes
Compact, not segmented block A/V =	0.31	Less heat loss by transfer	Yes
Most windows located on the south orientation	87%	Beneficial (positive) thermal balance, passive gains cover min. 40% of the heat demand	Yes
Windows – cooling in summer	Shutters, green	Minimization of overheating in summer	**
Achieved tightness test	n50 =0.62-1		No
Elimination of thermal bridges (infrared camera test)	~0 (assumption)	Tests to confirm the design objectives have not been made yet	***

\* Verification by direct measurement of energy consumption after 3 heating seasons

\*\* Verification during the operation of the building in summer 2016

\*\*\* Verification will be carried out using the infrared camera (winter)

## 5. Summary and conclusions

This article presents the building designed as a passive building which is under construction in Podlaskie region by Podlaskie Passive Building Centre (PCBP).

On the basis of the analysis of the building design documentation, calculations and participation in tightness test of the building it was found that the building meets the characteristics of a passive building, except for tightness test with slightly exceeded limit values. It is therefore necessary to seal the uncontrolled leaks.

It has been estimated that despite very good thermal insulation of the external partitions the reduction of energy demand in comparison to a standard building will be 3.22 toe only. Thus, the main factor to meet the characteristics of a passive building was achieved through limiting the heat loss through air ventilation heat recovery (recuperator, ground heat exchanger). Ventilation losses are estimated at ~9% of total demand for heat for heating the building.

All the calculation values of U factor, heat demand reduction  $\Delta Q$  and the need for heat for heating purposes, presented in Tables 2, 3 and 4, were made by the authors of this article.

## References

- [1] Feist W., Munzenberg U., Thumulla J., *Podstawy budownictwa pasywnego*, Polski Instytut Budownictwa Pasywnego, Gdańsk 2009.
- [2] *Budynki pasywne – mistrzowie oszczędzania energii*, Krajowy Ruch Ekologiczno-Społeczny, 2006.
- [3] Rozporządzenie Ministra Gospodarki z dnia 10 sierpnia 2012 r. w sprawie szczegółowego zakresu i sposobu sporządzania audytu efektywności energetycznej, wzoru karty audytu efektywności energetycznej oraz metod obliczania oszczędności energii, Dz.U. 2012, poz. 962.
- [4] Rydzewski A. i inni, *Projekt architektoniczny budynku biurowego Łubniki gm. Zabłudów*, ARH+, Białystok 2013.





MARTA NOWAK\*, MICHAŁ KOŁACZKOWSKI\*\*

## NEW DIMENSION FOR STRAW CONSTRUCTION

### NOWY WYMIAR BUDOWNICTWA ZE SŁOMY

#### Abstract

The rising interest in the ecological and energy-saving constructions include the whole life cycle of building – starting from materials and ending with remains that a building leaves in the environment. The holistic view of the ecological construction leads to increase in the interest in constructions made from straw. This article focuses on the technology using straw bales in modern buildings. To a great extent the straw bale method fulfils modern, ecological trends because of low production costs, low energy use during production and biodegradation, among others. The article describes physical parameters specific for straw bale and gives examples of current projects of modern buildings made with this technology.

*Keywords: straw bale, straw, ecological construction*

#### Streszczenie

Rosnące zainteresowanie budownictwem ekologicznym i energooszczędnym obejmuje cały cykl życiowy budynku – od produkcji materiałów do śladów w środowisku, jakie budynek po sobie zostawia. Holistyczna wizja budownictwa ekologicznego doprowadziła do wzrostu zainteresowania budownictwem ze słomy. W artykule skoncentrowano się na technologii wykorzystania w nowoczesnym budownictwie sprasowanych kostek słomy – *straw bale*. *Straw bale* w znacznym stopniu odpowiadają współczesnym, ekologicznym trendom, między innymi, ze względu na niski koszt produkcji, niskie zużycie energii przy produkcji oraz biodegradowalność. W artykule opisano parametry fizyczne cechujące *straw bale* oraz podano przykłady aktualnych realizacji nowoczesnych budynków z wykorzystaniem tej technologii.

*Słowa kluczowe: straw bale, słoma, budownictwo ekologiczne*

**DOI: 10.4467/2353737XCT.15.407.5038**

\* MSc. Marta Nowak, Institute of Architectural Design, Faculty of Architecture, Cracow University of Technology.

\*\* M.Sc. Michał Kołaczkowski, Institute of Building Materials and Structures, Faculty of Civil Engineering, Cracow University of Technology.

## 1. Introduction

Straw is a natural material that has been used in construction for ages. Despite the various possibilities of forming modern wall barriers, straw still remains an attractive material both because of the ecological, economical and usage reasons. Straw constructions are often associated with buildings made in traditional architecture, build in accordance with principles handing down from generation to generation. In this article the authors would like to present products made of straw – straw bale as a building material with specified technical parameters and show that also buildings with modern form that fulfil current technical conditions can be constructed in the straw bale technique.

## 2. Continuity of the tradition

Nowadays more than 1/3 of Earth population still lives in buildings made from clay and straw [1]. Already from the prehistoric times, when people searched for shelter and dug holes in the ground and covered them with dry grass, materials like clay and straw have belonged to the most common building materials. Straw was already used in the oldest type of constructions like plaited frame from cane, dried grass and straw, filled with clay, which can still be noticed in Africa. In ancient times straw was one of the basic ingredients of dried bricks. Straw, as a commonly available material was also used as a material filling load-bearing constructions. In Europe and particularly among Slavic tribes popular were wooden frame structures filled with mixture of clay, straw and wood. Invention of cutting and pressing machine in 1860s revolutionized usage of straw as a separate load-bearing material. In consequence of achieved weight and volume, the pressed straw was stable enough to bear roof and later also the whole floor. This technique was used in America, where Americans within the act on farmsteads started to settle in the lowland area in Nebraska. In this area wood was almost unavailable and because of that the buildings were made from pressed straw formed in rectangular bales – straw bales.

According to the architecture researcher Roger Welsch the oldest documented building made with straw bale technique was a unicameral school raised in 1886 or 1887 [3]. Because unprotected straw was an attractive source of food for local animals, in 1902 the straw walls

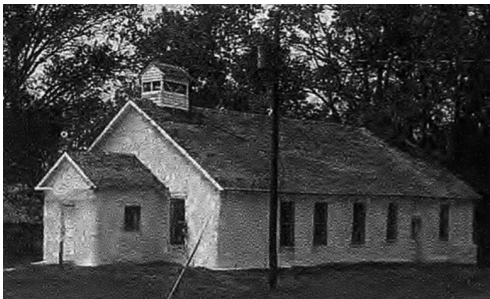


Fig. 1. Pilgrim Holiness Church, Nebraska 1928 [2]

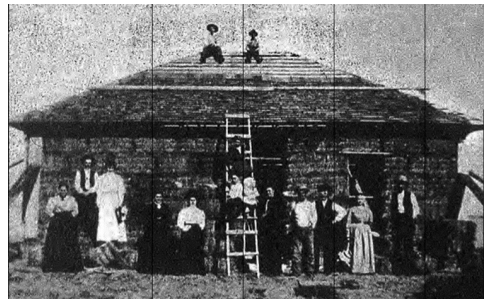


Fig. 2. Simonton House, Nebraska 1908 [2]

began to be covered with cement-lime plaster or clay layer. In Nebraska different type of straw buildings were constructed, starting from utility rooms, through houses and ending with public buildings like churches or offices. This technique was so popular that between 1895 and 1930 70 buildings were built in Nebraska and 13 of them can still be admired today [4]. In Europe the first commercial building made in straw bale technique was constructed in England in 1989. At the height of the ecological movements and an idea of “do it yourself” constructions from straw are getting popular from the beginning of 1990s. Until 1995 about 40 buildings in England were built with this technique, also in France and Norway, whereas in 2001 in Europe more than 400 [5].

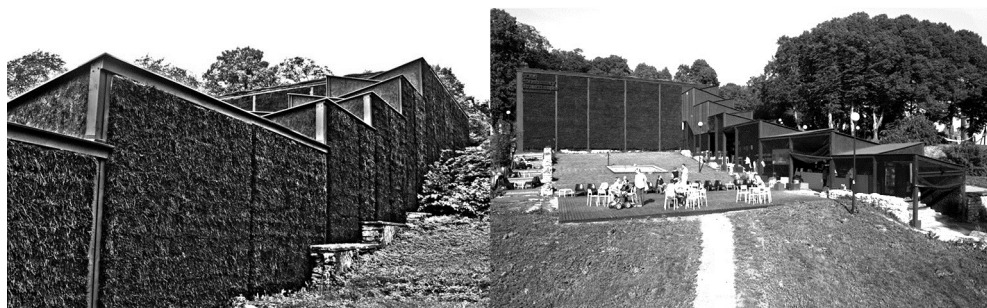


Fig. 3. Temporary Theatre Building – No99 Straw Theatre, Tallinn 2011 [6]

Nowadays both residential and public buildings like schools, warehouses, theatres, offices are made in accordance to the straw bale technique. One of the most innovative solutions was constructed in 2011 in Tallinn and it was a building of theatre with area of 440 m<sup>2</sup> made by the Estonian design office Salto Architects. This is an example of a temporary building that was constructed because of Tallinn being the European Capital of Culture. Modern objects with flat roof and cascade entrance was a wooden form filled with straw blocks. In this building straw blocks were not protected because in authors’ opinion this underlined a natural life cycle of the material. In order to emphasize the meaning of this place (the theatre was located in the city centre, along with old fortifications) the walls of the theatre were coloured with sprays to black [6].



Fig. 4. University Building in Nottingham, Great Britain 2012 [7]

In 2012 in Great Britain, a modern academic building at the Agricultural University in Nottingham was put in use and was built with straw bale technique as designed by Make Architects. The construction of this building consists of wooden, prefabricated castes filled with straw bales. In order to produce straw bales, straw from the cultivable field belonging to university was used and that is located about 200 m from the campus. Construction system was cheap and fast in installation which was perfectly fitting to the ecological and economical policy of the university. Four-storey building with an area of 3000 m<sup>2</sup> has a number of functions: labs, workshops and offices are located here. Among others, modern form is stressed with flat roof and oversized glasses [7].

### 3. Straw as a building material

Straw bale consists of pressed cereals formed in bundles with rectangular and rolled shape. The construction uses bundles in rectangular shape – as a filling material, located between construction elements or used to build load-bearing walls. In Poland straw blocks can be used in buildings as a building product admitted to unit application in a building object according to act from 16th April 2004 on building products (Journal of laws No. 92, unit 881 as amended). To the best materials used in the straw bale technique belongs straw made from wheat, spelt and rye, because it is the most durable product. According to Gernot Minke [4] straw bales can be divided into three groups: small – of about 35 cm height (h), about 50 cm width (w), 50-120 cm length (l), medium – of about 50 cm h, about 80 cm w, about 70–240 cm l and jumbo: about 70 cm h, 120 cm w, 120–300 cm l. Because of the weight of jumbo blocks it is necessary to use some heavy equipment. According to GSBN (Global Straw Building Network) the relative humidity of straw bales during storage and building shall be at the level of below 14%. The bale can fulfil its bear-loading function when its volume density is more than 90 kg/m<sup>3</sup>. It is also recommended that straw is without weeds because they are less durable and decompose much faster than plain straw so they can cause destabilisation of the bales. The pressed straw is characterised by very favourable heat conductivity coefficient  $\lambda$  which helps in using this solution in energy-saving houses. The coefficient  $\lambda$  fits into the range of 0.0337-0.086 W/m·K and depends on density of blocks, structure of fibres (parallel or perpendicular to the direction of heat transition), humidity of straw and, to a limited extend, also on the type of straw [3]. According to the code EN 13823 [8] the straw bales can be included to the combustible products with limited liability to spontaneous combustion – group B. A wall made from straw bales that are covered on both sides with 3-cm-thick clay plaster can achieve certified flame resistance of F-30-B [4]. It should be stressed, that thanks to pressing, the straw gets less flammable in comparison with loose straw and the fire insulation is more efficient because of the proper wall plaster. The basic advantage of wall construction in straw bale technique is forming a favourable microclimate with natural materials, together with limitation of building exploitation costs. Nowadays, straw belongs to the basic materials used in ecological construction among others because of the fact that production of straw blocks absorbs relative small amount of energy 14 MJ/m<sup>3</sup>, almost 77 times lower than production of mineral wool (1077 MJ/m<sup>3</sup>) [3]. The straw bale can be one of the most economical material in construction because of the general availability of straw. Each year Poland produces 29 million tonnes of straw, particularly cereal

and rape straw. Generally it is used in form of feed, bedding or ground fertilizer (because of high silicon content). Nowadays, because of agricultural mechanisation in Poland, surplus of straw is at the level of 12 millions tones each year [9]. All this features are considerate while preparing ecological characteristic e.g. LEED, BREEM that are needed while performing prestigious projects.

#### 4. Example of usage of straw bales in residential building designed in accordance with modern architecture

##### 4.1. General description of building

A house in Raciechowice was designed in wooden construction with straw bales as a material to infill outer walls. As of preparation of this article, this building is in the construction stage. It represents modern architecture trends and propagate houses with minimalistic form, so without eaves, with big glazed surface, where day part is connected with the garden. The problem connected with straw protection from the unfavourable weather conditions is solved here by application of proper finishing materials and thanks to shaping the form with construction overhanging. Popular materials used in modern residential construction with natural materials are connected in this building. The object is designed as a two-storey building, without basement. Dimensions of the building in plan are  $24 \times 14$  m and height in ridge is about 8.5 m. The construction is made from wooden frames, made from truss columns of the exterior walls, roof trusses and floor joists. The distance between frames is 90 cm because of the omission of roof windows and because of the dimensions of straw bales.

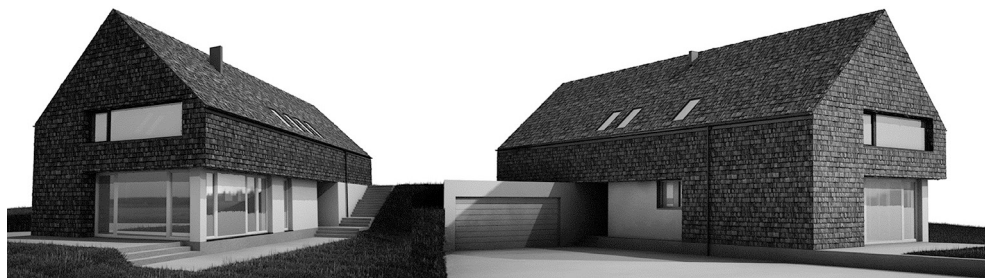


Fig. 5. A detached house, Raciechowice 2015

##### 4.2. Construction of exterior walls

The exterior walls with filling made from straw are characterised by relatively high thickness that normally is greater than 35 cm, which is the result of requirements for the thermal insulation. In case of the house in Raciechowice the exterior walls are 45 cm thick – straw bales with dimensions of 45 cm  $\times$  40 cm height  $\times$  45 cm length were used. It is worth stressing that dimensions of straw bales shall be specified already during the design stage of the building together with proper position of construction elements in such a way

that the smallest number of bales has to be cut during the construction. In case of such thick walls the thickness of foundation walls is problematic as they shall be above the ground level for a minimum of 30 cm in order to protect the straw from rain water. In this object 30 cm thick reinforced concrete foundation walls were used and overhangs were made of the wooden construction from the exterior side by 15 cm. The details concerning support of wall with wooden construction and filling made from straw bales with reinforced concrete foundation wall are presented at Fig. 6. The overhanging of the ground floor wall allowed to install thermal insulation of the foundation walls, without obligation to be moved out from the face of the ground floor wall. Making the foundation walls with width of the ground floor wall would be connected with excessive usage of materials and unnecessary increase of investment costs, as well as with insulation problems.

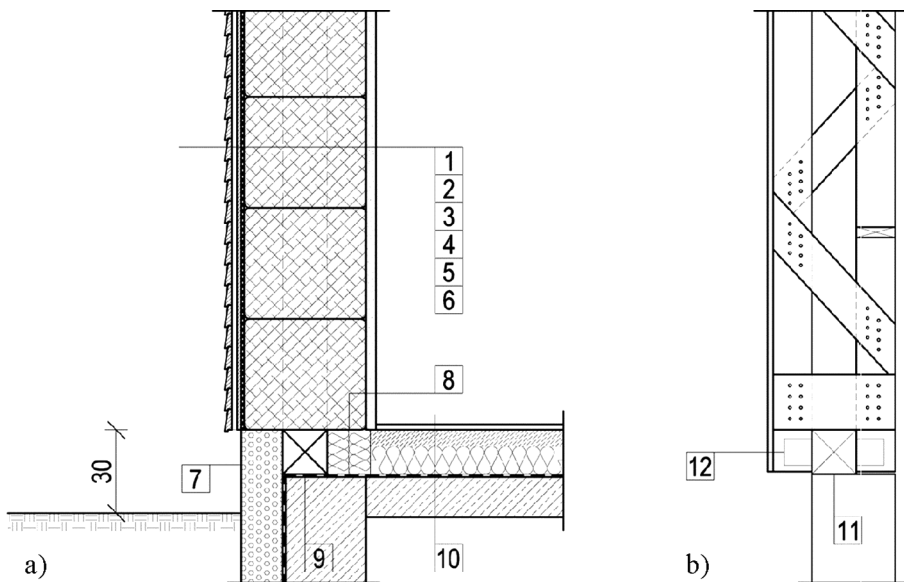


Fig. 6. Details of straw bale wall support on the reinforced concrete foundation: a) finished wall, b) wooden structure made from boards connected with nails; 1 – wooden shingle, 2 – ventilated air gap, 3 – planking, 4 – wind insulation, 5 – straw bales and wooden structure, 6 – clay plaster, 7 – thermal insulation XPS, 8 – thermal insulation EPS, 9 – damp-proof course, 10 – layers of flooring on the ground, 11 – wall plate, 12 – angle bracket

In order to calculate the thermal insulation of the wall the less favourable value of the heat transfer coefficient  $\lambda$  for straw bale that is given in the literature  $\lambda = 0.086 \text{ W/m}\cdot\text{K}$  was assumed. The thermal resistance ( $R$ ) of 45 cm thick straw layer by the assumed secured heat transfer coefficient level, was  $R = 5.23 \text{ m}^2\cdot\text{K/W}$ . In order to achieve the same thermal resistance by application of thermal insulation made from mineral wool, it shall be used 18–23 cm thick layer, depending on  $\lambda = 0.035\text{--}0.045 \text{ W/m}\cdot\text{K}$ . By assuming that price of straw is about 11.10 PLN/m<sup>2</sup> wall (price of the used bale was 2.00 PLN) and the average price of mat made from mineral wool 20 cm thick is 20 PLN/m<sup>2</sup>, the use of thermal insulation with straw is about twice cheaper. The energy consumption by production of 1 m<sup>2</sup> of thermal insulation

in accordance with assumptions described in point 2 of this article is about 30 times lower than in case of straw. Because of the above mentioned reasons and the will to use natural materials, the investors decided to make walls in accordance with the straw bale technique. However, the mineral wool was used to insulate the roof in order to achieve the maximum floor space in the attic by the limited acceptable height of building.

#### 4.3. Shape of roof and finishing of exterior partitions

Traditional roofs are made with eaves with length from 0.5 to 1.0 m. In the modern forms they are designed without eaves because of the aesthetic reasons, so the walls are much more exposed to weather conditions. Critical points are in edge of the roof and walls. The Fig. 7 presents solutions made in house in Raciechowice.

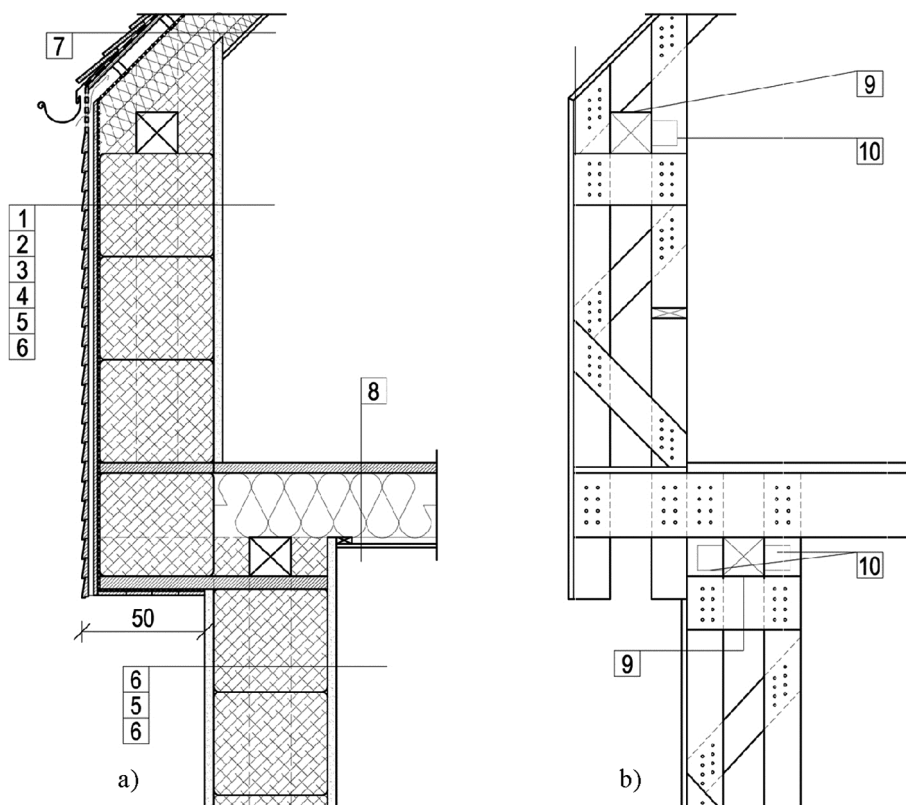


Fig. 7. Detail of first floor wall overhanged towards ground floor wall: a) finished wall, b) wooden structure made from boards connected with nails; 1 – wooden shingle, 2 – ventilated air gap, 3 – planking, 4 – wind insulation, 5 – straw bales and wooden structure, 6 – clay plaster, 7 – roof layers, 8 – ceiling layers, 9 – beam, 10 – angle bracket

In order to protect from the negative influence of rain and melting snow on the walls in the first floor a uniform finishing of walls and roof was designed in the form of a wooden



shingle. The contrast between wood and clay gives opportunity to achieve interesting architectonic effects. Because of that the house in Raciechowice except from application of wooden shingle, consists of some walls in the ground floor that were covered with clay plaster. In order to cover exterior walls in the ground floor with clay plaster an overhang of the first floor construction was made for about 0.5 m. Also the surface of all interior walls was covered with clay plaster. Except from the aesthetic reasons the clay plaster is characterised by a very good moisture vapour permeability. Diffusion resistance factor of the clay plaster can be compared to diffusion resistance factor of lime plaster. The clay plaster that is put inside thank to very good sorption performance helps to regulate proper air humidity in the building [3].

## 5. Summary

In this article the most important physical features of straw bales and walls made from this material are presented which shall be considered while designing buildings. The authors focused on the use of straw as a material to infill load-bearing structure. By proper construction and way of storage, straw bales have parameters that allow to compete with popular materials used to make thermal insulation of a wall, like mineral wool or polystyrene. The examples of public objects in Europe with modern form and residential object constructed nowadays in Poland listed in the article confirm the thesis that the straw bale technique does not have to be associated with traditional architecture from 19th and 20th century, but can be an interesting alternative for modern constructions.

## References

- [1] Kelm T., *Architektura ziemi. Tradycja i współczesność*, Oficyna Wydawnicza Politechniki Warszawskiej, Warszawa 2014.
- [2] Eisenberg D., Hammer M., *Strawbale Construction and Its Evolution in Building Codes*, Building Safety Journal online, 2, 2014, 25–29.
- [3] Swentzell Steen A., Steen B., Bainbridge D., Eisenberg D., *The straw bale house*, Chelsea Green Publishing, Chelsea 1994.
- [4] Minke G., Mahlke F., *Building with Straw. Design and Technology of a Sustainable Architecture*, Birkhäuser, Basel 2005.
- [5] <http://www.compaillons.eu/blog-rfcp/articlelemoniteurfr>, online: 06.06.2015.
- [6] <http://www.salto.ee/no99-straw-theatre/>, online: 06.06.2015.
- [7] <http://www.makearchitects.com/projects/gateway-building/>, online: 06.06.2015.
- [8] EN 13823: 2002-02: *Reaction to fire tests for building products – Building products excluding floorings exposed to the thermal attack by a single burning item*.
- [9] <http://bioenergainvest.pl/>, online: 06.06.2015.

# BUILDING MATERIALS, ENVIRONMENT



AGATA PAWŁOWSKA\*, MICHAŁ ZIELINA\*

## ANALYSIS OF WATER INTAKE SCREEN'S PERFORMANCE UNDER VARIOUS CONDITIONS

---

### ANALIZA PRACY CZERPNI W RÓŻNYCH WARUNKACH

#### Abstract

The article presents the problem of ichthyofauna protection in aquatic ecosystems. One of the possible solutions to protect the fish and fry in the water intakes is the use of properly designed water intake screens. The article presents the results of numerical calculations performed in Autodesk Simulation CFD software considering the performance of water intake screen under various conditions.

*Keywords: water intake, water intake screen, ichthyofauna*

#### Streszczenie

W artykule przedstawiono problem ochrony ichtiofauny w ekosystemach wodnych. Jednym z możliwych rozwiązań stosowanych w celu ochrony ryb i narybku w ujęciach wodnych jest wykorzystanie odpowiednio zaprojektowanej czerpni. W artykule zamieszczono wyniki obliczeń numerycznych wykonanych w programie Autodesk Simulation CFD uwzględniające pracę czerpni w różnych warunkach.

*Słowa kluczowe: ujęcie wody, głowica ujmująca wodę, ichtiofauna*

**DOI: 10.4467/2353737XCT.15.398.5029**

---

\* MSc. Agata Pawłowska, PhD. Student, Assoc. Prof. DSc. PhD. Eng. Michał Zielina, Institute of Water Supply and Environmental Protection, Faculty of Environmental Engineering, Cracow University of Technology.

## 1. Introduction

Water intake, which is the first element of a water supply system plays a fundamental role in its functioning. Therefore, it is especially important to design a proper water intake. Technical and economic aspects have to be taken into consideration as well as the fact that water intake may be a threat i.e. lead to injury or death of fish or fry inhabiting or migrating near the water intake. Potential losses of fish can be caused by its entrainment or impingement. Entrainment takes place when a fish is drawn into a water intake and cannot escape. Impingement occurs when an entrapped fish is held in contact with the intake screen and is unable to free itself. The degree of negative impact of water intake on the ichthyofauna depends on the number, size, arrangement of ichthyofauna and swimming ability of individuals, as well as the water velocity, inflow into the intake and depth at which the intake is installed. Other important factors are the type and size of water intake and the mesh size of a screen [1].

In order to protect fish and fry from entrainment, behavioural or physical barriers are installed in water intakes. The purpose of behavioural barriers is to deter the fish from getting to areas that may pose a threat to them. There are different types of behavioural barriers: louvers, light and sound behavioural devices, air bubble curtains, hanging chains, water jet curtains, electric fields and other [2, 3]. The barriers require an activity from the fish, and therefore their efficiency significantly depends on the ability of fish to swim.

Another, and the most popular, method of protecting fish and fry from entrainment by surface water intakes is the use of physical barriers [2]. These are the intakes equipped with special screens. The use of physical screens in place of water intake is recommended in case of small and medium size water supplies. The appropriate design of a screen is largely dependent upon the species and the size of fish requiring protection. Proper installation and maintenance/cleaning of the screen are also important and ensure satisfactory operation of the screen [1]. The screens can come in different shapes. These can be flat screens with circular or square cross section and box or cylindrical screen. According to [2] when a screen has round mesh holes, the size of mesh depends on the size of fish and fry and should be lower than 2.38 mm for fry and lower than 6.53 mm for fish with length greater than 60 mm. Usually the perforation of such screens is about 50–60% [2, 3], meaning that mesh holes represent 50–60% of the total screen area. The cylindrical screen is the most widely applied submerged screen concept. It consist of fully submerged screen modules placed at the intake and gravity diversion conduits. These designs may include a single screen module or multiple screen modules where larger diversion flow rates are required [4].

## 2. Material and methods

In order to check the performance of water intake screen under various conditions the Autodesk CFD software was used. The programme provides computational fluid dynamics (CFD) simulation, which is a simulation technique that mathematically simulates fluid flow and heat transfer.

CFD simulation works by iteratively solving mathematical approximations of the Navier-Stokes and Energy Equations to reach the solution. The software iterates these equations over the entire simulation model until an unchanging (converged) solution is attained.

The  $k$ -epsilon turbulence model is the most common model used in CFD to simulate mean flow characteristics for turbulent flow conditions. It is a double equation model which gives a general description of turbulence by means of two transport equations. It is typically more accurate than the constant eddy viscosity model, but more computationally intensive and slightly less robust. It is not as resource intensive as the RNG model (based on Re-Normalisation Group methods), but still provides good results. The  $k$ -epsilon turbulence model's equations are as follow:

For turbulent kinetic energy  $k$ :

$$\frac{\partial(\rho k)}{\partial t} + \frac{\partial(\rho k u_i)}{\partial x_i} = \frac{\partial}{\partial x_j} \left[ \frac{\mu_t}{\sigma_k} \frac{\partial k}{\partial x_j} \right] + 2\mu_t E_{ij} E_{ij} - \rho \epsilon \quad (1)$$

For dissipation  $\epsilon$ :

$$\frac{\partial(\rho \epsilon)}{\partial t} + \frac{\partial(\rho \epsilon u_i)}{\partial x_i} = \frac{\partial}{\partial x_j} \left[ \frac{\mu_t}{\sigma_\epsilon} \frac{\partial \epsilon}{\partial x_j} \right] + C_{1\epsilon} \frac{\epsilon}{k} 2\mu_t E_{ij} E_{ij} - C_{2\epsilon} \rho \frac{\epsilon^2}{k} \quad (2)$$

where:

- $\rho$  – fluid density,
- $t$  – time,
- $x_i, x_j$  – coordinates,
- $u_i$  – velocity component in corresponding direction,
- $E_{ij}$  – component of rate deformation,
- $\mu_t$  – eddy viscosity,
- $\sigma_k, \sigma_\epsilon, C_{1\epsilon}, C_{2\epsilon}$  – adjustable constants.

The first step is to create a geometry. It was assumed that the water intake screen is cylindrical. The water intake screen's (part of the screen where water enters) dimensions are as follows: diameter – 500 mm, length – 1000 mm.

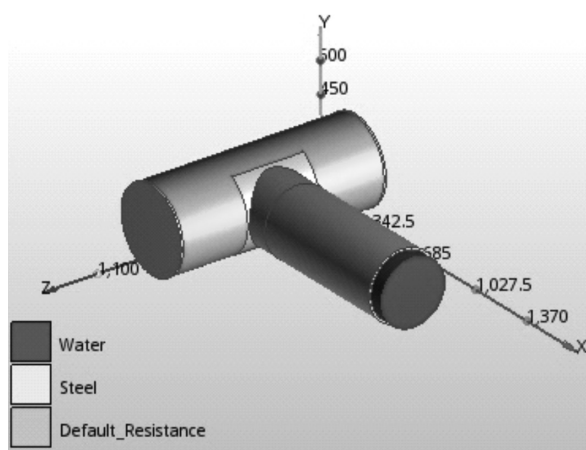


Fig. 1. Geometry model

Then a material of each part of the screen was determined and added. The screen material is stainless steel 304. As it does not affect the results of the simulation while it helps to reduce the analysis time, it was assumed that the resistance of the main part of the screen is 50% instead of taking into account huge amount of round mesh holes. Water flows into the screen through permeable surface (Default\_Resistance in the Fig. 1), the rest part of the screen is impermeable. Outflow surface of the water is named “water” in the Fig. 1.

The next step is to define boundary conditions. It was assumed that the water intake screen is installed in the tank on the depth of 3 m. The appropriate pressure and the outflow from the screen were assumed as the boundary conditions.

The pressure was calculated as:

$$p_{tot} = p_0 + p_h = p_0 + \rho \cdot g \cdot h \quad (3)$$

where:

- $p_{tot}$  – pressure [Pa],
- $p_0$  – atmospheric pressure – 101325 [Pa],
- $\rho$  – water density [ $\text{kg}/\text{m}^3$ ],
- $g$  – gravitational acceleration,  $h$  – depth [m].

Simulations were done concerning that water is an incompressible fluid and that there is a steady state.

Simulations were done in order to check the inlet velocity and the approach velocity values according to the USA guidelines [2] presented in the Tab. 1.

Table 1

**The acceptable inlet velocity and the approach velocity according to the USA guidelines [2]**

Fish/fry size [mm]	Approach velocity measured 8cm in front of the screen [m/s]	Inlet velocity [m/s]
Fry < 60	$\leq 0.06$	$\leq 0.15$
Fish $\geq 60$	$\leq 0.12$	

### 3. Results

There were simulations of two scenarios performed. In the first one it was assumed that outflow from the screen is 250  $\text{m}^3/\text{h}$ , then the average inlet velocity equals to 0.15 m/s. The second one concerns outflow increased to 320  $\text{m}^3/\text{h}$ .

The parameter especially important in terms of ichthyofauna protection is the approach velocity measured 8cm in front of the screen [2]. The results of approach velocity along Z-axis ( $X = 200$ ,  $Y = 250$ ,  $Z$ ) are presented in the Fig. 2 for Scenario 1.

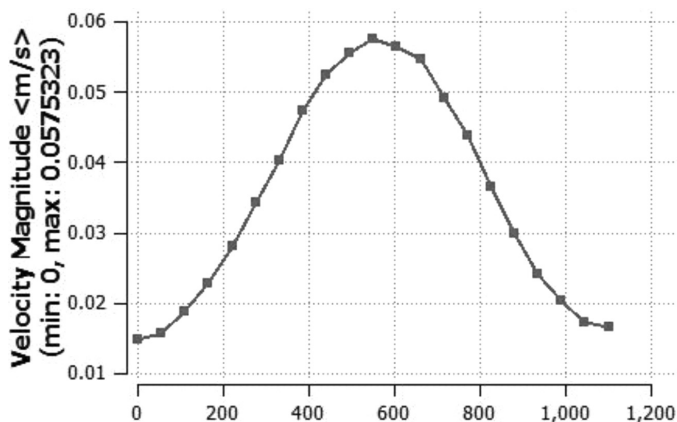


Fig. 2. Velocity distribution in Scenario 1 along Z-axis 8 cm in front of the screen

It can be seen that the maximum velocity value (0.058 m/s) is lower than the maximum acceptable approach velocities presented in the Tab. 1 for fish and fry as well.

The outflow from the screen is increased what is checked in Scenario 2. When the outflow increases to 320 m<sup>3</sup>/h the average inlet velocity equals to 0.18 m/s. The pressure and degree of perforation remains unchanged. The approach velocity distribution is shown in the Fig. 3.

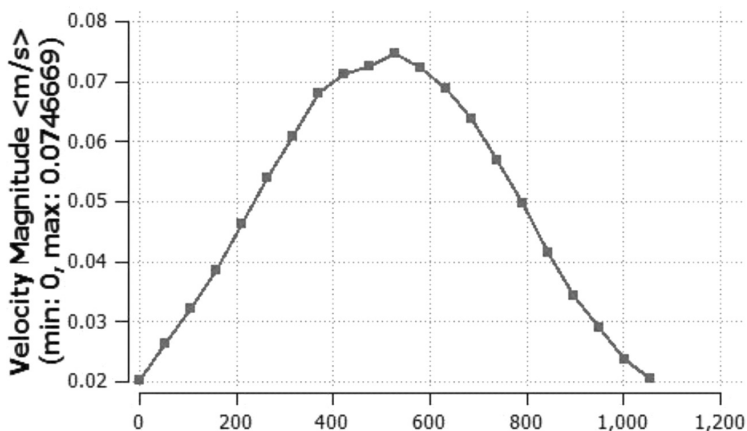


Fig. 3. Velocity distribution in Scenario 2 along Z-axis 8 cm in front of the screen

According to the obtained plot shown in the Fig. 3. the maximum velocity equals to 0.075 m/s. It can be said that the increased outflow is safe for fish (with minimal body length of 60 mm) as the velocity is lower than 0.12 m/s. A fry (with body length lower than 60 mm) could be endangered due to entrainment or impingement as the maximum velocity is higher than 0.06 m/s. It is impossible to determine a value of inlet velocity as the CFD programme provides averaged results of velocity on the screen's edge.



Additionally, the results of velocity distribution are shown in the Fig. 4., and Fig. 5. and the pressure drop is presented in the Fig. 6.

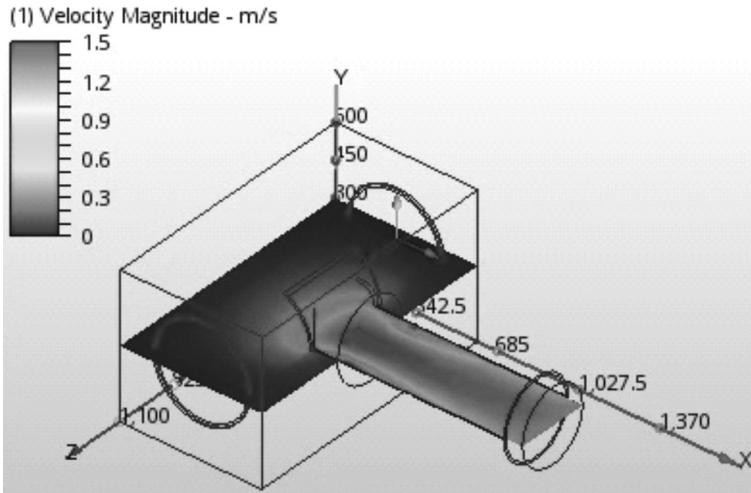


Fig. 4. Velocity distribution in Scenario 2

As expected the velocity is higher inside the manifold (discharge pipe), where it reaches 1.5 m/s unlike in the perforated, inlet part of the screen. In order to show the range of velocity more visible in this Scenario the plot of velocity value along X-axis (X, Y = 250, Z = 500) was done.

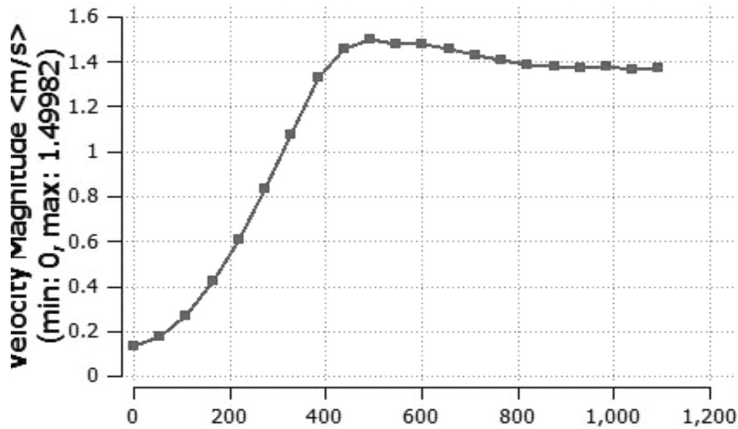


Fig. 5. Velocity distribution in Scenario 2 along X-axis

Another important parameter in the screen work’s analysis is pressure. The Fig. 6. presents pressure drop inside the screen along X-axis (X, Y = 250,500).

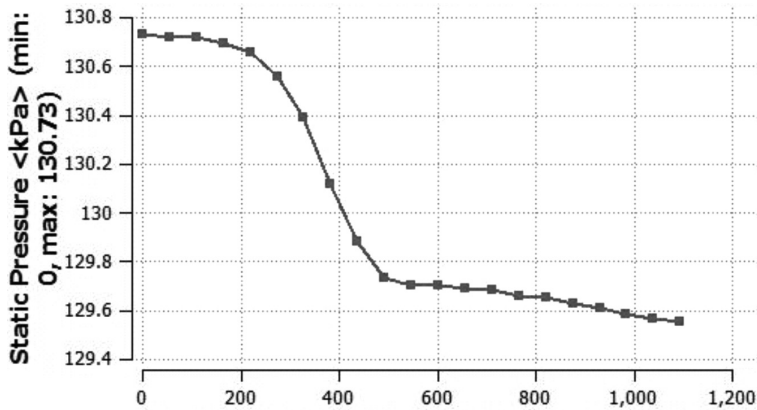


Fig. 6. Pressure drop in Scenario 2 along X-axis

It can be seen that the maximum static pressure is in the perforated, intake part of the screen and it exceeds 130.75 kPa. At the outlet of the screen static pressure is 129.58 kPa. The difference between inlet and outlet equals to 1.17 kPa which means that pressure head loss during flow is 0.12 m.

#### 4. Conclusions

The numerical simulations allow to get qualitative and quantitative results of examined issues. Thanks to the simulation performed it is possible to determine the velocity and pressure distribution. The pressure distribution obtained in accordance with water intake capacity enables to determine pressure loss during the flow inside the screen.

Velocity and pressure are essential parameters in designing water intake screens protecting the fish and fry as well as preventing from retraction of ice, slush ice, debris from the bottom and larger polluting objects in a river.

The conditions presented in Scenario 1 are safe in terms of ichthyofauna protection. The results of velocity range in Scenario 2 are acceptable from hydraulic point of view. However, Scenario 2 can be dangerous for fry as the maximum approach velocity in front of the screen is higher than the acceptable one. Nevertheless, during the design of water intake screen, the size of the fish and fry inhabiting and migrating in the vicinity of the water intake is a key aspect and each case needs to be taken into consideration individually.

#### References

- [1] Freshwater Intake End-of-Pipe, *Fish Screen Guideline*, Department of Fisheries and Oceans, Ottawa, Ontario, Canada, 1995.
- [2] *Fish Protection at Water Diversions. A Guide for Planning and Designing Fish Exclusion Facilities*, Department of the Interior Bureau of Reclamation Denver, Colorado, USA, 2006.

- [3] *Fish Protection Technologies: a Status Report* E.P. Taft, Environmental Science & Policy 3, 2000, S349-S359, USA.
- [4] Jamieson D., Bonnett M., Jellyman D., Unwin M., *Fish screening: good practice guidelines for Canterbury*, NIWA Client Report: CHC2007-092, October 2007.
- [5] Toro E.F., *Riemann Solvers and Numerical Methods for Fluid Dynamics: A Practical Introduction*, Springer, 2009.
- [6] Jiyuan Tu, Guan Heng Yeoh, Chaoqun Liu, *Computational fluid dynamics: a practical approach*, Elsevier, 2008.
- [7] Middlestadt F., Gerstmann J., *Numerical Investigations on Fluid Flow through Metal Screens*, Munich, Germany 2014.

MARTA PLASKACZ-DZIUBA\*, MARCIN CICHOSZ, BARTŁOMIEJ IGLIŃSKI,  
ROMAN BUCZKOWSKI

## AUTOCLAVED AERATED CONCRETE WITH AN ADDITION OF WASTE FROM SEMI-DRY FLUE GAS DESULFURIZATION PROCESS – THERMAL STABILITY AND XRD INVESTIGATIONS

---

### AUTOKLAWIZOWANY BETON KOMÓRKOWY Z DODATKIEM ODPADU Z INSTALACJI PÓLSUCHEGO ODSIARCZANIA SPALIN – ANALIZA TERMOGRAWIMETRYCZNA ORAZ RENTGENOGRAFICZNA

#### Abstract

The article presents the results of research on autoclaved aerated concrete (AAC) produced according to the manufacturer recipe and modified AAC with the addition of waste from the semi-dry flue gas desulfurization installation. Produced cubes of concrete were analysed using thermogravimetry in a temperature regime of 0–1200°C in order to determine thermal stability. Samples were also tested using X-ray diffractometer to determine the differences in the content of tobermorite 1.1 nm, the compound which is responsible for the mechanical properties of tested concrete.

*Keywords: autoclaved aerated concrete, semi-dry flue gas desulfurization, x-ray diffraction, thermogravimetry*

#### Streszczenie

W artykule przedstawiono wyniki badań autoklawizowanego betonu komórkowego (ABK) wyprodukowanego według przepisu producenta oraz zmodyfikowanego ABK z dodatkiem odpadu z instalacji odsiarczania spalin metodą półsuchą. Wyprodukowane kostki betonu poddano analizie termicznej w reżimie temperaturowym 0–1200°C w celu określenia stabilności termicznej oraz badaniu dyfraktometrem rentgenowskim w celu określenia różnic w zawartości tobermorytu 1.1 nm, składnika odpowiedzialnego za parametry wytrzymałościowe betonu komórkowego.

*Słowa kluczowe: autoklawizowany beton komórkowy, odsiarczanie metodą półsuchą, dyfraktometria rentgenowska, termogravimetria*

DOI: 10.4467/2353737XCT.15.401.5032

---

\* MSc. Marta Plaskacz-Dziuba, PhD. Marcin Cichosz, PhD. Bartłomiej Igliński, Assoc. Prof. Roman Buczkowski, Department of Chemical Proecological Processes, Faculty of Chemistry, Nicolaus Copernicus University in Toruń.

## Signatures

- FGD – flue gas desulfurization
- AAC – autoclaved aerated concrete
- AACS – autoclaved aerated concrete standard
- AACM – autoclaved aerated concrete modified
- ABKS – autoklawizowany beton komórkowy standardowy
- ABKM – autoklawizowany beton komórkowy modyfikowany

## 1. Introduction

The waste from the semi-dry flue gas desulfurization (FGD) is currently inapplicable, what makes it an useless material, whose utilization is associated with additional costs. Unlike the waste from wet FGD, where the product is a synthetic gypsum, widely used in industry, mainly in the production of building materials [1]. The applicability of waste from semi-dry FGD in the production of autoclaved aerated concrete could be an interesting alternative for manufacturers [2]. However, the composition of the analyzed, unstable waste whose main component is calcium sulfite, requires tests before usage as a substitute for gypsum.

## 2. Experiment

### 2.1. Waste from the semi-dry flue gas desulfurization

The waste obtained in the semi-dry FGD method consists of calcium sulfite –  $2\text{CaSO}_3 \cdot \text{H}_2\text{O}$  (15–75%), calcium sulfate –  $\text{CaSO}_4 \cdot 2\text{H}_2\text{O}$  (2–30%), unreacted lime –  $\text{CaO}$ ,  $\text{Ca(OH)}_2$  (0–25%), limestone –  $\text{CaCO}_3$  (1–30%), calcium chloride –  $\text{CaCl}_2 \cdot n\text{H}_2\text{O}$  (1–15%), moisture (1–10%) and others (e.g. chlorides, sulfates, silicates of sodium, potassium, magnesium, iron, aluminum). The exact composition depends on a wide range of factors, e.g. type of sorbent, type of fuel used in power station, operating conditions during desulfurization process, and composition of fumes. Due to the high content of sulfate (IV) calcium any possible use as a synthetic gypsum must be subjected to a detailed analysis because of the instability of sulphates on the IV oxidation degree.

### 2.2. Autoclaved aerated concrete production

The studied autoclaved aerated concrete blocks (AACS and AACM) were obtained in the industrial conditions with retaining the existing manufacturer production process parameters [3].

The test product was produced as follows: to 4600 kg of slime with a 64% average content of silica 545 kg of cement was added, 180 kg of lime and 200 kg of gypsum or waste product from the FGD installation. Samples were taken from both the surface and the center

of prepared blocks. Collected research material was triturated in a mortar, and then placed in a hermetic vessel with a capacity of 200 ml.

Samples with a signature G were taken from the top of a particular cube, whereas samples with signature D and S were taken from the center of a tested block. Figure 1 shows a diagram of sampling for analysis.

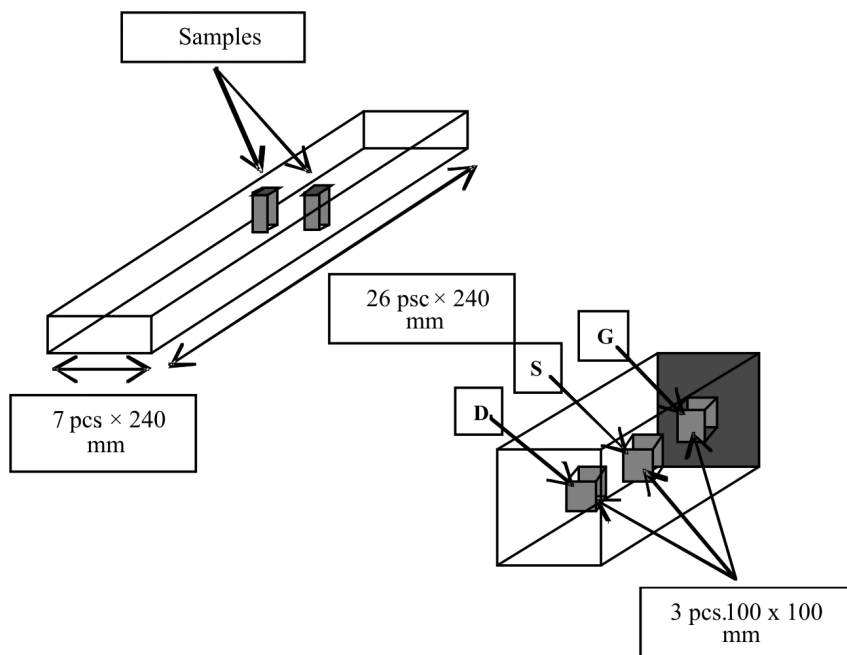


Fig. 1. Diagram of samples for analysis

### 2.3. Termogravimetric analysis

The thermal analysis was performed, for four randomly selected samples of AACS and AACM, to estimate the thermal stability of the produced building materials. Thermograms of the two samples are given in Figure 2. Beton 1 is the sample of AACS, while beton 2 is the sample of AACM.

Thermograms shown in Figure 2 illustrate that the material marked as beton1 and beton 2 have a low moisture content (approximately 3%). The minimal endothermal effect within a temperature range 500–550°C is a result of dehydration of calcium hydroxide. The loss of mass at a temperature of about 650–700°C is caused by decarboxylation. A significant exothermal effect at about 800–850°C is related to transformation of calcium silicate into wollastonite, and there is no change in weight during this process. Decomposition of sulphates occurs only at temperatures of about 1000 °C. For the above reasons, it is allowed to conclude that the tested materials made of AAC are characterized by high thermostability.

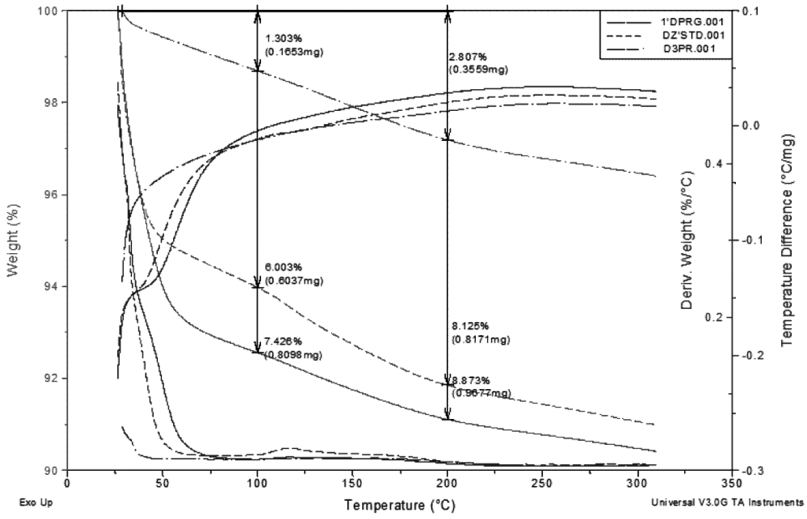


Fig. 2. Thermogram of two randomly selected samples, AACS (beton1) and AACM (beton2)

Figures 3–5 show the results of thermal analysis for the various samples marked as D, S, G respectively for AACS (STD) and AACM (PR and PRG). Analyses confirmed the results for dried material (marking 3) as well as for the material 1 and 2 (1-AACM and 2-AACS).

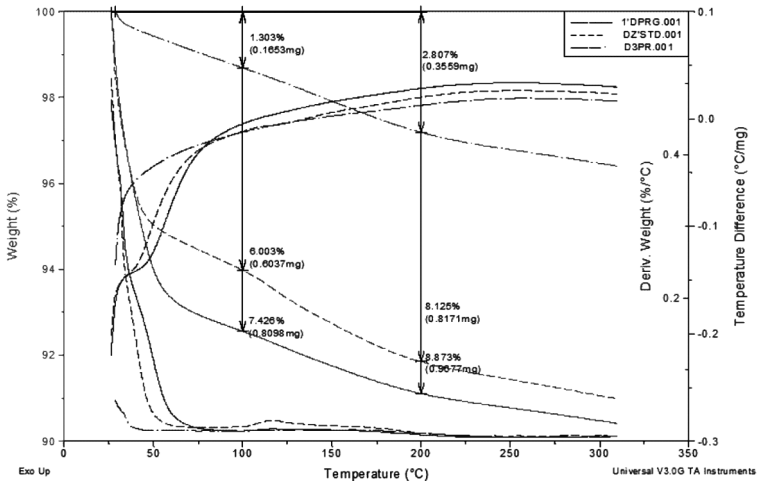


Fig. 3. Thermogram for sample D

Typical flow of thermal processes characterizes the analyzed materials. The release of weakly bound water appears at temperature about 100°C. Afterwards, dehydration of tobermorite and other forms of hydrated calcium silicates occurs at temperature range of 150–200°C.

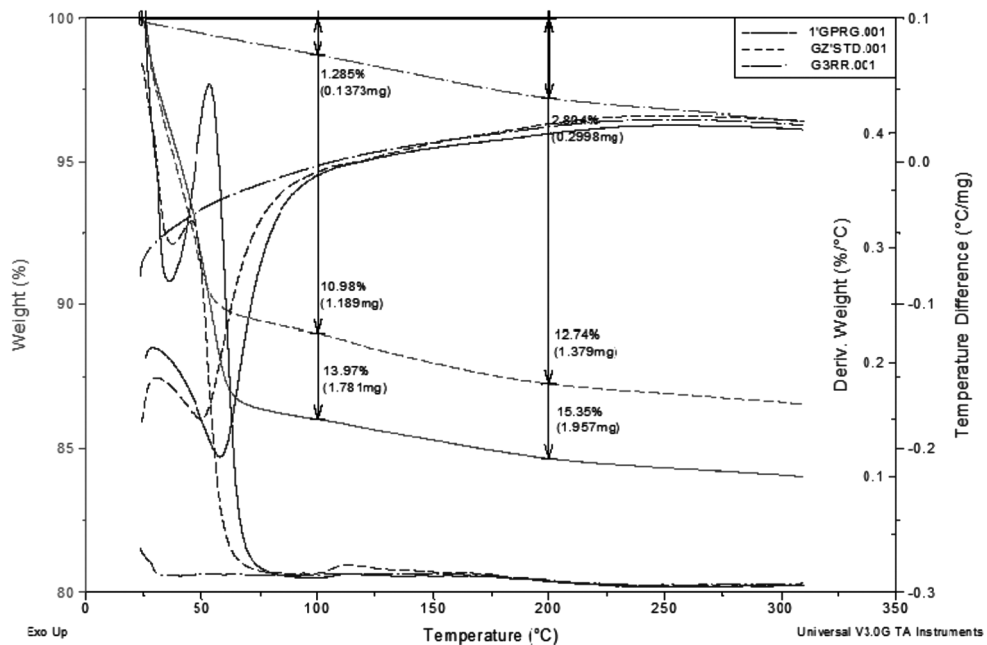


Fig. 4. Thermogram for sample G

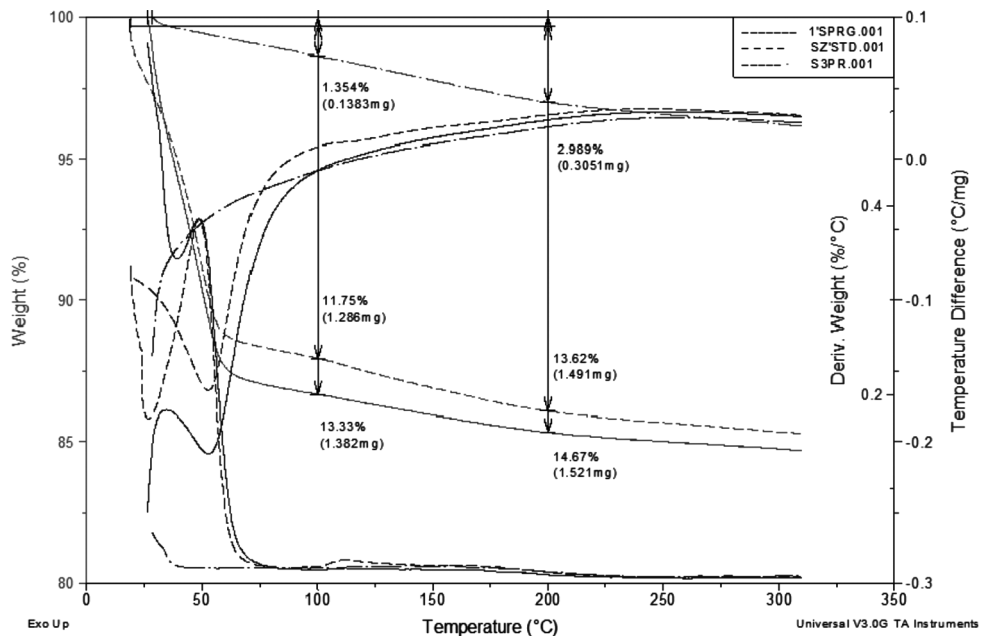


Fig. 5. Thermogram for sample S



Analyzes explicitly show that the sample marked 3 had been dried before testing. Samples D contain less free water up to 200 °C than samples G and S. In the tested temperature range no significant differences between the ABKS A ABKM were detected.

#### 2.4. X-ray diffraction

To analyze the effect of adding calcium sulfite to AAC, the content of tobermorite-1.1nm was taken. Tobermorite is a crystal structure, with chemical formula  $\text{Ca}_5\text{Si}_6\text{O}_{16}(\text{OH})_2 \cdot 4(\text{H}_2\text{O})$ , forming during the process of autoclaving AAC. The presence of tobermorite-1.1nm as a binding material provides a well-structured autoclaved aerated concrete (AAC) with good mechanical properties [4].

Averaged samples for analysis were prepared by taking the material in an amount of about 20g from five different locations of the particular concrete block and milled in an impact mill for 15 minutes. The obtained grist was subjected to diffractometric analysis. Nine measurements were performed for the selected angular range 28–31° for samples with the extension .PR or .PRG with the addition of calcium sulfite and extension .STD with the addition of calcium sulfate [5]. Table 1 summarizes all the results obtained during X-ray diffraction analysis.

Table 1

**Specification of signals and their intensity**

Sample	Intensity [cps] (Position °2Th0)		Average Intensity [cps](Position °2Th)	
	28.9	30	28.9	30
1'D PRG	732	255	690	259
1'G PRG	745	247		
1'S PRG	772	275		
G3 PR	543	202		
D3 PR	756	280		
S3 PR	591	145		
D2' STD	436	219	670	362
G2' STD	681	335		
S2' STD	894	532		

Table 1 shows that the average signal intensity for tested samples, with the addition of calcium sulfite (.PR and .PRG) and with the addition of calcium sulfate, is very similar and their value adjustments are 689.8 and 670.3 cps for angle 28.9 °2Th. Differences in the intensity of the angle °2Th 30 position were observed. Respectively, for AACM average intensity amounts to 259 cps, whereas for AACs it's 362 cps. Figure 6 shows results for 9 tested AAC samples.

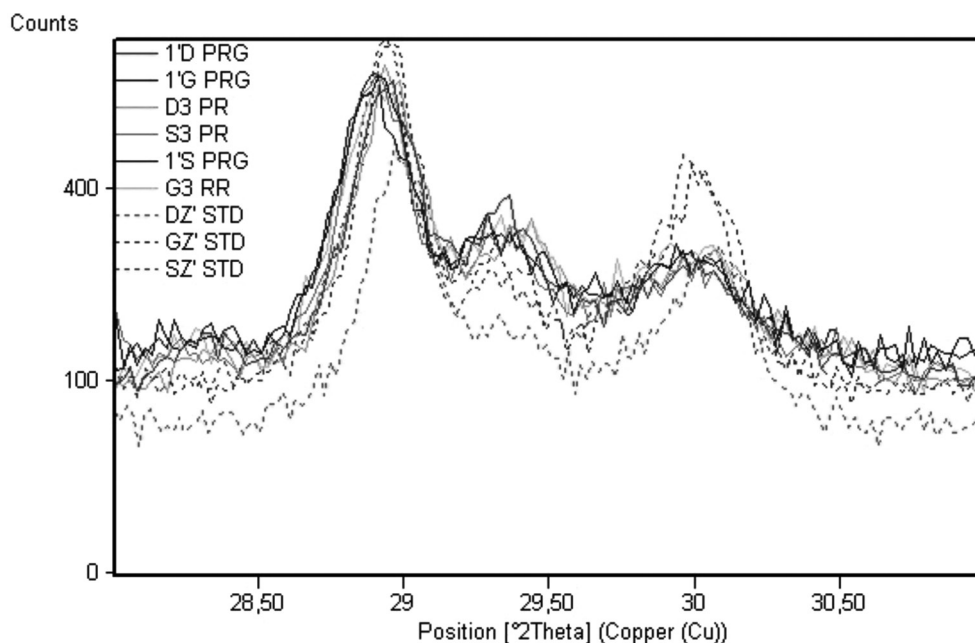


Fig. 6. Comparison of registered diffractograms

### 3. Results and discussion

Obtained thermograms show no significant differences in physicochemical transformations associated with heating of analyzed materials, especially in the area of temperature corresponding to rising and curing batched concrete mix before hydrothermal treatment in the process of autoclaving. Decomposition of sulphates occurs only at temperatures of about 1000°C, which is essential for safe functioning of autoclaves (especially the danger of corrosion due to sulfur dioxide desorption) and during exploitation AAC in the construction works. X-ray powder diffractometry analysis were performed to examine the differences in characteristic signal intensities of tobermorite 1.1 nm in the samples AACS and AACM. The obtained results show that the intensity of the signal for an angle 28.9° is similar for both, ABKS and ABKM, samples and amount to respectively 670 and 690 cps. In comparison, the intensity for an angle 30° differs significantly for the studied materials. For AACS it amounts to 362 cps, whereas for AACM it's 259 cps, what reflects lower content of the tobermorite-1.1 for modified concrete samples. This result may suggest that the addition of semi-dry FGD waste to the AAC has an impact on the formation of this compound in structure of concrete.

## References

- [1] Trzepierczyńska I., *Charakterystyka i możliwość utylizacji odpadów z odsiarczania spalin*, *Ochrona Środowiska*, 1(64), 1997.
- [2] Turnock D., *Environmental problems and policies in East Central Europe: A changing agenda*, *GeoJournal* 54, 2001, 485–505.
- [3] Kikuma J., Tsunashima M., Ishikawa T., Matsuno S., Ogawa A., Matsui K., Sato, *In situ time-resolved X-ray diffraction of tobermorite synthesis process under hydrothermal condition*, *IOP Conf. Series: Materials Science and Engineering* 18, 2011, 022017.
- [4] Jasiczak P., Mikołajczak P., *Technologia betonu modyfikowanego domieszkami i dodatkami*, Wyd. Politechniki Poznańskiej, F1997.
- [5] Hartmann A., Khakhutov M., Buhl J. Ch., *Hydrothermal synthesis of CSH-phases (tobermorite) under influence of Ca-formate*, *Materials Research Bulletin* 51, 2014, 389–396.

ANNA WASSILKOWSKA, KAROLINA KUC, MICHAŁ ZIELINA\*

## A STUDY OF THE COMPOSITION OF CEMENT MORTAR LINING IN WATER AND SEWAGE PIPELINES

### SPRAWDZENIE SKŁADU POWŁOKI CEMENTOWEJ W RURACH WODOCIĄGOWYCH I KANALIZACYJNYCH

#### Abstract

Cementation of iron water and sewage pipes is a standard procedure that is used to ensure internal protection against corrosion. In order to reduce leaching of chemical elements from coating to water, the neutral impact of cement coating on the water is of major importance. In the present study, the elemental composition of the cement mortar lining, taken from the new cast iron pipes with a diameter of 100 and 150 mm, has been investigated. A reference sample was made from Portland cement. Studies using scanning electron microscopy revealed an increased contents of titanium in the sewage pipes coating and also aluminum and alkali in water pipe coatings.

*Keywords: ductile iron pipe, blast furnace cement, Portland cement, centrifugal lining, energy dispersive spectroscopy*

#### Streszczenie

Cementowanie żeliwnych przewodów wodociągowych i kanalizacyjnych jest standardowym zabiegiem stosowanym w celu zapewnienia wewnętrznej ochrony przewodów przed korozją. W celu ograniczenia stopnia ługowania zanieczyszczeń z wykładziny do wody szczególne ważne jest, aby powłoka zachowywała się neutralnie w stosunku do wody, z którą ma kontakt. W obecnej pracy zbadano skład pierwiastkowy powłok cementowych pobranych z nowych rur żeliwnych o średnicy 100 i 150 mm. Próbkę porównawczą wykonano z cementu portlandzkiego. Badania z użyciem skaningowego mikroskopu elektronowego ujawniły podwyższoną zawartość tytanu w powłokach w przewodach kanalizacyjnych oraz glinu i alkaliów w powłokach w rurach wodociągowych.

*Słowa kluczowe: rury żeliwne, cement hutniczy, cement portlandzki, cementowanie wirowe, spektrometria dyspersji energii*

**DOI: 10.4467/2353737XCT.15.404.5035**

\* PhD. Eng. Anna Wassilkowska, MSc. Eng. Karolina Kuc, Assoc. Prof. DSc. PhD. Eng. Michał Zielina, Institute of Water Supply and Environmental Protection, Faculty of Environmental Engineering, Cracow University of Technology.

## 1. Introduction

Ductile iron pipes used in water and wastewater are supplied as standard with cement-mortar lining [1–4]. The function of cement-mortar lining is to reduce the susceptibility to corrosion and the frictional resistance of pipelines. Cement coating must meet a number of standard requirements [3, 4] for example, have the appropriate thickness, cracks width, compression resistance. Due to the quality of drinking water and coating durability, numerous studies are devoted to the investigation of chemical elements leaching from coating to water [5–7].

Recently [8], more attention has been paid to the structural characterization of factory cement coatings. In contrast to the cement-mortar applied on construction site, they exhibit not only better density, but also a gradient distribution of the components across the coating thickness. The mortar is poured into pipe spinning with high rotation velocity. This causes separation of the coarse concrete components on the wall of the pipe and on the coating surface – solidification of dense and very smooth layer consisting of cement laitance. Because the cement binder is a critical component of the concrete, it can be expected that under the same operation conditions of cemented iron pipes, changes of technological properties of cement coating will be different for a homogeneous and layered structure.

Regardless of whether the concrete mixture was applied on the new iron pipes, or the renovation of old pipes was performed, the corrosion resistance of coating is determined by the type of cement used and the tightness and strength of hardened concrete (properties varying considerably over time) [9]. For factory cement lining of iron water pipes, the blast furnace cement is used, as its chemical and mineral composition have a smaller impact on the quality of tap water than Portland cement mortar [7]. The wastewater pipes are used with alumina cement mortar lining, which has better resistance to fermentation tanks and certain acids, as well as increased wear resistance under normal flow conditions [10]. The use of aluminous cement for water pipes is not recommended, as it may cause a dangerous increase in the concentration of alumina dissolved in water [5–7].

The aim of this study was to investigate the chemical composition of the coating cement for water pipes supplied by different manufacturers and compare the results with studies lining for a typical sewer pipe.

## 2. Experimental method

The materials for the study consisted of three cast iron pipes from different suppliers, lined with standard cement mortar coating. The collected samples were determined as follows: *E* and *S* – coating of water pipes with a diameter 150 mm, *B* – a coating of sewer pipe with a diameter 100 mm. Macroscopic inspection included visual inspection of the appearance and colour of the lining surface (Fig. 1) and measurement of coating thickness using a micrometer screw (Table 1). It was assumed, that the comparative test will be made with Portland cement. The sample M was taken from the pipes, which are part of the laboratory equipment, as described in Ref. [6]. Concrete mix was prepared from cement CEM I 42.5R and fine sand in relation 1:1 with the addition of water, which guaranteed water-cement ratio  $w/c = 0.3$ . The coating was applied manually in the laboratory, hence the lack of segregation of components in its cross section.

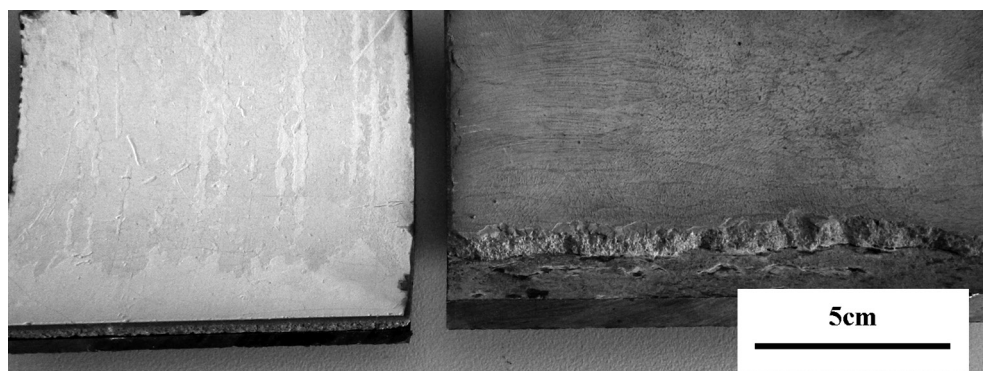


Fig. 1. Image of the factory cement lining: specimens S (on the left) and B (on the right)

Table 1

**Dimensions of investigated material: DN – nominal pipe diameter;  
G<sub>1</sub> – lining thickness; G<sub>2</sub> – laitance thickness**

Specimen	DN	G <sub>1</sub> , mm	G <sub>2</sub> , mm
M	–	6.0	–
E	150	8.2	1.8
S	150	5.3	2.0
B	100	5.0	1.4

The chemical composition of the surface of the cement-mortar lining has been analyzed using a scanning electron microscope HITACHI S-3400N, equipped with an energy dispersive X-ray spectrometer (EDS) manufactured by *ThermoScientific*. Microscope mode is variable vacuum, allowing to test the natural state of surface of an electrically non-conductive specimen. A single area of analysis was  $2.5 \times 1.5$  mm. A similar study was carried out for the comparative coating *M*.

### 3. Results and discussion

For various cements based on Portland cement clinker, the difference in the composition of the upper layer of the cement coating surface has been expected, due to differences in the composition and the respective proportions of clinker minerals, undergoing binding and hardening. Table 1 shows that the estimated thickness of the cement laitance ( $G_2$ ) does not depend on the overall thickness of the coating ( $G_1$ ). Microscopic photographs of the Surface coating (Figs. 2–5) disclosed qualitatively different characteristics: open porosity (*M* and *S*), small cracks (*E* and *S*) and roughness (*M* and *B*). On the Surface of the sample *E* showing a part of the slag, which confirms the use of cement of CEM III class. For comparison only of the Surface of the sample – the typical spectrum is given in the next picture to the structure from Fig. 2 to Fig. 5. More particularly, for spin-coating applied, it is the cement laitance.

Comparative coating *M* matured in different natural conditions than factory-allied, but according to the literature [11, 12], should show typical composition of clinker: 62–68% CaO, 18–25% SiO<sub>2</sub>, 4–8% Al<sub>2</sub>O<sub>3</sub>, 2–4% Fe<sub>2</sub>O<sub>3</sub>, 0.5–0.6% MgO, 0.8–3.0% SO<sub>3</sub>, 0.4–3.0% N<sub>2</sub>O+K<sub>2</sub>O. For Portland cement, hydrated silicates, aluminates and ferrites calcium proceeds to form ettringite-like compounds, portlandite (called “slaked lime”), and tobermorite silicate phase (gel substance with high fineness) [9]. It is known that, in contrast to Portland cements (*M*), blast furnace cement contain less lime, more silica and generally more alumina [9]. The calculation of the composition of the oxide phase in Portland cement clinker is pointless here, since the analysis of coatings was carried out by semi-quantitative method – the results are compared in Table 2.

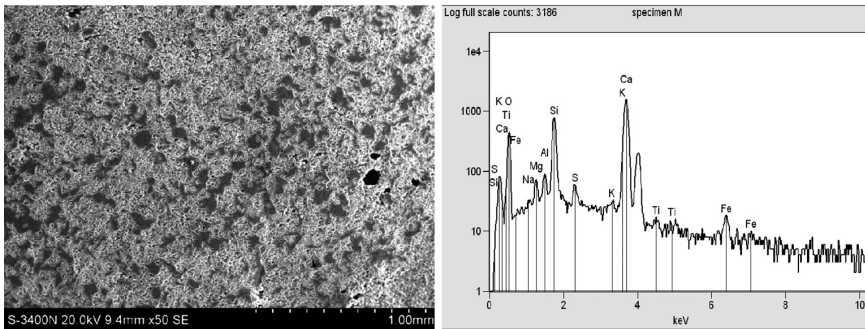


Fig. 2. Surface analysis of a reference Portland cement lining (specimen M)

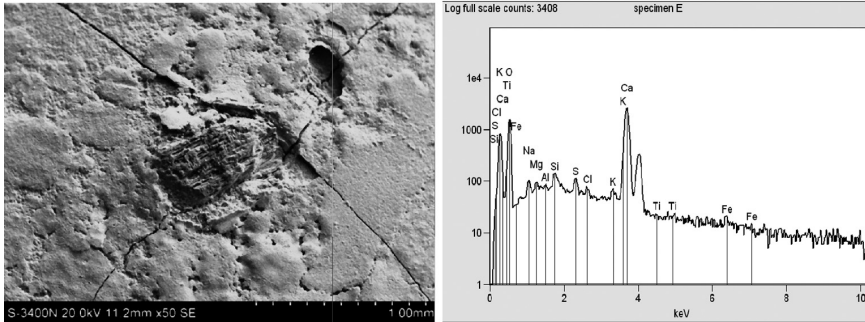


Fig. 3. Surface analysis of a cement-mortar lining from water supply pipe (specimen E)

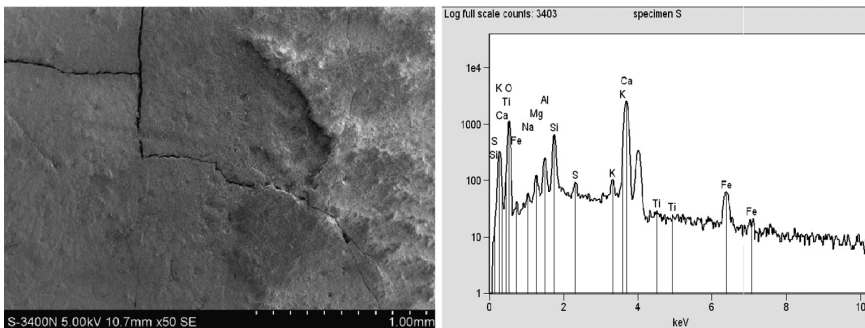


Fig. 4. Surface analysis of a cement-mortar lining from water supply pipe (specimen S)

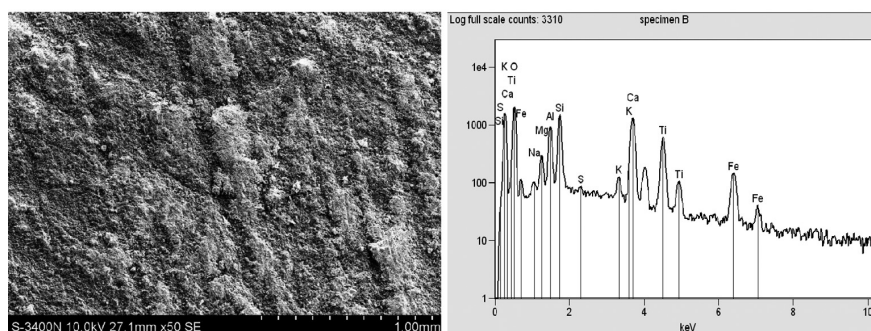


Fig. 5. Surface analysis of a cement-mortar lining from sewage pipe (specimen B)

Table 2

#### Results of quantitative EDS analysis of cement-mortar lining surface

Specimen	Elemental composition [weight %]										
	<i>Ca</i>	<i>Si</i>	<i>Al</i>	<i>Fe</i>	<i>Ti</i>	<i>Mg</i>	<i>Na</i>	<i>K</i>	<i>S</i>	<i>Cl</i>	<i>O</i>
M	32.0	9.5	0.8	0.8	0.2	0.7	0.2	0.1	0.6	0.0	55.1
E	26.8	1.3	0.5	0.5	0.0	0.4	0.8	0.5	0.6	0.2	68.2
S	27.6	4.2	1.7	1.6	0.1	0.8	0.3	0.5	0.3	0.0	63.0
B	10.7	7.5	4.9	2.9	7.4	1.5	0.7	0.5	0.1	0.0	63.7

The results for water pipe linings showed that specimen (*S*) contains more silica and iron-aluminate than the specimen (*E*); the linings have also different content of magnesium, sodium and sulfur. The composition of cement lining (*B*) shows a large amount of aluminate phases, higher concentration of Mg and, above all, the presence of Ti in quantities equal to Si. According to [13] titanium dioxide is „self-cleaning” on concrete surfaces, neutralizes organic compounds and prevents the emergence of fungi and lichen on the air.

#### 4. Conclusions

The composition of the various cement-mortar linings applied internally to ductile iron pipes has been examined by means of scanning electron microscope. It was found by comparative method that:

- Centrifugally lined in a factory cement-mortar linings have a significantly lower open porosity and better surface smoothness, than those applied by projection method (on site, in the lab), through macroscopic separation of the cement-laitance layer;
- Sewerage coating is different from water coating not only in color and absence of cracks; in addition to higher aluminum content, a high concentration was measured for titanium, which in the form of nanooxide acts as a photo catalyst in special concretes;



- Factory cement-mortar lining of water pipes exhibit several-fold differences in aluminum and iron content. In both specimens chromium and lead were not detected;
- In contrast to Portland cement, the factory coatings exhibited higher alkaline content.

## References

- [1] Dąbrowski W., Żuchowski D., *Powłoki cementowe jako wewnętrzne zabezpieczenie rurociągów przed korozją*, Gaz, Woda i Technika Sanitarna, 9, 2013, 371–375.
- [2] Bonds R.W., *Cement mortar linings for ductile iron pipes*, Ductile Iron Pipes Association, DIP-CML/3-0.5/3.5M, 2005.
- [3] PN-EN 598+A1:2010, Rury, kształtki i wyposażenie z żeliwa sferoidalnego oraz ich połączenia do odprowadzania ścieków – Wymagania i metodyka badań.
- [4] EN 545:2010, Ductile iron pipes, fittings, accessories and their joints for water pipelines – Requirements and test methods.
- [5] Meland I.S., *Durability of mortar linings in ductile iron pipes*, National Research Council Canada, 1999, 170–179.
- [6] Zielina M., Młyńska A., Żaba T., *Przenikanie zanieczyszczeń z wyprawy cementowej do wody pitnej w przewodach wodociągowych po cementowaniu*, w: *Zaopatrzenie w wodę, jakość i ochrona wód*, Dymaszewski i in. (red.), Poznań, Toruń 2014, 533–544.
- [7] Neville A., *Effect of cement paste on drinking water*, Materials and Structures, 34, 2001, 37–372.
- [8] Bąk J., Dąbrowski W., Dąbrowska B., Wassilkowska A., *Jakość przewodów z żeliwa sferoidalnego i ich warstw ochronnych*, Rynek Instalacyjny, 11, 2014, 74–77.
- [9] Gruener M., *Korozja i ochrona betonu*, Wydawnictwo Arkady, Warszawa 1983.
- [10] Information on: <http://www.pamline.pl/pdf/saint-gobain-siec-kanalizacyjna.pdf>.
- [11] Bobrowski A., Gawlicki M., Łagosz A., Nocuń-Wczelik W., *Cement. metody badań. Wybrane kierunki stosowania*, Wydawnictwa AGH, Kraków 2010.
- [12] Fiertak M., Dębska D., Stryzewska T., *Chemia dla inżynierów budownictwa*, Politechnika Krakowska, Kraków 2011.
- [13] Kohutek Z. (Ed.), *Beton przyjazny środowisku*, Wydawnictwo SPBT, Kraków 2008.

GABRIELA ZEMELKA \*

## FATE OF THREE HERBICIDES (TEMBOTRIONE, NICOSULFURON AND S-METOLACHLOR) ON SOIL FROM LIMAGNE REGION (FRANCE)

### WPLÝW TRZECH HERBICYDÓW (TEMBOTRION, NICOSULFURON I S-METOLACHLOR) NA GLEBĘ Z REGIONU LIMAGNE (FRANCJA)

#### Abstract

The laboratory studies of pesticides involves a number of ways and methods. It has become especially important nowadays when pesticides is common for people to use. The increasing risk of these chemicals has forced the Legislating Authorities in France to set up recommendations on the use of pesticides and established *Ecophyto 2018* program. This paper and research are the part of an interdisciplinary project funded by CPER (Contract between the State and Region), FEDER and the Région Auvergne.

The objective of this research is to characterize the fate of 3 herbicides (tembotrion, S-metolachlor, nicosulfuron) belonging to different chemical families on soil from Limagne region in France. The author have performed the experiments with the dry samples of soil which were polluted in the laboratory by spraying pesticide solutions. The work focused on one of the main processes governing the adsorption on surface of solid phase. The results of the research shown that the impact of pesticides is greatly dependent on their family origin as well as on the environmental conditions and the type of soil. Further studies have to be carried out to better understand actions and behaviour of the pesticides in the soil.

*Keywords: herbicide, black soil, Limagne – France*

#### Streszczenie

Naukowe badania pestycydów obejmują wiele sposobów i metod badań laboratoryjnych. Są one szczególnie istotne w dzisiejszych czasach, kiedy popularne stało się stosowanie pestycydów. Wzrost zagrożenia tymi substancjami, zmusił organy prawa we Francji do utworzenia zaleceń dotyczących ich stosowania i wprowadzenia programu *Ecophyto 2018*. Artykuł i przedstawione w nim badania są częścią interdyscyplinarnego projektu sponsorowanego przez CPER (Umowa między Państwem i Regionem), FEDER i Région Auvergne.

Celem badań jest scharakteryzowanie losów 3 herbicydów (tembotrion, S- metolachlor, nicosulfuron), należących do różnych rodzin chemicznych w glebie z regionu Limagne we Francji. Autor prowadził badania na glebie zanieczyszczonej roztworami pestycydów. Badania te skoncentrowane były na jednym z głównych procesów dotyczących adsorpcji na powierzchni fazy stałej. Wyniki badań pokazały, że wpływ pestycydów jest znacznie uzależniony od ich pochodzenia chemicznego, jak również od warunków środowiskowych i gleby. Dalsze badania powinny być prowadzone w celu lepszego zrozumienia działania i zachowania pestycydów w glebie.

*Słowa kluczowe: herbicyd, czarna ziemia, Limagne – Francja*

**DOI: 10.4467/2353737XCT.15.405.5036**

\* MSc. Eng. Gabriela Zemelka, PhD student, Cracow University of Technology.

## 1. Introduction

One of the main processes governing the dissemination and fate of pesticides in agricultural soils is adsorption on surface of the solid phase. These interactions play a key role not only in the transport of pesticides but also in their biodegradation, by acting on their bioavailability and on the microbial metabolic activity. Therefore the understanding and measurement of the pesticide retention and degradation are the key steps in risk assessments of their persistence and contribution to pollution [10].

The objective of laboratory studies was to characterise the fate of 3 pesticides belonging to different chemical families in soils from Limagne region. Nicosulfuron (sulfonylurea), S-metolachlor (acetanilide) and tembotrione (triketone), known to be usually applied sequentially during the growing season of maize [4, 13, 14, 16]. Soil from Limagne region (Auvergne, France) was formed under continental climate, very cold in winter, very wet during the spring thaw and very hot and dry in summer. That soil was classified as Vertisol which is very fertile and lead to high production yields [3, 9]. That is why monitoring the fate of pesticides in this area is a major environmental and health concern. In order to better understand the mechanism involved in transfer/transformation processes of pesticides, research was carried to identify the role of the soil component on the different pesticide adsorption. Laboratory microcosm experiments were conducted to assess the dissipation of each pesticide in this soil.

## 2. Materials and methods

### 2.1. Preparation of soil sample

Samples were separated into 3 fractions depending on their size by physical treatments ( $50\ \mu\text{m} < \Phi < 500\ \mu\text{m}$ ;  $2\ \mu\text{m} < \Phi < 50\ \mu\text{m}$ ;  $\Phi < 2\ \mu\text{m}$ ) according to the procedure described on Figure 1. Bulk soil (air-dried and sieved at 2mm) was used.

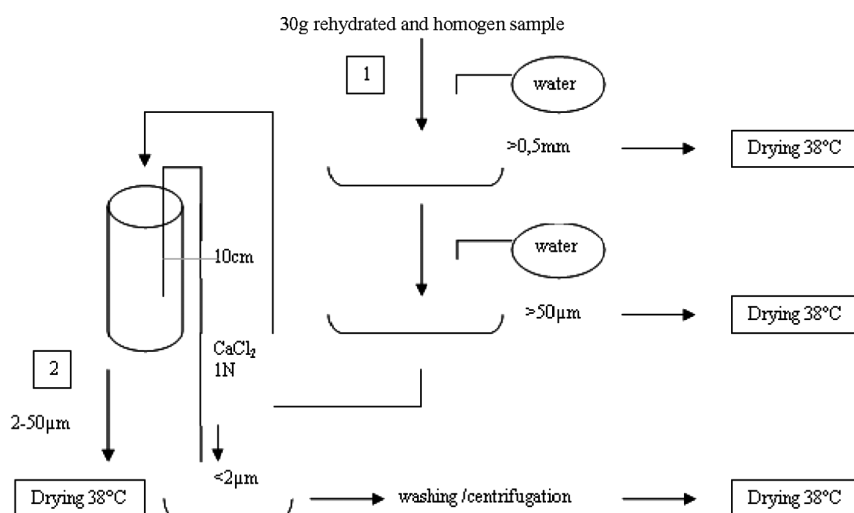


Fig 1. Steps of the soil fractioning [17]

30 g of soil were put into container and cover sample with 2L of water. Fraction obtained contained carbonates and organic matter. Water was removed every 8 hours by special pipe and a vacuum pump and moved to the other container.  $\text{CaCl}_2$  1N was put to accelerate settling. After 1 week the fraction  $<0.5$  mm was placed in a plastic pot and an ultrasonic bath for 15 minutes and sow in  $50\ \mu\text{m}$  and  $5\ \mu\text{m}$  sieve. The fraction  $< 2\ \mu\text{m}$  should be washed to remove Cl-ions made during the addition of  $\text{CaCl}_2$  1N. It was centrifuged twice during 15 minutes and speed 4000 rpm. The samples were placed in a crystallizer and dried at  $38^\circ\text{C}$ .

## 2.2. Stability of pesticides

Three different solution pesticides of tembotrione, nicosulfuron, S-metolachlor with the same concentration ( $100\ \mu\text{M}$ ) were prepared. The solutions were kept 7 days in Infors HT Multitron Incubator. They were shaken with a speed 140rpm in  $27^\circ\text{C}$  under lights simulating the solar spectra. Every day solutions were weighted. Distilled water was given in amount which disappeared from the flask. 1ml of solutions were taken by automatic pipette and moved into the eppendorf. The solutions were weighed again. New weight was recorded. Samples were frozen at  $-20^\circ\text{C}$  until HPLC analyses.

## 2.3. Microcosms

Six microcosms were prepared, two for each pesticide with two moisture contents (25 and 35%). Therefore six different solutions of pesticides: tembotrione 35% ( $142\ \mu\text{M}$ ) and 25% ( $200\ \mu\text{M}$ ), nicosulfuron 35% ( $142\ \mu\text{M}$ ) and 25% ( $200\ \mu\text{M}$ ), S-metolachlor 35% ( $142\ \mu\text{M}$ ) and 25% ( $200\ \mu\text{M}$ ) were prepared. Each one was sprayed on 200g of air-dried and sieved bulk soil into different containers. Control of water content was checked every week, the day before sampling (Fig. 2). Soil (3.5 g) was contaminated with 1.5 mL of pesticide at different concentrations in centrifuge tubes. After 15 minutes ( $T_0$ ) and 20 hours ( $T_{20}$ ), 20 mL of solvent was added and the suspension was shaken for 24 h. After centrifugation (1200 rpm for 15 min), supernatants were put in a freezer ( $-20^\circ\text{C}$ ) until HPLC analyses (Fig. 2.). The same protocol was carried out with a soil samples of each microcosm once a week (samples taken in triplicate) and extracted with ultra pure water for tembotrione and nicosulfuron and a mixture of  $\text{MeOH}/\text{H}_2\text{O}$  4/1 for S-metolachlor [11].

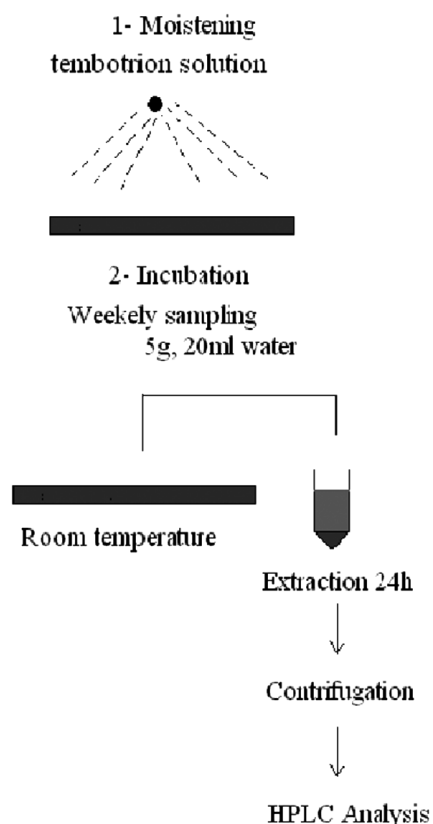


Fig. 2. Microcosm experiments on the example of tembotrione [17]

## 2.4. Sorption experiment-Kinetics

1 g of dry soil with 3mL of Volvic® water (natural mineral water from France) was used. The soil samples were shaken (Heidolph Reax2) for 12 hours in 20°C before the day of experiment. The supernatant was removed after centrifugation (Thermo KR22i Jouan) at 12000 rpm for 15 min. 3 mL of pesticide solution in distilled water (pH = 6) was pipetted into the container. The samples were shaken again for 1/2, 1, 1 1/2, 2, 3, 4, 6, 8, 20 and 24 hours in 20°C. Centrifugation was used again. HPLC analysis of supernatant was conducted. Each measurement was performed three times.

## 2.5. Sorption experiment-Isotherms

The author prepared various concentrations solution of pesticide were prepared (10  $\mu\text{M}$ , 20  $\mu\text{M}$ , 30  $\mu\text{M}$ , 50  $\mu\text{M}$ , 70  $\mu\text{M}$ , 100  $\mu\text{M}$ ). The process of preparing samples is the same like in adsorption kinetics.

1 g of clay was used and preconditioning with 3 mL of Volvic water (natural mineral water from France). Samples were shaken (Heidolph Reax2) for 12 hours in 20°C before the day of experiment. Centrifugation (Thermo electron corporation KR22i Jouan) 12000 rpm for 15 min was used. Then supernatant was removed. 3mL of various concentrations solution pesticide were pipetted into the 6 containers. Samples were shaken in 20°C for 4 or 6 hours according to the pesticide studied. HPLC analysis of supernatant was conducted. Each measurement was performed three times.

## 3. Results

The results of pesticide stability showed that a strong decrease of S-metolachlor was observed within the first day. Almost 70% has disappeared. Tembotrione and nicosulfuron were stable.

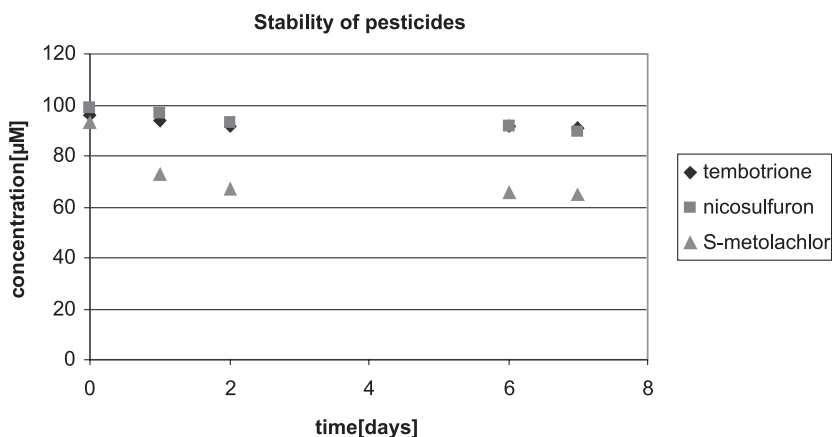


Fig. 3. Photostability of tembotrione, S-metolachlor and nicosulfuron (100  $\mu\text{M}$ ) [17]

The results of pesticide dissipation in microcosms are presented on Fig 4.

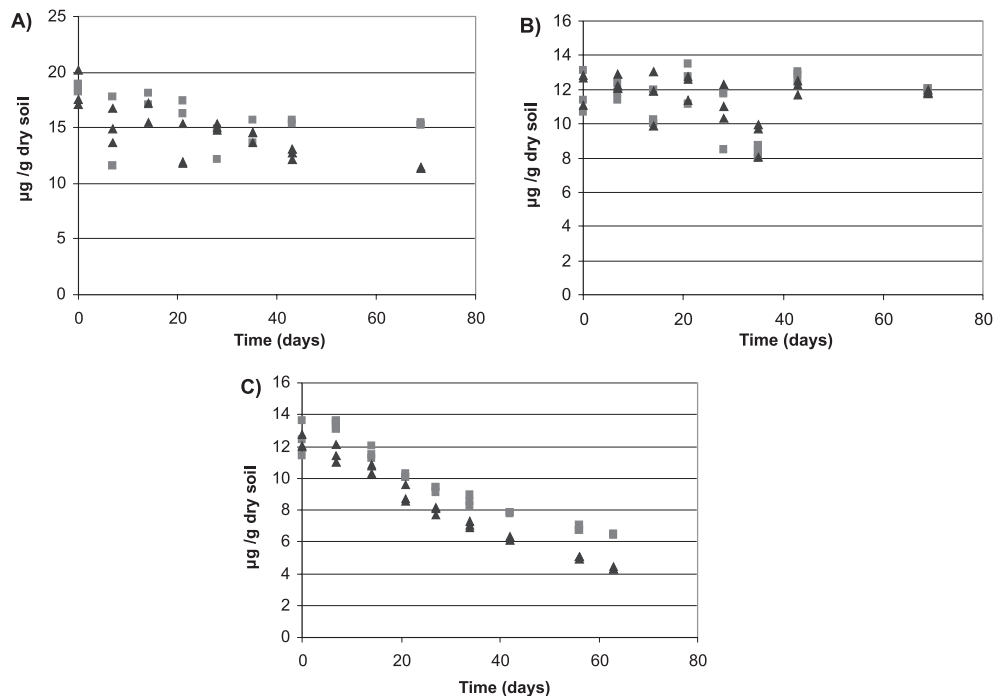


Fig. 4. Dissipation of (A) tembotrione, (B) nicosulfuron and (C) S-metolachlor in microcosms with 25% (■) and 35% (▲) soil moisture [17]

Nicosulfuron is persistent as the final concentration after 69 days of incubation is the same as the initial one. Tembotrione dissipated very slowly but a decreasing tendency of its concentration is observed with time. The less persistent herbicide is nicosulfuron as 50% and 70% have disappeared within 69 days of incubation for 25 and 35% of soil moisture, respectively [10].

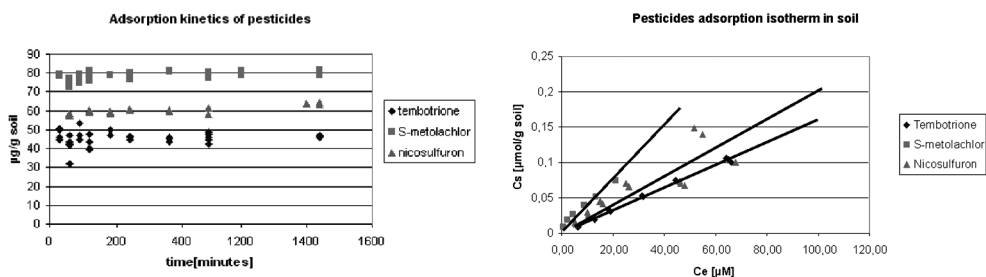


Fig. 5. Adsorption kinetic of pesticides Fig 6. Adsorption isotherms of pesticide in soil [17] in soil [17]

Kinetics studies showed a quick adsorption, and equilibrium soon reached which is shown on the graphs (Fig. 5). The graph of tembotrione adsorption kinetics shows that the most stable time of adsorption is 6 hours and for nicosulfuron and S-metolachlor is 4 hours. After that time concentration of the analytes did not change.

The results of pesticide adsorption isotherms showed that tembotrione displays the lowest adsorption capacity and S-metolachlor displays the greater adsorption behavior (Fig. 6).

#### 4. Discussion

Degradation is the process of pesticide breakdown after application. This can be done by microorganisms, chemical reactions and light or photodegradation [2,6]. S-metolachlor and nicosulfuron have the potential to move into the water due to their high water solubility [12]. These three pesticides are quite stable under those conditions (temperature, light, humidity). Degradation from irradiation was comparatively slow. The contribution of a photolytic mechanism of degradation is therefore limited. Moreover, no other chemical degradation was observed (hydrolysis).

The dissipation could be observed due to sorption process on soil particles or organic matter and/or to biodegradation by microorganisms present in soil. To discriminate both these processes and to understand better the role of the different components of soil, adsorption experiments were carried out with each pesticide.

Kinetics studied showed that the diffusion through the heterogeneous matter and accessibility to the adsorption sites are high. Consequently, 4h and 6h of pesticide/soil contact time were chosen for adsorption isotherm experiments [1, 5, 8].

Adsorption coefficients ( $K_d$ ) of the 3 herbicides adsorbed on soil from Limagne region follows the variation:  $K_d$  (S-metolachlor) >  $K_d$  (nicosulfuron) >  $K_d$  (tembotrione). The same behavior is observed than reported in the literature [7, 15]. The most soluble herbicide, tembotrione displays the lowest adsorption capacity. Because of the negative charge of its ionic form, interaction of tembotrione with surface of metal oxides, carbonates and clays is unfavorable. Differently, S-metolachlor displays the greater adsorption behavior. Due to its low solubility and its high  $K_{oc}$ , this herbicide has a greater tendency to be adsorbed by the soil organic matter. This is probably the reason why, it has great capability to be immobilized on Limagne Vertisol. The major components are soil organic matter and clays. In Vertisols, clays mineral is vermiculite, which is very specific.

#### 5. Conclusion

In summary, the present results show that the fate of pesticides is greatly dependent on their chemical structure and corresponding physico-chemical properties as well as on the environmental conditions and type of soil. In this soil, our work focused on one of the main processes governing the fate of pesticide: adsorption/desorption with solid particles that was studied in detail but also on a global view of the pesticide dissipation under environmental conditions. Tembotrione, S-metolachlor and nicosulfuron were not strongly adsorbed by

the soil. The results showed that S-metolachlor had the highest percentage of adsorption. Nicosulfuron and tembotrione that were much less sorbed were found to be respectively, persistent and slightly dissipated in soil. We can then assume that biodegradation by soil microorganisms, known to be another important dissipation process in the soil, is not very active for both these pesticides under the conditions used in the experiments. To conclude, Further studies have to be carried out to better understand actions and behaviour of the pesticides in the soil.

#### Acknowledgment

This work is part of an interdisciplinary project funded by CPER (Contract between the State and Region), FEDER and the Région Auvergne.

I would like to thank my supervisors Dr. Pascale Besse-Hoggan and Pr. Claude Forano for help at my scientific research during my stay at University Blaise Pascale in Clermont-Ferrand in France (Erasmus research program).

I would like to thank the reviewer of this paper for his valuable comments.

#### References

- [1] Bedmar F., Daniel, P. Costa J., Giménez D., *Sorption of acetochlor, S-metolachlor, and atrazine in surface and subsurface soil horizons of Argentina*, Environ. Toxicol. Chem., vol. 30, 2011, 1990–1996.
- [2] Benzi, M., Robotti, E., Gianotti, V., *HPLC-DAD-MSn to investigate the photodegradation pathway of nicosulfuron in aqueous solution*, Anal. Bioanal. Chem., vol. 399, 2011, 1705–1714.
- [3] Bornand M., Dejou J., Robert M., Roger L., *Composition minéralogique de la phase argileuse des Terres noires de Limagne (Puy de Dôme). Le problème des liaisons argiles-matière organique*, Agronomie, vol. 4 (1), 1984, 47–62.
- [4] Bowman, B.T., *Mobility and persistence of the herbicides atrazine, metolachlor and terbuthylazine in plainfield sand lysimeters*, Environ. Toxicol. Chem., vol. 8, 1989, 485–491.
- [5] Cao P., Wang X., Liu F., Zhao E., Han L., *Dissipation and residue of S-metolachlor in maize and soil*, Bull Environ Contam Toxicol, vol. 80, 2008, 391–394.
- [6] Dimou A.D., Sakkas, V.A., Albanis, T.A., *Metolachlor photodegradation study in aqueous media under natural and simulated solar irradiation*, J. Agric. Food Chem., vol. 53, 2005, 694–701.
- [7] Foo K.Y., Hameed B.H., (2010) *Insights into the modeling of adsorption isotherm systems*, Chem.Eng. J., 156, 2-10.
- [8] Gonzalez J.M., Ukrainczyk L., *Adsorption and desorption of nicosulfuron in soils*, J. Environ. Qual., vol. 25(6), 1996, 1186–1192.
- [9] IUSS Working Group WRB, *World Reference Base for Soil Resources 2014. International soil classification system for naming soils and creating legends for soil maps*, 2014, 97–100.



- [10] Mamy L., Barriuso E., Gabrielle B., *Environmental fate of herbicides trifluralin, metolachlor, metamitron and sulcotrione compared with that of glyphosate, a substitute broad spectrum herbicide for different glyphosate-resistant crops*, Pest Management Science, vol. 61, 2005, 905–916.
- [11] Nelieu S., Perreau F., Guichon R., Seguin F., Bry Ch., Einhorn J., *Monitoring and effects of nicosulfuron in aquatic mesocosms: development of a simple analytical procedure and evidence for low toxicity to phytoplankton communities*, Anal Bioanal Chem, vol. 382, 2005, 108–114.
- [12] PPDB=Pesticide Properties Database-University of Hertfordshire, (online) homepage: <http://sitem.herts.ac.uk/> (date of access: 2013-06-20).
- [13] Regitano J. B., Koskinen W. C., *Characterization of Nicosulfuron Availability In Aged Soils*, Journal of Agricultural and Food Chemistry, vol. 56, 2008, 5801–5805.
- [14] Santel H.J., *Laudis® OD – a new herbicide for selective post-emergence weed control in corn (Zea mays L.)*, Bayer CropScience Journal, vol. 62, 2009, 95–108.
- [15] Si Y., Takagi K., Iwasaki A., Zhou D., *Adsorption, desorption and dissipation of metolachlor in surface and subsurface soils*, Willey Interscience, vol. 65, 2009, 956–962.
- [16] Tarara G., Fliege R., Desmarteau D., Kley C., Peters B., *Environmental fate of tembotrione*, Bayer CropScience Journal, vol. 62, 2009, 63–73.
- [17] Zemelka G., *Fate of three herbicides (tembotrione, nicosulfuron and S-metolachlor), alone or in mixture, in Limagne plane soil*, Rapport de Stage Master 2, Institut de Chimie de Clermont-Ferrand, 2013.

MICHAŁ ZIELINA, ANNA MŁYŃSKA, TADEUSZ ŻABA\*

## EXPERIMENTAL RESEARCH ON DETERIORATION OF DRINKING WATER QUALITY AFTER CEMENT MORTAR PIPE LINING

### EKSPERYMENTALNE BADANIA NAD POGARSZANIEM JAKOŚCI WODY PITNEJ PO CEMENTOWANIU PRZEWODÓW WODOCIĄGOWYCH

#### Abstract

In the paper the results of experimental research on the deterioration of drinking water quality after cement mortar lining were presented. The experiments were conducted in the renovated water pipeline section in Cracow. Based on the results, the expected degree of leaching of the pollutants from cement mortar to drinking water for specified lengths and diameters of renovated pipes, as well as water velocities, was estimated.

*Keywords: cement mortar lining, water quality, water pipes*

#### Streszczenie

W niniejszym artykule przedstawiono wyniki badań eksperymentalnych nad pogarszaniem się jakości wody do picia po cementowaniu przewodów wodociągowych. Pomiary przeprowadzono na odcinku jednej z krakowskich magistral poddanej renowacji z zastosowaniem wykładziny cementowej. Na podstawie uzyskanych pomiarów przeanalizowano jakiego stopnia ługowania zanieczyszczeń z powłoki cementowej do wody można się spodziewać przy określonych długościach i średnicach przewodów poddanych renowacji oraz prędkościach przepływającej wody.

*Słowa kluczowe: cementowanie, jakość wody, przewody wodociągowe*

**DOI: 10.4467/2353737XCT.15.406.5037**

\* Assoc. Prof. DSc. PhD. Eng. Michał Zielina, MSc. Eng. Anna Młyńska, PhD. Eng. Tadeusz Żaba, Institute of Water Supply and Environmental Protection, Faculty of Environmental Engineering, Cracow University of Technology.

## 1. Introduction

One of the most commonly used trenchless water pipe renovation methods is cement mortar lining. It is mainly used for steel and cast iron pipes. This method is performed, after thorough cleaning, by the spraying of cement mortar onto the inner surface of the pipeline. A rotary head, which is pulled through the pipeline at a constant speed, is used for spreading the cement mortar inside the pipe during renovation [1, 2], which provides a uniform layer of cement mortar. In turn, the cementation of new pipes during manufacturing in a factory is a different process. During the cementation the pipe rotates rapidly around its own axis. It provides a much smoother surface of coating than in the case of cement mortar lining made directly on a building site. Moreover, the rotation of the pipe around its own axis causes the movement of sand grains towards the pipe wall. In consequence, the fine-grained structure of cement mortar characterised by low seepage is formed [3]. The final thickness of the cement coating should be in the range between 3 mm and 10 mm. The coating thickness depends on the pipe material and its diameter [4].

The popularity of cement mortar lining technique is due to its simplicity and relatively low costs. Additionally, the method is characterised by a quite short renovation time, guaranteeing a minimal interruption of water supply to the consumers. Cementing provides two forms of protection against corrosion: active and passive. It also protects the pipe by an encrusting and void-filling calcite phenomenon. Therefore, renovation by cement spraying is considered to be a very effective method for solving drinking water quality problems in the long term [5, 6]. Active corrosion protection is provided by a very thin layer of water (a few micrometers) which is formed between the cement coating and the pipe wall. This layer has a very high pH at which the corrosion process is reduced or avoided [7].

However, it is often noted that directly after cement mortar spraying some of the drinking water quality parameters may deteriorate. In the case of soft water, which has a low content of carbonate and bicarbonate, contact of water with a newly applied cement coating may lead to leaching of calcium hydroxide – a component of the cement lining. It causes an increase in the pH of water and a decrease in the mechanical strength of the protective coating [7]. In turn, high values of pH can contribute to the dissolution and leaching of aluminium and chrome from the cement mortar into the water [8] and also other chemical elements such as lead, zinc, nickel, arsenic, cadmium, vanadium and copper. The amount of leached chemical elements from the concrete coating into the water depends on the type of applied cement. For example, use of high alumina cement contributes to the leaching of a significant quantity of aluminium into the water. In the case of high-calcium cements, leaching of large amount of calcium from the coating into the water is observed and, as a consequence, a significant rise of water pH [9].

Pipe diameter is another parameter that is significant for determining the concentration of chemical elements in the water after contact with the cement mortar coating in the pipeline. The volume of the circular pipe section rises proportionally to the square of the inner pipeline diameter, while the inner wall surface of the pipe section rises only proportionally to the diameter. Therefore, the larger the pipe diameter, the smaller the volume of water per cement mortar unit surface area (Fig. 1), consequently the larger the pipe diameter, the smaller the influence of the cement mortar on the water quality [10].

The impact of the cement mortar lining on the deterioration of drinking water quality in a short period after renovation was analysed in the paper. Full-scale experiments were conducted soon after renovation of water main section in Cracow. soon after renovation of the water main section of the water distribution network in Cracow. pH, alkalinity, concentration of calcium, aluminium and heavy metals such as chromium, lead and cadmium were measured in water samples collected before and after the newly renovated pipeline. Based on the results of the experimental research, the expected degree of leaching of pollutants from the cement mortar into the drinking water for specified lengths, diameters of renovated pipes and also water velocities was estimated.

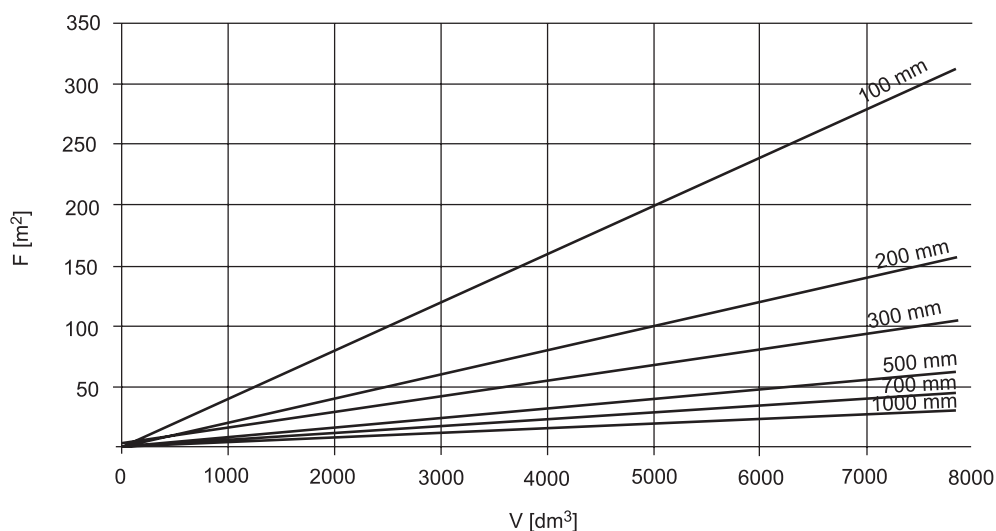


Fig. 1. The dependence of the water volume on the coating surface for few different pipeline diameters

## 2. Material and methods

The renovated water main section is located along one of the main streets in Cracow. The 500 mm diameter pipeline is made of steel and is 725 metres long. In a place where the pipeline passes under the road, a 110.5 metres-long section was renovated by cured-in-place pipe method in which a resin-saturated felt tube made of polyester and nylon fibers was pulled into the corroded pipe. The rest of the 614.5 metres of water main was renovated by cement mortar lining. The process of renovation was preceded by hydrodynamic cleaning with the aim of removal of accumulated pollution and corrosion products. Cleaning equipment powered by a water pump produced a pressure of discharge water of almost 100 MPa. The cement mortar lining process was conducted by centrifugal spreading of cement mortar on the inner surface of the pipe using a rotary head (Fig. 2). The cement coating thickness was equal to approximately 10 mm. The expected thickness of cement lining was achieved by providing a constant flow of cement mortar from the rotary head and its constant rotation speed and suitable rate of movement of the spraying equipment along the water pipe.



Fig. 2. Rotary head for cement mortar lining water pipes (author's photo)

For the preparation of the cement mortar, Portland cement CEM I 42.5 R – manufactured by CEMEX – was mixed with quartz sand in a ratio of 1 to 1. Next, water was added to the mixture, maintaining quite a low water-to-cement ratio equal to 0.35. After the completion of the cement mortar lining, one day of curing the cement mortar is required. After this time, the renovated pipe was filled with water and the water was kept for 6 days under working pressure. After this period of time a pressure test was conducted. For half an hour the water pressure was maintained at 10 bars. At the end the pipe was flushed with a velocity of 0.2 m/s for 6 hours before returning to usage.

### 3. Results

Water samples were collected before, during and 5 hours after flushing at the inflow to (sample No. 1) and the outflow from (samples No. 2-5) the renovated section of pipeline. The temperature of the collected samples was around 5°C. Each of the samples was tested in the lab for pH, alkalinity and concentration of chemical elements such as aluminium, chromium, calcium, cadmium and lead. The results of the pH and alkalinity tests are presented in Table 1. After half an hour from the start of the pipe flushing, the pH increased above 10 but decreased for the next ten hours, reaching a value of 9 at the end. It is supposed that this increase of pH was due to the impact of the fresh cement lining on the water. However, quite a quick decrease of pH after a few hours is probably caused by the 6 days of water retention which preceded the flushing and also the relatively large diameter and short length of the cemented pipe. In other cases pH is expected to exceed 9.5 – the limitation value for drinking water in the Polish Ministry of Health Regulation [11].

Concentrations of aluminium, calcium and heavy metals such as chromium, cadmium and lead in the collected samples are presented in Table 2. Concentrations of heavy metals were all under instrument detection limits, so it can be stated that the risk of drinking water contamination by leaching of heavy metals from fresh cement mortar lining seems to be negligible under the investigated conditions. Only a high increase of aluminium concentration, significantly exceeding the maximum limitation predicted by the Polish Health Ministry Regulation [11] and [12] (0.2 mg/l), was observed soon after the beginning of the flush. The aluminium concentration gradually decreased and, 5 hours after flushing, reached the

same value at the beginning of the renovated pipe as at the end. Since during flushing the aluminium concentration was kept around the standard limitation, there is the potential risk of exceeding this value under other renovation conditions such as a smaller diameter, longer pipe, different cement, water quality and velocity, shorter flushing or omitting, preceded flushing, and six days retention time. The analysis of calcium shows a small increase in concentration at the beginning of the flushing process and a gradual decrease until the end. There is no significant influence on water quality in the short period but long-term leaching of calcium can devastate the mortar cement coating layer

Table 1

**pH and alkalinity in collected water samples**

No.	Sampling place	The time from the start of water pipe flushing [h]	pH	Alkalinity [mmol/l]
1	Inflow to the renovated pipe		7.75	1.20
2	Outflow from the renovated pipe	0,5	10.13	0.85
3		3	8.40	1.40
4		6	8.10	1.40
5		11	9.05	1.20

Table 2

**Concentrations of chemical elements in collected water samples**

No.	Sampling place	The time from the start water pipe flushing [h]	Aluminium [mg/l]	Chromium [mg/l]	Calcium [mg/l]	Cadmium [mg/l]	Lead [mg/l]
1	Inflow to the renovated pipe	0	0.043	< 0,002	61.44	< 0.001	< 0.005
2	Outflow from the renovated pipe	0,5	0.064	< 0,002	21.02	< 0.001	< 0.005
3		3	0.293	< 0,002	61.72	< 0.001	< 0.005
4		6	0.172	< 0,002	64.23	< 0.001	0.007
5		11	0.052	< 0,002	46.33	< 0.001	< 0.005

It was considered, based on the experiments, that the greatest risk of drinking water quality contamination in the short term after cement mortar lining renovation is due to aluminium leaching. Based on the experimental measurements presented in Table 2, growth of aluminium concentrations at the end of the freshly cemented pipe were calculated for

different possible flow velocities, pipe lengths and diameters. The results of the calculations are presented in Figures 3 and 4. The calculations took into account preceded flushing, 6 days water retention, pressure test and 6 hours of flush. Figure 3 presents the results of the calculation for water drinking flow velocity equal to 0.5 m/s, and Figure 4 presents the results for 1.0 m/s velocity.

Growth in aluminium concentration increases proportionally to the length of cement mortar lined pipe and decreases proportionally to the pipe diameter. So, the smaller the diameter and the longer the renovated pipe, the greater the risk of pollutant leaching from the cement mortar into the water. The higher the velocity of water in the pipeline, the shorter the contact time with the cement coating. The shorter the contact time with the cement coating, the smaller the growth of aluminum concentration. So, the higher the water velocity, the smaller the growth of aluminum concentration. In Figures 3 and 4, two velocities, 0.5 m/s and 1.0 m/s, were taken into account. Assuming an inversely proportional dependence between water velocity and growth in aluminum concentration, a two times smaller growth in aluminium concentration for 1.0 m/s velocity is expected than for 0.5 m/s.

Since the maximum limitation of aluminum concentration in drinking water based on [12] is equal to 0.2 mg/l, a growth in concentration equalling 0.1 mg/l appears to be dangerous and should not be allowed. For 0.5 m/s velocity, such a high growth of aluminium is expected to appear if a 200 mm diameter pipe is a minimum 3 km long, or if a 500 mm diameter pipe is more than 8 km long. Of course, allowable growth in aluminium concentration depends on the aluminium concentration in the water produced by the treatment plant and the flushing time period.

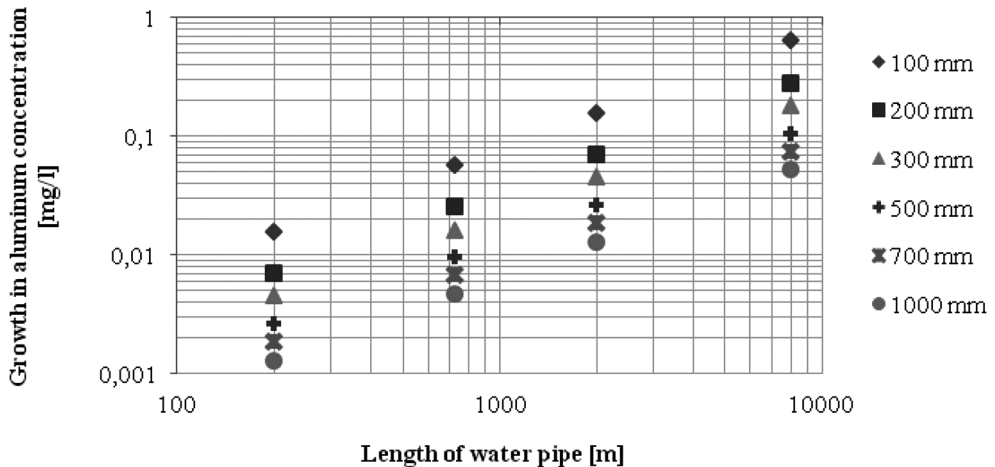


Fig. 3. Growth in aluminum concentration depending on the length and diameter of a freshly renovated cement mortar lined pipe for 0.5 m/s velocity

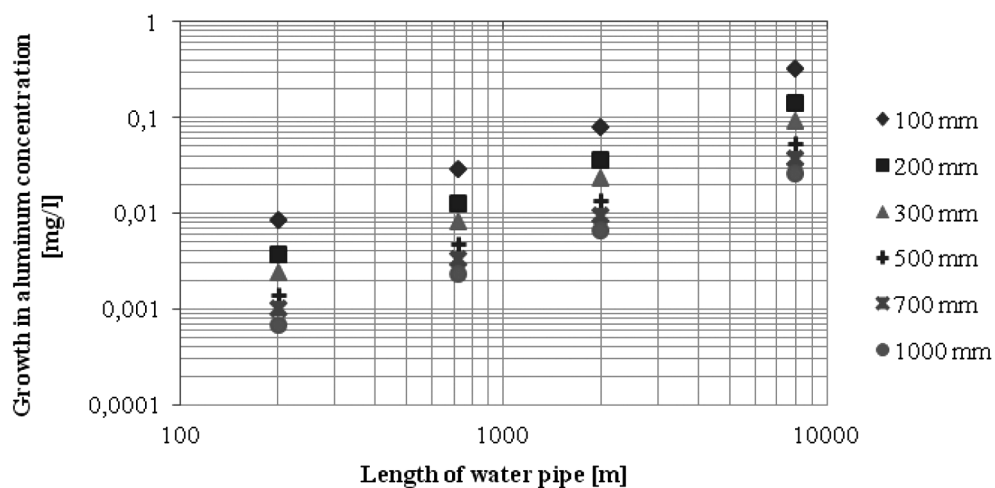


Fig. 4. Growth in aluminum concentration depending on the length and diameter of a freshly renovated cement mortar lined pipe for 1.0 m/s velocity

#### 4. Conclusions

Despite cement mortar lining of water pipes being a common method of renovation due to its many advantages, it was noted that, directly after application of the cement mortar inside the pipeline, some quality parameters of drinking water may deteriorate. The results of experimental research performed on a steel water pipe section with a diameter of 500 mm and length of 725 m shows that the greatest risk of deterioration in water quality is related to the increase in pH value and leaching of aluminium from the cement mortar into the water. Under experimental conditions it was observed that the risk of water contamination by chemical elements as chromium, lead or cadmium is negligible.

Based on the conducted experiments it was possible to estimate the potential growth of aluminium concentration after cement mortar lining for different pipe lengths and diameters at velocities of 0.5 m/s and 1.0 m/s. Calculations were conducted based on contact time, assuming linear direct dependence of leached metals growth on pipe length and linear reversely proportional dependence on pipe diameter and water flow velocity.

Based on the experimental measurements and calculations, growth in aluminium concentration exceeding 0.1 mg/l is probable if the renovated 500 mm diameter pipe is a minimum 8 kilometres long and water flow velocity is not faster than 0.5 m/s for the same as the experimental conditions other than pipe diameter, length and velocity.

The curves showing the growth of aluminum concentration in drinking water after contact with the freshly cemented pipes enable finding of the maximum length of water pipe characterised by a specific diameter that can be once renovated without the risk of leaching aluminium from the cement mortar into the water exceeding the aluminum concentration limit for drinking water.



## Acknowledgment

The research has been financed by Polish National Science Center under the research project No 2648/B/T02/2010/39.

## References

- [1] Damodaran N., Pratt J., Cromwell J., Lazo J., David E., *Customer acceptance of water main structural reliability*, AwwaRF, 2005.
- [2] American Water Works Association, *Rehabilitation of water mains*, Manual of water supply practices: AWWA Manual M28, Denver 2001.
- [3] North American Society for Trenchless Technology, *Cement Mortar Lining (nonreinforced)*, March 1999.
- [4] DVGW W 343, *Zementmörtelauskleidung von erdverlegten Guß- und Stahlrohrleitungen; Einsatzbereiche, Anforderungen und Prüfungen*
- [5] Deb A., Silbert L. K., Schoder H., *Decision support system for distribution system piping renewal*, AwwaRF and AWWA, 2002, 26–28.
- [6] American Water Works Association, *Internal corrosion control in water distribution systems*, Manual of water supply practices: AWWA Manual M58, Denver 2011.
- [7] Bonds R.W., *Cement – mortar linings for ductile iron pipe*, Ductile Iron Pipe Research Association (DIPRA), report DIP-CML/3-05/3,5M, 2005, Alabama, USA.
- [8] Deb A., McCammon S. B., Snyder J., Dietrich A., *Impacts of lining materials on water quality*, Water Research Foundation, 2010.
- [9] Zielina M., Dąbrowski W., Radziszewska-Zielina E., *Cement mortar lining as a potential source of water contamination*, International Journal of Environmental, Ecological, Geological and Mining Engineering, 2014, vol. 8, no. 10, 628–631.
- [10] Dąbrowski, W., Głód, K., *Cementowanie rurociągów*, Chemia Przemysłowa, z. 4, 2011, 40-43.
- [11] Rozporządzenie Ministra Zdrowia z dnia 29 marca 2007 roku w sprawie jakości wody przeznaczonej do spożycia przez ludzi. (Dz.U. 2007 nr 61 poz. 417).
- [12] United States Environmental Protection Agency, Secondary drinking water standards.

MAJA BARTOSZEK\*, MICHAŁ JUSZCZYK\*\*

## SELECTED PROBLEMS OF BIM-BASED PLANNING OF CONSTRUCTION WORKS – CASE STUDY

---

### WYBRANE PROBLEMY PLANOWANIA ROBÓT BUDOWLANYCH Z WYKORZYSTANIEM BIM – STUDIUM PRZYPADKU

#### Abstract

The article presents the problem of planning works based on the BIM model of a building. The authors briefly discuss the possibility of using BIM as a tool for planning works, and then present the case study. In the case study method in a synthetic manner the planning process presents works based on a model residential building construction. The advantages and opportunities as well as the problems of using BIM as a basis for the planning process of construction works are discussed and commented in the conclusions.

*Keywords: BIM, scheduling, construction planning, BIM based planning*

#### Streszczenie

W artykule przedstawiono problematykę planowania robót budowlanych na podstawie modelu BIM obiektu budowlanego. W zwięzły sposób omówiono możliwości wykorzystania BIM jako narzędzia do planowania robót budowlanych, a następnie przedstawiono studium przypadku. W syntetyczny sposób przedstawiono proces planowania robót budowlanych w oparciu o model konstrukcji budynku mieszkalnego. We wnioskach omówiono i skomentowano zalety i możliwości, a także wybrane problemy wykorzystania modeli BIM w procesie planowania robót budowlanych.

*Słowa kluczowe: BIM, harmonogramowanie, planowanie realizacji robót budowlanych, planowanie oparte na BIM*

**DOI: 10.4467/2353737XCT.15.392.5023**

---

\* Eng. Maja Bartoszek, Datacomp sp. z o.o.

\*\* PhD. Eng. Michał Juszczyk, Institute of Construction and Transportation Engineering and Management, Faculty of Civil Engineering, Cracow University of Technology.

## 1. Introduction

Civil engineering is nowadays important part of, generally speaking, industry. To make construction process faster and more efficient engineers tend to invent more and more sophisticated methods both of buildings' design and constructing of the structures. A constant trend of improvement of construction planning and control through the whole period of works performed on a building site is needed and should be started from the very beginning of construction works start, or even before that time.

One of the most common problems associated with such situations is lack of communication and management systems, which are not effective enough to react instantaneously. The only way to get a solution of these types of problems could be usage of software which is more flexible, intuitive and comprehensive.

In this paper, there is Building Information Modeling (BIM) to be described as an irreplaceable tool in future construction management systems. It shows basic rules which need to be followed during BIM-based management of construction works. The aim of this article is to present concisely selected problems of the process of construction works planning. The case study for a certain structural model of a residential building is included in the paper. The starting point is the analysis of the model. The authors presented successive stages of the planning process (quantity take-off and scheduling) aided by the selected BIM tools (computer applications) which are currently developed in Poland.

This paper topic alludes to the previous works and research (i.a. [4, 7, 10] made by the academics from the Institute of Construction and Transportation Engineering and Management, Cracow University of Technology) in the field of widely understood applications of BIM in construction management.

## 2. BIM as a tool in construction planning and management

According to Smith [8] BIM (a building information model) "(...) is a digital representation of the physical and functional characteristics of a facility. As such it serves as a shared knowledge resource for information about a facility forming a reliable basis for decisions during its life-cycle from inception onward."

"Building Information Modeling (BIM) is one of the most promising developments in the architecture, engineering and construction (AEC) industries. With BIM technology, an accurate virtual model of a building is constructed digitally. When completed, the computer-generated model contains precise geometry and relevant data needed to support the construction, fabrication, and procurement activities needed to realize the building" [2].

According to these definitions, on one hand, BIM is a process of modelling information, on the other collection of building information data, a spatial representation of a structure. Actually, BIM is all of it itself and even more.

The starting point is a 3D model of a building which contains geometry and other adjectives such as building components (walls, windows, stairs etc.) and its characteristics and parameters. However simulation of a building behavior is also possible on the grounds of those features.

According to another definition BIM can be related to as an intelligent simulation of architecture. According to them, there are six main characteristic of such simulation [east]:

- digital,
- spatial (3D),
- accessible,
- measurable (quantifiable, dimension-able, and query-able),
- comprehensive (encapsulating and communicating design intent, building performance, constructability, and include sequential and financial aspects of means of method),
- durable (usable through all phases of facility’s life).

Those characteristic may seem idealistic and hard to be fulfilled at once. As a modern tool in construction industry, there is a belief that in the next few years all of the demanded features will be achieved.

Furthermore, there are a lot of mistakes and misunderstandings about what actually the BIM technology is. First of all, BIM models must be not only 3D, but also represent other pieces of information (attributes), for example cost. What is more, BIM model must be equipped with parametric intelligence – it means that they must be equipped with a possibility to adjust their position and proportions. Those models cannot be inconsistent or uncountable. Also, they must reflect all changes on each possible view, not to confuse and inhibit the programming and working on the model.

From the perspective of construction works planning process BIM which is understood as model of a building, database or storage of important information, may serve as a source of knowledge necessary for quantity take-off analysis and then schedule development. It must not be forgotten that the use of BIM tools (that is software, computer applications) are inevitable to make the most of the information stored in the model.

### 3. Initial analysis of the model

The case study presented in this paper was carried out for the structural model of a residential building. Basic information about the building is set together in the Table 1. The model is presented in the Fig. 1.

Table 1

**Basic information about the building under consideration**

Building type:	– residential building – single family house, – small-size garage is integrated with the house structure.
Numer of storeys:	– no storeys below ground level, – two storeys above ground (ground floor and attic floor).
Foundations:	– foundation slab made of reinforced concrete, (below the slab, respectively styrofoam layer and sand-and-gravel bedding), – four spot footings in the corners of the structure outside the foundation slab (onto them, wooden frame as the part of the roof structure).
Walls:	– masonry ceramic load-bearing walls made of blocks of 25 cm in thickness (prefabricated lintels are to be installed above windows and entrance door), – cores in the load bearing walls made of reinforced concrete,
Slab:	– monolithic floor slab between ground floor and first floor,
Roof:	– gabled roof – collar-beam type of structure, – wooden frame as a part of the roof structure (posts made of glued wood).

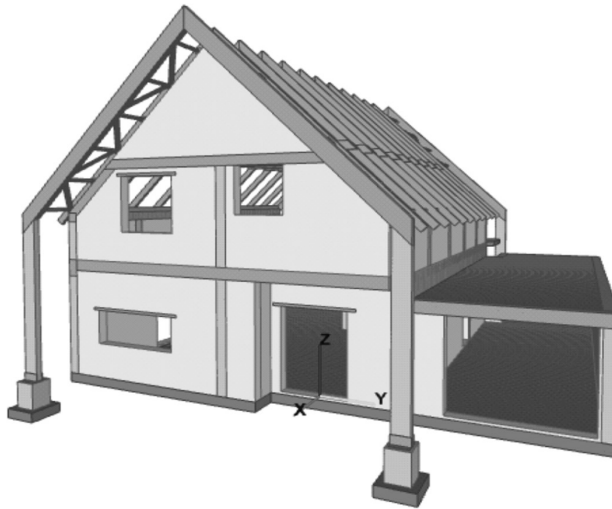


Fig. 1. The view of the model

The starting point for the planning process was the analysis of the model. The analysis revealed both some design and model correctness problems which may affect the process of construction works planning. The first issue was to rework and correct the model before the start of the planning. As the model was delivered as IFC file type, an IFC viewer (namely BIM Vision by Datacomp sp. z o.o.) has been used in order to check out the model. All the discovered deficiencies were presented to the design team and the model was corrected. Some selected problems revealed in the course of the analysis, are presented and briefly discussed below.

### 3.1. Internal structure of the elements comprising the model

Fundamental project structure division is presented in the Fig. 2.

So called “IFC structure” of the model was needed to be done for easier and more effective way of working on the quantity takeoff; such segregation has been added to the model. If it had not been done at this stage, each element of the construction (even every single reinforcing bar) would must be manually assigned to the adequate floor. Such a manual manner of work makes it unnecessary to use BIM technology – there is no improvement or automation in comparison with traditional way of project scheduling.

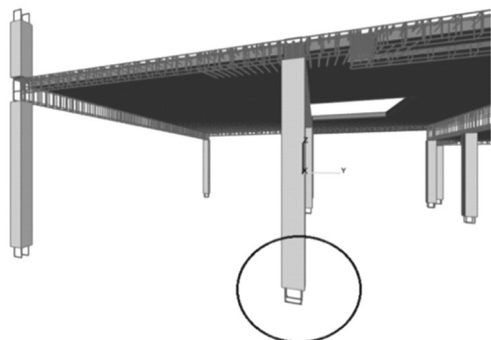
Adequate annotation of construction elements

From point of view of scheduling, proper management of construction works is essential. That is why a designer must be sure that every stage of the project execution is consequent and there is no doubt that all the structural rules are kept safely. Such a situation occurs clearly in case of starters – special reinforcing bars which are responsible for good connection and proper continuation of two construction elements designed to work as one system. An example is connection of the foundation slab and the columns on the ground floor. Comparison of rebar allocation is depicted in the Fig. 3.

Lp.	Model	Nr	Podstawa	Opis robót
1	<input checked="" type="checkbox"/>		Kosztorys	- Czystochowa
2	<input checked="" type="checkbox"/>	1	Rozdział	- Roboty budowlane
3	<input checked="" type="checkbox"/>	1.1	Grupa	- Undefined
4	<input checked="" type="checkbox"/>	1.1.1	Grupa	- Single-family house (dom jednorodzinny)
5	<input checked="" type="checkbox"/>	1.1.1.1	Grupa	- Foundations (fundamenty)
6	<input checked="" type="checkbox"/>	1.1.1.1.1	Element	+ Reinforcement (zbrojenie)
154	<input checked="" type="checkbox"/>	1.1.1.1.2	Element	+ Slabs (plyty grube)
156	<input checked="" type="checkbox"/>	1.1.1.1.3	Element	+ Footing (ławy i stopy)
161	<input checked="" type="checkbox"/>	1.1.1.1.4	Element	+ Frame mounting (mocowanie ramy gl.)
174	<input checked="" type="checkbox"/>	1.1.1.1.5	Element	+ Columns (słupy)
179	<input checked="" type="checkbox"/>	1.1.1.2	Grupa	+ Ground floor (parter)
411	<input checked="" type="checkbox"/>	1.1.1.3	Grupa	+ First floor (piętro)
505	<input checked="" type="checkbox"/>	1.1.1.4	Grupa	+ Roof (dach)

Fig. 2. IFC structure of the model

Before correction:



After correction:

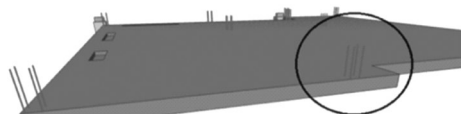


Fig. 3. Example of corrections made to the reinforcing bars assignments

When the schedule is to be done, design team must ensure that the starters are installed on the level of foundation slab (they must be prepared as the part of slab reinforcement, in spite of the fact that they are not actually the construction element of the slab). The same situation has been observed on the upper floor. After those rebar remarks have been launched (with great care of static part of calculations and design of reinforced concrete structure) also technological order of works execution could be conserved.

#### Practical approach to concrete placement

The figure shows how the model has been changed in order to facilitate concrete placement process. On the left of the Fig. 4 – proper execution and creation of strong enough bonds between neighbouring concrete elements (slabs, beams and columns) demanded by designing rules would be impossible. On the right of the Fig. 4 (after model corrections) – concrete placement will be easier and a gain of technological properties unquestionable.

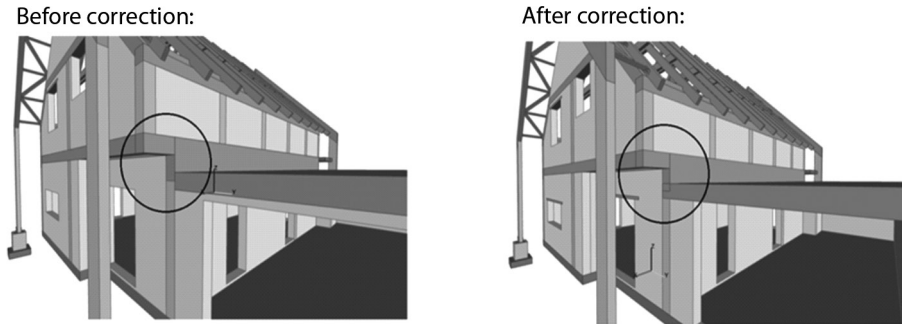


Fig. 4. Example of corrections made in the concrete elements' connections

The problems revealed in the course of the analysis might be related to unavoidable human errors or usage of repeatable blocks of elements during the model development process. (In the light of the analysis results the choice of IPD (Integrated Project Delivery) approach seems to be a promising option. Early involvement of contractors, consultants, fabricators and other specialists in the design process is expected to reduce errors and deficiencies on the very early stage of design process. More details about the IPD can be found i.a. in [3] and [9])

#### 4. BIM-model-based quantity takeoff and schedule

Two next steps described in the following chapter are the actual parts of the planning process. The first step was the quantity takeoff and the second step was the scheduling. The most important advantage of the BIM model usage is the ability to get automatically or semi-automatically the quantities of construction works (compare with e.g. [2]). “All BIM tools provide capabilities for extracting counts of components, area and volumes of spaces, material quantities and to report these in various schedules” [2]. However it must not be forgotten that the degree of accuracy depends on the model itself and the way it is developed. A list of the elements with their quantities read directly from the model is a starting point to scheduling.

##### 4.1. Quantity takeoff

The quantity takeoff was prepared with use of Zuzia BIM application (BIM software tool which is being developed by Datacomp sp. z o.o.). The process itself is very easy – selected construction element or group of elements has been automatically counted (area, length of chosen edge, volume or weight) and assigned to the element or group of elements presented on the model. Such an operation has been performed on the entire model. Not only each level of construction (foundations, ground floor, first floor, roof structure) has been described directly on the basis of quantity survey, but also automatically each variant of construction element has been registered and summed up (e.g. for the entire building, posts with dimension of  $25 \times 25$  cm comprises  $2.886 \text{ m}^3$  of concrete). The exemplary part of the work is depicted in the Fig. 5.

Model	Podstawa	Opis robót	J.m.	Ilość	Ilość jedn.	Ilość całkowita
1		Jednostkowe ceny pozycji projektu				
2		Slupy				
3	Element	rama; 14'37	m3			0,864
4	Element	slup; 25'25	m3			2,886
6		oponowanie/obrot	m2			
7	Element	slup; 25'25	m3			0,700
8		CONCRETE/C30/37	???			
9		Belki				
34		Zbrojenie				
43		ściany				
60		Płyty grube				
65		Lawy i stopy				

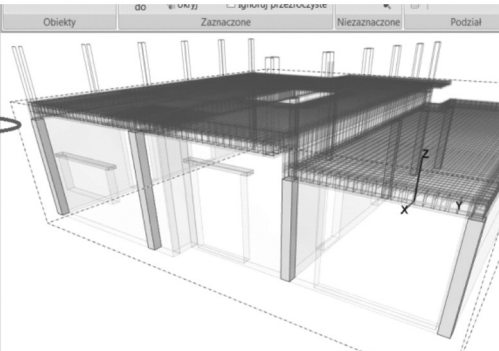


Fig. 5. Transfer of the quantity information from the model – example for RCT columns

There were few challenges met during quantity takeoff determination. As no BIM specific rules of measurement have been yet developed in Poland it was necessary to make the most of the catalogue base which is traditionally used in the process of cost estimation.

When all the quantities have been revealed in quantity takeoff, direct assignation of resources and their normative consumption connected with each type of an element has been determined.

#### 4.2. Development of construction works schedule

Development of the schedule was continued with use of Zuzia BIM application. It noteworthy that an arrangement of an IFC-structure of a model (i.a. definition of stroeys/ levels and elements assigned to the levels/stoereys) in the model directly determines tasks which are to be carried out during construction phase. There is a possibility however to group any types of element and the elements themselves. Nevertheless, its usage for schedule arrangement is hard to be launched and unclear and there is the threat, that merging of position causes disintegration of the model and the quantity takeoff.

The most complicated case occurs for reinforcement. On grounds of clarification of construction elements, such a classification could be made regarding bar diameter. The division facilitates distinction of similar bars' properties on each level of the building. Then the quantity takeoff appears more understandable and transparent. Unfortunately, it does not help to plan more accurate schedule of construction works. It would be like that if the division has been made into parts of the foundation reinforcement (for example group 1: footing, group 2: slab, group 3: columns). The more the groups, the more accurate schedule may become.

It must be emphasized however, that this type of classification (regarding e.g. bar diameter) is very troublesome during planning phase. In order to prepare precise schedule such a division must be made by a designer of a model. From point of view of a person constructing the schedule only classification regarding similar location is reasonable.

The durations of the tasks was assumed as deterministic and assessed on the basis of the simple formula (compare with [1, 4]):



$$D = \frac{TA}{ns} \quad (1)$$

where:

$D$  – duration of an activity (here in days),

$A$  – quantity of a construction work,

$T$  – the time required to complete a unit of work by a standard crew (measured in man hours or machine hours per measurement unit of a construction work),

$n$  – the number of workers or machines assigned to the task,

$s$  – number of working hours per shift.

The details of the duration assessment is depicted in Fig. 6.

Nr	Nazwa	Widoczny	Il. godz. pracy	r-g koszt.	r-g	Il. prac.	r-g / prac.	m-g	m-g / sprz.	Il. dni liczona	Ilość dni rob.	Czas trwania
1.1.1	- Single-family house (dom jednorodzinny)	<input checked="" type="checkbox"/>										53
1.1.1.1	- Foundations (fundamenty)	<input checked="" type="checkbox"/>										47
1.1.1.1.1	+ Reinforcement (zbrojenie)	<input checked="" type="checkbox"/>	8		152	5	30	21	21	4	4	
1.1.1.1.2	+ Footing (ławy i stopy)	<input checked="" type="checkbox"/>	8		3	1	3	1	1	1	1	
1.1.1.1.3	+ Slabs (płyty grube)	<input checked="" type="checkbox"/>	8		16	2	8	3	3	1	1	
1.1.1.1.4	+ Columns (slupy)	<input checked="" type="checkbox"/>	8		7	1	7	1	1	1	1	
1.1.1.1.5	+ Frame mounting (mocowanie ramy gł.)	<input checked="" type="checkbox"/>	8		0	2		0	0			
1.1.1.2	- Ground floor (parter)	<input checked="" type="checkbox"/>										17
1.1.1.2.1	+ Walls (ściany)	<input checked="" type="checkbox"/>	8		295	7	42	48	48	6	6	
1.1.1.2.2	+ Reinforcement (zbrojenie)	<input checked="" type="checkbox"/>	8		146	5	29	20	20	4	4	
1.1.1.2.3	+ Columns (slupy)	<input checked="" type="checkbox"/>	8		35	4	8	4	4	1	1	
1.1.1.2.4	+ Beams (belki)	<input checked="" type="checkbox"/>	8		226	10	22	15	15	3	3	
1.1.1.2.5	+ Slabs (płyty grube)	<input checked="" type="checkbox"/>	8		249	10	24	13	13	3	3	
1.1.1.3	- First floor (piętro)	<input checked="" type="checkbox"/>										19
1.1.1.3.1	+ Walls (ściany)	<input checked="" type="checkbox"/>	8		155	5	31	25	25	4	4	
1.1.1.3.2	+ Reinforcement (zbrojenie)	<input checked="" type="checkbox"/>	8		11	3	3	2	2	1	1	
1.1.1.3.3	+ Columns (slupy)	<input checked="" type="checkbox"/>	8		22	3	7	2	2	1	1	
1.1.1.3.4	+ Beams (belki)	<input checked="" type="checkbox"/>	8		85	10	8	6	6	1	1	
1.1.1.4	- Roof (dach)	<input checked="" type="checkbox"/>										7
1.1.1.4.1	+ Columns (slupy)	<input checked="" type="checkbox"/>	8		19	3	6	1	1	1	1	
1.1.1.4.2	+ Beams (belki)	<input checked="" type="checkbox"/>	8		122	6	20	7	7	3	3	

Fig. 6. Table with details of duration assessment for the tasks in the schedule

For the tasks enlisted in the Fig. 6 value of the nominator in the formula (1) has been calculated automatically on the basis of the information extracted from the model (quantities) and obtained from the catalogue base (normative consumption of man-hours [r-g] or machine-hours [m-g] for a certain construction work). Assumptions about the number of working hours per shift and number of workers assigned to a certain construction work had to be made in the course of planning process.

#### 4.3. Final arrangement of construction works schedule

The work starts with foundation reinforcement preparation and placement. As there is a lot of rebar, the task takes four days with man power of five reinforcement fixers. When it is finished, both footing and foundation slab is to be poured with concrete. Technological delay is required, that is why ground floor walls are planned to be constructed nine days after the slab execution and the week no. 2 may be recognized as a gap week. When the process of walls bricking up is

nearly finished first stage of ground floor reinforcement (column's reinforcement) preparation is planned to be started. Columns are located between masonry walls and are to be constructed after them, what reduces amount of needed formwork. Two-sided one is to be mounted and concrete placed in order to create the columns. Another part of the schedule is the roof structure construction. Main frame made from wood comprises columns mounted on the foundation columns (placed onto the spot footing) and beams. Execution of the rest of roof structure is planned to be finish at the same time as frame, but the frame does not require the gable wall in contrast to beams comprising roof truss (collar-ties, rafters, cross-beams and other wooden and metal elements). Final arrangement of the tasks in the schedule is presented in the Fig. 7.

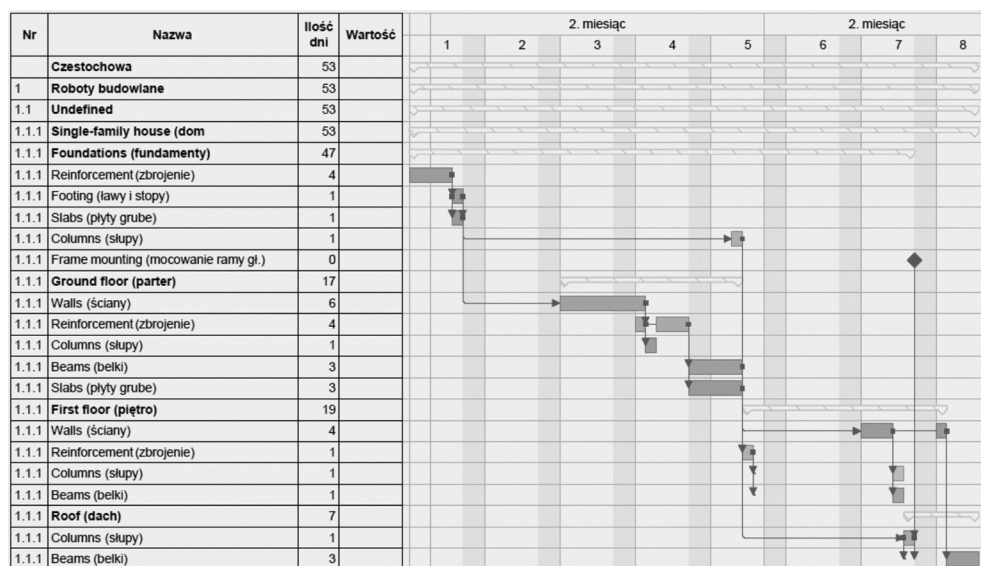


Fig. 7. Final arrangement of the tasks in the schedule – plan of construction works

## 5. Summary and conclusions

Implementation of BIM provides numerous number of possibilities concerning all the building engineering matters. BIM is especially beneficial in the field of construction project management. The models developed as 4-, 5- or even 6D constitute a collection of the data (database information) related to the successive construction stages, moreover they can also be a basis for maintenance and operating system long after the construction process is finished. Any type of building element can be launched into the model – every type of installation, architectural consideration or even a landscape planning.

The starting point for the quantity takeoff, cost estimation and planning is a model. Preparation of a model that ensures sufficiently precise, consistent and well organized information is a task which requires a discipline, experience and skills from the design team. On the one hand, each building structure may be composed of millions of elements, on the other hand division of those element into groups can be infinitely long process, actually not

this much important for designers as for people responsible for planning. Some requirements for the models as a basis for quantity takeoff and schedule can be listed as follows:

- elements in the model structure should be ordered in a way which allows for generating adequate work breakdown structure for the purposes of planning and schedule,
- distinction of the storeys/levels in the building's structure and assignment of the building's elements to the storeys/levels is essential,
- the elements in the adequate storeys/levels should be ordered in a way which reveals the technological order of execution of construction works,
- adequate model-based work breakdown structure is a condition for proper planning and schedule,
- quality of the schedule depends on the quality of a model.

The software exploited by the authors in the course of planning process (ZuziaBIM) allows to improve some of the possible deficiencies of the model. It is possible to correct the structure of the model's elements in the scheduling module to some extent. The way of operating on the model seems to be rather intuitive. For these people who met the concept and the tools for a building designing and construction management before, usage of BIM should not be troublesome. Such a program as ZuziaBIM (well-known cost estimation tool on Polish market) has been developed recently in order to operate on \*.ifc files. (BIM software backgrounds is described i.a. in [6].)

The future of the construction management seems to be strictly connected to BIM-based solutions. It must be emphasized however, that none of program or concept is able to replace a reasonable human who is able to evaluate the given assistance (in a form of software), reject unnecessary gadgets and take advantage of the modern world's opportunities for the most efficient project management outcomes.

#### Acknowledgements

BIM Vision and Zuzia BIM software by the courtesy of Datacomp sp. z o.o. Model BIM of the residential building by the courtesy of M.A.D. Engineers sp. z o.o.

#### References

- [1] Cooke B., Williams P., *Construction Planning, Programming and Control*, Wiley-Blackwell 2009.
- [2] Eastman C., Teicholz P., Sacks R., Liston K., *BIM Handbook – a guide to Building Information Modelling for Owners, Managers, Designers, Engineers and Contractors*, John Wiley & Sons, Hoboken, New Jersey 2008.
- [3] Griem P., *Integrated Project Delivery Using BIM*, Structure Magazine, April 2009.
- [4] Hendrickson C., Au T., *Project Management for Construction*, Prentice Hall, International Edition 1989.
- [5] Juszczak M., Zima K., *Building Information Modeling in Construction Process*, TECH-STA 2010, Management and Technologies for Sustainable Development in the Building Industry, 8-th International Conference, Prague 2010.

- [6] Kozłowska M., Sabol L., *Innovation approaches to building project preparation and realization*, Czasopismo Techniczne z. 1-B/2010, Wydawnictwo Politechniki Krakowskiej.
- [7] Leśniak A., Zima K., *Selected problems of cost estimating using BIM*, Creative Construction Conference 2012, June 30–July 3 2012, Budapest, Hungary.
- [8] Smith D.K., *An Introduction to Building Information Modeling (BIM)*, Journal of Building Information Modeling, Fall 2007.
- [9] The American Institute of Architects, California Council, *Integrated Project Delivery – A Working Definition*, McGraw Hill, 2007.
- [10] Zima K., *Integracja dokumentacji w procesie budowlanym z wykorzystaniem modelowania informacji o budynku*, Budownictwo i Architektura, 12(1), 2013.



MAGDALENA FURMANEK, KRZYSZTOF ZIMA\*

## ANALYSIS OF A PASSIVE DESIGN SPORTS HALL: CONSTRUCTION AND USE

---

### ANALIZA BUDOWY I EKSPLOATACJI PASYWNEJ HALI SPORTOWEJ

#### Abstract

This article presents an analysis of how the construction and insulation materials used for the walls of a sports hall built according to passive design affect the overall construction costs. The authors also attempt to answer whether the objective of achieving the lowest possible energy consumption in a building is actually economically sound. Cost analyses will be carried out to this end, the optimum insulation thickness will be determined, and the time necessary to balance the investment expenditure will be calculated for an energy-efficient construction project.

*Keywords: cost analysis, energy-efficient construction, passive buildings*

#### Streszczenie

W artykule, posługując się przykładem hali sportowej, wybudowanej w technologii budownictwa pasywnego, przeprowadzono analizę dotyczącą wpływu materiałów konstrukcyjnych i izolacyjnych ścian na ogólne koszty budowy. Autorzy podejmą także próbę odpowiedzi na pytanie, czy dążenie do uzyskania jak najmniejszego zużycia energii w budynku jest uzasadnione ekonomicznie. Zostaną w tym celu przeprowadzone analizy kosztowe, wyliczenia optymalnej grubości izolacji oraz obliczenie czasu zwrotu inwestycji energooszczędnej.

*Słowa kluczowe: analizy kosztowe, budownictwo energooszczędne, budynki pasywne*

**DOI: 10.4467/2353737XCT.15.388.5019**

---

\* PhD. Eng. Krzysztof Zima, Eng. Małgorzata Furmanek, Institute of Construction and Transportation Engineering and Management, Faculty of Civil Engineering, Cracow University of Technology.

## 1. Introduction

The construction sector is a particularly important part of implementing any sustainable development concept. A significant majority of sustainable development concepts refers to the problem of economic growth harmonization and the management of economic and natural resources [1]. The concept of energy-efficient buildings is receiving a great amount of attention. Faced with the rapid growth of energy carriers price, we are looking for solutions that would reduce the demand for energy, and thus costs [4]. There is no doubt that construction of such facilities is beneficial for the natural environment, but is it a 100% economically feasible proposition? In Poland, similar to the majority of the European Union countries, we are witnessing the gradual introduction of legal regulations limiting energy consumption in newly constructed, as well as in renovated or modernized, buildings. The European Union has issued numerous directives in recent years aimed at improving energy efficiency of buildings. The gradual process of introducing more and more stringent requirements related to energy consumption levels in construction has led to a considerable reduction in this area [4]. Energy standards for passive buildings vary according to the country and the type of structure being built, yet they have one thing in common – a low coefficient of energy consumption. The term passive building has received a lot of publicity throughout the world, and now it is regarded by investors and designers as prestigious [3].

The energy efficiency classification for buildings has never been clearly defined. Different definitions are valid in different countries, depending on the point of reference [4].

This article uses the classification developed by the Society for Sustainable Development. The point of reference in this classification is the operational energy indicator. The more stringent requirements for insulation properties of construction barriers may serve the purpose of defining the boundary values which are considered exemplary. Yet, in the opinion of numerous experts, in the context of power generation based on new energy sources, they may prove too strict [6].

## 2. Passive sports hall

The sports hall which is the subject of the analysis has been built at 3rd LO (Comprehensive High School) in Kraków. It was approved for use on 1 September 2014.

The parameters of the hall:

- The area covered by the planned facilities: 1,866.0 m<sup>2</sup>
- Total net area: 1,874.4 m<sup>2</sup>
- Gross volume of the above-ground storeys: 16,362.6 m<sup>3</sup>
- Height (stated in order to determine the technical requirements): 10.42 m.

Since the hall has been built with passive construction technology, its energy demand is less than 15kWh/m<sup>2</sup> per year (Fig. 1). In order to achieve such low levels of energy consumption, a number of solutions had to be implemented during the construction process, e.g. excellent thermal insulation (the walls – 30 cm of polystyrene foam, the roof – 40 cm of polystyrene foam + 10 cm of polyurethane foam, floor – 40 cm of polystyrene foam), triple pane windows, solar panels and an air exchange unit with a recuperator.

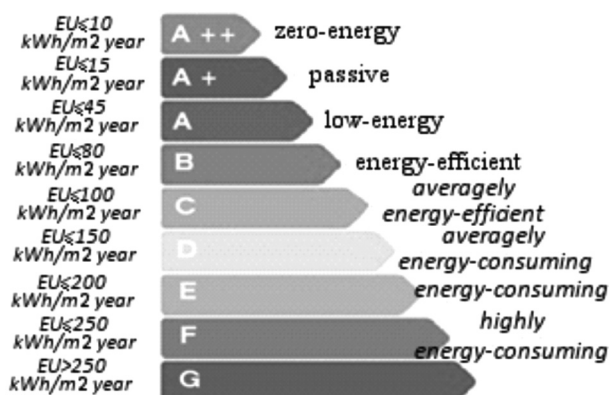


Fig. 1. Energy efficiency classification of buildings. Source: the authors, based on [4]

There are no thermal bridges in the building; it is effectively air-tight and generally meets the design specifications, which has been confirmed by photos taken during an inspection with the use of a thermal imaging camera (Fig. 2a, b).

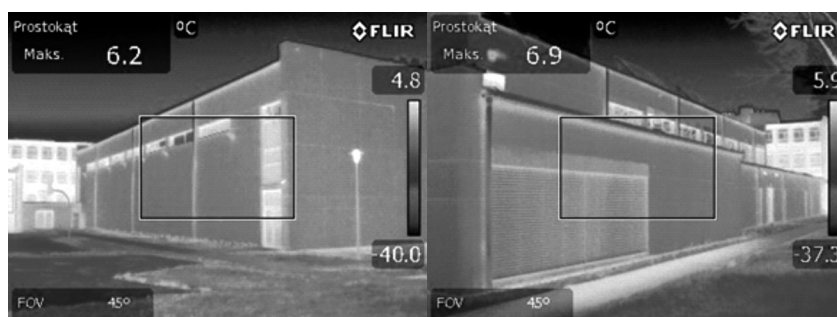


Fig. 1. A thermal image of the sports hall, a) northern façade, b) southern façade

### 3. Cost analysis

#### 3.1. The construction cost of the sports hall

The total cost of the sports hall construction amounted to approximately 6.5 million PLN. The analysis presented below takes into account only the architectural cost estimate, which included the following: external walls, internal walls (ground floor and first floor), internal plasters, wall facing, paint, suspended ceilings, foundations, thermal insulation, floors, a roof over the arena (roofing material), PVC profiles, wood profiles, metalwork, thermal insulation for the external walls, bathrooms and changing room furnishings, office furnishings, and sports equipment. The cost estimate for the above elements, done by the authors for the purpose of this paper, with the use of Zuzia 11 software, amounts to 2,414,805.59 PLN.



The main question that is usually asked in projects of this type is whether the construction costs could be reduced. The analysis must therefore focus on the assessment of how the general cost estimate value is affected by the type of material used to build the external walls of the hall, as well as the type of windows that have been installed in the building.

### 3.2. Analysis of cost estimate variants

Table 1 presents the materials which were used for the external walls of the hall, and table 2 displays the analysed alternative materials. Table 3 in turn shows the total estimated costs for each variant.

Table 1

**The sports hall external wall technical parameters for variant 1**

Material	d [cm]	$\lambda$ [W/mK]
Thin-layer polymer architectural coating	0.01	0.1200
SILKA N25 calcium-silicate blocks	25.00	0.4600
Fasada Platinum polystyrene foam panels	30.00	0.0032
Regular plaster	1.00	0.8200
Wood wool acoustic panels	3.50	0.0700

Source: Own work.

Table 2

**The sports hall external wall technical parameters for alternative variants**

Material	d [cm]	$\lambda$ [W/mK]
POROTHERM T&G type 25 wall hollow bricks	25.00	0.3130
YTONG cellular concrete class PP4/0.6S+GT	24.00	0.1600
Rockwool mineral wool panels	30.00	0.4600
Fasada Platinum polystyrene foam panels	15.00	0.0032

Source: Own work.

The analysis also includes two types of windows: the triple panel window  $U = 0.7 \text{ W/m}^2\text{K}$  and the double panel window  $U = 0.7 \text{ W/m}^2\text{K}$ , which is reflected in the results of calculations for different variants in individual cost estimates.

Table 3

**Distribution of construction costs in PLN for individual variants**

Insulation	Polystyrene foam 30 cm		Polystyrene foam 15 cm		Mineral wool 30 cm	
	windows double pane	windows triple pane	windows double pane	windows triple pane	windows double pane	windows triple pane
SILKA	2 367 137.30	2 414 805.59	2 323 727.54	2 371 395.83	2 364 939.71	2 412 608.00
POROTHERM	2 361 838.58	2 409 506.87	2 318 428.82	2 366 097.11	2 359 640.99	2 407 309.28
YTONG	2 388 501.43	2 436 169.72	2 345 091.67	2 392 759.96	2 386 303.84	2 433 972.13

Source: Own work.

The reference variant, which has been implemented in reality, is the one with external walls made of the following materials: Silka + 30 cm polystyrene foam and triple pane windows. If we reduce the insulation thickness by half and use windows of a lower coefficient  $U[W/m^2K]$ , the calculations presented in table 3 indicate that the greatest savings could be achieved in the following variants:

- Porotherm + 15 cm polystyrene foam + double pane windows (3.99% cost reduction as compared to the reference variant, i.e. 96,376.77 PLN),
- Silka + 15 cm polystyrene foam + double pane windows (3.77% cost reduction – 91,078.05 PLN).

**4. Operational energy**

The operational energy (OE) demand is defined by the amount of energy required annually for heating (or cooling), ventilation and tap water heating [4]. The OE calculations for the analysed sports hall (Tab. 4) have been done with the use of the BuildDesk Energy Certificate software.

Each alternative design variant involves an increase in the hall's energy consumption. The cheapest variants, as compared to passive technology, result in energy consumption increases of:

- 73.90% – Porotherm + 15 cm polystyrene foam + double pane windows,
- 39.96% – Silka + 15 cm polystyrene foam + double pane windows.

Table 4

**Operational energy demand in kWh/m<sup>2</sup> per year for individual variants**

Insulation	Polystyrene foam 30 cm		Polystyrene foam 15 cm		Mineral wool 30 cm	
	windows double pane	windows triple pane	windows double pane	windows triple pane	windows double pane	windows triple pane
SILKA	17.04	14.94	20.91	18.66	17.56	15.44
POROTHERM	22.11	19.83	25.98	23.59	22.64	20.34
YTONG	19.77	17.56	22.73	20.43	20.20	17.98

Source: Own work.

### 5. The time necessary to balance the investment expenditure

The simple time necessary to balance the investment expenditure may be calculated from the following formula:

$$SPBT = \frac{N}{\Delta O} \quad (1)$$

where

$N$  – the investment expenditure

$\Delta O$  – the savings

The time needed to balance SILKA + 30 CM POLYSTYRENE FOAM + TRIPLE PANE WINDOWS as compared to the cheaper solutions:

- POROTHERM + 15 CM POLYSTYRENE FOAM + DOUBLE PANE WINDOWS – 27 years,
- SILKA + 15 CM POLYSTYRENE FOAM + DOUBLE PANE WINDOWS – 47 years.

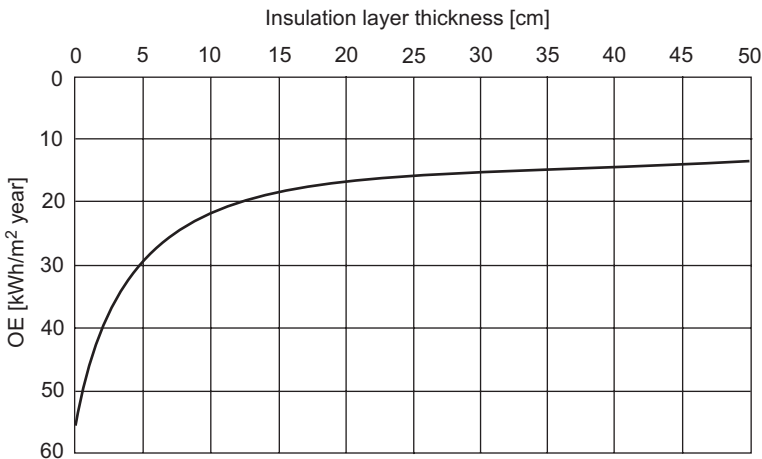


Fig. 3. Dependence of the insulation layer thickness on the operation energy demand for the passive sports hall Source: the authors.

It could be observed (Fig. 3) that, at a certain point, further increasing the insulation thickness no longer significantly reduces the operational energy consumption. The costs related to the additional insulation grow, yet the energy consumption drops only slightly, which results in the lengthening of the time necessary to balance the investment expenditure.

## 6. Optimal insulation thickness

The differences in construction costs between the promoted cost-efficient variant and the expensive one may – in the case of a sports hall – amount to almost 100% (Fig. 4).

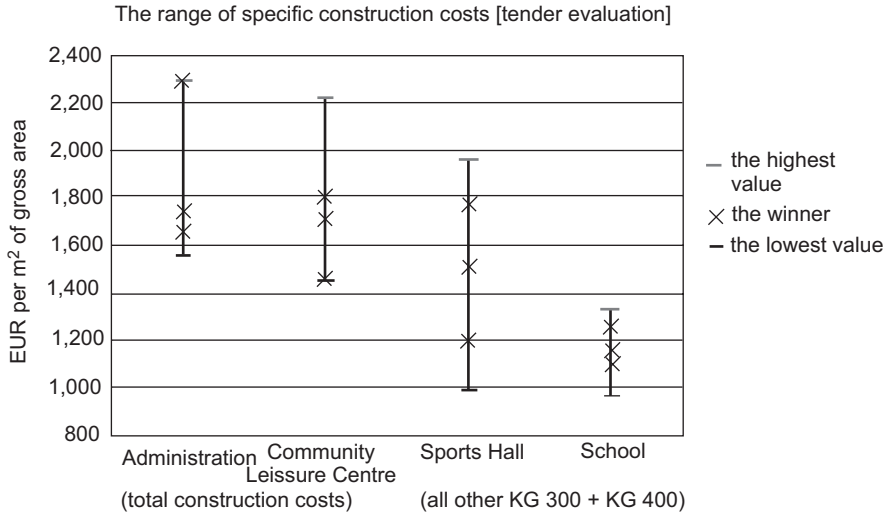


Fig. 4. “Cost efficiency” of architectural designs in comparison with additional costs of energy-efficient construction. Source [2]

Given such a huge difference in investment expenditure for the same construction project, we are impelled to ponder the question concerning the optimal insulation layer thickness [2]. The decision on the insulation layer thickness rests with the designer. The present cost of thermal insulation material and the cost of heating supply are known. The remaining factors are not quite known, although they are foreseeable, e.g. the discount rate value or the rates of energy cost increase above the inflation level in future years. The optimal insulation thickness formula (2) is shown below [5]:

$$d_{\text{opt}} = \lambda \sqrt{\frac{G_0 \sum_{i=1}^n \frac{(1+s)^i}{(1+r)^i}}{\lambda K}} \quad (2)$$

- $d_{\text{opt}}$  – optimal insulation thickness,
- $\lambda$  – heat conduction coefficient of the basic thermal insulation material,
- $G_0$  – annual heating cost ratio as related to 1 m<sup>2</sup> of barrier [PLN/m<sup>2</sup>],
- DD – number of heating degree-days
- $G$  – energy cost [PLN/GJ],
- $N$  – period of benefiting from the effects of warm weather [summer],
- $S$  – rate of heating cost increase over the inflation rate in time,

- $r$  – discount rate,  
 $K$  – insulation material cost *loco* construction site [PLN/m<sup>3</sup>],  
 $R_0$  – thermal resistance of the barrier's layers other than the thermal insulation (the ground) together with heat transfer resistance on the surface of barriers.

Given the following values of the relevant parameters: DD – 3050.1; G – 90 PLN/GJ;  $\lambda$  – 0.0032; K – 215 PLN/m<sup>3</sup>;  $R_0$  – 1.2265; inflation – 6% and the energy prices increase – 5%, the optimal values of insulation thickness for different periods of benefiting from the effects of warm weather are showed in Table 5.

Table 5

#### Optimal insulation thickness for the analyzed sports hall

Period of benefiting from the effects of summer	10	20	30	40	50
Optimal insulation thickness [cm]	18	20	21	22	23

Source: Own work.

## 7. Conclusions

The energy consumption of a building results – to a great extent – from the low thermal insulation of its walls (25–35%), so the design stage should include the process of optimization leading to a determination of the most economically feasible thermal insulation thickness [4].

Frequently, striving to meet the standards of a passive building is not accompanied by immediate financial gains, and a thick insulation layer is not indispensable for the optimal functioning of a building. In this article an analysis was made for the purpose of determining the best economic solutions in the context of construction costs and subsequent use of external wall insulation. An analysis was also performed in order to determine the best insulation thickness in relation to the expected period of use.

## References

- [1] Belniak S., Głuszak M., Zięba M., *Budownictwo ekologiczne. Aspekty ekonomiczne*, PWN, Warszawa 2013.
- [2] Bretzke A., *Benefits of the Passive House Standard in Schools: cost-effectiveness and user convenience*, Conference Proceedings for the 2009, International Conference on Passive Houses, Passivhaus Institut.
- [3] Dudzińska A., *Komfort cieplny w pasywnym budynku hali sportowej w Słomnikach*, Czasopismo Techniczne z. 2-B/2010, Wydawnictwo Politechniki Krakowskiej, 65–72.
- [4] [http://www.eip-cz-pl.eu/cz/files/Workshopy/02/ZURAWSKI\\_Budynki.pdf](http://www.eip-cz-pl.eu/cz/files/Workshopy/02/ZURAWSKI_Budynki.pdf) (14.04.15)

- [5] Rudczyk-Malijewska E., *Jaką grubość powinna mieć izolacja cieplna w przegrodach zewnętrznych budynków?*, IZOLACJE 3/2010.
- [6] Żurawski J., *Certyfikacja energetyczna przegród budowlanych*, Doradca Energetyczny, 4/2007, 35–37.



ANNA JOŃCZY, KRZYSZTOF ZIMA\*

## ANALYSIS OF SOLUTIONS FOR EXTERIOR WALLS IN THE BIM MODEL USING THE AHP METHOD

---

### ANALIZA WARIANTÓW ŚCIAN ZEWNĘTRZNYCH W MODELU BIM Z WYKORZYSTANIEM METODY AHP

#### Abstract

This paper presents selected variants of thermal insulation for external walls of single family homes. The main aim of this article is to analyze the technological and economical solutions based on the BIM model. The technical and economic analysis concerns the calculation and evaluation of both the costs of constructing the walls and the energy demand of the model building designed by the authors. The last part of the paper compares and prioritises proposed solutions in regard to the accepted assessment criteria using the AHP method, which allows for selecting the best solution.

*Keywords: AHP method, BIM, cost estimation, exterior walls*

#### Streszczenie

W artykule przedstawiono wybrane warianty izolacji cieplnej ścian zewnętrznych domów jednorodzinnych. Głównym celem artykułu jest analiza technologiczna i ekonomiczna rozwiązań oparta na modelu BIM. Analiza techniczna i ekonomiczna dotyczy obliczania i oceny zarówno kosztów budowy ścian, jak i zapotrzebowania na energię budynku zaprojektowanego przez autorów. W ostatniej części artykułu porównano proponowane rozwiązania i priorytety w odniesieniu do przyjętych kryteriów oceny z wykorzystaniem metody AHP, która pozwala na wybór najlepszego rozwiązania.

*Słowa kluczowe: metoda AHP, BIM, kosztorysowanie, ściany zewnętrzne*

**DOI: 10.4467/2353737XCT.15.391.5022**

---

\* Eng. Anna Jończy, PhD Eng. Krzysztof Zima, Institute of Construction and Transportation Engineering and Management, Faculty of Civil Engineering, Cracow University of Technology.



## 1. Introduction

The development of energy-efficient construction has become very dynamic in recent years. Care for high-quality thermal comfort in buildings, the desire to minimize the impacts of energy consumption on the environment and the reduction in expenses for heating are all tasks that require computer assistance. In addition, systematically tightening regulations compel the use of modern techniques for improving the facilities built.

This paper presents selected variants of thermal insulation for external walls of single family homes. The main aim of this article is to analyze the technological and economical solutions based on the BIM model. Technical and economic analysis concerns the calculation and evaluation of both the costs of constructing the walls and the energy demand of the model building designed by the authors. Calculation and analysis are based on the BIM model, presenting the possible workflow, which includes an automation of the calculations of the building energy demand and cost calculations.

The last part of the paper compares and prioritises proposed solutions in regard to the accepted assessment criteria using the AHP method, which allows for selecting the best solution.

## 2. Innovative methods for creating buildings – Utilization of BIM technology in modern construction

Progress and the development of computer technology have made it possible to transfer the design process from paper to the computer screen [1]. The foundations of BIM technology date back to the late twentieth century, when programmers tried to develop software allowing one to illustrate the processes taking place in the building designer's imagination. Initially, the exchange of industry data was not possible due to the lack of a common format, and the first versions of the programs only created mock-ups of future buildings on which self-generated drawings were based. After several years of development, the IFC standard (Industry Foundation Classes) was created, which is currently adopted by most leading IT companies creating software for the construction industry. As a result, cooperation between branches is now possible regardless of the software [2].

BIM is defined by the National BIM Standard as “a digital representation of physical and functional characteristics of a facility” and “shared knowledge resource for information.” In another words, we could say that BIM means a building, which can be created in the virtual world, from the conceptual stage to implementation. BIM is an organizing concept that contributes in the lifecycle of a facility by creating and managing a building's data in a convenient way [3]. That digital model developed in 5D technology can be used to make design decisions, develop a coherent and complete construction documentation, perform subsequent analysis of collected data for estimating the profitability and investment costs, and ultimately the management of the built object as well [4].

An object created in BIM has all the possible parameters of the actual building (Fig. 1). However, a virtual building created this way is not only an ordinary geometrical model dressed in nice textures, creating attractive visualizations for the client. With BIM technology, each element is a digital prototype of the building's physical components: walls,

columns, windows, doors, stairs, etc. As a result, the BIM model allows us to understand the building before its construction even begins, as well as to catch errors in the design before its implementation. Because its energy efficiency is known, it is possible to control the cost of construction and materials, as well as the cost of maintaining the building throughout its life cycle already at the design stage. The database can include a wide array of information about the structure, including geometry, material, manufacturing and assembly techniques, tolerances, costs, and even information to support supply chain management, or it may include only some of these [5].

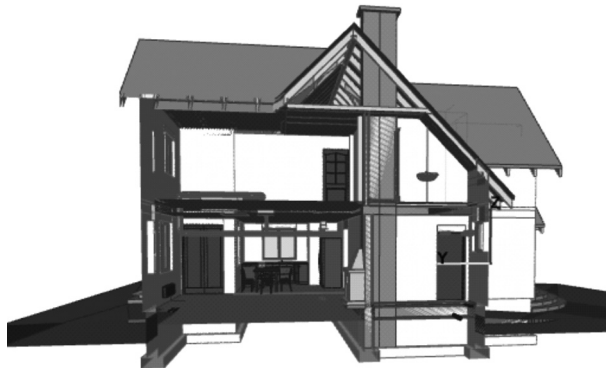


Fig. 1. Model of a building in BIM

BIM technology is used at the stage of design development so that all participants in the investment process may become involved in the creation of the facility. Because cooperation is based on 3D models, changes made by one party are immediately seen by others. This results in saving time that had previously been spent on coordinating and adapting all of the documentation to the changes made in 2D. Therefore, BIM also facilitates the close cooperation of specialists.

The model's level of detail and the ease of sharing information between sectors makes it simpler to introduce design changes, thus enabling contributors to simulate the costs and the energy demand. For these reasons, the universality of the use of BIM models in the world is growing at a dynamic pace, and this technology is already recognized as a worldwide standard.

### 3. Decision-making based on BIM

Decision-making based on BIM technology consists of collecting data from engineering analysis, cost analysis, etc., in a single model. Information from databases is added to the 3D model. It is easy to calculate the energy demand from the designed building or to create a realistic visualization of the facility so that the potential customer can easily imagine the finished product. Such a model can be also loaded into a cost estimation program and present the estimate in a transparent manner (Fig. 2).

Estimating the cost in a program based on BIM technology, equipped with a 3D model viewer, we can save a substantial amount of time. Such a system allows users to move bills of quantities obtained directly from virtual models in order to estimate and obtain a quote at any stage of the project. Therefore the estimate is based on the bill of quantities obtained from a virtual model of the building. Such a system eliminates accounting errors and elements included in the bill of quantities which are related to the blueprints, so it is possible to skip single parts. Dimensional elements appear in the browser as slides (Fig. 3), so there is no need for the estimator to consider whether the given element was already measured. This innovative application is adaptable and can use models developed in any CAD system compatible with BIM.

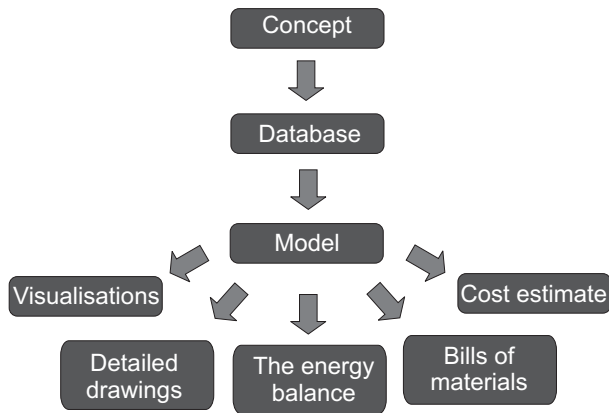


Fig. 2. Diagram of the BIM process

The BIM model can automatically provide a section of data needed to perform cost calculation (bill of quantities, scope of calculation and list of materials), leaving the cost estimator with the remaining elements. The remaining work is dependent on the regulations relating to cost estimation and the individual assessment of the cost estimator [6].

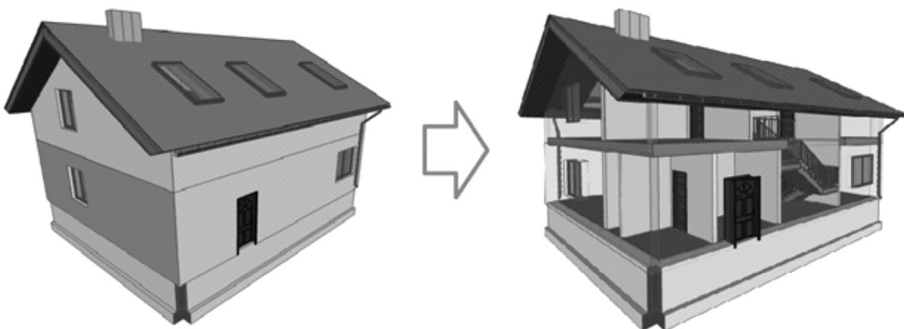


Fig. 3. Presentation of the quantity takeoff process in BIM

The integration of a BIM model with a decision-making tool and sustainability metrics addresses the difficulties of making decisions earlier in the design/build process, and allows for specific sustainability trade-off analyses to be conducted, using the actual building conditions and characteristics [7]. Figure 4 presents the model's architecture for cost calculations with environmental factors. The exemplary model determines the processes for data analysis, considering all criteria and specifications. This analysis is applied to project and sustainable information, environmental factors, environmental performance, and unit cost calculations, using input requirements. The main aim of the presented model is a 3D-BIM sustainable design of the building, which contains a list of the selected sustainable materials and their environmental impacts, as well as cost calculations for the chosen variant.

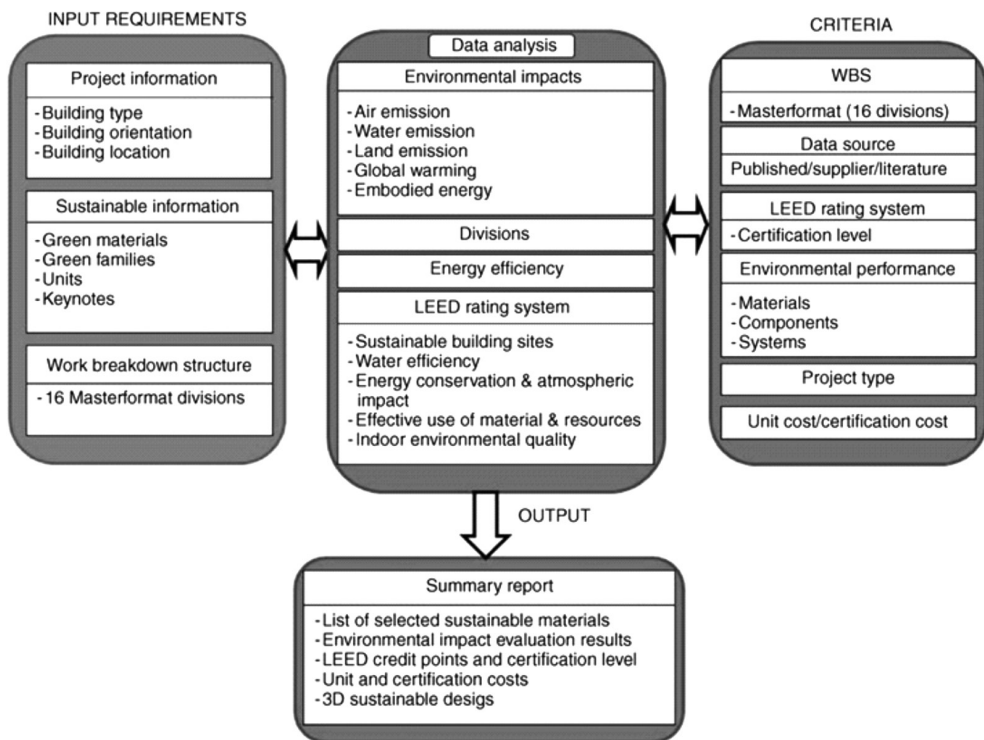


Fig. 4. Model architecture [3]

#### 4. BIM based analysis

##### 4.1. Basic technical parameters of the analysed building

The model of the building on which the technological and economic analyses of external walls were carried out is a single-storey, single-family house with a habitable attic. The building designed by the authors for the analysis has a rectangular footprint with the

dimensions  $12.68 \text{ m} \times 10.83 \text{ m}$ . Its shape is a truncated rectangular prism with a gable roof. The house consists of a ground floor and a habitable attic, without a basement. The basic data of the building's geometry: total area:  $253.2 \text{ m}^2$ , usable area:  $213.4 \text{ m}^2$ , area of the building envelope:  $327.5 \text{ m}^2$ , volume:  $605.57 \text{ m}^3$ .

The external walls of the building consist of a structure made of clay masonry units Porotherm P+, which are 30 cm thick and contain a 12 cm thermal insulation layer. The total thickness of the envelope is 46 cm.

Individual layers of the external wall include: 2 cm – interior plaster, 30 cm – Porotherm P+W 30 hollow masonry unit, 12 cm – thermal insulation, 2 cm – external plaster.

#### 4.2. Thermal insulation of external walls and thermal transmittance of the building

Three variants of insulation have been used for the technical and economic analysis:

- EPS 040 FASSADA foamed polystyrene made by Austrotherm.
- ISOVER TF Profi mineral rock wool.
- EPS 031 FASSADA PREMIUM graphite-enhanced foamed polystyrene made by Austrotherm.

Below is a list of coefficients of thermal conductivity  $\lambda$  and the applied thicknesses of thermal insulation materials, as well as the values of the heat transfer coefficient  $U$ , obtained by the external walls of the building after the application of the given type of thermal insulation (Table 1).

Table 1

##### Material data of thermal insulation and thermal transmittance values obtained

Material	EPS	Mineral wool	Graphite-enhanced EPS
Thermal conductivity coefficient [W/m · K]	0.40	0.36	0.31
Thickness [m]	0.12	0.12	0.12
Thermal transmittance coefficient $U$ [W/m <sup>2</sup> · K]	0.22	0.21	0.19

Source: Own work

#### 4.3. Building energy demand

The values of heating energy and total energy consumption, calculated using ArchiCAD 18, software based on BIM technology, as well as the maximum values of these quantities required for energy efficient buildings and passive buildings are shown in the figure below (Table 2).

As can be seen from the above results, the use of each of the analysed material meets the requirements for energy-efficient buildings, but none of the variants of the solution provides the level required for passive buildings.

Table 2

**Energy demand in relation to the different variants of the building's thermal insulation**

Type of energy	EPS	Mineral wool	Graphite-enhanced EPS	Permissible value for	
				energy-efficient building	passive building
Heating energy [kWh/m <sup>2</sup> · year]	31.54	30.58	29.61	70	15
Total energy consumption [kWh/m <sup>2</sup> · year]	131.29	130.33	129.36	250	120

Source: Own work

#### 4.4. Cost analysis of the building

The cost analysis was limited to estimating the cost of the construction of external walls. The list of the costs of different types of thermal wall insulation is presented in Table 3.

Table 3

**Energy demand in relation to the different variants of the building's thermal insulation**

EPS	Mineral wool	Graphite-enhanced EPS
PLN 4433.43	PLN 6166.23	PLN 5520.99

Source: Own work

### 5. Analysis of the profitability of different variants of thermal insulation using AHP

The Analytic Hierarchy Process (AHP) is a multi-criteria decision analysis method. It is applied in order to find solutions for multi-criteria decision problems. Specifying the importance of the criteria is performed by a pairwise comparison on a 1–9 scale. The scale ranges from 1/9 for 'least valued than' to 1 for 'equal,' and to 9 for 'absolutely more important than,' covering the entire spectrum of the comparison [8]. The AHP method consists of two phases: the creation of a structure and performing an evaluation of the hierarchical structure.

A list of the criteria for particular variants and the evaluation criteria are presented in Table 4.

Table 4

**Material data of thermal insulation and thermal transmittance values obtained**

Criterion	EPS	Mineral wool	Graphite-enhanced EPS
Thermal transmittance coefficient U	0.22	0.21	0.19
Thickness [m]	0.12	0.12	0.12
Total energy consumption [kWh/m <sup>2</sup> · year]	131.29	130.33	129.36
Cost	PLN 4433.43	PLN 6166.23	PLN 5520.99

Source: Own work

Table 5 shows an example matrix of relative significance adjusted to the normalized value.

Table 5

**Matrix of relative significance adjusted to the normalized value – an example for C3**

C3	W1	W2	W3	→	C1	W1	W2	W3
W1	1.00	0.33	0.20		W1	0.11	0.08	0.13
W2	3.00	1.00	0.33		W2	0.33	0.23	0.22
W3	5.00	3.00	1.00		W3	0.56	0.69	0.65

Source: Own work

The hierarchy general ranking table, as a final score of calculations is shown in Table 6.

Table 6

**Hierarchy general ranking**

GP	C1	C2	C3	C4	W
Wg	0.406	0.044	0.309	0.241	
W1	0.083	0.333	0.106	0.633	0.289
W2	0.193	0.333	0.260	0.106	0.223
W3	0.724	0.333	0.633	0.260	0.488
SUMA	1.406	1.044	1.309	1.241	

Source: Own work

The consistency check in the hierarchy general ranking was calculated: CR for C1 equals 0.063, C2 equals 0.000, C3 equals 0.031, C4 equals 0.031. Therefore, the consistency check succeeds, all CR values are less than 0.1. With the established criteria in the AHP method, variant 3 (Graphite-enhanced EPS) proved to be the most advantageous option.

## 6. Conclusion

The use of solution variants allows for a quick assessment of the solutions. The use of decision-making support using AHP as a module for the BIM model expands the information available to the decision-maker. From the cases analysed in this paper, it can be inferred that:

- The use of EPS 040 FASSADA costs PLN 4433.43, which allows building an exterior wall with the thermal transmittance coefficient of  $0.22 \text{ W/m}^2 \cdot \text{K}$
- The use of ISOVER TF Profi mineral wool reduces the heat permeability by 4.5%, and provides durability to the heat-insulating material, but increases the expense of thermal insulation by 28%
- Construction of thermal insulation using graphite-enhanced EPS 031 FASSADA PREMIUM increases the level of thermal insulation by 13.5% compared to regular EPS and 9.5% to mineral wool, whereas the cost of this solution is 20% higher than the price of regular expanded polystyrene and 10.5% lower than mineral wool.

In summary, it can be said that, depending on the expectations from the building being designed, it is possible to use cheaper materials with average thermal properties (EPS), more expensive materials with better technical parameters such as graphite-enhanced EPS, or expensive – but also more durable materials – such as mineral wool. Using the AHP analysis, however, it is possible to select the best solution, taking multiple criteria into account.

## References

- [1] Juszczuk M., *Technologia BIM i podejście IPD*, Przemysł Drzewny, 2/2013, 44-49.
- [2] [http://www.archicad.pl/materialy\\_prasowe/Archicad\\_BIM.html](http://www.archicad.pl/materialy_prasowe/Archicad_BIM.html), online: 28.12.2014.
- [3] Jrade A., Jalaei F., *Integrating building information modelling with sustainability to design building projects at the conceptual stage*, Building Simulation, 6, 2013, 429-444.
- [4] Juszczuk M., Zima K., *Building Information Modeling in construction process*, Proceedings of TECHSTA 2010 – Management and Technologies for Sustainable Development in the Building Industry (on CD), Prague 2010, 241-246.
- [5] See R., *Building information models and model views*, Journal of Building Information Modeling, 2007, 20-25.
- [6] Zima K., Leśniak A., *Limitations of Cost Estimation Using Building Information Modeling in Poland*, Journal of Civil Engineering and Architecture, 7, 2013, 545-554.
- [7] Bank L.C., McCarthy M., Thompson B.P., Menassa C.C., *Integrating BIM with system dynamics as a decision-making framework for sustainable building design and operation*, Proceedings of the First International Conference on Sustainable Urbanization, Hong Kong 2010, 40-48.
- [8] Vaidya O.S., Kumar S., *Analytic hierarchy process: An overview of applications*, European Journal of Operational Research 169, 2006, 1-29.





AGNIESZKA LEŚNIAK\*, BARTŁOMIEJ SZEWCZYK\*

## SELECTION OF A SPORTS FLOORING TYPE

---

### WYBÓR WARIANTU WYKONANIA PODŁOGI SPORTOWEJ

#### Abstract

The article presents a classification of sports floors based on the type of deformations to which they are subjected and gives several examples of possible methods of their manufacture and installation. Three variants of sports flooring have been suggested for a selected sports venue and, subsequently, a multi-criteria comparative analysis has been carried out for the variants taking into account the following criteria: cost, installation time, suitability for various sports disciplines and other extra-sport purposes as well as the floor thickness.

*Keywords: sports flooring, multi-criteria analysis*

#### Streszczenie

W artykule zaprezentowano podział podłóg sportowych związany z rodzajem odkształceń, którym ulegają. Podano przykłady trzech wariantów podłogi sportowej i porównano je pod względem kosztu i czasu realizacji. Dla proponowanych wariantów przeprowadzono również wielokryterialną analizę porównawczą, uwzględniając przy tym: koszt i czas realizacji, możliwości zastosowania do różnych dyscyplin sportowych i celów pozasportowych oraz grubość podłogi.

*Słowa kluczowe: podłogi sportowe, analiza wielokryterialna*

**DOI: 10.4467/2353737XCT.15.409.5040**

---

\* PhD. Eng. Agnieszka Leśniak, MSc. Eng. Bartłomiej Szewczyk, Institute of Construction and Transportation Engineering and Management, Faculty of Civil Engineering, Cracow University of Technology.

## 1. Introduction

The selection of the right sports flooring is a key factor in designing any sports hall since the degree to which it will serve its function properly depends mainly on the structure of the floor. A sports floor is a type of special purpose flooring that must accommodate the intensive and diverse movements of people practicing sport. Therefore it is designed and made with two fundamental objectives in view: comfort and safety of users, which, in consequence, will reduce the risk of injury. Additionally, it must provide the right surface finish effect (friction) and movement dynamics so as to ensure the highest possible level of performance.

The article presents the types of sports flooring which are in use contemporarily. Three possible variants of sports flooring have been suggested, their cost and installation times estimated, and the most suitable variant has been selected on the basis of the adopted criteria.

## 2. Classification of sports floors

The classification of sports flooring contained in standard [1] is based on the type of deformations to which they are subjected. Four types of sports floors may thus be differentiated:

### – Area-elastic floors

Applying a point force causes deflection over a relatively large area around the point of application of the force [2]. This type of floors may be found in two structural variants: over a grid of joists or over a composite grid of plywood or particle board laid alternately [3]. These floors are characterized by a considerable height, yet, owing to their structure, they fully meet the requirements of professional sports people.

### – Point-elastic floors

Applying a point force causes deflection only close to the point of application of the force [2]. Point-elastic floors are composed of two layers: the underlying elastic layer and the surface synthetic layer [4]. It may take the form of a thick sports floor cover with an underlying layer made of elastic foam [5]. The main feature of point-elastic floors is their relative thinness. Due to their soft surface, they are a good option for school gyms and recreational facilities.

### – Combi-elastic floors

They combine area-elastic floors with a point-elastic surface [4]. The area of deformation is large in the load distribution layer. On the surface, however, it is limited precisely to the area directly under loading [2]. Combined systems are universal in their applications, as they are suitable for practicing professional sports without compromising safety. However, they also have the deficiencies of both area-elastic and point-elastic floors, such as considerable structural height or limited options of placing heavy sports equipment or spectator stands on them.

### – Mixed-elastic floors

The area of deflection is small, but clearly extends beyond the point of application of the force. The floor deflection characteristics are between those of a point-elastic floor and an area-elastic floor [2]. It is a combination of a point-elastic floor with a surface stiffening component [4]. Due to the introduction of the surface stiffening component, the floor of this type does not induce muscle fatigue of its users, retaining at the same time a relatively soft surface. Moreover, such floors are low in height and lightweight.

### 3. Analysis of the selected variants of sports flooring

#### 3.1. The suggested variants of sports flooring

Three possible variants of flooring have been suggested for the sports hall selected as an example, with the area of 526 m<sup>2</sup>:

– **Variant I – area-elastic sports floor**

Area-elastic floor over a grid of pine joists, 16 mm × 50 mm in cross-section, laid crisscross, with a subfloor of 16 mm thick pine boards nailed in an open-work fashion. The spacing of the lower layer of joists is every 50 cm, while of the upper one – every 31.5 cm. The surface made of polished oak parquet planks covered with three coatings of anti-slip paint.

– **Variant II – point-elastic sports floor**

Point-elastic floor of Omnisports REFERENCE sports flooring – 6.5 mm thick – glued directly to the base. Having been rolled out and glued, the floor covering is cut to fit and heat welded at joints.

– **Variant III – combi-elastic sports floor**

Combi-elastic floor over a grid of two layers of pine joists, 16 mm × 50 mm in cross-section, laid crisscross, with a subfloor of two layers made of 12 mm-thick waterproof coniferous plywood. The spacing of the lower layer of joists is every 50 cm, while of the upper one – every 31.5 cm. Epoxy surfacing poured on site over the underlayment of rubber granules laid over the subfloor.

#### 3.2. The cost and time of installation

A detailed cost estimate according to [6], has been prepared for each variant. The following input data were used in the estimation process:

- man-hour fee – 14.34 PLN,
- materials purchase cost index – 6.40% of the materials cost,
- indirect cost index – 65.00% of the labor and equipment use cost,
- profit index – 10.90% of the labor, equipment use and indirect costs,
- prices of materials and equipment use – average market prices.

Next, the composition of working teams was determined and so were the times needed for installation of individual variants. The comparison of the estimated price components for each variant has been presented in Table 1.

Table 1

**Comparison of the floor installation costs in individual variants. Source: the author**

Variant	Labor [PLN]	Materials [PLN]	Equipment [PLN]	Indirect cost [PLN]	Profit [PLN]	Estimated net price [PLN]
Variant I	22,041.96	123,382.62	1,751.73	15,450.69	4,274.95	166,901.95
Variant II	5,410.70	67,744.59	165.14	3,628.06	1,003.89	77,952.38
Variant III	17,857.34	154,494.25	1,352.19	12,474.64	3,451.53	189,629.95

The variant of point-elastic floor is characterized by the lowest values of all the components: labor, materials and equipment use. The variant of area-elastic floor has the highest of all the compared labor and equipment use costs. The combi-elastic floor, on the other hand, requires the highest expenditure on materials. Since this component has the largest share in the estimated price, variant III of the floor is the most expensive.

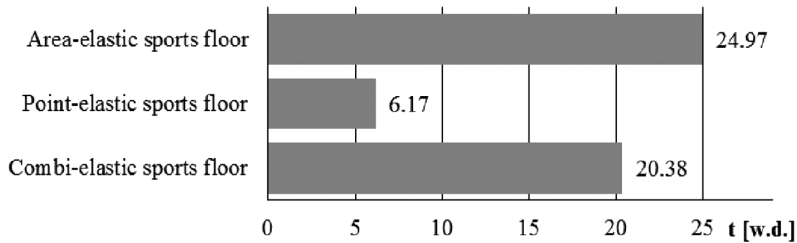


Fig. 1. Comparison of the installation times of the suggested sports flooring variants.  
Source: the author

The shortest installation time, which is slightly more than 6 working days (8-hour working day), characterizes the point-elastic floor variant, whereas the area-elastic floor variant, requiring 28 working days, is the longest to assembly. Significant differences in the installation times of the individual floor variants result from the considerable difference in the number of layers in the structure of those variants. The point-elastic floor is basically one ready-made sports floor covering requiring solely to be glued to the base and heat welded at the joints. In contrast, the two remaining variants require installation of a joist grid, a subfloor and the surface. They are then definitely more labor consuming.

#### 4. Multi-criteria comparative analysis

Multi-criteria analysis may be used to select, out of a set of analyzed variants, the best variant or a sub-set of variants which are “good enough.” It may also serve the purpose of arranging the variants from the best to the least advantageous. It is applicable when the decision-making process requires considering more than one criterion. In order to select the most advantageous variant of sports flooring, a multi-criteria comparative analysis has been carried out, in which the following four evaluation criteria were adopted:

- Criterion I – the cost of installation,
- Criterion II – the time of installation,
- Criterion III – functionality (for sports disciplines and extra-sport purposes),
- Criterion IV – the height of the floor structure.

The values of individual constituent measures are: the estimated net price and the times of installation presented in the previous chapter. The suitability of the individual variants for sports disciplines and extra-sport purposes has been graded arbitrarily on a six-grade scale, on the grounds of information included in [3]. The thickness has been determined measuring the layers from the base to the surface. Table 2 presents the values of individual constituent measures applied to the variants according to the adopted criteria of evaluation.

Table 2

**Values of constituent measures applied to the variants according to the adopted criteria of evaluation. Source: the author**

Criterion	Criterion character	Measure of the variant		
		Variant I	Variant II	Variant III
C I – the cost of installation	Inhibitor	166,901.95 PLN	77,952.38 PLN	189,629.95 PLN
C II – the time of installation	Inhibitor	24.97 w.d.	6.17 w.d.	20.38 w.d.
C III – functionality	Stimulus	5	2	4
C IV – thickness	Inhibitor	97 mm	6.5 mm	86 mm

The Neumann-Morgenstern coding has been applied in this paper, i.e. a constituent measure has been replaced by the ratio of the difference between this measure and the worst measure in a given criterion and the difference between the best and the worst measures in this criterion [7]. Table 3 presents the encoded measures of the variants according to the adopted criteria.

Table 3

**Encoded measures of variants according to the adopted criteria of evaluation. Source: the author**

Criterion	Criterion character	Measure of the variant		
		Variant I	Variant II	Variant III
C I – the cost of installation	Inhibitor	0.20	1.00	0.00
C II – the time of installation	Inhibitor	0.00	1.00	0.24
C III – functionality	Stimulus	1.00	0.00	0.67
C IV – thickness	Inhibitor	0.00	1.00	0.12

The following weighted indicators have been adopted:  $v_1 = 0.3$ ;  $v_2 = 0.1$ ;  $v_3 = 0.5$ ;  $v_4 = 0.1$ ; it has been decided that the most important criterion would be the suitability of the floor for sports disciplines and extra-sport purposes due to the special function performed by sports flooring.

The corrected summative indicator [7] has been applied for the purpose of a synthetic evaluation of the variants, calculated according to formula (1).

$$J_i = \sum_{j=1}^m (z_{ij} \cdot v_j) \quad (1)$$

where:

- $z_{ij}$  – encoded measure of the  $i$ -th variant in relation to the  $j$ -th criterion,
- $v_j$  – weight of the  $j$ -th criterion,
- $m$  – number of criteria.

**Summative indicators for the variants. Source: the author**

Summative indicator	Variant I	Variant II	Variant III
$J$	0.56	0.50	0.37

As a result of the comparative analysis (Table 4), variant I – the area-elastic sports floor – must be considered the most advantageous in the light of the adopted criteria, since the summative indicator for this variant has the highest value  $J_1 = 0.56$ . Variant II – the point-elastic sports floor – has a slightly lower summative indicator value –  $J_2 = 0.50$ . The least advantageous variant, according to the adopted criteria, is variant III – the combi-elastic sports floor –  $J_3 = 0.37$ .

## 5. Conclusions

The suggested variants of sports floors differ considerably in cost and time of installation as well as in functionality and technical specifications. The multi-criteria comparative analysis has indicated the most advantageous variant in the light of the adopted criteria. However, selecting a sports flooring type, the investor should also consider other factors (which have been disregarded in the example), such as e.g. the prevailing sports discipline, the age of users or whether the sports practiced in the facility are amateur or professional. They will undoubtedly facilitate selection of the best option.

## References

- [1] PN-EN 14904:2009. Nawierzchnie terenów sportowych – Nawierzchnie kryte przeznaczone do uprawiania wielu dyscyplin sportowych – Specyfikacja.
- [2] website American Sports Builders Association [www.sportsbuilders.org](http://www.sportsbuilders.org).
- [3] website of sports floors manufacturer [www.haro-sports.com](http://www.haro-sports.com).
- [4] website of sports facilities contractor [www.descol.nl](http://www.descol.nl).
- [5] website of floors manufacturer [www.tarkett.pl](http://www.tarkett.pl).
- [6] Plebankiewicz E. *Podstawy kosztorysowania robót budowlanych*, Wydawnictwo Politechniki Krakowskiej, Kraków 2007.
- [7] Szwabowski J., Deszcz J., *Metody wielokryterialnej analizy porównawczej: podstawy teoretyczne i przykłady zastosowań w budownictwie*, Wydawnictwo Politechniki Śląskiej, Gliwice 2001.

## CONTENT

Artur Borowczyński, Dariusz Heim: Supplementary lighting control in office room with minimized glazing area .....	3
Henryk Nowak, Paweł Noszczyk: Application of the active IR thermography for the detection of non-uniformity of materials in building partitions .....	9
Katarzyna Nowak-Dzieszko, Małgorzata Rojewska-Warchał: Simulation of night cooling in a single dwelling of a large panel building .....	15
Andrzej Smoleń: Performance analysis of the hybrid power system used for supplying the autonomous road light installations .....	23
Katarzyna Franczyk, Alicja Kowalska-Koczwara: Analysis of the influence of shaping steel hall pillars of its dynamic characteristics .....	31
Paweł Gałek: An attempt to evaluate the application of 3D scanners in construction diagnostics and tests .....	39
Alicja Kowalska-Koczwara, Paweł Kiszka: Analysis of the influence of reinforced concrete beam-and-slab floor forming on dynamic characteristics of a building.....	45
Dawid Łątka, Michał Repelewicz: The influence of superstructure stiffness on internal forces distribution in raft foundations.....	51
Izabela Murzyn, Joanna Dulińska, Marek Wazowski: An experimental and numerical assessment of the dynamic characteristics of the footbridge located over the national expressway DK-1 .....	57
Dawid Pawłowski, Maciej Szumigała: An experimental and theoretical study of deflections of BFRP RC beams .....	63
Dawid Pawłowski, Maciej Szumigała: Short-term cracking in BFRP RC beams – experimental and theoretical analysis.....	71
Donatas Aviža, Zenonas Turskis, Adam Święcicki: An empirical analysis of the Lithuanian and Polish normative requirements and their influence on the payback of a thermo-insulation layer of an external wall detail.....	79
Barbara Dulińska: Sustainable development in cities designed in accordance with the Smart City concept .....	87
Wojciech Duliński: Sustainable airport passenger terminal design – the review of selected examples.....	93
Irena Ickiewicz, Ewelina Kowalczyk: Passive building – verification of achieved effects.....	99
Marta Nowak, Michał Kołaczkowski: New dimension for straw construction.....	107
Agata Pawłowska, Michał Zielina: Analysis of water intake screen's performance under various conditions .....	115
Marta Plaskacz-Dziuba, Marcin Cichosz, Bartłomiej Igliński, Roman Buczkowski: Autoclaved aerated concrete with an addition of waste from semi-dry flue gas desulfurization process – thermal stability and XRD investigations .....	123
Anna Wassilkowska, Karolina Kuc, Michał Zielina: A study of the composition of cement mortar lining in water and sewage pipelines.....	131
Gabriela Zemełka: Fate of three herbicides (tembotrione, nicosulfuron and S-metolachlor) on soil from Limagne region (France).....	137
Michał Zielina, Anna Młyńska, Tadeusz Żaba: Experimental research on deterioration of drinking water quality after cement mortar pipe lining .....	145
Maja Bartoszek, Michał Juszczak: Selected problems of BIM-based planning of construction works – case study .....	153
Magdalena Furmanek, Krzysztof Zima: Analysis of a passive design sports hall: construction and use.....	165
Anna Jończy, Krzysztof Zima: Analysis of solutions for exterior walls in the BIM model using the AHP method .....	175
Agnieszka Leśniak, Bartłomiej Szewczyk: Selection of a sports flooring type .....	185



## TREŚĆ

Artur Borowczyński, Dariusz Heim: Uzupełniające sterowanie oświetleniem w pomieszczeniu biurowym o zminimalizowanej powierzchni przeszklenia .....	3
Henryk Nowak, Paweł Noszczyk: Zastosowanie termografii aktywnej do detekcji niejednorodności materiałowych w przegrodach budowlanych .....	9
Katarzyna Nowak-Dzieszko, Małgorzata Rojewska-Warchał: Symulacja nocnego chłodzenia w pojedynczych mieszkaniach w budynku z wielkiej płyty .....	15
Andrzej Smoleń: Analiza wydajności hybrydowego układu zasilania autonomicznego systemu oświetlenia drogowego.....	23
Katarzyna Franczyk, Alicja Kowalska-Koczwara: Analiza wpływu kształtowania słupów hali stalowej na jej charakterystyki dynamiczne.....	31
Paweł Gałek: Próba oceny możliwości zastosowania skanerów 3D w diagnostyce budowlanej i badaniach.....	39
Alicja Kowalska-Koczwara, Paweł Kiszka: Analiza wpływu kształtowania modelu stropu płytowo-żebrowego na charakterystyki dynamiczne budynku .....	45
Dawid Łątka, Michał Repelewicz: Wpływ sztywności nadbudowy na wielkość sił wewnętrznych w płytach fundamentowych .....	51
Izabela Murzyn, Joanna Dulińska, Marek Wazowski: Doświadczalne i numeryczne wyznaczanie charakterystyk dynamicznych kładki dla pieszych usytuowanej nad DK-1 .....	57
Dawid Pawłowski, Maciej Szumigała: Ugięcia belek zbrojonych prętami bazaltowymi BFRP – badania laboratoryjne i rozważania teoretyczne .....	63
Dawid Pawłowski, Maciej Szumigała: Krótkotrwałe zarysowanie belek zbrojonych prętami bazaltowymi BFRP – analiza teoretyczna i doświadczalna .....	71
Donatas Aviža, Zenonas Turskis, Adam Święcicki: Analiza litewskich i polskich wymagań ochrony cieplnej oraz ich wpływ na czas zwrotu termoizolacji ściany zewnętrznej.....	79
Barbara Dulińska: Zrównoważony rozwój w miastach projektowanych zgodnie z ideą Smart City	87
Wojciech Duliński: Zrównoważony rozwój w projektowaniu pasażerskich terminali lotniczych – przegląd wybranych przykładów .....	93
Irena Ickiewicz, Ewelina Kowalczyk: Budynek pasywny – weryfikacja uzyskanych efektów .....	99
Marta Nowak, Michał Kołaczkowski: Nowy wymiar budownictwa ze słomy .....	107
Agata Pawłowska, Michał Zielina: Analiza pracy czerpni w różnych warunkach.....	115
Marta Plaskacz-Dziuba, Marcin Cichosz, Bartłomiej Igliński, Roman Buczkowski: Autoklawizowany beton komórkowy z dodatkiem odpadu z instalacji półsuchego odsiarczania spalin – analiza termograwimetryczna oraz rentgenograficzna .....	123
Anna Wassilkowska, Karolina Kuc, Michał Zielina: Sprawdzenie składu powłoki cementowej w rurach wodociągowych i kanalizacyjnych .....	131
Gabriela Zemełka: Wpływ trzech herbicydów (tembotrion, nicosulfuron i S-metolachlor) na glebę z regionu Limagne (Francja).....	137
Michał Zielina, Anna Młyńska, Tadeusz Żaba: Eksperymentalne badania nad pogarszaniem jakości wody pitnej po cementowaniu przewodów wodociągowych .....	145
Maja Bartoszek, Michał Juszczyk: Wybrane problemy planowania robót budowlanych z wykorzystaniem BIM – studium przypadku .....	153
Magdalena Furmanek, Krzysztof Zima: Analiza budowy i eksploatacji pasywnej hali sportowej ...	165
Anna Jończy, Krzysztof Zima: Analiza wariantów ścian zewnętrznych w modelu BIM z wykorzystaniem metody AHP .....	175
Agnieszka Leśniak, Bartłomiej Szewczyk: Wybór wariantu wykonania podłogi sportowej .....	185

## LISTA RECENZENTÓW

Belniak Stanisław, Cracow University of Economics, Poland  
Berliński Nikolai, Odessa State Environmental University, Ukraine  
Biliński Tadeusz, University of Zielona Góra, Poland  
Błaszczński Tomasz, Poznań University of Technology, Poland  
Błazik-Borowa Ewa, Lublin University of Technology, Poland  
Bomberg Marek, McMaster, Hamilton, On, Canada  
Brząkała Włodzimierz, Wrocław University of Technology, Poland  
Đurica Pavol, University of Žilina, Slovakia  
Dzierżanowski Grzegorz, Warsaw University of Technology, Poland  
Eberhardsteiner Josef, Technische Universität, Wien, Austria  
Gruba Piotr, University of Agriculture in Cracow, Poland  
Hasan M. Abdullah, Bangabandhu Sheikh Mujibur Rahman Agricultural University, Bangladesh  
Hájek Petr, Czech Technical University in Prague, Czech Republic  
Heim Dariusz, Łódź University of Technology, Poland  
Henková Svatava, Brno University of Technology, Czech Republic  
Horszczaruk Elżbieta, West Pomeranian University of Technology, Szczecin, Poland  
Katunský Dušan, Technical University of Košice, Slovakia  
Kisilewicz Tomasz, Cracow University of Technology, Poland  
Klemm Katarzyna, Łódź University of Technology, Poland  
Kuc Sabina, Cracow University of Technology, Poland  
Licholaj Lech, Rzeszow University of Technology, Poland  
Łapko Andrzej, Białystok University of Technology, Poland  
Malinowski Anton Antonowicz, National University Lviv Polytechnic, Ukraine  
Mang Herbert, Technische Universität, Wien, Austria  
Pilecka Elżbieta, Cracow University of Technology, Poland  
Plebankiewicz Edyta, Cracow University of Technology, Poland  
Pogorzelski Jerzy, Białystok University of Technology, Poland  
Radziszewska-Zielina Elżbieta, Cracow University of Technology, Poland  
Šlanhof Jiří, Brno University of Technology, Czech Republic  
Sobczak-Kupiec Agnieszka, Cracow University of Technology, Poland  
Sobotka Anna, AGH University of Science and Technology, Poland  
Spišáková Marcela, Technical University of Košice, Slovakia  
Struková Zuzana, Technical University of Košice, Slovakia  
Tažiková Alena, Technical University of Košice, Slovakia  
Tchórzewska-Cieślak Barbara, Rzeszow University of Technology, Poland  
Tichá Alena, Brno University of Technology, Czech Republic  
Vranayová Zuzana, Technical University of Košice, Slovakia  
Wekezer Jerzy, Florida State University College of Engineering, Tallahassee, USA  
Zielina Michał, Cracow University of Technology, Poland  
Zimoch Izabela, Silesian University of Technology, Poland